Development of a Transient System Model of Mobile Air-Conditioning Systems

T. L. Hemami and W. E. Dunn

ACRC TR-143 September 1998

For additional information:

Air Conditioning and Refrigeration Center
University of Illinois
Mechanical & Industrial Engineering Dept.
1206 West Green Street
Urbana, IL 61801

(217) 333-3115

Prepared as part of ACRC Project 78
Modeling, Diagnostics, and Control
for Mobile Air-Conditioning Systems
W. E. Dunn and N. R. Miller, Principal Investigators

The Air Conditioning and Refrigeration Center was founded in 1988 with a grant from the estate of Richard W. Kritzer, the founder of Peerless of America Inc. A State of Illinois Technology Challenge Grant helped build the laboratory facilities. The ACRC receives continuing support from the Richard W. Kritzer Endowment and the National Science Foundation. The following organizations have also become sponsors of the Center.

Amana Refrigeration, Inc.
Brazeway, Inc.
Carrier Corporation
Caterpillar, Inc.
Copeland Corporation
Dayton Thermal Products
Delphi Harrison Thermal Systems
Eaton Corporation
Ford Motor Company
Frigidaire Company
General Electric Company
Hill PHOENIX
Hydro Aluminum Adrian, Inc.
Indiana Tube Corporation
Lennox International, Inc.
Modine Manufacturing Co.
Peerless of America, Inc.
The Trane Company
Whirlpool Corporation
York International, Inc.

For additional information:

Air Conditioning & Refrigeration Center
Mechanical & Industrial Engineering Dept.
University of Illinois
1206 West Green Street
Urbana IL 61801

217 333 3115

DEVELOPMENT OF A TRANSIENT SYSTEM MODEL OF MOBILE AIR-CONDITIONING SYSTEMS

Tara Lynn Hemami, Ph.D.
Department of Mechanical and Industrial Engineering
University of Illinois at Urbana-Champaign, 1998
W. E. Dunn, Advisor

ABSTRACT

A transient model was developed to predict the behavior of the vapor compression cycle of a mobile air-conditioning system. Mobile air-conditioning systems operate in a transient mode due to variations in compressor speed, variations in condenser air flow rate, and the controls strategy such as clutch-cycling. We developed a model to simulate start-up transients, clutch cycling transients, city-driving transients, and shut-down transients including the following charge redistribution.

Our transient model treats the components in a vapor compression refrigeration system including the compressor, condenser, orifice tube, evaporator, and accumulator. The heat exchangers are divided into a series of constant-volume cells. The conservation of mass, conservation of energy, and conservation of momentum equations are applied to each cell. The number of cells and/or the volume of the cells can be changed between simulations in order to change the resolution of the model. The accumulator model is a modification of the heat exchanger model which constrains the outlet to always be vapor. The orifice tube model and the compressor model are semi-empirical.

The model is validated with steady-state and transient data obtained from a test facility specifically designed to simulate mobile air-conditioners. The steady-state model predicts most of the system parameters to within ±15%. The transient model predicted the behavior of the city driving cycle, compressor shut-down, compressor start-up, and clutch-cycling simulations well.

An important part of the system model is calculating the refrigerant properties correctly. We developed refrigerant property routines to the calculate equilibrium thermodynamic properties in the liquid, vapor, two-phase liquid-vapor, and supercritical region using the Modified-Benedict-Webb-Rubin equation of state. Our property routines accurately solve for a given output property for applicable combinations of input properties. They also accurately predict whether the refrigerant is in the single-phase or two-phase region. The property routines agree extremely well with the experimental data found in the literature.

Table of Contents

List of Tables

List of Figures

Nomenclature

English Symbols

a	Helmholtz energy
a°	Ideal gas contribution to the Helmholtz energy
$\bar{a}$	Real gas contribution to the Helmholtz energy
A	Area
Bo	Boiling number $\left(\frac{\dot{Q}/A_{cs}}{G\,h_{fg}}\right)$
c_p	Specific heat at constant pressure
c_v	Specific heat at constant volume
c_v°	Ideal gas specific heat
C	Heat capacity rate $\left(\dot{m}c_p\right)$
CF	Clearance factor
Co	Convection number $\left[\left(\frac{\rho_g}{\rho_f}\right)^{0.5}\left(\frac{1-x}{x}\right)^{0.8}\right]$

C_r	Ratio of minimum heat capacity to maximum heat capacity in a heat exchanger $\left[\frac{(\dot{m}c_p)_{min}}{(\dot{m}c_p)_{max}}\right]$
D	Diameter
D_{eff}	Effective diameter
D_H	Hydraulic diameter
E_{CB}	Augmentation factor for two-phase convective boiling heat transfer
E_{NB}	Augmentation factor for two-phase nucleate boiling heat transfer
f	Friction factor, Fraction
f_Q	Heat transfer fraction $\left(\frac{\dot{Q}}{\dot{W}}\right)$
f_I	Irreversibility fraction $\left(\frac{\dot{I}}{\dot{W}}\right)$
F_{fric}	Friction loss per unit volume
Fr	Froude number $\left(\frac{V^2}{gD}\right)$
g	Acceleration of gravity, Gibbs free energy
G	Mass flux (ρV)

h	Enthalpy, Heat transfer coefficient
j	J-factor (dimensionless heat transfer correlation)
k	Thermal conductivity
K	Minor pressure losses coefficient
$\dot{I}$	Compressor irreversibility ($T_{in}\,\dot{S}_{internal}$)
L	Length
m	Mass
$\dot{m}$	Mass flow rate
M	Mach number $\left[\frac{V}{ss}\right]$
n	Polytropic exponent, Number, Unit normal
$\dot{N}$	Compressor speed (revolutions per second)
NTU	Number of transfer units $\left[\frac{UA}{(\dot{m}c_p)_{min}}\right]$
P	Pressure
PD	Piston displacement
Pe	Peclet number $[Re_L Pr]$

Pr	Prandtl number $\left(\frac{\mu c_p}{k}\right)$
Pr_l	Liquid Prandtl number $\left(\frac{\mu_l c_{p,l}}{k_l}\right)$
q''	Heat transfer per unit area
$\dot{Q}$	Heat transfer rate
r	Nondimensional compressor speed $\left(\frac{\dot{N}}{\dot{N}_{ref}}\right)$
R	Thermal resistance, Ideal gas constant
Re	Reynolds number $\left(\frac{GL}{\mu}\right)$
Re_D	Reynolds number based on diameter $\left(\frac{GD}{\mu}\right)$
Re_l	Superficial liquid Reynolds number $\left(\frac{GD(1-x)}{\mu_l}\right)$
Re_{lo}	Liquid only Reynolds number $\left(\frac{GD}{\mu_l}\right)$
RPM	Compressor speed (rounds per minute)
s	Entropy

S	Degrees of subcooling, Slip ratio $\left(\frac{V_g}{V_f}\right)$, Surface area
$\dot{S}$	Rate of entropy production
ss	Speed of sound
t	Time, Thickness
T	Temperature
u	Internal energy
UA	Overall heat transfer coefficient
v	Specific volume
V	Velocity
Vol	Volume
Vol_D	Displacement volume
W	Work
$\dot{W}$	Power
We	Weber number $\left(\frac{G^2 D}{\sigma \rho}\right)$
x	Mass quality $\left(\frac{m_{vapor}}{m_{total}}\right)$

X_{tt}	Turbulent-turbulent Lockhart Martinelli parameter
z	Distance (parallel with the gravity vector)

Greek Symbols

α	Void fraction $\left(\frac{A_{vapor}}{A_{total}}\right)$
δ	Density ratio $\left(\frac{\rho}{\rho_{crit}}\right)$
Δ	Difference
ε	Heat exchanger effectiveness
ϕ	Mass flux quality $\left(\frac{\dot{m}_{vapor}}{\dot{m}_{total}}\right)$
γ	Specific heat ratio $\left(\frac{c_p}{c_v}\right)$
η	Efficiency
η_{mech}	Mechanical efficiency
η_{rev}	Reversible efficiency
η_v	Volumetric efficiency

θ	Angle between refrigerant line and vertical
ρ	Density
σ	Surface tension
μ	Viscosity
τ	Temperature ratio $\left(\frac{T}{T_{crit}}\right)$, Time constant, Fluid shear stress

Subscripts

air	Air properties
acc	Accumulator
c	Condenser
calc	Calculated
cell	Cell property
cond	Condenser
comp	Compressor
crit	Critical property
cs	Cross sectional
cv	Control volume

e	Evaporator
evap	Evaporator
f	Saturated liquid property
fg	Difference between the saturated vapor property and the saturated liquid property
fric	Friction
g	Saturated vapor property
i	Ideal
in	Inlet properties
isen	Isentropic
l	Liquid
lo	Liquid only
lam	Laminar
min	Minimum
minor	Minor losses
max	Maximum
n	Node properties
out	Outlet properties

pred	Predicted
ref	Reference
sat	Saturation property
sub	Subcooled
super	Superheated
surf	Surface
tot	Total
tur	Turbulent
wall	Wall properties
v	Vapor
Vol	Volume

Chapter 1
Introduction

Mobile air conditioners are designed to cool the cabins of automobiles and heavy machinery. These systems are vapor compression refrigeration systems similar to room air-conditioners, refrigerators, and heat pumps. However, mobile systems differ from other air conditioning and refrigeration systems because their operation is always transient. The compressor is driven by a belt from the vehicle engine crankshaft; and as a result the compressor speed varies with engine speed independently of vehicle load. The condenser air-flow is provided by a combination of fans and the ram-effect flow; consequently, it varies with vehicle speed.

The primary design criterion for a mobile air-conditioner is too cool the cabin as quickly as possible after vehicle start-up. A cabin can reach 130 °F or more when the vehicle has been parked in direct sunlight. The system is overdesigned for less extreme operating conditions which occur after the cabin temperature has been pulled down to a comfortable level. A control strategy must be employed to regulate the excess capacity. A common control strategy is to cycle the compressor on and off using a clutch. Clutch cycling adds to the transient behavior of the system.

Because the system is inherently transient, a transient system model should be used to design a mobile air conditioner. The first part of this thesis is concerned with developing a transient model design tool for mobile air conditioning systems. This transient model must accurately simulate start-up transients, shut-down transients, and the following charge redistribution after shutdown. Also, the model must be able to simulate changes in the input conditions such as the compressor speed, heat exchanger air flow rates, and inlet heat exchanger air temperatures.

This model is intended to be a design tool in which different components and control strategies can be tested under actual operating conditions. Our mobile air-conditioning model provides a complete description of the thermodynamic state, refrigerant mass flow rates, and refrigerant mass distribution in a vapor compression system.

In Chapter 2 we shall provide a background of mobile air-conditioning system, air-conditioning models, and review the current state of the art in transient air-conditioning modeling. The structure of the transient model and the transient component models will be developed and validated with experimental data in Chapter 3. The component models will be

combined to create a system model that will also be validated with steady-state experimental data in Chapter 4. In Chapter 5 we shall validate the models with transient driving cycle, shut-down, start-up, and clutch cycling data.

An important part of the system model is calculating the refrigerant properties correctly. The second portion of this thesis discusses thermodynamic properties and the development of refrigerant property routines. Property routines determine one thermodynamic property from two other independent properties. A transient system model can call the property routines thousands of times per problem. The property routines must

1) Accurately determine the phase of the refrigerant and solve for the refrigerant properties,
2) Provide versatility with respect to the input properties,
3) Have a convenient user interface,
4) Quickly solve for the refrigerant properties, and
5) Provide results for different refrigerants.

In Chapter 6 we discuss single component refrigerant properties, the general algorithm for calculating refrigerant properties, and currently available property routines. In Chapter 7 we summarize our property routines and specifically discuss the user interface, equation of state, and search routines. We then determine the robustness of the property routines and validate the property routines with experimental data.

This work results in a robust model which can accurately model all transients in a mobile air-conditioning system between system start-up and shutdown and the subsequent charge distribution. The model uses our refrigerant property routines which consistently converge on the correct properties. This model is directly useful for studying clutch-cycling mobile air-conditioners but it could be easily extended to model other control strategies or vapor compression systems.

Chapter 2
Overview of Mobile Air-Conditioning System Models

This chapter provides background on mobile air-conditioning systems and transient system models. First, we shall summarize some of the key features that make mobile air-conditioning systems unique from other vapor compression systems. Next, an overview of transient system and transient component models is provided. Finally, we shall discuss some important transient vapor-compression models in the literature.

2.1 Description of Mobile Air-Conditioning Systems

Mobile air-conditioning systems are vapor-compression refrigeration systems designed for automotive and heavy-machinery applications. This description of mobile air-conditioning systems will focus on how they differ from stationary vapor-compression systems (e.g. refrigerators, heat pumps, room air-conditioners, etc.). It is important to note these differences because much of the literature on transient vapor-compression models is for stationary systems. We shall describe these differences in terms of the (a) specific components, (b) design criteria, (c) controls strategy, and (d) controls methods.

2.1.1 Specific Components

First, we shall discuss how the compressor, heat exchangers, and expansion device differ between mobile and stationary systems.

Stationary systems use a hermetic compressor powered by an internal electric motor whereas mobile systems use an external-drive compressor powered by a shaft connected to the vehicle engine. In mobile systems, the compressor speed changes with the engine speed independently of the air-conditioning load, and the compressor is turned on and off with a clutch. In most stationary systems the compressor speed remains constant. Some prototype stationary systems have variable-speed compressors wherein the compressor speed changes to match the cooling load. Several mobile systems use a variable displacement compressor which is discussed in Section 2.1.4.3.

An important design criterion in mobile systems is to reduce the size and weight of the components (discussed in Section 2.1.2). As a result, the automotive industry has adopted many compact and efficient heat exchanger designs such as plate-fin evaporators and micro-

channel condensers which are not commonly seen in stationary systems at present. Another difference relates to the airflow over the condenser. In refrigerators and heat pumps, the airflow is provided exclusively by a fan. In automotive systems, the flow is a combination of fan-induced and ram-effect flow. The fan provides most of the flow at low vehicle speeds whereas the ram-effect provides most of the air flow at high vehicle speeds.

The standard constant-area expansion device is an orifice tube in mobile systems and a capillary tube in stationary systems. In stationary systems, capillary tubes are sometimes run parallel to the suction line creating a counterflow heat exchanger. Some stationary and mobile systems also use thermal expansion valves (TXVs) as an expansion device.

2.1.2 Design Criteria

The design criteria are a very important difference between stationary and mobile systems. Mobile air-conditioning systems are required to provide a comfortable vehicle cabin temperature and humidity level under a variety of conditions. These systems must be designed to keep the cabin cool on an extremely hot day in Arizona and to dehumidify a cabin on a cool rainy day in Maine. Mobile systems are traditionally designed for the most extreme operating condition which is rapid cabin temperature pulldown. After a vehicle has been sitting in the sun on a summer day, the cabin temperature can be upwards of 130 °F. Consumers want the air-conditioning system to pull this temperature down to comfortable levels quickly. As a result of this design criterion, the system is typically oversized for most normal operating conditions.

Other important design criteria include minimizing the size and weight of the component and minimizing both initial manufacturing costs and future warranty costs. With automotive manufacturers pushing towards longer warranties, reliability has become a greater concern.

The most important design criterion in a stationary system is energy efficiency because it is regulated by the federal government. Stationary systems generally pulldown the indoor environment temperature on the order of hours rather than minutes, and they are usually working against a cooler initial temperature. Minimizing manufacturing and warranty costs are also an important design criterion.

2.1.3 Control Objectives

Mobile air-conditioning systems have two basic controls objectives. The first is to maintain the cabin at the correct temperature. The second is to prevent frost from forming on the evaporator. If the outlet evaporator air temperature falls below the freezing point of water, then frost forms on the evaporator coils reducing airflow to the cabin and evaporator efficiency.

The standard method of operating mobile systems is to employ a controls strategy (summarized in Section 2.1.4) to maintain the evaporator refrigerant temperature at approximately 35 °F. This strategy results in maximum cooling and maximum dehumidification at all times. Since the system is sized for pulldown conditions, the passenger compartment will become too cold during less extreme operating conditions unless the system capacity is modulated. This can be accomplished using a blend door to divert a portion of the cool air from the air conditioning system through the heating core.

Stationary systems must also be controlled to maintain the indoor environment at the correct temperature. Compressor cycling (Section 2.1.4.1) and variable-area expansion valves (Section 2.1.4.2) are the most common control methods used to achieve this objective. In a room air conditioner, the system is designed for the evaporator to operate around 40-50 °F and thus frost formation is automatically avoided.

2.1.4 Control Methods

In the following sections we shall discuss control methods for mobile air conditioners. Clutch cycling and variable-area expansion valves are the two most common methods whereas variable-displacement compressors and suction throttling are less common. All of these control methods are also applicable to stationary systems but compressor cycling is the most common strategy followed by variable-area expansion valves. Another control strategy used in some prototype stationary systems is a variable-speed compressor. This strategy is not practical for mobile systems and is not discussed here.

2.1.4.1 On-off Control

On-off control typically use a constant-area expansion valve such as an orifice tube. A pressure sensor at the exit of the evaporator controls whether the compressor clutch is engaged or disengaged. The clutch disengages when the pressure falls below the low-pressure set point and engages when the pressure reaches a high-pressure set point. During highway operation, the clutch can cycle on and off several times per minute. Clutch cycling systems have an accumulator between the evaporator and compressor to prevent liquid refrigerant from flowing into the compressor. A transient model is most important for this type of system because of the extreme transient nature caused by the compressor constantly turning on and off.

The main advantages of clutch cycling systems are that the control algorithm is simple to implement and the expansion valve has no moving parts which can fail. For these reasons, this is the most common control strategy in American-made automobiles.

A disadvantage of clutch cycling systems is that the compressor cycling causes swings in the discharge temperature. Also, the horsepower required to drive a compressor can

represent a significant portion of the engine output. The driver can sometimes feel the drop in power when the compressor is engaged. Also, there is excessive wear on the compressor because it is constantly stopping and restarting.

2.1.4.2 Variable-Area Expansion Valve Systems

Variable-area expansion valves control the refrigerant temperature at the outlet of the evaporator by changing the expansion valve opening. Two types of variable-area expansion valves are thermal expansion valves (TXV) and electronic expansion valves (EEV).

A TXV maintains a constant superheat at the evaporator exit. The outlet temperature is measured using a thermal bulb filled with refrigerant. The refrigerant can either be the same refrigerant as in the system or a combination of refrigerants depending on the desired characteristics. The bulb is connected to the outlet of the evaporator. The refrigerant in the bulb expands or contracts depending on the temperature at the outlet of the evaporator. The orifice opening is determined by the difference between the refrigerant pressure in the bulb and the sum of the refrigerant pressure at the outlet of the expansion valve and a spring force which tends to close the valve. If the heat load increases, the evaporator superheat increases. The refrigerant in the bulb expands and increases the expansion valve opening. As a result, the refrigerant flow increases and decreases the refrigerant outlet temperature. A more detailed explanation of TXVs is provided by Eaton Automotive Controls (1993). TXVs are common in Japanese-made automobiles.

Another type of expansion valve is the electronic expansion valve (EEV). EEVs are currently experimental in mobile and stationary air-conditioning system. The throat opening is controlled by an electric signal provided by a microprocessor. The microprocessor can use a variety of inputs such as the outlet refrigerant pressure or the compressor speed and a more sophisticated control algorithm to determine the optimal valve opening.

Since variable-area expansion systems are designed to maintain superheated refrigerant at the evaporator exit, an accumulator is not needed before the compressor. Typically, a receiver-dryer is placed between the condenser and the TXV. A receiver-dryer is a reservoir for refrigerant which is designed to only allow liquid to flow out.

The advantage of TXV control is that the system is operated at a high level of efficiency. Maximum heat exchanger efficiency occurs when all of the refrigerant in the evaporator is two-phase. Since a TXV controls outlet temperature, a small amount of superheat is typically maintained.

One disadvantage of TXV systems is that the expansion valve has moving parts which can fail. Another problem is that the system can become unstable or "hunt." Hunting occurs when the valve alternates between opening too wide and opening too small without coming to a

steady-state value. Hunting is caused by a wrongly sized valve or the system operating in an unusual way.

2.1.4.3 Variable-Displacement Compressor Systems

A variable-capacity compressor changes its displacement volume to maintain the evaporator pressure at a constant value which is slightly above the freezing point of water. If the evaporator load is reduced, then the evaporator temperature and pressure decrease. The suction pressure decreases which causes the compressor displacement and capacity to also decrease. More information on the details of the behavior of variable-displacement compressors can be found in Skinner and Swadner (1985) and Tojo et al. (1990). These systems usually have an orifice tube but can also use a TXV (Inoue et al., 1988).

Variable-displacement compressor systems have the advantage of running continuously so there is no cycling load on the engine or swing in outlet air temperature. However, these compressors are more complex than constant-displacement compressors and can be less reliable. These factors can lead to higher warranty costs and dissatisfied customers.

2.1.4.4 Suction Throttling Systems

Suction throttling uses a valve at the outlet of the evaporator to control the evaporator pressure. The valve maintains the outlet evaporator pressure at a constant value independent of the compressor inlet pressure and the cooling demand. This maintains the evaporator above the freezing temperature of water.

This strategy has the advantage that the compressor runs continuously. However, suction throttling is extremely inefficient and results in an unacceptable fuel economy penalty. Suction throttling is rarely used in current production vehicles.

2.2 Transient System Models

A dynamic model is needed to simulate mobile air conditioning systems because they are inherently transient. Steady-state models are useful for designing a system for one specific operating point or determining an average energy efficiency. Transient models are useful for studying system behavior during more realistic operating conditions such as start-up, shut-down, clutch-cycling, or city driving cycles.

Transient models capture different phenomena than do steady-state models such as refrigerant charge migration throughout the system, thermal capacitance of the components, and energy storage in the refrigerant. Some possible output from transient models include energy efficiency, changes in evaporator air outlet temperature, and changes in drivability (i.e., compressor torque). Transient models are also important in determining possible problems in

system operation such as liquid slugging of the compressor, evaporator charge starvation, TXV hunting, or refrigerant pressure spikes.

The inputs of both steady-state and transient models are compressor speed, evaporator and condenser air temperatures, condenser and evaporator air mass flow rates, and the refrigerant charge. The model outputs include the refrigerant state (pressure, temperature, enthalpy, etc.) throughout the system, refrigerant flow rate, outlet air temperatures, compressor torque, and refrigerant flow rate.

Transient system models are composed of separate component models discussed in Section 2.3. Section 2.3 also describes the types of equations needed to model each component. The solution technique for the equations is discussed in Section 2.4. Section 2.5 describes how to predict the refrigerant charge in a system.

The remainder of this section provides an overall perspective of transient models. Transient system models are developed to capture different transient phenomena. The next section specifically describes the transient conditions that occur during system operation and how they affect the input conditions to the model. The following two sections describe the objectives of transient models and the classification of the model equations.

2.2.1 Transients in Mobile Air-Conditioning System Operation

Different transients affect mobile vapor-compression systems such as load transients, vehicle transients, on/off transients, and controls transients. All of these transients except vehicle transients also affect stationary systems.

Load transients (from the viewpoint of the air conditioning systems) occur when the evaporator inlet temperature changes. The most extreme load transient occurs during pulldown. Load transients also result from temporal variations in the net heat flux to the passenger compartment. Such variations arise from changes in the solar input, the convective heating or cooling of the vehicle exterior, and air exchange through an open door or window. Also, load transients can occur by the vehicle occupant varying the set point of the conditioned air. Since the thermal capacitance of the vehicle interior is fairly large, these transients are relatively slow. The cabin generally takes many minutes to reach a new steady-state after a load transient occurs.

Vehicle transients are changes which the moving vehicle imposes on the air-conditioning system and correlate directly with the acceleration and deceleration of the vehicle. These transients include changes in the compressor speed and condenser airflow. Vehicle transients do not occur when the vehicle is operating at a constant speed.

On/off transients occur when the clutch turns on and off. These transients occur during system start-up, system shut-down, or clutch cycling. In a clutch-cycling system, on/off

transients occur frequently except when the system is turned off (and the clutch is disengaged) or when there is an extremely high steady-state load and the clutch does not cycle. High steady-state loads occur on hot days when the fresh air enters with evaporator core rather than recirculated air. When the clutch engages (disengages), the compressor speed accelerates (decelerates) to the speed of the engine (zero) quickly. The on/off transient itself occurs on the order of tenths of seconds to seconds. On/off transients affect the vapor-compression system by causing the refrigerant mass flow rate to go zero when the clutch is turned off or to go to a steady-state nonzero value when the clutch is turned on. After an on/off transient, the vapor compression system takes minutes to reach a new steady-state value.

On/off transients are much more difficult to model than the other transients. Most other transients can be modeled as small deviations from a steady-state model. On/off transients represent large deviations from steady-state. When the compressor is turned off, situations completely different from steady-state conditions occur. For example, the refrigerant mass flow rates go to zero or can become negative. Also, subcooled liquid refrigerant can exist in the evaporator or the condenser can become entirely superheated vapor.

Other transients relate to other controls strategies besides clutch cycling such as changing the area of an expansion valve, changing the area of a suction throttling valve, or changing the displacement of a variable-displacement compressor. The time constant for thermal expansion valves is dependent on the thermal capacity of the thermal bulb and it can be on the order of seconds or tens of seconds. The suction throttling valve and variable-displacement compressor react to changes in the system pressure and have faster time constants.

2.2.2 Objectives of System Models

The objective of a transient system model dictates the types of equations and the type of solution techniques. Four different objectives are (a) system design, (b) controls implementation, (c) energy efficiency studies, and (d) qualitative studies.

Transient design models are used to optimize system performance in transient operation by varying components, refrigerant (for studying alternative refrigerants), or controls strategy. The most useful design models can simulate all of the above types of transients although most design models do not attempt that. Transient design models can also be used to test a system in failure modes (such as charge loss) or extreme operating conditions (such as extremely high ambient temperatures). These models must be validated with experimental data and must be accurate enough to provide confidence in the conclusions. Design models are also important in understanding transient phenomena observed in real data. Simplified transient design models can be used as a starting point for controls and energy efficiency models.

Models developed for real-time controls applications must be simple enough to run on a microprocessor in real-time during system operation. Controls models take inputs measured in real time such as system pressures or temperatures. The model then calculates actuator outputs such as fan speeds, electronic expansion valve opening, or the compressor speed or displacement. Some possible controls objectives include preventing evaporator frosting, increasing system efficiency, maintaining constant outlet air temperatures, reducing system noise, or preventing liquid from flowing into the compressor. Control models must be able to model all transients to correctly control the system at all times. However, it is very difficult to develop a simple model that captures all operating conditions. Often simple heuristic models are used for extreme transients such as start-up or shut-down. Controls models must also agree with transient data.

The standard method of calculating the energy efficiency of refrigerators and heat pumps is to use a steady-state model. Transient models take into account the loss in efficiency during start-up and shut-down. Usually energy efficiency models are a simple modification of steady-state models or simplifications of transient models.

Qualitative system models have not been compared to laboratory data and can only be used as the first step in the design process. These models are used to qualitatively understand refrigerant migration, thermal capacitance, and other transient phenomena. Also, qualitative models can help obtain a general understanding of the differences between different control strategies and design parameters on system performance. However, further analysis is needed before making a definitive conclusion because the models have not been compared with laboratory data.

2.2.3 Classification of System Model Equations

The objective of the model dictates which type of transient model is utilized. We shall define the different classifications of system models as fundamental, quasi-steady-state, time constant, and empirical models.

A fundamental mathematical model uses the transient conservation equations to represent the system. These models are used for design and detailed systems analysis. A simplified fundamental model can be used in conjunction with system control algorithms. Fundamental models can be simplified to quasi-steady-state models by setting the derivatives equal to zero.

In a quasi-steady-state model, the input parameters change with time, but the governing equations are steady-state. This type of model is accurate only for very slow transients such as load transients. Quasi-steady-state models can be used for any of the above purposes as long as the transient are slow enough.

Time-constant models represent the transient response of the heat transfer and refrigerant migration with a time lag of the steady-state response. Time constants are useful for simulating repeatable transients such as heat pump or refrigerator cycling. This type of model is typically used for energy efficiency calculations.

Empirical models are based on experimental data and use a mathematical equation to correlate the inputs and the outputs. The form of the equation relates only loosely to any physical phenomenon and is chosen because it correlates well with the experimental data. Empirical transient models are often based on quasi-steady-state or time-constant models.

2.3 Transient Component Models

A transient system model is a combination of transient component models. A complete system model includes models for the evaporator, condenser, expansion valve, compressor, and other components such as the accumulator, refrigerant lines, and control valves. Each component model can be classified as belonging to one of the above groups, and more than one classification can be used in a system model.

The following sections provide an overview of the component models and categorize the models in order to better understand the literature review (Section 2.6). We shall concentrate on fundamental models for each component. If the fundamental model is too complex for systems models, alternative modeling approaches are discussed.

2.3.1 Heat Exchanger Models

A heat exchanger model is developed by applying the conservation of mass, conservation of energy, and conservation of momentum to the refrigerant, heat sink fluid, and heat exchanger wall. Each of these sections is dealt with separately.

2.3.1.1 Refrigerant Model

When the conservation equations are applied to the refrigerant, a standard simplification is to model the refrigerant flowing in the tube as one-dimensional. Therefore, the scalar velocity in the x direction is defined as V. Other refrigerant variables are the density (ρ), pressure (P), internal energy (u), enthalpy (h), and temperature (T). Geometry variables include the volume (Vol), the area (A), internal diameter (D), and the angle between the refrigerant line and the vertical (θ). The differential forms of the conservation of mass, conservation of momentum, and conservation of energy are

$$\frac{\partial \rho}{\partial t} + \frac{\partial (\rho V)}{\partial x} = 0, \tag{2.1}$$

$$\frac{\partial (\rho V)}{\partial t} + \frac{\partial \left(\rho V^2\right)}{\partial x} = \rho g \cos\theta - \frac{\partial P}{\partial x} + F_{fric}, \text{ and} \tag{2.2}$$

$$\frac{\partial \left[\rho\left(u + \frac{V^2}{2} + gz\right)\right]}{\partial t} + \frac{\partial \left[\rho V\left(h + \frac{V^2}{2} + gz\right)\right]}{\partial x} = \frac{\dot{Q}}{Vol} + V\rho g\cos\theta. \tag{2.3}$$

The friction loss per unit volume is defined as

$$F_{fric} = \frac{1}{D} f \frac{1}{2} \rho V^2. \tag{2.4}$$

f is the Darcy friction factor. The heat transfer between the wall and refrigerant is

$$\dot{Q} = A_{inside} h_{ref} \left(T_{wall} - T_{ref}\right). \tag{2.5}$$

where h_{ref} is the heat transfer coefficient between the refrigerant and the wall. One method of solving the above equations is to discretize the partial derivatives and solve the resulting implicit equations (Chen and Lin, 1991; Nyers and Stoyan, 1994; MacArthur and Grald, 1989; Murphy and Goldschmidt, 1986; and Gruhle and Isermann, 1985).

An alternative method of developing a heat exchanger model is to integrate the conservation equations or equivalently use a control volume approach. The integral or control volume equations for the conservation of mass, conservation of momentum, and conservation of energy are

$$\frac{dm}{dt} = \dot{m}_{in} - \dot{m}_{out}, \tag{2.6}$$

$$\frac{d(mV)}{dt} = \dot{m}_{in} V_{in} - \dot{m}_{out} V_{out} + mg\cos\theta + \left(P_{in} - P_{out}\right) A_{cs} + F_{fric} Vol, \tag{2.7}$$

and

$$\frac{d\left[m\left(u+\frac{V^2}{2}+gz\right)\right]}{dt} = \dot{m}_{in}\left(h_{in}+\frac{V_{in}{}^2}{2}+gz_{in}\right) - \dot{m}_{out}\left(h_{out}+\frac{V_{out}{}^2}{2}+gz_{out}\right) + \dot{Q} \quad (2.8)$$

These ordinary differential equations can be solved using standard techniques such as Euler's method (Mitsui, 1987; Chi and Didion, 1982; and Dhar and Soedel, 1979b) or Runge-Kutta (Vargas and Parise, 1995). Other methods used to solve the equations are differential/algebraic equation solvers (Colding et al., 1991). Ploug-Sorensen et al. (1997) and Ginsberg (1994) developed their codes for specific software packages, EASY5 and Sinda/Fluint, respectively.

Frequent approximations used to simplify the equations include neglecting gravity ($mg\cos\theta$ and gz), neglecting kinetic energy ($V^2/2$), and neglecting the viscous dissipation, $V(F_{fric}Vol)$.

He et al. (1997) linearized the differential equations around an operating point and used a standard linear equation solver. The resulting equations are only valid for small perturbations around the operating point and result in a model useful for control purposes.

Another way of writing the governing equations is to apply the conservation equations separately to the liquid and vapor phases (Sami et al., 1987). An extra term is needed in the conservation equations which corresponds to the mass transfer between the vapor and liquid phases.

An important part of the heat exchanger equations is determining the heat transfer coefficients and the pressure drop parameters. A lumped-parameter model uses a single parameter to describe these complicated phenomena over the entire control volume. This simplification is generally used in system models since the details of each component are not as important as the interaction of the components. Alternatively, the parameters are integrated over the entire length of the control volumes.

Two types of heat exchanger models are cell models and zone models. The difference between these models lies in the definition of the control volumes.

Cell Models

A cell model divides the heat exchanger into a series of constant volume sections. The resolution of the model can be changed by increasing or decreasing the number of cells in different model runs. Simplified transient models often use a single cell model to describe the condenser and evaporator (Vargas and Parise, 1995; Darrow et al., 1991; Cherng and Wu,

1989; and Chi and Didion, 1982). More accurate models use multiple cells and solve an increased number of equations (Ploug-Sorensen et al., 1997; Sami and Zhou, 1995; Sami and Comeau, 1992; Chen and Lin, 1991; MacArthur and Grald, 1989; Mitsui, 1987; Gruhle and Isermann, 1985; and Yasuda et al., 1983).

One advantage of cell models is that the number of cells is constant for a given run and consequently the number of equations remain constant during the run. Using a large number of cells increases accuracy at the expense of computation time.

Zone Models

The control volumes in a zone model are the liquid, two-phase, and vapor regions. Because the boundaries between the control volumes change with time, this model is also called a moving boundary model. During transient operation, the zones can appear or disappear. Zone models have been used in transient models by He et al. (1997), Nyers and Stoyan (1994), Ginsberg (1994), Colding et al. (1991), and Dhar and Soedel (1979a).

An advantage of zone models is that they provide good accuracy with only a few equations to be solved numerically. Also, the state variables of each zone can be different. For example, pressure and temperature can be the state variables of the single-phase regions, and temperature and quality can be the state variables of the two-phase regions.

A disadvantage is that a new transient variable, the length of the zone, is introduced. Another disadvantage is that the number of zones in a heat exchanger can vary during transient operation. For example, at start-up the entire condenser might be two-phase. After some time a superheated region occurs and later a subcooled region occurs. The number of equations required in the condenser model changes as the number of zones change. These discontinuities create a programming challenge for the modeler.

2.3.1.2 Heat Sink Fluid Model

The heat sink fluid of a heat exchanger can be either air (or theoretically any other gas) or water (or any other liquid). The heat sink fluid affects the vapor compression system by changing the inlet air or water temperature to the evaporator and condenser. Models of the heat sink fluid vary greatly in complexity. The simplest models only provide an inlet air or inlet water temperature to the refrigeration model. More detailed models couple the vapor compression model to a heat transfer simulation of the cooled environment.

The same conservation equations which apply to the refrigerant (Equations 2.6, 2.7, and 2.8) apply to the air. The transients on the airside of the heat exchanger are commonly modeled as steady-state. The most important airside property, the outlet air temperature, is determined from the conservation of energy equation.

$$0 = \dot{m}_{air} c_{p,air} \left(T_{air,in} - T_{air,out}\right) - h_{air} A_{outside} \left(T_{air,in} - T_{wall}\right) \quad (2.9)$$

This type of model is used by Mitsui (1987) and MacArthur and Grald (1989). More complex models include all three differential equations across the heat exchanger (Chi and Didion, 1982 and Ginsberg, 1994). The next step in complexity is to model the room or cabin with a lumped capacitance model (Ploug-Sorensen et al., 1997 and Vargas and Parise, 1995). Bajpai (1994) calculates the solar heat load on an automobile which is an input to their design model, and Cherng and Wu (1989) include a 3-D model for an automotive passenger compartment.

If the ambient air is humid, then water will condense on the evaporator. Both the latent and sensible heat load must be taken into account in the transient models. Humidity is included in the following models: Ginsberg (1994), Kyle et al. (1993), Sami et al. (1987), Mitsui (1987), and Cherng and Wu (1989).

2.3.1.3 Heat Exchanger Wall Model

The model for the heat exchanger wall couples the air model with the refrigerant model. This model incorporates the heat capacitance of the wall and is used to calculate the temperature of the wall.

$$c_{p,wall} m_{wall} \frac{dT_{wall}}{dt} = h_{ref} A_{inside} \left(T_{ref} - T_{wall}\right) - h_{air} A_{outside} \left(T_{wall} - T_{air,in}\right) \quad (2.10)$$

Heat exchanger wall models are not necessary when the thermal capacitance of the wall is very small. In that case the inlet air temperature is used instead of the wall temperature in Equation 2.5; the refrigerant temperature is used instead of the wall temperature in Equation 2.9. He et al. (1997), Nyers and Stoyan (1994), Chen and Lin (1991), Mitsui (1987), Gruhle and Isermann (1985), Yasuda et al. (1983), Chi and Didion (1982), and Dhar and Soedel (1979a) include transient models for the heat exchanger walls.

2.3.2 Compressor Models

Mobile air-conditioning systems use external drive compressors which are powered by the vehicle engine. Heat pumps and refrigerators generally use hermetic compressors where an electric motor is encased in the compressor housing. The main difference between modeling external drive and hermetic compressors is modeling the heat transfer. We shall discuss modeling the heat transfer in compressors in the next section and the compression process in the following section.

2.3.2.1 Conservation of Energy

The conservation of energy principle is applied to the refrigerant in the compressor to determine the outlet enthalpy. The control volume formulation of the conservation of energy of the refrigerant is as follows.

$$\frac{\partial\left[m\left(u+\frac{V^2}{2}\right)\right]}{\partial t} = \dot{m}_{in}\left(h_{in}+\frac{V_{in}{}^2}{2}\right) - \dot{m}_{out}\left(h_{out}+\frac{V_{out}{}^2}{2}\right) - \dot{Q}_{comp} + \dot{W}_{comp} \tag{2.11}$$

A common simplification is to neglect the transient term. Two parameters, work and heat, can either be simulated analytically or determined experimentally.

The work is generally modeled as a quasi-steady-state process. It can be specified empirically as a function of inlet conditions, outlet conditions, and compressor speed (Murphy and Goldschmidt, 1985). Alternatively, work can determined from an overall compressor efficiency given input power (Ginsberg, 1994 and Chi and Didion, 1982).

Heat transfer models vary greatly in complexity. Simple models lump the entire heat transfer coefficient between the refrigerant and the air into one or two parameters (Chi and Didion, 1982 and Ginsberg, 1994). This type of model is valid for external drive compressors. More complex hermetic compressor models can include heat transfer coefficients between the suction line, discharge line, electric motor, shell, oil sump, and compressor. Since mobile air conditioners have external drive compressors we shall not go into the details of these complex models. Models that treat hermetic compressors are Chen and Lin (1991), Dhar and Soedel (1979a), MacArthur and Grald (1989), and Murphy and Goldschmidt (1985).

The outlet enthalpy can also be determined from the isentropic efficiency (Ploug-Sorensen et al., 1997; Darrow et al., 1991; Colding et al., 1991; and Mitsui, 1987). It is defined as

$$\eta_s = \frac{\dot{W}_{min}}{\dot{W}} \tag{2.12}$$

This equation does not discriminate between heat and work. The heat transfer and other irreversibilities are lumped into a single efficiency which can be constant or a function of the compressor parameters.

2.3.2.2 Compression Process

The goal of modeling the compression process is to determine the mass flow rate, the output pressure, or the input pressure given two of these properties. Three types of compression models are fundamental, theoretical, and empirical.

Precisely modeling the compression phenomena is quite complicated. Fundamental models describe the events in the compressor cylinder as a function of crankcase angle, mass flow rate through the valves, valve dynamics, compressor kinematics, and heat transfer within the valves and through the cylinders. The most accurate models are three dimensional and have more detail than is necessary for a system model. Simpler fundamental models simulate each compressor stroke with a conservation of energy equation and a conservation of mass equation (Chen and Lin, 1991; Sami et al., 1987; and Yasuda et al., 1983). The mass flow rates in and out of the compressor are determined using the valve characteristics.

Theoretical (or first principles) models use certain assumptions and simplifications such as modeling the compression as a polytropic process or using a volumetric efficiency. The most common theoretical models use volumetric efficiency (Ginsberg, 1994; Gruhle and Isermann, 1985; Mitsui, 1987; Vargas and Parise, 1995). The volumetric efficiency is defined as the actual mass of fluid per cycle divided by the theoretical mass of fluid per cycle.

$$\eta_v = \frac{\dot{m}}{\rho_{in}\, Vol_D\, \dot{N}} \tag{2.13}$$

Vol_D is the piston displacement. Colding et al. (1991), Darrow et al. (1991), and Ploug-Sorensen et al. (1997) determined the volumetric efficiency empirically. Chi and Didion (1982) use the polytropic expansion coefficient to determine the volumetric efficiency. Other models such as He et al. (1997) use an empirical equation with the polytropic coefficient. Theoretical models are useful to study the effect of compressor parameters (such as piston displacement) on system behavior.

Purely empirical models do not provide any insight to the physical processes in the compressor. However, they are accurate and computationally efficient. Empirical models are simple to implement because they do not require any knowledge of the geometry or materials of the compressor. Murphy and Goldschmidt (1985) and Kyle et al. (1993) use purely empirical models.

2.3.3 Expansion Valve Models

The purpose of an expansion valve is to control the refrigerant mass flow rate through the system by throttling the refrigerant from the condenser to the evaporator. In automotive and heavy machinery systems, the expansion valve is typically either an orifice tube or a thermal expansion valve (TXV). An orifice tube is a constant area device. The area of a TXV is mechanically controlled by the evaporator outlet temperature. A third type of expansion device is a capillary tube which is used in refrigerators. A capillary tube is a small diameter tube which acts as a constant throttle.

A new type of expansion valve is an electronic expansion valve (EEV). The opening of the valve is actuated by an electric signal. Several system models use EEV as a control output. EEVs models are similar to orifice tube models except that the orifice opening is a function of the control input.

The expansion valve model determines the inlet pressure, outlet pressure, or mass flow rate given the other two properties and other information. Orifice tubes and TXVs are modeled as having no heat input or work input so the inlet enthalpy is equal to the outlet enthalpy. Capillary tubes are much longer and are sometimes run parallel to the suction line creating a counterflow heat exchanger. Modeling heat transfer is important when a suction-line heat exchanger is present.

2.3.3.1 Orifice Tubes

During steady-state operation, the orifice tube has either two-phase or subcooled refrigerant at the inlet and always has two-phase refrigerant at the outlet. The mass flow rate through the orifice tube is generally thought of as "choked" although it is weakly dependent on the outlet pressure. During start-up conditions, the mass flow rate is too small for the flow to be choked. A transient model must take into account all of these conditions.

A simple and rather inaccurate orifice tube model is based on Bernoulli's equations applied to an orifice. This model assumes steady, adiabatic, frictionless, incompressible flow with a uniform velocity profile and no external work.

$$\dot{m} = C_{orifice} A_{cs} \sqrt{2\rho(P_{in} - P_{out})} \tag{2.14}$$

Bernoulli's equation does not take into account that the flow is choked. He et al. (1997) and Nyers and Stoyan (1994) use this type of model.

More accurate models replace the outlet pressure in Equation 2.11 with a pseudo-outlet pressure which accounts for the choked flow (Kyle et al., 1993 and MacArthur and Grald,

1989). The form of the pseudo-outlet pressure has been determined experimentally. This type of model can be fairly accurate; however, it only works when the flow is choked.

2.3.3.2 Thermal Expansion Valves

A TXV has a bulb filled with refrigerant attached to the refrigerant tube at the outlet of the evaporator. The bulb can either contain the same fluid as the rest of the system or a different refrigerant. The temperature and therefore the pressure in the bulb are a function of the outlet temperature of the evaporator. The valve area is controlled by the pressure difference between the pressure at the exit of the evaporator and the pressure in the thermal bulb. A TXV is typically tuned to maintain several degrees of superheat at the evaporator exit.

Models for the flow through the expansion valve are similar to models for an orifice tube except the area is variable. Colding et al. (1991) and Mitsui (1987) apply Bernoulli's equations; Gruhle and Isermann (1985) utilize a modified Bernoulli's equations. Sami and Zhou (1995) and Sami and Comeau (1992) use an empirical equation for the mass flow rate.

The area of the expansion device is simulated as a linear function of the pressure difference between the minimum valve opening and the maximum valve opening (Kyle et al., 1993 and Yasuda et al., 1983). Ginsberg (1994) takes the derivative of this formula to provide the transient response. A quasi-steady-state model assumes that the bulb temperature is equal to the temperature of the refrigerant at the evaporator outlet. A more accurate model uses transient differential conservation equations to model the heat transfer between the evaporator tube and the refrigerant in the feeler bulb (Mitsui 1987 and Yasuda et al. 1983).

2.3.3.3 Capillary Tubes

Since mobile air-conditioning systems are not designed to use capillary tubes, we shall only discuss them briefly for the sake of completeness. Capillary tubes are long, small-diameter tubes used in refrigerators and room air conditioners. They are often placed next to or inside the suction line which forms an efficient counterflow heat exchanger. The sub-cooling and consequently the mass flow rate from the condenser are increased and the superheat into the compressor is increased.

Capillary tubes models are similar to heat exchanger models. The conservation equations are applied to a series of control volumes. The major difference is that the flow becomes choked in the capillary tube. An iterative process is usually employed to determined whether the tube is choked or not. Ploug-Sorensen et al. (1997), Chen and Lin (1991), Sami and Comeau (1992), and Murphy and Goldschmidt (1986) model capillary tubes.

2.3.4 Other Component Models

Other refrigeration components in a vapor-compression system include the accumulator, refrigerant lines, and receiver. The accumulator is a tank between the evaporator and the compressor which is designed to prevent liquid refrigerant from flowing into the compressor. Modeling the accumulator is very important in transient operation because the amount of liquid refrigerant it contains varies significantly during transient operation. Accumulators are included the following models: MacArthur and Grald (1989), Chi and Didion (1982), and Dhar and Soedel (1979a).

Refrigerant pipes between components usually have a small amount of heat transfer and pressure drop compared to the other components. If desired, these can be modeled in a manner similar to one cell of a heat exchanger. Refrigerant lines between the condenser and orifice tube contain liquid or two-phase refrigerant and are important for a proper mass inventory. Ginsberg (1994) includes a model for refrigerant pipe.

Receiver-dryers are used in TXV systems between the condenser and the valve. Either two-phase or liquid refrigerant flows into the receiver and only liquid refrigerant exits to the expansion valve. Colding et al. (1991) and Mitsui (1987) simulate a receiver.

2.4 Solution of System Models

After combining the component models to create a system model, the next step is to solve the equations. The resulting equations are generally a set of differential and algebraic equations. If the conservation equations are formulated as PDE's as in Equations 2.1, 2.2, and 2.3 then the partial derivatives are approximated with a difference formula and the equations are solved. If the conservation equations are formulated as ODE's (Equations 2.6, 2.7, and 2.8) then a standard integration technique such as Runge-Kutta can be employed. One more obstacle to be overcome is that the conservation equations are stiff.

A system of initial-value, stiff, ordinary differential equations has widely varying time constants. Some components of the solution decay very quickly while other components decay very slowly. It is generally thought that the conservation of momentum makes the equations stiff because it has a much shorter time constant than either the conservation of mass or the conservation of energy. If the steady-state conservation of momentum equation is used instead of the transient equation, then the equations are no longer stiff. If the transient conservation of momentum equation is used, a special algorithm such as Gear's method (Gear, 1968) must be used.

2.5 Void fraction, Quality, and Refrigerant Charge Prediction

The final aspect of system modeling we shall discuss is refrigerant charge prediction which is one of the most important and challenging parts of developing a refrigeration model. In the system, refrigerant exists in three different phases, subcooled liquid, superheated vapor, and a saturated mixture of liquid and vapor. Determining the amount of charge in the liquid and vapor sections is trivial; the average density of the single-phase refrigerant is multiplied by the volume of that section. In the two-phase section, the void fraction must be used to determine the correct amount of charge.

Quality is an important variable in determining refrigerant charge in the two-phase region. The mass quality of refrigerant in a two-phase region is defined as the ratio of the vapor mass to the total mass.

$$x = \frac{m_{vapor}}{m_{total}} \tag{2.15}$$

The mass flux quality is defined as the ratio of the vapor mass flow rate to the total mass flow rate.

$$\phi = \frac{\dot{m}_{vapor}}{\dot{m}_{total}} \tag{2.16}$$

Typically the mass flux quality is also represented by the variable x. The mass quality and the mass flux quality are not necessarily equal and to avoid confusion we shall give them different symbols.

The void fraction is defined as the vapor-flow cross sectional area divided by the total area.

$$\alpha = \frac{A_{vapor}}{A_{total}} \tag{2.17}$$

Using basic algebra, we can determine that the mass quality is related to the void fraction in the following way.

$$\alpha = \frac{1}{1+\left(\frac{1-x}{x}\right)\left(\frac{\rho_g}{\rho_f}\right)} \tag{2.18}$$

In order to find the void fraction at an interface, the mass flux quality must be used. The void fraction must be used to calculate the charge in the two-phase region because the liquid and vapor refrigerant move at different velocities. The slip ratio is defined as the vapor velocity divided by the liquid velocity.

$$S = \frac{V_{vapor}}{V_{liquid}} \tag{2.19}$$

Using algebra, one can derive the following equation for void fraction.

$$\alpha = \frac{1}{1+S\left(\frac{1-\phi}{\phi}\right)\left(\frac{\rho_g}{\rho_f}\right)} \tag{2.20}$$

The simplest way to calculate the void fraction is to assume that the slip ratio is unity and the liquid and vapor refrigerant move at the same velocity. This assumption is called the homogeneous model.

$$\alpha = \frac{1}{1+\left(\frac{1-\phi}{\phi}\right)\left(\frac{\rho_g}{\rho_f}\right)} \tag{2.21}$$

Comparing Equation 2.18 to Equation 2.21, we note that the mass quality and the mass flux quality are equal when the homogeneous assumption is employed. It follows that the mass can be calculated from

$$m = \frac{Vol}{\left(x\frac{1}{\rho_g} + (1-x)\frac{1}{\rho_f}\right)}. \tag{2.22}$$

The homogeneous model is common in transient models because it greatly simplifies the calculation of mass (Ploug-Sorensen et al., 1997 and Nyers and Stoyan, 1994). The homogeneous model is inaccurate because the vapor refrigerant moves at a faster velocity than

the liquid refrigerant. As a result, the homogeneous model overpredicts the void fraction and underpredicts refrigerant mass.

Many different correlations for the void fraction exist. It is typically a function of refrigerant mass flux quality, saturation densities, and liquid and vapor viscosity. Rice (1987), Bridges and Bullard (1995), and Farzad and O'Neal (1994) summarize and compare the accuracy of various void-fraction correlations.

Several different void-fraction correlations are employed in published transient models. Mitsui (1987) uses Equation 2.20 although the specific slip ratio correlation is not specified. MacArthur and Grald (1989) utilizes the Zivi void fraction model. Yasuda et al. (1983) uses Hughmark mass flow rate dependent model and Sami et al. (1987) employs a drift flux model.

To calculate the refrigerant mass from the void fraction an average quality, α_{cv}, is determined by integrating the mass flux quality from the inlet to the outlet of the control volume. Rice (1987) provides a detailed explanation of the different assumptions which can be employed to perform this integration. Then the mass of the refrigerant in the two-phase region is then determined by

$$m = \left(\alpha_{cv}\rho_g + (1-\alpha_{cv})\rho_f\right)\text{Vol.} \tag{2.23}$$

An assumption used in the model by He et al. (1997) is a time-invariant mean void fraction assumption based on Wedekind et al. (1978). With experimental verification, Wedekind showed that the mean void fraction remains relatively constant in the two-phase region during most operation. He et al.'s model is written for controls purposes and does not capture start-up or shut-down transients where this assumption would be quite poor.

2.6 Current State of the Art

The following sections summarize the transient models available in the literature today. These sections are divided into mobile system models and other vapor compression models. Mobile system models are placed in their separate section because most transient models were designed to study the cycling losses, start-up, or shut-down of heat pumps or refrigerators. Heat pump and refrigerator systems models do not necessarily include variable compressor speed and variable air flow rates. The cycling times of these systems are longer than for mobile air-conditioners, so they operate at steady state for an extended period of time.

2.6.1 Mobile System Models

2.6.1.1 Steady-state Models

Steady-state automotive air-conditioning models were developed by Bajpai (1994) and Kyle (1993). Bajpai's model is an expert system steady-state design tool for automotive air-conditioning systems developed for General Motors Corporation. The design tool includes three components: 1) a database of vehicles and air-conditioning components, 2) a conventional numerical and thermodynamic analysis program, and 3) an air-conditioning knowledge base. The knowledge base contains several heuristic "rules of thumb" for air-conditioning design which were acquired from HVAC design engineer experts. Bajpai does not discuss the details of the model and only presents an expert systems method of determining steady-state operating conditions. This model is not compared to experimental data.

Kyle (1993) developed the Automotive Heat Pump Model (AHPM). This model is based on the Oak Ridge National Lab residential heat pump model (Fisher, 1983). The automotive model incorporates several different submodels which are unique to automotive systems such as a variable-speed, belt-driven open compressor and plate-fin evaporator. The documentation for the automotive and heat pump models provides detailed explanations of the equations and correlations used. These models provide a good starting point for the development of a transient model. The AHPM is not compared with experimental results.

2.6.1.2 Transient Models

Transient automotive models were developed by Cherng and Wu (1989) and Mitsui (1987). The Cherng and Wu refrigeration system model is fairly simple and quasi-steady-state. The main thrust of this model lies in the fact that a 3-D, finite-difference model is used to predict the vehicle cabin temperature.

Mitsui (1987) documented a transient design model for automotive air-conditioners to compare TXV control with EEV control. The heat exchanger models have multiple cells and the evaporator model includes both sensible and latent heat transfer. The compressor model is steady-state and utilizes the volumetric efficiency and the isentropic efficiency. The TXV model includes the conservation of energy between the evaporator refrigerant and feeler bulb refrigerant and uses Bernoulli's orifice equation to determine the mass flow. The compressor speed and the evaporator superheat are inputs to the EEV controller. When the compressor shuts off the expansion valve is fully closed to prevent refrigerant charge from migrating from the condenser to the evaporator. For a short period of time after the compressor turns on, the valve is opened fairly large to provide adequate mass flow into the evaporator. After that period of time, PID control is used to regulate the superheat. This control method showed

increased evaporator cooling capacity compared with TXV control immediately after start-up in both the model and experiments. This model is adequate for comparing controls algorithms; however, it cannot perform a start-up simulation from zero pressure difference in the evaporator and condenser.

2.6.2 Transient Refrigeration and Heat Pump Models

The majority of transient models available in the literature today are for refrigerators, heat pumps, and room air conditioners. These models are classified depending on their purpose: a) design, b) controls, c) energy efficiency, and d) qualitative.

2.6.2.1 Design Models

Ploug-Sorensen et al. (1997) developed a domestic refrigerator system model using a general dynamic system modeling package Sinda/Fluint. Sinda/Fluint was developed at NASA and is capable of simulating steady-state and dynamic behavior of fluid pipe networks. This simulation code contains empirical equations for single-phase and two-phase pressure drops, single-phase and two-phase heat transfer coefficients, and properties of common fluids including several refrigerants. The model developed by Ploug-Sorensen et al. (1997) consists of a multi-cell heat exchanger model and an efficiency-based compressor model. The capillary tube is modeled similarly to the heat exchangers. A clutch-cycling simulation model was compared to data, and the simulated cabinet temperature and condenser pressure agree well with data. The simulated evaporator pressure decreases much faster than the empirical evaporator pressure. This error makes it difficult to simulate clutch-cycling systems controlled by evaporator pressure.

MacArthur and Grald (1989) developed a general transient model which simulates the start-up and shut-down of a heat pump. The model simulates both open and hermetic compressors as well as the engine and the engine-speed controller. The limiting assumptions of the model are that pressure is constant in the evaporator and condenser. The model is compared to data from a 3-ton hermetic heat pump and a 2-ton open compressor heat pump during start-up. The compressor mass flow rate, condenser pressure, and evaporator pressure from the model compare well with the start-up data. The model predicts shutdown well although the reported time scale is on the order of minutes.

A dynamic model of a refrigeration system was developed by Colding et al. (1991) to compare different strategies for the condenser fan to control the condenser pressure. The speed of the condenser fan is controlled to maintain the condenser pressure at a preset value. When the fan is turned on, the heat transfer between the refrigerant and the air increases so the condenser temperature and pressure decrease. This preset pressure is optimized to minimize

overall energy consumption of the system. The model is validated with an experimental set-up using on/off control of the condenser fan. This simple model does not capture all of the transients in the refrigerant temperatures but it does capture the general trends. Colding et al. concluded that the system consumes 4% less energy using proportional control rather than on/off control of the condenser fan.

Yasuda et al. (1983) developed a dynamic model to study the hunting phenomenon of TXV systems. The models includes a complete vapor-compression system. Transient conservation equations model the refrigerant in the feeler-bulb. The model is compared yo transient data in which a step change is imposed on the static superheat. The static superheat is the temperature which causes the expansion valve to open. The model successfully simulated an increase in the static superheat. Under these conditions, the system exhibits an underdamped response and comes to a new steady-state value. When the static superheat was decreased, the experimental system began oscillating or hunting. The initial model did not capture this phenomenon. Yasuda et al. theorized that hunting is caused by liquid droplets entrained in the slightly superheated flow cause a temperature decrease in the pipe wall where the feeler bulb is located. This effect could significantly alter the control loop and cause hunting. They modeled this phenomenon by adjusting the refrigerant side heat transfer coefficient when the outlet evaporator superheat is less than 5 K. This adjusted model successfully predicted the hunting. The model only captures small perturbations from steady-state values, and it is not clear if it accurately captures the reasons for hunting.

Another dynamic model (DAHP) was developed to predict the performance of heat pumps using alternative pure refrigerants (Sami and Duong, 1991 and Sami et al., 1987). First, Sami et al. (1987) used a phase model to describe the heat exchanger which Sami and Duong (1991) changed to a multi-cell model. Sami et al. (1987) compared a quasi-steady-state model with start-up experimental data, and the general trends agreed well after the initial 10 seconds. Sami and Duong (1991) discretized the transient equations and solved them iteratively. This transient model was not compared to experimental data. Sami and Comeau (1992) and Sami and Zhou (1995) modified the above model to use nonazeotropic refrigerant mixtures. The Carnahan-Starling-DeSantis (CSD) equation of state was used to determine the properties of the mixture. The steady-state values from the model compare well with the experimental data; however, the initial transients have some differences in overshoot and time response.

Darrow et al. (1991) developed a simple model to predict the transient behavior of a water chiller. This model is appropriate for modeling systems in which the transients are controlled by the thermal mass of the components rather than the refrigerant migration. Therefore, this model only takes into account heat transfer and neglects hydrodynamic effects. The evaporator, condenser, and chiller are each treated as a single perfectly mixed zone, and

the refrigerant distribution in the system is assumed to be constant with respect to time. The three transient equations in the model are the conservation of energy for the condenser temperature, evaporator temperature, and chiller temperature. This model accurately predicts the transient temperatures of a water chiller plant after start-up. This type of model is not appropriate for modeling automotive systems because the transients associated with refrigerant migration are at least of the same magnitude (if not longer) than the transients associated with the thermal capacitance.

Several models were developed as a general transient design tool. Chen and Lin (1991) developed a dynamic simulation of a refrigerator which optimizes the combination of system components to reduce energy consumption. The model consists of transient models for the heat exchangers, compressor, and capillary tube and the general temperature trends compare well with experimental start-up data. Their start-up data begins with a large pressure differential between the condenser and the evaporator. The pressures agree well except for the initial derivative of the evaporator pressure. The goal of the optimization is to vary some parameters, such as capillary tube diameter and length, in order to reduce overall compressor power. No results from the optimal matching technique are reported.

Chi and Didion (1982) also developed transient model for heat pumps (TRPUMP) for general design purposes. The heat exchanger model is a single-cell, lumped-parameter model which uses constant coefficients for the heat transfer and pressure drop parameters. The components included in this model are the electric motor, compressor, shafts, electric fans, heat exchangers, accumulator, and thermal expansion valve. The compressor is modeled using volumetric and compression efficiencies and a heat transfer analysis. The pressure and temperature results compare well with experimental data on system start-up; however, the first start-up data point is not until 30 seconds after start-up.

2.6.2.2 Controls Models

Controls models are dynamic models used during real-time system operation for controls purposes. The models take inputs from the system (e.g., temperatures, pressures, or compressor speed) and use a model and control algorithms to compute outputs (e.g., expansion valve opening, fan speeds, or compressor speeds). These models must be computationally simple enough to provide real-time results. The following models use different methods to achieve this goal.

He et al. (1997) developed a lumped-parameter model for a heat pump or refrigeration system for multivariable control. This model was developed to control the evaporator refrigerant pressure and outlet superheat during quasi-steady-state operation. The model is not designed to capture the dynamics of start-up or shut down. The heat exchanger models use

zones or moving interfaces which accurately predicts the superheat at the exit of the evaporator. The transient model is linearized around a steady-state operating condition, and it is only valid for small deviations from this point. The condenser pressure, evaporator pressure, and evaporator superheat are predicted fairly well for step changes in the compressor speed and the expansion valve opening. The original linearized model based on conservation principles was eleventh-order; however, it was found that the system dynamics can be described by a fourth-order model. He et al. proposed to use this model with a multi-input, multi-output (MIMO) control technique using to extend the performance limits of the system.

Nyers and Stoyan (1994) document a model to control the evaporator in a heat pump. The evaporator is divided into multiple cells, and the transient conservation of mass, energy, and momentum equations are discretized over each cell. Also, the conservation of energy equation is applied to the evaporator wall and the secondary fluid which in this case is water. The models of the expansion valve, compressor, and condenser all consist of single lumped-parameter equations. The difference equations are solved for a sinusoidal condenser temperature input. The results show how the refrigerant pressure, quality, and velocity oscillate through the length of the evaporator. Improvements to the condenser, compressor, and expansion valve models are necessary before this model can be used for real-time control purposes. It is not clear if a multiple-cell heat exchanger model can be solved quickly enough to be practical for real-time controls applications.

Crawford and Shirey (1987) and Crawford and Woods (1985) developed a method for developing a purely empirical model from performance data for a heat pump system. The empirical equations correlate each model output to the model inputs. For example, the indoor air temperature is a function of outdoor air temperature, solar heat load, wind speed, and heat pump energy consumption. The coefficients for the empirical equations are obtained by gathering large amounts of data from the heat pump system during normal operation and then using a linear least-squares technique to determine the coefficients. As a result, the coefficients for the empirical model are only accurate for the specific heat pump system from which the performance data were acquired. The model requires fairly simple calculations which can be incorporated into an on-line optimal control application. The model predicts the indoor air temperature well; however, a large amount of data is needed to ensure that the empirical model is valid in all operating extremes.

2.6.2.3 Energy Efficiency Models

The main purpose of energy efficiency models is to calculate power consumption and cooling capacity of a system. Generally, these models are simpler than design models.

O'Neal and Katipaluma (1993) developed a time-constant model to determine the performance of air conditioners during cycling. A single time constant is used to correlate the capacity at start-up to the steady-state capacity. This time constant is determined for a single specific system. The time constant equation is then integrated to determine the cooling load factor (the ratio of the capacity during a given on-time divided by the capacity produced by the unit operating at steady-state) for the entire cycle. An important nondimensional time variable appears in these equations which is the fraction on time divided by the product of the time constant and the cycling rate. In comparison with experimental data, the single time constant method is shown to predict the cooling load factor fairly well.

2.6.2.4 Qualitative System Models

Qualitative system models are intended to understand the dynamics of the vapor-compression system and the effects of system parameters on these dynamics. These models are defined as qualitative because they have not been verified with experimental data.

Boeing Computer Services (BCS) developed a vapor compression library (Ginsberg, 1993) for use with its program, EASY5. EASY5 (Tollefson, 1992) is a family of software programs used to model and analyze dynamic systems. EASY5 is graphically based and allows the user to create a system by connecting icons for each of the components. One advantage of the EASY5 system is a feature called switch states. It allows the user to indicate when a discontinuity in the model occurs. For example, a discontinuity occurs when the flow switches from laminar to turbulent. Switch states allow for the code to efficiently recognize and integrate through discontinuities. BCS's vapor compression library includes zone models for the condenser and evaporator, an efficiency based compressor model, thermal expansion valve, and refrigerant pipe. It is not known how well the model performs as a design tool, but it is useful for studying the effects of the system parameters on transient behavior.

Vargas and Parise (1995) developed a simplified transient model to compare the energy consumption and room temperature variation between two heat pump control strategies. A clutch-cycling control strategy is compared to a closed loop feedback control of the compressor speed. The input to the controller is the room temperature and a power-law controller regulates the voltage to the compressor. Mass migration between the evaporator and the condenser is prevented by modeling a theoretical expansion valve which always exactly matches the compressor mass flow rate. The result of the model shows that the feedback controller conserves energy and maintains a more stable temperature.

Murphy and Goldschmidt (1984, 1985, and 1986) wrote a series of papers analyzing the transients associated with residential air-conditioner cycling. The first paper (1984) qualitatively discusses transient pressure and temperature data during cycling. They attribute

most of the cycling efficiency losses to charge migration rather than thermal capacitance. A simple model which simulates start-up transients (1985) consists of a compressor, condenser, and capillary tube. Experimental pressure and temperature data are used instead of a mathematical evaporator model. They concluded that lighter condensers and shorter capillary tubes decrease the time it takes for the capillary tube to flood and for the system to reach steady state. During shutdown (1986), the heat exchangers are modeled as tanks with inflows and outflows. The capillary tube and the pressure equalization valve in the compressor connect the condenser and evaporator tank. From this model it is concluded that if the pressure must be equalized between the condenser and evaporator after shutdown then the cycling losses are minimized when the thermal capacitance of the heat exchangers is minimized.

Gruhle and Isermann (1985) developed a model to study the hunting phenomenon of TXV systems. This model includes a fairly detailed multiple cell evaporator model but it does not include a condenser model. The opening of the TXV is a direct function of superheat. Gruhle and Isermann model captures oscillations of the liquid-dry out point for steady input conditions. They believe the fluctuations are caused by the strong nonlinear course of the heat transfer coefficient. Hunting was simulated by modeling the TXV as a proportional controller. Gruhle and Isermann concluded that replacing the TXV with an electronic expansion valve (EEV) and applying a suitable control algorithm with a lower gain can reduce hunting.

Dhar and Soedel (1979a,b) developed a general transient model for vapor compression heat pumps. A unique aspect of this model is that it includes oil migration. Most of the oil remains in the hermetic compressor. Oil exits the compressor by leaking past the piston ring and by being carried into the compressor cylinders by the suction gas. All of this oil then migrates to the accumulator. The mass flow rate of oil back to the compressor is dependent on the mass flow rate of refrigerant out of the accumulator. The heat exchangers are simulated using zone models. Each control volume is considered to behave as a stirred tank; the outlet conditions are equal to the bulk conditions within the control volume. The heat transfer is modeled using an electrical circuit analogy with thermal resistances and thermal capacitances. The model results show the trends of pressure, oil migration, and mass flow rates after start-up but it was not compared to experimental data.

2.7 Conclusions

In this chapter, we have provided an overview of mobile air-conditioners and transient system models of vapor-compression systems. Mobile air-conditioners are unique from other vapor-compression systems in their components, design criteria, objectives, and control methods. Most transient vapor compression models documented in the literature are for heat

pumps and refrigerators. Currently, no transient models exists which are capable of simulating all of the transients in a mobile air-conditioning system.

Chapter 3
Transient System Model

This chapter provides a description of the transient system model for a mobile air-conditioning system. The requirements of the model are that it must be fully transient and accurately model all phases of operation from start-up to shut-down including the subsequent charge redistribution. The model must allow for a variable-speed compressor and variable air flow rates over the heat exchangers.

Section 3.1 describes the overall organization for the model. Section 3.2 provides a brief overview of the experimental data used to verify the model. Sections 3.3-3.8 summarize the component models and Section 3.9 summarizes the steady-state and transient solution technique.

3.1 System Model Organization

Our transient model consists of the refrigerant circuit in a vapor compression refrigeration system. The system contains a compressor, condenser, orifice tube, evaporator, and accumulator (Figure 3.1). At this stage of development, only pure refrigerant is modeled but at a later date the model can be modified to include a refrigerant-oil mixture.

The system model consists of three different types of component models: (1) the heat exchanger model (Sections 3.3-3.5), (2) the compressor model (Section 3.6), and (3) the orifice tube model (Section 3.7). The accumulator model (Section 3.8) is an extension of the heat exchanger model. Each component model is designed to use enthalpy (h), pressure (P), and mass flow rate ($\dot{m}$) as inlet and outlet properties. All other refrigerant properties employed in the component models such as density (ρ), temperature (T), and velocity (V) are calculated from these three basic properties.

The thermodynamic refrigerant properties are computed from property routines summarized in Chapters 6 and 7. The transport properties for R134a are summarized in Appendix A and the dry air properties are summarized in Appendix B.

The heat exchanger model divides the refrigerant circuit into a series of constant volume cells. The conservation of mass, conservation of energy, and conservation of momentum equations are applied to each cell. During a given simulation, the number of cells and the volume of each cell remain constant. As a result, the number of equations also remains

constant. The number of cells and/or the volume of the cells can be changed between simulations in order to change the resolution of the model. For example, in a low-resolution model the evaporator can be divided into a few cells while in a high-resolution model it can be divided into ten, twenty, or more cells. The cell model does not need to be modified for start-up or shutdown and it allows for any refrigerant mass distribution in the system.

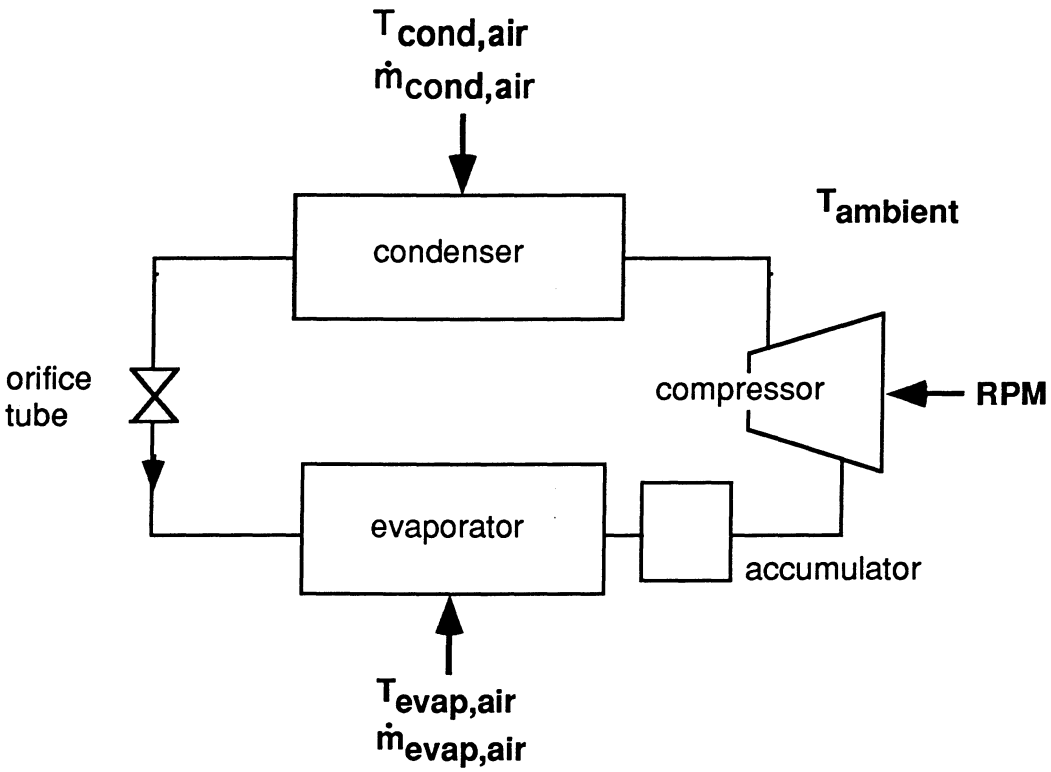

Figure 3.1 Mobile air-conditioning orifice tube system schematic.

In the system model, the refrigerant loop is divided into two series of cells as shown in Figure 3.2. The first series of cells is designated condenser cells and covers the components between the compressor and the orifice tube. The second series is designated evaporator cells and covers the portion of the loop between the orifice tube and the compressor. The compressor model and orifice tube model (which are inherently algebraic in nature) link these two groups of cells together. In Figure 3.2 the subscripts "c" and "e" refer to the condenser and evaporator cells, respectively. The additional subscript "n" designates nodal properties which are at the inlets and outlets of cells as opposed to the cell-centered properties.

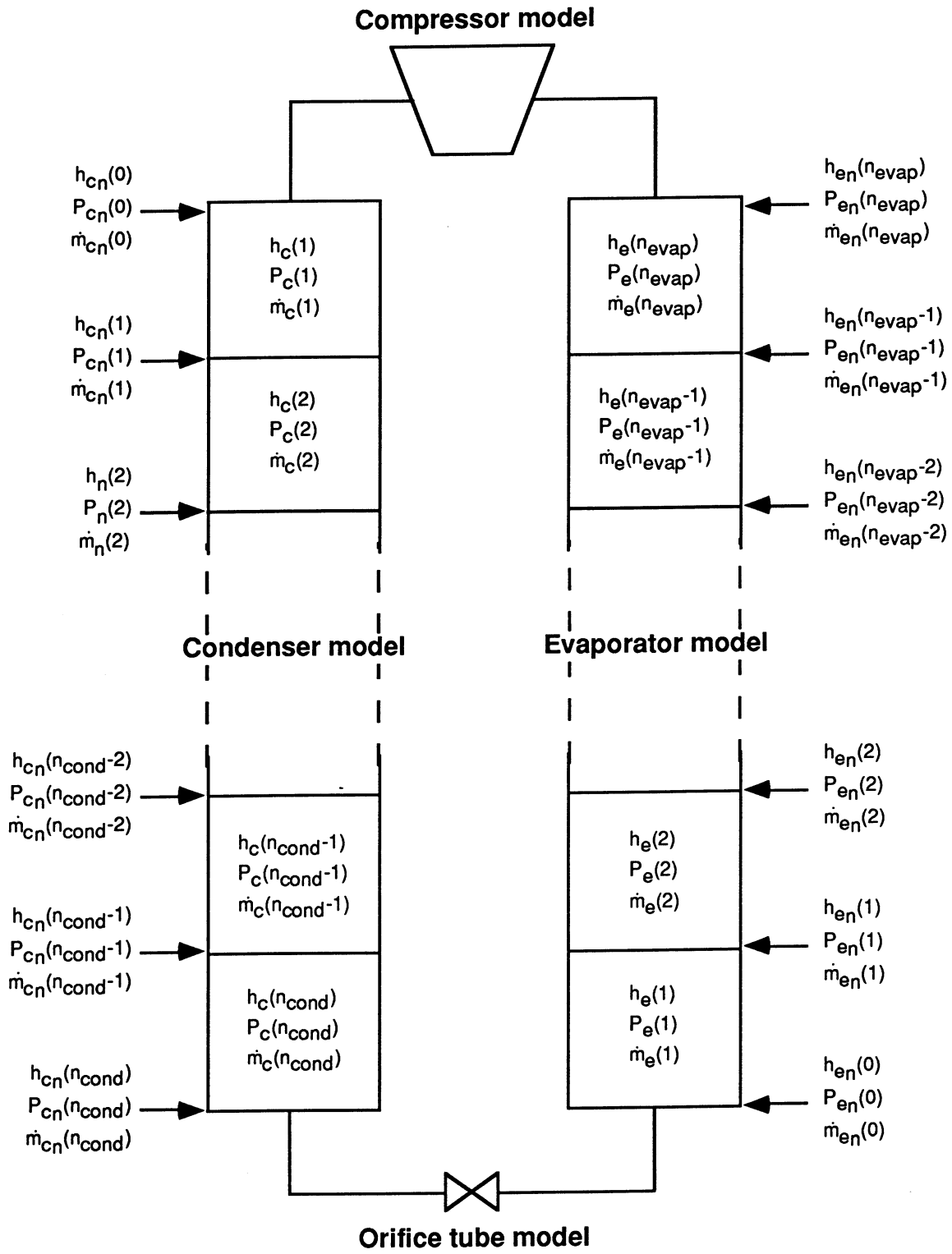

Figure 3.2 System model organization.

In our model, the evaporator is divided into six cells, and the condenser is divided into seven cells. Also, the refrigerant line between the condenser and evaporator is modeled as a single cell. This refrigerant line is included in the model because it contains subcooled refrigerant during steady-state operation and thus a large amount of the refrigerant mass.

Our model operates in three different modes: (a) as a steady-state model, (b) as a compressor-on transient model, and (c) as a compressor-off transient model. Table 3.1 lists the inputs for each of these models.

Inputs	**Steady-state**	**Transient**	
		Compressor-on	**Compressor-off**
compressor speed	single	time	time
$T_{evap,air}$	single	time	time
$T_{cond,air}$	single	time	time
$\dot{m}_{evap,air}$	single	time	time
$\dot{m}_{cond,air}$	single	time	time
$T_{ambient}$	single	time	time
m_{ref} or $T_{sub,cond}$	single		
Initial conditions (refrigerant state points)		single	single
Compressor inlet/outlet conditions			time

Table 3.1 Inputs to system models. "single" indicates that the input is needed at a single time. "time" indicates that this input is time dependent.

In Table 3.1, $T_{evap,air}$ and $\dot{m}_{evap,air}$ are the average air temperature and air mass flow rate through the evaporator. Likewise $T_{cond,air}$ and $\dot{m}_{cond,air}$ are the average air temperature and air mass flow rate through the condenser. The heat exchanger model allows for each cell to have different inputs in order to study the effects of air temperature and air mass flow rate gradients. Because all of our experimental data is well mixed, we used a single average air temperature and average mass flow rate. The ambient air temperature, $T_{ambient}$, enters the analysis through its effect on the compressor, accumulator, and refrigerant lines. In an actual automotive system, all of these components are in the engine compartment and the ambient temperature can be computed from an underhood heat transfer analysis. In our experimental

setup (Section 3.2), all of these components are surrounded by room temperature air, thus we always used a single ambient temperature in our model/data comparisons.

The outputs from the model are the refrigerant state points (enthalpy, pressure, and mass flow rate) throughout the system and the compressor power. The following sections summarize when the steady-state and transient models are used.

3.1.1 Steady-state Model

The steady-state model is a convenient alternative to the fully transient model. The equations for the steady-state model are the same as those for the transient model except that all of the time derivatives are set equal to zero. The steady-state model can be used to verify the steady-state heat transfer, pressure drop, and mass flow rate correlations for each of the components. The steady-state model can also serve as an expedient means to obtain a starting point for the transient model once the system is fully in operation. One input to the model is the refrigerant mass. It is difficult to accurately predict the refrigerant mass, and small errors in the refrigerant mass prediction can lead to large deviations in the system operating conditions. As a result, it is often more convenient to use one other state parameter as an input. We use the condenser subcooling because we can compute it very accurately.

3.1.2 Compressor-on Transient Model

This model is transient and determines the time dependent output of the system when the compressor is operating. The time dependent inputs to this model are (a) compressor speed, (b) evaporator inlet air temperature, (c) condenser inlet air temperature, (d) evaporator air mass flow rate, (e) condenser air mass flow rate, and (f) ambient temperature. The model also requires a set of refrigerant state points as initial conditions. The model can start from a cold start condition where all of the pressures are equal and all of the mass flow rates are zero. Alternatively, the steady-state model can be used to obtain initial conditions for the transient model to bypass the start-up condition. The model equations form a closed loop around the system.

3.1.3 Compressor-off Transient Model

During shutdown, the clutch is disengaged and the compressor ramps down to zero. The compressor-off model is used once the compressor speed equals zero. As a result, this model is primarily used to study the pressure equalization and refrigerant mass migration after compressor shutdown. It can be used during both clutch-cycling and final compressor shutdown. When the compressor is off, it acts as a closed valve so the refrigerant no longer flows in a complete loop. Rather it redistributes itself through the orifice tube and eventually

come to a steady-state condition where all of the refrigerant pressures in the system are equal and the mass flow rates are zero.

This model is different than the compressor-on model because the system equations no longer form a closed loop. Because the temperatures and pressure at either side of the compressor become decoupled, additional inputs are required. The outlet compressor temperature is specified to simulate the cooling of the refrigerant between the compressor and condenser. Also the inlet and outlet compressor mass flow rates are set to zero. These inputs are summarized with the compressor model in Section 3.6. The heat exchanger, orifice tube, and accumulator equations are the same for the compressor-on model and the compressor-off model.

3.2 Experimental Data for Model Validation

The experimental data used for the model validation were obtained from a test facility specifically designed to test mobile air-conditioners developed in the Air Conditioning and Refrigeration Center (ACRC) at the University of Illinois at Urbana-Champaign. The compressor speed and the air flow through the heat exchangers are controlled by variable-speed motors. The inlet air temperatures to the evaporator and condenser and the humidity addition to the evaporator are also controlled. The test facility was developed by Weston (1996) and Rubio-Quero (1995). Collins (1996), Wandell (1997), and Whitchurch (1997) made further modifications to the test facility.

All of the tests were performed on a Ford Crown Victoria air conditioning system with R134a refrigerant. Figure 3.3 provides a schematic of the measurements taken in the test facility. The refrigerant temperature and pressure are measured at every state point in the facility. The refrigerant mass flow rate is measured with a Micro Motion™ flow meter at the exit of the condenser. This flow meter only gives accurate measurements for single-phase liquid or vapor refrigerant. The air flow rates are measured with venturi flow meters. The air temperatures are measured at the inlet and outlet of the heat exchangers with a grid of thermocouples. Inlet and outlet humidity levels are measured in the evaporator and a single humidity measurement is in the condenser air loop. The experimental data from the test facility were validated by Rubio-Quero. The air and refrigerant capacity agree within 10% for the condenser and 10% for the evaporator for dry-evaporator data.

Oil is circulating with the refrigerant and provides lubrication to the compressor. A real-time oil concentration sensor is installed in the liquid line between the condenser and the orifice tube. Wandell (1997) reported that between 2% and 10% oil is circulating in the refrigerant loop.

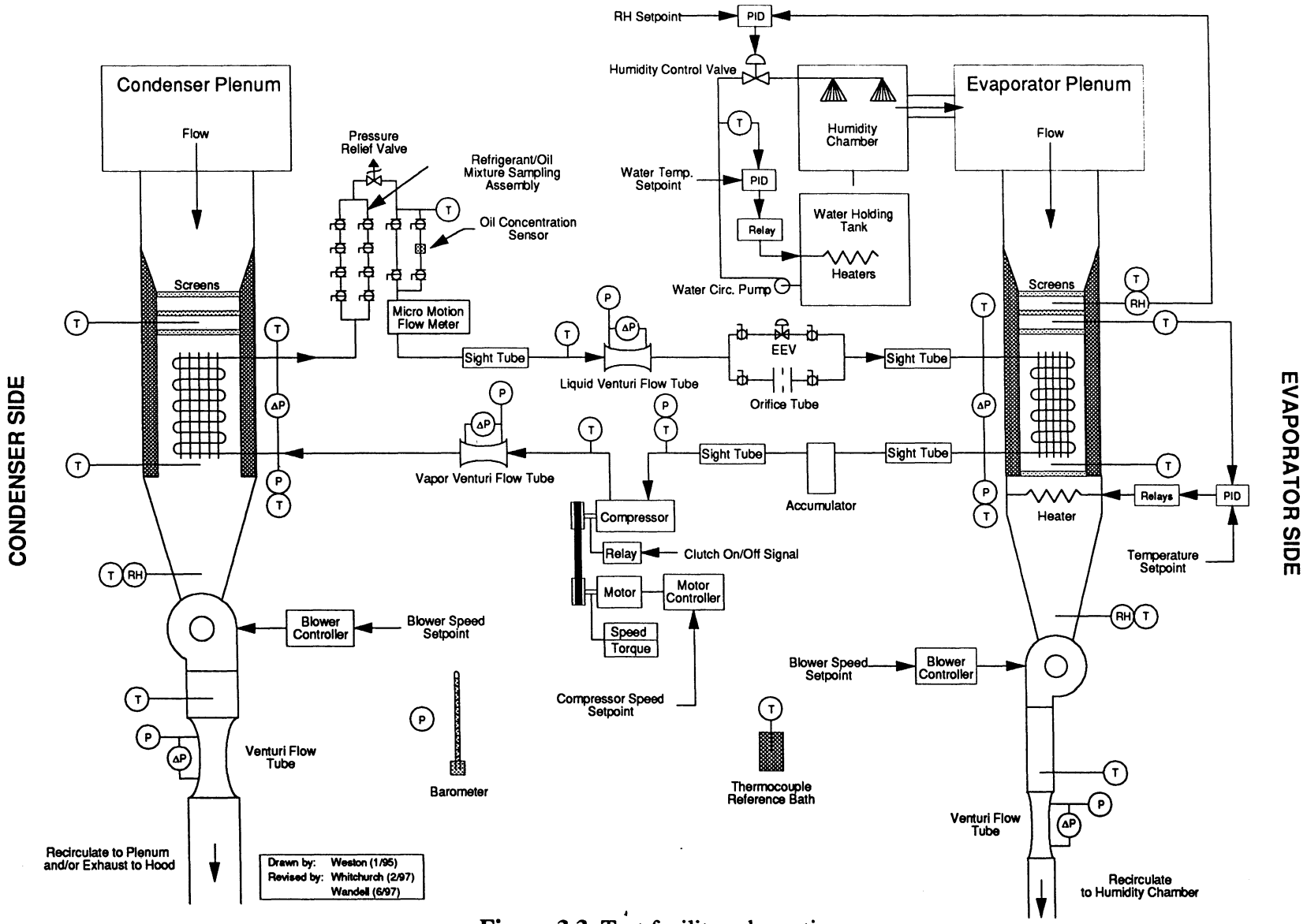

Figure 3.3 Test facility schematic.

In the remainder of this chapter , the components models are validated with steady-state data. Different steady-state data sets were obtained by Rubio-Quero, Collins, and myself, Hemami (Table 3.2). Minor modifications were made to the test facility between each data set. The most obvious differences between the data sets were that different sized orifice tubes and different amount of refrigerant were used in the system.

Data set	Date	Orifice tube	Refrigerant mass
Rubio-Quero	Spring 1995	brown	1.02 kg (2.25 lb.)
Collins	Winter 1996	green	1.34 kg (2.95 lb.)
Hemami	Summer 1997	orange	1.34 kg (2.95 lb.)

Table 3.2 Steady-state data used to validate the model.

3.3 Heat Exchanger Models

The following heat exchanger model is used for the evaporator, condenser, and all modeled refrigerant lines. This section summarizes equations in the heat exchanger model while Section 3.4 and Section 3.5 summarize the correlations for the evaporator and condenser, respectively.

3.3.1 Heat Exchanger Equations

A control volume approach is used to model the heat exchangers (Section 2.3.1.1). The primary assumptions in this model are (a) the volume of each cell is constant, (b) the refrigerant flow is one-dimensional along the tube axis, (c) energy and mass transfer only occur by convection, and (d) pure refrigerant is flowing in the tubes.

Recall from Equation 2.6, the conservation of mass principle is written as

$$\frac{dm}{dt} = \dot{m}_{in} - \dot{m}_{out}, \tag{3.1}$$

where m is the refrigerant mass and $\dot{m}$ is the refrigerant mass flow rate.

Recall from Equation 2.7 the conservation of momentum is expressed as

$$\frac{d(mV)}{dt} = \dot{m}_{in}V_{in} - \dot{m}_{out}V_{out} + mg\cos\theta + (P_{in} - P_{out})A_{cs} + F_{fric}Vol. \tag{3.2}$$

V is the average scalar velocity in the x direction which is down the length of the refrigerant tube. P is the pressure, and the friction loss per unit volume is F_{fric}. In writing the momentum equation, $F_{fric}Vol$ is replaced by

$$F_{fric}Vol = (\Delta P_{fric} + \Delta P_{minor})A_{cs} \tag{3.3}$$

where

$$\Delta P_{fric} = \frac{L}{D} f \frac{1}{2} \rho V^2 \tag{3.4}$$

and

$$\Delta P_{minor} = K \frac{1}{2} \rho V^2. \tag{3.5}$$

We neglect the effects of gravity in Equation 3.2 because elevation differences are small. We also neglect the transient terms in the conservation of momentum equation because the time constant associated with the changes in the redistribution of momentum is much smaller than for mass or energy. Including the full transient form of the conservation of momentum equation makes the resulting system of equations stiff.

Combining the above assumptions and definitions results in the final form of the conservation of momentum equation.

$$0 = \dot{m}_{in} V_{in} - \dot{m}_{out} V_{out} + (P_{in} - P_{out} - \Delta P_{fric} - \Delta P_{minor})A_{cs} \tag{3.6}$$

The conservation of energy equation for the heat exchanger is

$$\frac{d\left[m\left(u + \frac{V^2}{2} + gz\right)\right]}{dt} = \dot{m}_{in}\left(h_{in} + \frac{V_{in}^2}{2} + gz_{in}\right) - \dot{m}_{out}\left(h_{out} + \frac{V_{out}^2}{2} + gz_{out}\right) + \dot{Q}_{ref} \tag{3.7}$$

Because changes in kinetic ($V^2/2$) and potential energy (gz) are small we may neglect these terms and use the simplified form

$$\frac{d(mu)}{dt} = \dot{m}_{in}h_{in} - \dot{m}_{out}h_{out} + \dot{Q}_{ref}. \tag{3.8}$$

The heat transfer between the heat exchanger wall and the refrigerant is

$$\dot{Q}_{ref} = h_{ref}A_{inside}(T_{wall} - T_{ref}). \tag{3.9}$$

The conservation of energy equation for the heat exchanger wall is

$$c_{p,wall}m_{wall}\frac{dT_{wall}}{dt} = \dot{Q}_{air} - \dot{Q}_{ref} \tag{3.10}$$

where

$$\dot{Q}_{air} = h_{air}A_{outside}(T_{air} - T_{wall}). \tag{3.11}$$

$A_{outside}$ is the effective external surface area accounting for fin effects.

Equation 3.10 is necessary when the thermal capacitance of the heat exchanger wall is important. This occurs primarily during start-up and shutdown. When the compressor has been operating continuously, the heat exchanger remains at a relatively constant temperature, and Equation 3.10 is not required. Under quasi-steady conditions, all of the heat transfer coefficients between the refrigerant and the air can be lumped into one overall parameter governing heat transfer between the refrigerant and the air.

$$UA = \frac{1}{R_{tot}} = \frac{1}{R_{ref} + R_{wall} + R_{air}} \tag{3.12}$$

Equation 3.8 becomes

$$\frac{d(mu)}{dt} = \dot{m}_{in}h_{in} - \dot{m}_{out}h_{out} + \dot{Q} \tag{3.13}$$

where

$$\dot{Q} = UA(T_{air} - T_{ref}). \tag{3.14}$$

In the steady-state model, the time derivatives are set to zero.

$$0 = \dot{m}_{in} - \dot{m}_{out} \tag{3.15}$$

$$0 = \dot{m}_{in}V_{in} - \dot{m}_{out}V_{out} + (P_{in} - P_{out} - \Delta P_{fric} - \Delta P_{minor})A_{cs} \tag{3.16}$$

$$0 = \dot{m}_{in}h_{in} - \dot{m}_{out}h_{out} + \dot{Q} \tag{3.17}$$

3.3.2 Determining the State Variables

Equation 3.1, 3.6, and 3.8 model the refrigerant flow in the heat exchanger. From these equations, we can solve for three variables which describe the state of the refrigerant. Two of the variables define the thermodynamic state of the refrigerant, and the third variable defines the velocity of the refrigerant.

The conservation equations are applied to constant volume cells. As a result we can bring the cell volume out of the time derivative.

$$\frac{dm}{dt} = Vol\frac{d\rho}{dt} \tag{3.18}$$

$$\frac{d(mu)}{dt} = Vol\frac{d(\rho u)}{dt} \tag{3.19}$$

From the above equations, it appears that the obvious choice for the state variable is density (ρ) and internal energy (u). When density is used as a state variable, a problem occurs in the liquid region. The liquid refrigerant is basically incompressible. A small error in the density can result in a very large error in the pressure. This effect can cause large problems in the transient solution when a cell switches from the two-phase to the liquid region.

Because of the above problems, we use pressure and enthalpy as the state variables. We chose to use mass flow rate instead of velocity as the third state variable. The mass flow rate is constant through the system during steady-state operation. Because of the variations of density

and cross sectional area throughout the system, the refrigerant velocity will vary over several orders of magnitude.

The transient solver predicts enthalpy and pressure as a function of time. We must be able to relate the time derivatives of enthalpy and pressure to the derivatives listed in Equations 3.18 and 3.19. We use the chain rule to calculate the time derivative of density.

$$\frac{d\rho}{dt} = \frac{\partial\rho}{\partial h}\frac{dh}{dt} + \frac{\partial\rho}{\partial P}\frac{dP}{dt} \tag{3.20}$$

In Equation 3.19, we replace internal energy, u, with the definition for enthalpy ($h = u + P/\rho$) and then simplify the derivative to obtain the final form for the time derivative in the conservation of energy.

$$\frac{d(mu)}{dt} = Vol\left[\frac{d(\rho h - P)}{dt}\right] = Vol\left[\rho\frac{dh}{dt} + h\frac{d\rho}{dt} - \frac{dP}{dt}\right] \tag{3.21}$$

The conservation of mass equation and the conservation of energy equation become

$$Vol\left[\frac{\partial\rho}{\partial h}\frac{dh}{dt} + \frac{\partial\rho}{\partial P}\frac{dP}{dt}\right] = \dot{m}_{in} - \dot{m}_{out} \tag{3.22}$$

and

$$Vol\left[\rho\frac{dh}{dt} + h\left(\frac{\partial\rho}{\partial h}\frac{dh}{dt} + \frac{\partial\rho}{\partial P}\frac{dP}{dt}\right) - \frac{dP}{dt}\right] = \dot{m}_{in}h_{in} - \dot{m}_{out}h_{out} + \dot{Q}_{ref} \tag{3.23}$$

3.3.3 Relating Cell Properties to the Inlet and Outlet Properties

The state variables, enthalpy, pressure, and mass flow rate, are the average properties in the refrigerant cell. We can directly compute other average cell properties such as T_{ref} in Equation 3.9 and ρ and V in Equations 3.4 and 3.5. We also need the inlet and outlet properties for each cell, so we must be able to relate these average cell properties to the inlet and outlet properties also used in the equations.

We use the upwind scheme to determine the enthalpy at the outlet of the cell.

$$h_{out} = h_{cell} \tag{3.24}$$

A similar scheme is used by Vargas and Parise (1995), Ginsberg (1993), MacArthur and Grald (1989), and Chi and Didion (1982).

3.4 Condenser Model

The equations for the steady-state (Equations 3.15-3.17) and transient (Equations 3.1, 3.6, 3.8, and 3.10) condenser model are summarized in Section 3.3. This section documents and validates the correlations for heat transfer and pressure drop due to friction and minor losses.

We modeled a Ford Crown Victoria condenser. It is a fin-tube heat exchanger and is made of an aluminum alloy. Figure 3.4 illustrates the general circuiting of the condenser refrigerant tubes. Here, the air flow is into the page. For the sake of discussion, we call the side where the air flow enters the heat exchanger the front, and the side where the air flow leaves the heat exchanger the rear. Two manifolds run down the left edge of the condenser, one manifold on the front side and one manifold on the rear side. Refrigerant enters the top of the manifold on the backside. The manifold feeds several round tubes in the first pass of the heat exchanger. Refrigerant flows across the back of the heat exchanger and then across the front as shown in Figure 3.4. The manifold on the front of the heat exchanger feeds the second pass. The refrigerant flows through the second pass and enters the back manifold. This manifold then feeds the third pass. From the third pass, the refrigerant enters the front manifold and then exists the condenser. At the entrance of the heat exchanger, the refrigerant is typically vapor and the passes have more tubes than at the exit of the heat exchanger where the refrigerant is typically liquid. The geometry calculations are summarized in Appendix C.

The schematic of Figure 3.4 is slightly different than the actual geometry of the Ford Crown Victoria condenser. In the actual condenser there are seven passes. Because we define each pass to be a single cell, the condenser is modeled using seven cells. Each cell has the same length of refrigerant tube but contains a different number of tubes. As a result, each cell has a different cross sectional area and a different volume. Treating the condenser in this manner implicitly assumes a perfect refrigerant distribution between the tubes in each pass.

3.4.1 Heat Transfer Correlations

Equation 3.12 determines the overall heat transfer coefficient for each cell of the heat exchanger. In the condenser model, the heat transfer coefficient through the refrigerant wall is

neglected. Only the air heat transfer coefficient and the refrigerant heat transfer coefficient are needed.

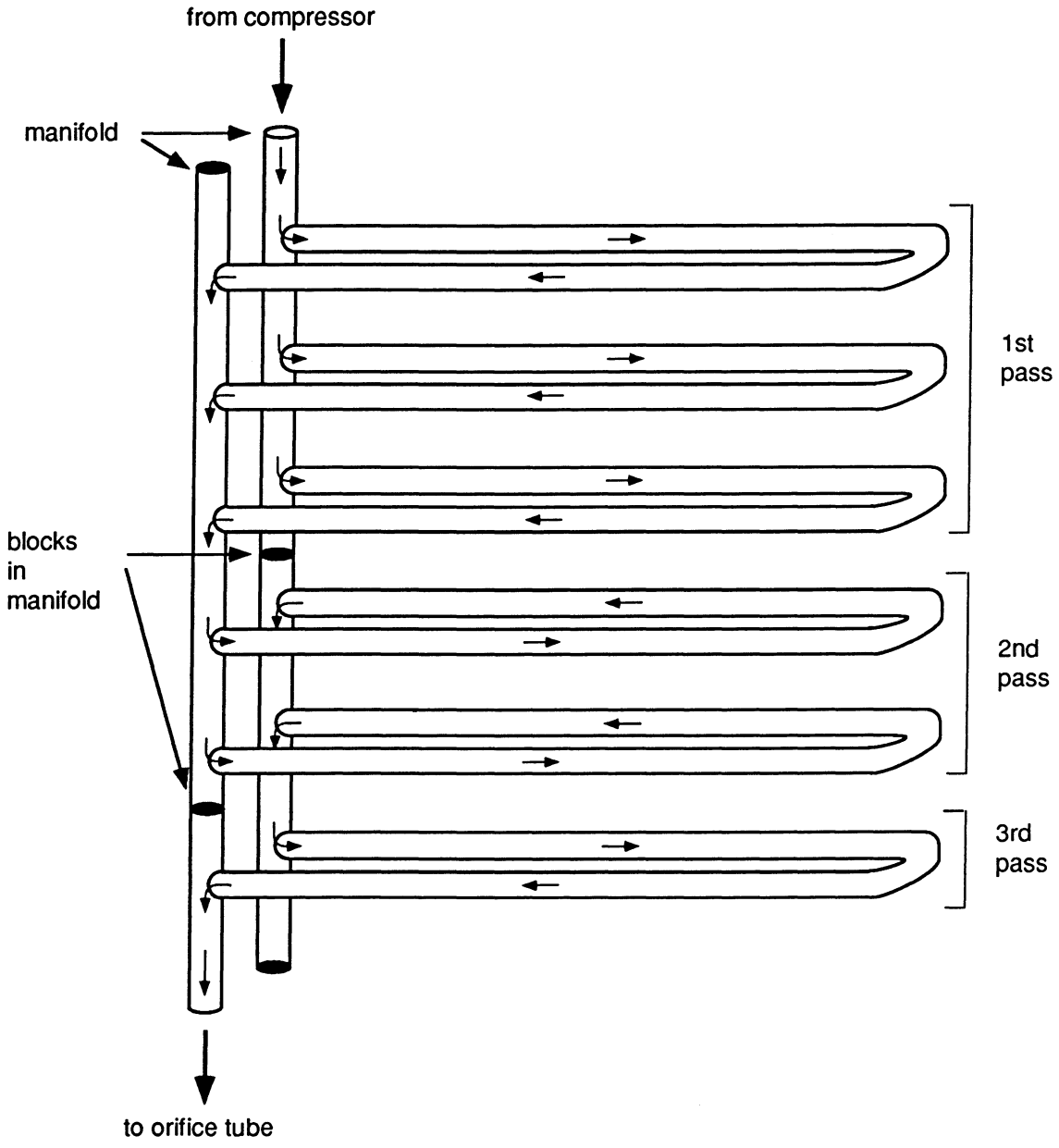

Figure 3.4 Illustration of refrigerant tube arrangement in the condenser. Air flow direction is into the page.

Vapor, liquid, and superheated vapor heat transfer correlations are needed for the refrigerant. These correlations were first used in the ACRC room air conditioner model RACMOD (Hahn, 1991). The heat transfer coefficient for the vapor is determined by the Hiller and Glicksman (1976) correlation and is based on circular tube data from Kays and London (1984).

$$h_{vapor} = c_1 c_p G Pr^{-2/3} Re_D^{c_2} \tag{3.25}$$

where

$$\begin{aligned} Re_D < Re_{lam} \quad & c_1 = 1.10647 \\ & c_2 = -0.78992 \\ Re_{lam} \le Re_D < Re_{tur} \quad & c_1 = 3.5194 \times 10^{-7} \\ & c_2 = 1.03804 \\ Re_D \ge Re_{tur} \quad & c_1 = 0.01080 \\ & c_2 = -0.13750 \end{aligned}$$

As noted by the Reynolds number range, this correlation is valid for laminar, turbulent, and transitional flow. The limits defined by Hiller and Glicksman is Re_{lam}= 3500 and Re_{tur}= 6000. We modified this limits to Re_{lam}= 3585 and Re_{tur}= 6560 to prevent discontinuities in the equations.

The liquid heat transfer correlation is the Dittus-Boelter equation (1930).

$$h_{liquid} = 0.023 \frac{k}{D} Re_D^{0.8} Pr^{0.3} \tag{3.26}$$

The two-phase flow correlation is from Dobson et al. (1994).

$$h_{two-phase} = 0.023 \frac{k_l}{D} Re_l^{0.8} Pr_l^{0.4} \left(1 + \frac{2.22}{X_{tt}^{0.889}}\right) \tag{3.27}$$

The Lockhart-Martinelli correlation for turbulent liquid and vapor flow, X_{tt}, is defined as

$$X_{tt} = \left(\frac{\rho_v}{\rho_l}\right)^{0.5}\left(\frac{\mu_l}{\mu_v}\right)^{0.1}\left(\frac{1-x}{x}\right)^{0.9}. \tag{3.28}$$

In our model, we use the simplified form of this curve fit determined by Jung and Radermacher (1989).

$$X_{tt} = 0.551\frac{P}{P_{crit}}\left(\frac{1-x}{x}\right)^{0.9} \tag{3.29}$$

The two-phase correlation (Equation 3.29) is only valid for annular flow. Dobson also provides a correlation for wavy flow but for this specific geometry and conditions the wavy flow equation is only valid if the mass flow rate is less than 0.001 kg/s. This mass flow rate is approximately ten times smaller than any mass flow rate occurring during steady-state conditions.

When the refrigerant is saturated liquid (x = 0) the two-phase correlation (Equation 3.25) does not exactly equal the liquid correlation (Equation 3.24). To prevent discontinuities in the equations, the liquid and two-phase correlations are weighted between x = 0.05 and x = 0.

$$\frac{h_{ref} - h_{liquid}}{h_{two-phase}(x=0.5) - h_{liquid}} = \frac{x}{0.5} \tag{3.30}$$

Similarly, the vapor (Equation 3.23) and two-phase (Equation 3.25) correlations are weighted between x = 0.95 and x = 1.

The heat transfer coefficient for the air side is determined from a plain fin correlation (Gray and Webb, 1986). The j-factor is determined from the following equations.

$$R_{factor} = 0.991\left[2.24\ Re_{D_{eff}}{}^{-0.092}\left(\frac{N}{4}\right)^{-0.031}\right]^{0.607(4-N)} \tag{3.31}$$

$$j = 0.14\, Re_{Deff}^{-0.328} \left(\frac{S_T}{S_L}\right)^{-0.502} \left(\frac{\delta}{D_{eff}}\right)^{0.0312} R_{factor} \tag{3.32}$$

where

$D_{eff} = D_{out} + 2t_{fin}$,

D_{out} = outer diameter,

t_{fin} = fin thickness,

N = number of tubes in air flow directon,

S_T = tube spacing transverse to air flow direction,

S_L = tube spacing in air flow direction, and

δ = fin spacing.

The heat transfer coefficient is then

$$h_{air} = G_{air}\, c_p\, Pr^{(2/3)}\, j\,. \tag{3.33}$$

The UA value is given by

$$UA_{cond} = \frac{1}{R_{ref} + R_{air}} = \frac{1}{\dfrac{1}{\eta_{surf} h_{air} A_{outside}} + \dfrac{1}{h_{ref} A_{inside}}}. \tag{3.34}$$

The equations for the surface efficiency, η_{surf}, are summarized in Appendix C.

3.4.2 Pressure Drop Correlations

Both friction and minor losses play an important role in predicting the pressure drop in the condenser. Frictional pressure drops occur both in the refrigerant tubes and the manifolds. Minor losses occur at the entrance and exit of the tubes, at the entrance and exit of the manifolds, and at the return bends. It is difficult to analytically determine the pressure drops for each of these factors, especially for two-phase flow.

We have developed an empirical equation to calculate pressure drop through the condenser. In the empirical equation, pressure is in Pascal (Pa) and mass flow rate is in kilograms per second (kg/s).

$$\Delta P_{fric} + \Delta P_{minor} = \left(-14088 + 2.4652 \times 10^6 \dot{m}\right) \frac{L_{cell}}{L_{tot}} \qquad \text{for } 0.01 < \dot{m} < 0.045 \quad (3.35)$$

$$\Delta P_{fric} + \Delta P_{minor} = 10564 \frac{\dot{m}}{0.01} \frac{L_{cell}}{L_{tot}} \qquad \text{for } \dot{m} \leq 0.01 \quad (3.36)$$

3.4.3 Steady-state Condenser Model Validation

The condenser model was validated with data from Rubio-Quero, Collins, and Hemami. Figure 3.5 show a comparison of the experimental capacity with the predicted capacity. The model agrees within 5% of the data. It is important to have a good capacity prediction to accurately predict outlet subcooling (Figure 3.6). The model predicts the subcooling within 6 K.

Figure 3.7 shows the pressure drop validation. The predicted pressure drop agrees within 20% of the experimental data. At the maximum pressure drop of approximately 90 kPa, a 20% error is 18 kPa or 2.6 psi. In the steady-state experimental data sets, the average condenser pressure is 1020 kPa (148 psi). 18 kPa is less than 2 percent of 1020 kPa which is negligible.

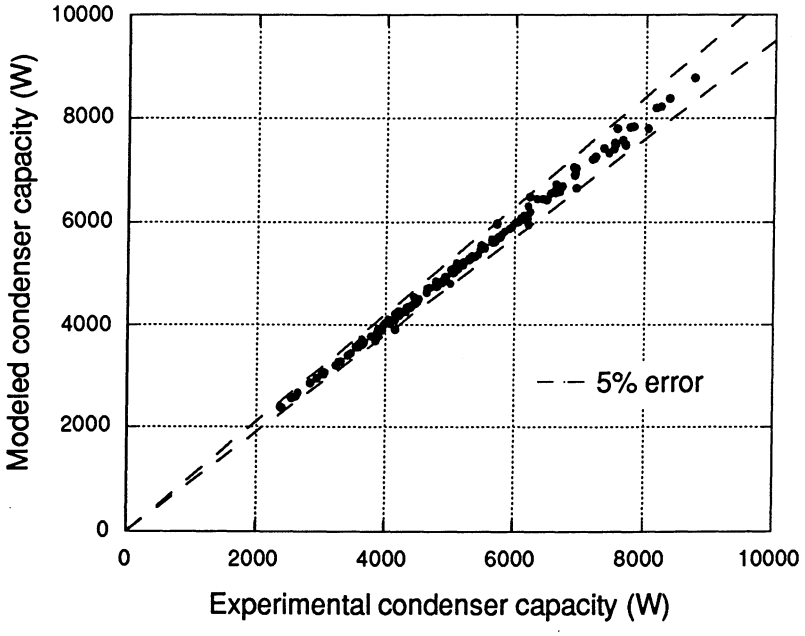

Figure 3.5 Comparison between experimental condenser capacity and modeled condenser capacity.

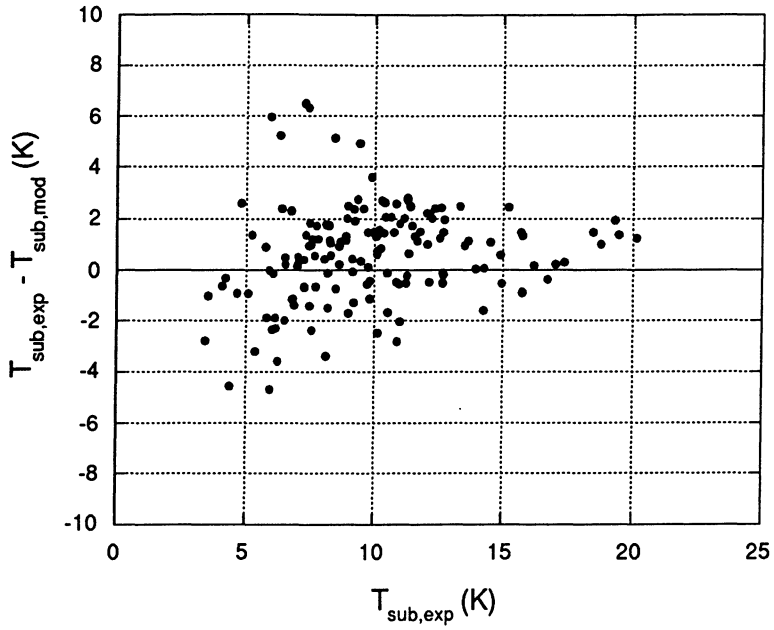

Figure 3.6 Error in condenser outlet subcooling prediction.

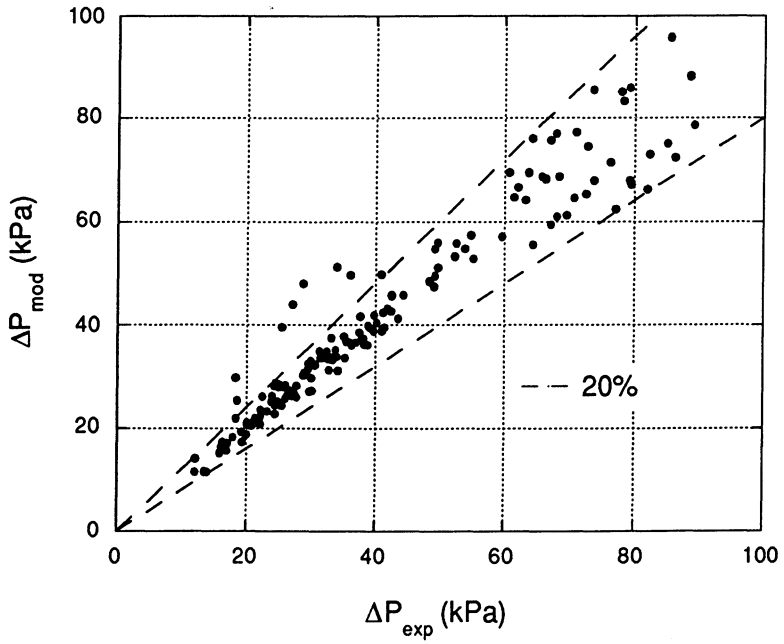

Figure 3.7 Comparison between experimental condenser pressure drop and modeled condenser pressure drop.

3.5 Evaporator Model

This section summarizes the correlations for the heat transfer coefficients and pressure drop parameters for the evaporator. The equations for the evaporator are documented in Section 3.3.

Plate-fin evaporators are typically used in mobile air-conditioners. They are constructed as a sandwich of flat plates with fins inbetween the plates. The refrigerant and air are carried between alternate pairs of plates in crossflow.

The specific plate-fin evaporator we modeled is designed for the Ford Crown Victoria. Figure 3.8 illustrates the general refrigerant circuiting of the heat exchanger. The refrigerant

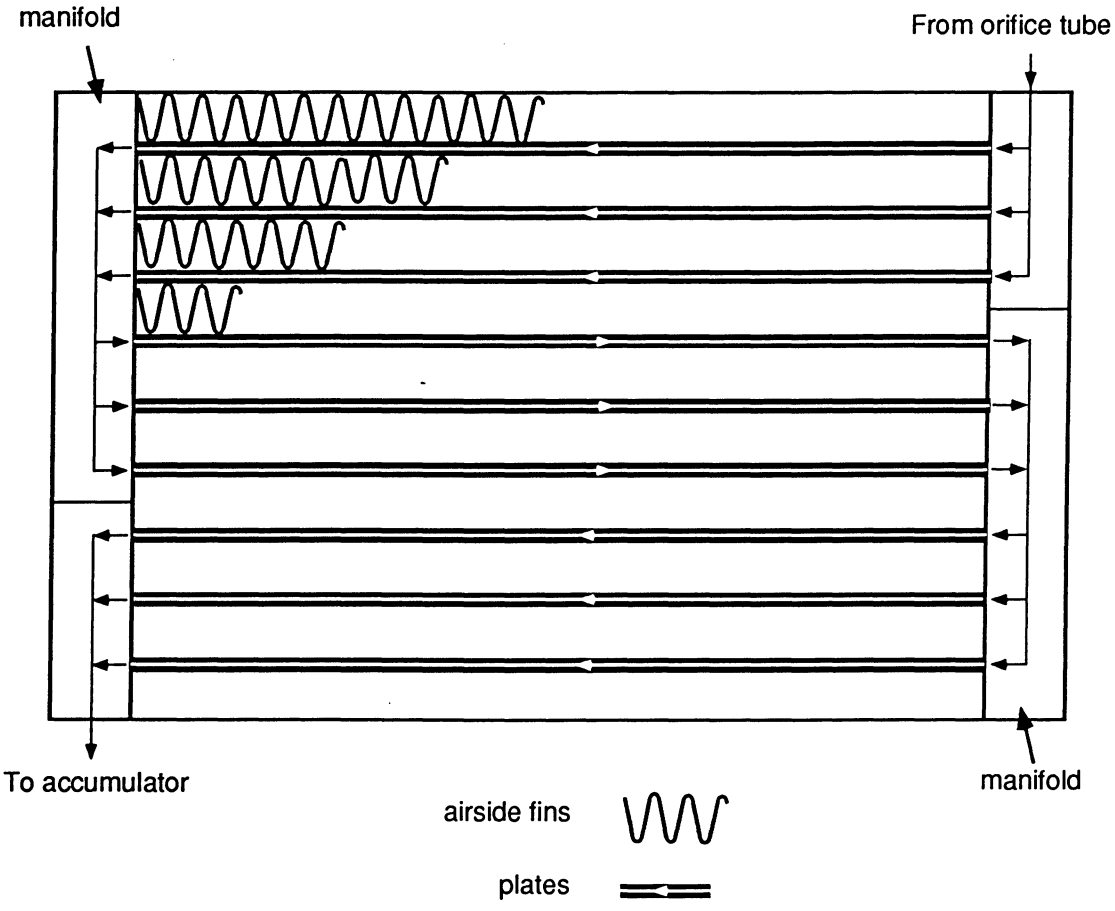

Figure 3.8 Illustration of refrigerant circuiting in the evaporator. Air flow is into the plane of the page.

enters a manifold on one side of the evaporator which feeds the first pass. The refrigerant flows across the length of the heat exchanger into the second manifold. This manifold then feeds the next pass. Each plate spans the length and width of the evaporator. The Ford Crown Victoria evaporator has three passes and each pass has approximately the same number of plates. Each of the passes is divided into two cells resulting in a total of six cells.

3.5.1 Heat Transfer Correlations

In the plate-fin evaporator, both the plates and fins are augmented to increase heat transfer. The heat transfer correlations are specifically dependent on the geometry of the augmentation. The refrigerant, wall, and air heat transfer coefficients are included in the overall heat transfer coefficient. The air and refrigerant geometry calculations are given in Appendix C.

3.5.1.1 Refrigerant Heat Transfer Correlations

During steady-state operation the refrigerant is either two-phase or superheated vapor. After compressor shutdown, the refrigerant can become pure liquid during certain situations. The liquid heat transfer coefficient is simply modeled by determining the saturated liquid (x = 0) heat transfer coefficient from the two-phase model.

Heat transfer in the refrigerant plates is enhanced by fins. The geometry of the fins resembles elongated dimples (Figure 3.9). No literature documenting the heat transfer coefficient for this specific geometry could be found; therefore, the fins are modeled as the similar serrated fin geometry (Figure 3.9). The heat transfer coefficient for the serrated fin single-phase refrigerant is from Robertson and Lovegrove (1983).

$$h_{vapor} = 0.2106 \frac{k}{D_H} Re_{D_H}^{0.62} Pr^{(1/3)} \tag{3.37}$$

The two-phase heat transfer coefficient is based from Kandlikar (1991) and can be modified for different types of plate-fins augmentations. The two-phase heat transfer coefficient is the larger of either the nucleate boiling (NB) or convective boiling (CB) heat transfer coefficient.

$$h_{two-phase} = \text{larger of} \begin{cases} h_{NB} \\ h_{CB} \end{cases} \tag{3.38}$$

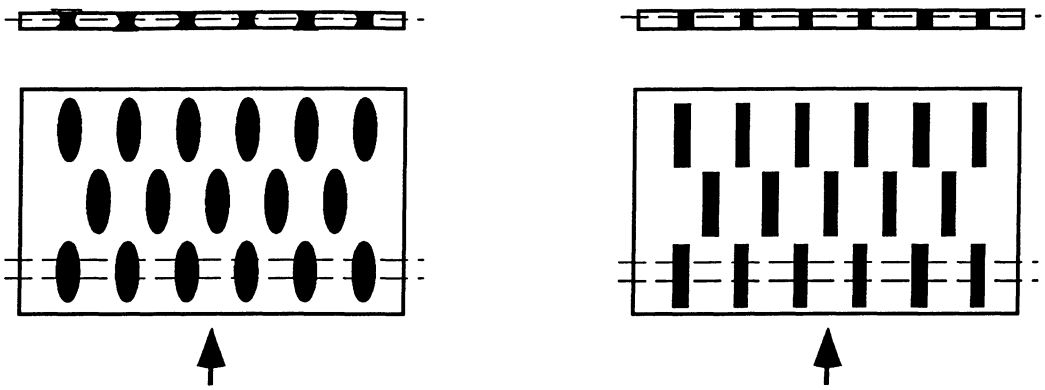

Figure 3.9 Comparison of actual evaporator plate geometry with modeled plate geometry.

These heat transfer coefficients are determined as follows.

$$h_{NB} = 0.6683\,Co^{-0.2}(1-x)^{0.8}h_{lo}E_{CB} + 1058\,Bo^{0.7}(1-x)^{0.8}F_{fl}h_{lo}E_{NB} \qquad (3.39)$$

$$h_{CB} = 1.136\,Co^{-0.9}(1-x)^{0.8}h_{lo}E_{CB} + 667.2\,Bo^{0.7}(1-x)^{0.8}F_{fl}h_{lo}E_{NB} \qquad (3.40)$$

F_{fl} is a fluid dependent parameter that is equal to 1.63 for R134a. The convection number, Co, is

$$Co = \left(\frac{\rho_g}{\rho_f}\right)^{0.5}\left(\frac{1-x}{x}\right)^{0.8}. \qquad (3.41)$$

The boiling number, Bo, is

$$Bo = \frac{\dot{Q}/A_{cs}}{G\,h_{fg}}. \qquad (3.42)$$

$\dot{Q}$ is determined from Equation 3.9 and is not known until the heat transfer coefficient is calculated. In order to avoid an iterative solution for the heat transfer coefficient, the boiling number is approximated by

$$Bo = \frac{h_{in} - h_{out}}{h_{fg}} \tag{3.43}$$

h_{in} and h_{out} refer to the inlet refrigerant enthalpy and the outlet refrigerant enthalpy to the cell, respectively. This approximation is exactly correct for steady-state flow.

E_{CB} is the augmentation factor for convective boiling and E_{NB} is the augmentation factor for nucleate boiling. For the fin geometry documented by Robertson and Lovegrove, Kandlikar determined that $E_{CB} = 1.20$ and $E_{NB} = 0.77$. The liquid correlation for heat transfer coefficient is from Robertson and Lovegrove (1983).

$$h_{lo} = 0.2106 \frac{k_l}{D_H} Re_{lo}^{0.62} Pr_l^{(1/3)} \tag{3.44}$$

3.5.1.2 Air-side Heat Transfer Correlations

The air-side fins are similar to louvered fins except that they are parallel to the flow rather than angled to the flow. The fins are actually more similar to offset-strip fins (Figure 3.10).

The air-side heat transfer coefficient is modeled with an offset-strip correlation from Manglik and Bergles (1995). This correlation is valid in laminar, turbulent, and transition region. The equations for the j factor are

$$j = c_1 Re_{D_h} \left(1 + c_2 Re_{D_h}^{1.34}\right)^{0.1} \tag{3.45}$$

where

$$c_1 = 0.6522 \alpha_{fin}^{-0.1856} \delta_{fin}^{3.767} \gamma_{fin}^{-0.2659} \tag{3.46}$$

$$c_2 = 5.259 \times 10^{-5} \alpha_{fin}^{0.504} \delta_{fin}^{0.456} \gamma_{fin}^{-1.055} \tag{3.47}$$

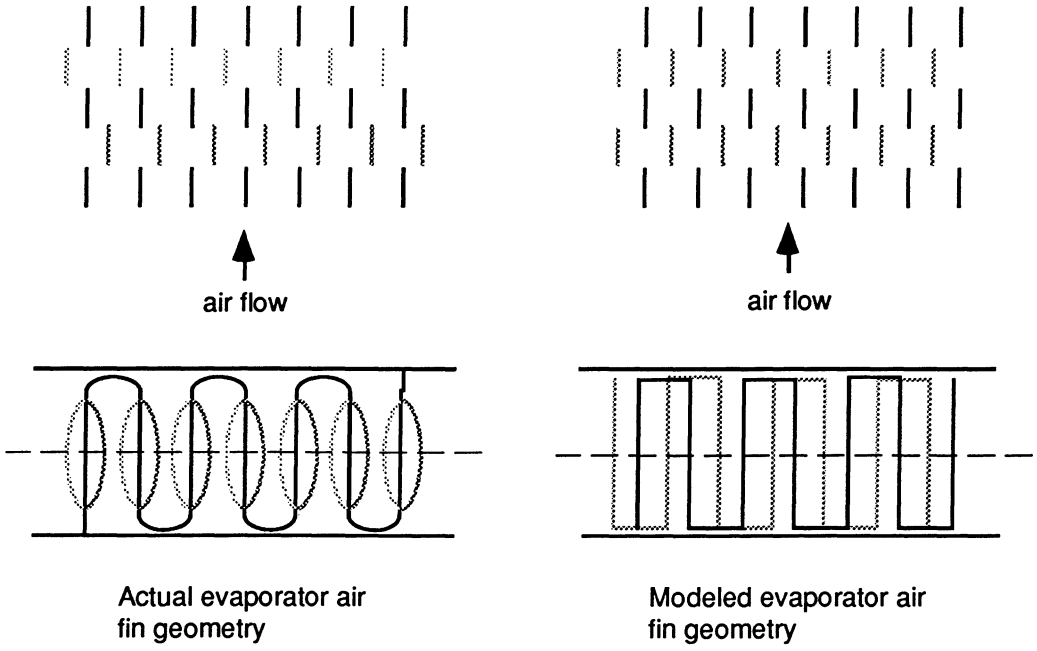

Figure 3.10 Comparison of actual evaporator airside fin geometry with modeled airside fin geometry.

$$\alpha_{fin} = \frac{s_{fin}}{h_{fin}} \tag{3.48}$$

$$\delta_{fin} = \frac{t_{fin}}{l_{fin}} \tag{3.49}$$

$$\gamma_{fin} = \frac{t_{fin}}{s_{fin}} \tag{3.50}$$

s_{fin}, h_{fin}, t_{fin}, and l_{fin} are the fin dimensions labeled in Figure 3.11. The Reynolds number is based on the hydraulic diameter which is defined by Manglik and Bergles.

$$D_h = \frac{4\,A_{cs}}{A_{surf}/L} = \frac{4 s_{fin} h_{fin} l_{fin}}{2(s_{fin} l_{fin} + h_{fin} l_{fin} + t_{fin} h_{fin}) + t_{fin} s_{fin}} \tag{3.51}$$

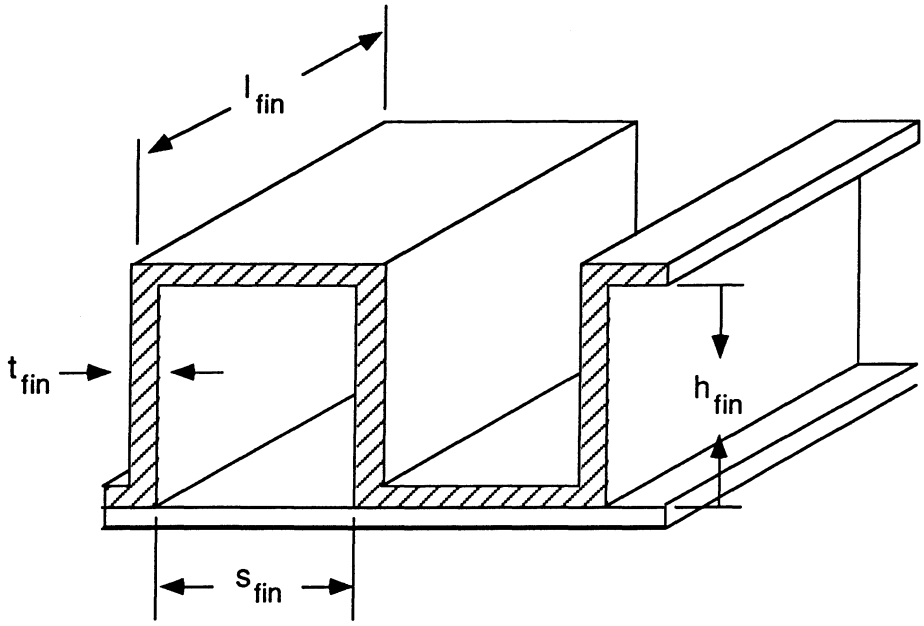

Figure 3.11 Offset strip fin geometry.

3.5.1.3 Wall Heat Transfer Correlations

The resistance for the wall is defined by

$$R_{wall} = \frac{t_{wall}}{k_{wall} A_{wall}} . \tag{3.52}$$

t_{wall} is the thickness of the wall, and A_{wall} is the surface area of the wall. The thermal conductivity of the wall is set to 173 W/m-K which is a reasonable average value for aluminum alloys.

3.5.1.4 Effectiveness-NTU Functions

The effectiveness-NTU functions are used to determine the final heat transfer. The important parameters are the ratio of the heat capacity rates, C_r, and the number of transfer units, NTU.

$$C_r = \frac{C_{min}}{C_{max}} = \frac{(\dot{m}c_p)_{min}}{(\dot{m}c_p)_{max}} \tag{3.53}$$

$$NTU = \frac{UA}{(\dot{m}c_p)_{min}} \tag{3.54}$$

If the refrigerant is two-phase, C_{max} is infinity and C_r becomes zero. The effectiveness-NTU correlation is independent of geometry.

$$\varepsilon = 1 - \exp(-NTU) \tag{3.55}$$

When the refrigerant is single-phase, the approximation for the effectiveness for both fluids unmixed is from Incropera and DeWitt (1990).

$$\varepsilon = 1 - \exp\left[\frac{NTU^{0.22}}{C_r}\left\{\exp\left(-C_r NTU^{0.78}\right) - 1\right\}\right] \tag{3.56}$$

3.5.2 Pressure Drop Correlations

An empirical curve fit is used to determine the minor losses and frictional pressure drop (Pa) as a function of mass flow rate (kg/s). This curve fit was determined from the data of Rubio-Quero, Collins and Hemami.

$$\Delta P_{fric} + \Delta P_{minor} = 8.45 \times 10^4 \frac{\dot{m}}{0.01} \frac{L_{cell}}{L_{total}} \quad \text{for } \dot{m} < 0.01 \tag{3.57}$$

$$\Delta P_{fric} + \Delta P_{minor} = \left(-1220 + 9.67 \times 10^5 \dot{m}\right) \frac{L_{cell}}{L_{tot}} \quad \text{for } \dot{m} \geq 0.01 \tag{3.58}$$

3.5.3 Steady-state Evaporator Model Validation

The steady-state evaporator model was compared with experimental data obtained by Rubio-Quero, Collins, and Hemami. The modeled capacity or heat transfer agrees within 5% of the experimental data (Figure 3.12). This results in the evaporator superheat being predicted within 8 K for the majority of the data points (Figure 3.13). The evaporator pressure drop is predicted within 25% for the majority of data points (Figure 3.14). The maximum difference between the modeled evaporator pressure drop and the experimental pressure drop is approximately 10 kPa which is less than 1.5 psi (Figure 3.15).

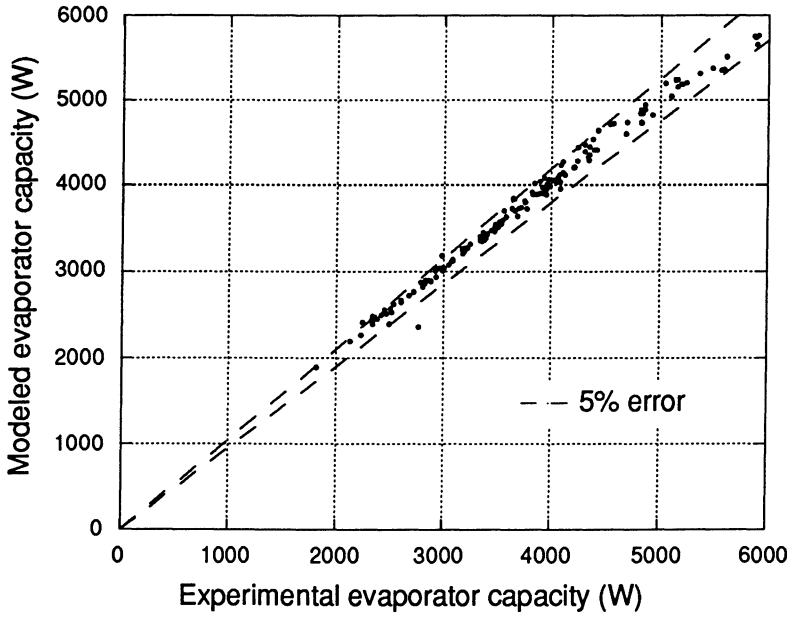

Figure 3.12 Comparison between experimental evaporator capacity and modeled evaporator capacity.

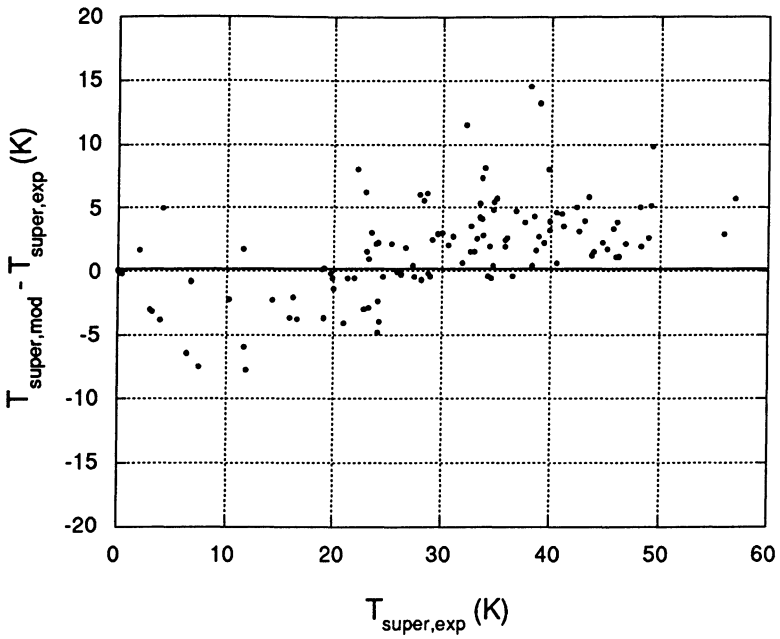

Figure 3.13 Difference between experimental evaporator superheat and modeled evaporator superheat.

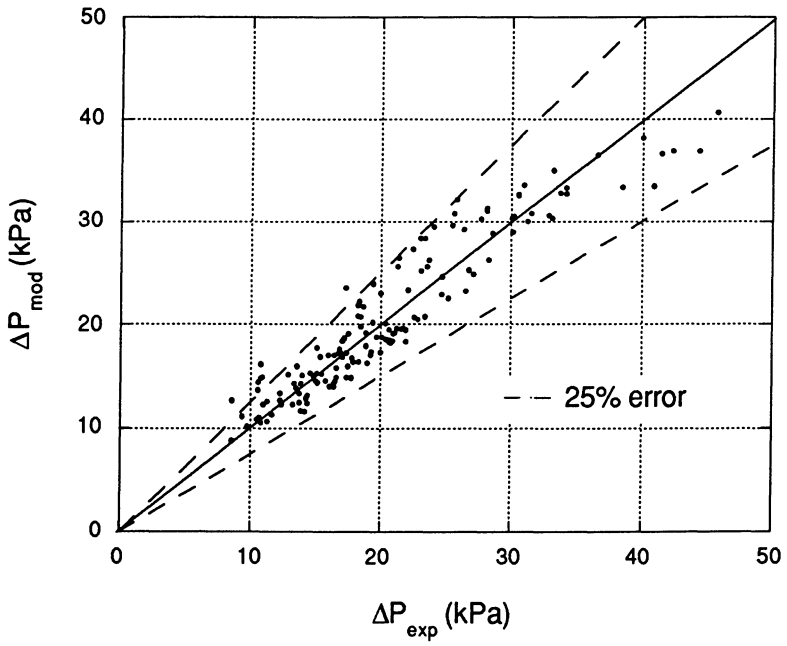

Figure 3.14 Comparison between experimental evaporator pressure drop and modeled evaporator pressure drop.

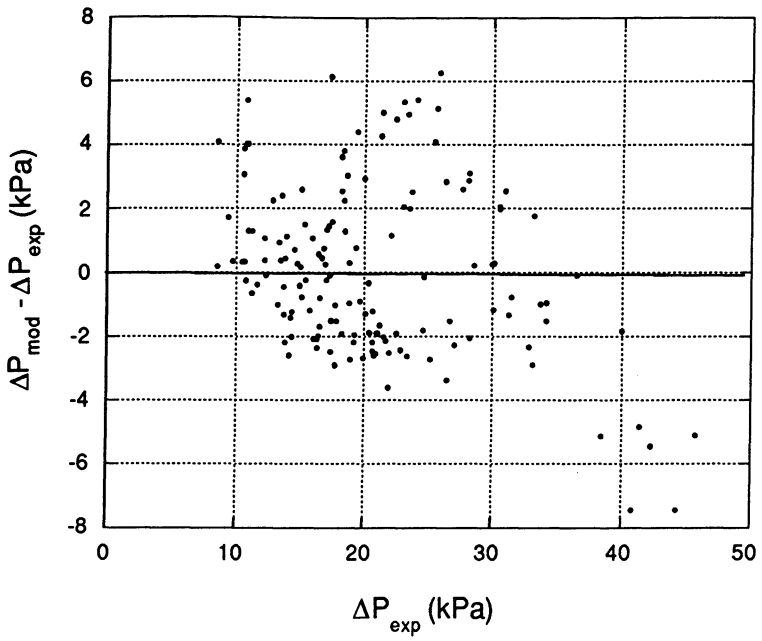

Figure 3.15 Difference between modeled evaporator pressure drop and experimental evaporator pressure drop.

3.6 Compressor Model

The compressor performs work on the vapor refrigerant exiting the accumulator in order to raise the pressure in the condenser. The following quasi-steady state model was developed for a Ford FS-10 externally-driven reciprocating compressor. The drive ratio for this compressor operating in a Ford Crown Victoria is 1.46 meaning that the compressor operates at a faster speed than the vehicle engine.

Figure 3.16 illustrates the input and output parameters of the compressor model. There are four input parameters to the compressor model.

(a) inlet pressure (P_{in}),
(b) inlet enthalpy (h_{in})
(c) exit pressure (P_{out})
(d) compressor speed ($\dot{N}$)

The output parameters from the compressor model are

(a) mass flow rate ($\dot{m}$),
(b) compressor power ($\dot{W}$), and
(c) exit enthalpy (h_{out}).

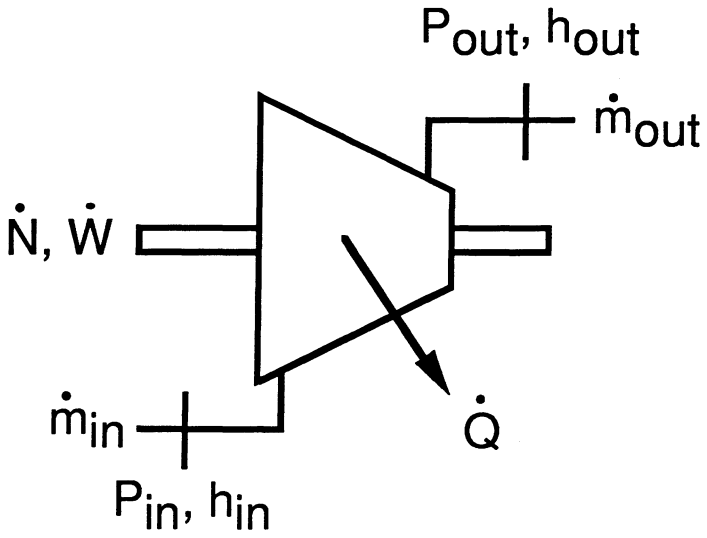

Figure 3.16 Compressor conceptualization.

Since we model the compressor as quasi-steady state, the inlet mass flow rate and the outlet mass flow rate are equal (Equation 3.62). The compressor heat transfer, $\dot{Q}$, may be required in a compressor model to determine the outlet enthalpy from the conservation of energy equation (Equation 3.63). However, it is generally of no practical interest as an output variable. The compressor power is modeled as positive into the compressor. The compressor heat transfer is modeled as positive out of the compressor.

Most compressor models are based on calorimetry data which are measurements of mass flow rate and compressor power (exit enthalpy is often omitted) for a wide variety of operating conditions. To fully define performance, the four inputs (three if compressor speed is fixed) noted above must each be varied independently. Fixing the inlet temperature or superheat eliminates one input variable although no information on the effect of this variable is then produced.

Our model is based on two sets of data taken for a single compressor. The first set of data was taken by Ford Motor Company in their compressor calorimetry laboratory. For each of five compressor speeds (600 RPM, 1000 RPM, 2000 RPM, 3000 RPM, and 5000 RPM), six pairs of compressor inlet and exit pressures were used giving a total of 30 tests. Superheat varied in the narrow range between roughly 8 °C and 10 °C. The second data set consists of 148 tests from our own facility obtained by Rubio-Quero, Collins, and Hemami. These data represent a random sampling of operating conditions. Table 3.3 compares the two data sets with respect to the key input parameters considered. The UIUC data generally involve a

narrower range of compressor speeds, lower pressures and higher superheat values. The two sets of data are characterized by different extremes yet have a significant area of overlap where direct comparisons are possible.

Two important issues must be considered when using calorimetry data. The first is transferability. Transferability is the extent to which performance data collected in one test facility can be transferred to another test facility or to an operating system. We shall discuss the transferability between the data obtained from the Ford Motor Company test facility and the UIUC test facility in Section 3.6.3. A second issue is manufacturing variability which is the variation among multiple units of the same compressor type. Since all of our experimental data was obtained from a single compressor, we do not analyze the effect of manufacturing variability.

Variable	Ford data	UIUC data
Number of data points	30	148
Minimum compressor speed [RPM]	600	847
Mean compressor speed [RPM]	2320	2172
Maximum compressor speed [RPM]	5000	3542
Minimum inlet pressure [kPa]	237.8	93.2
Mean inlet pressure [kPa]	316.1	179.2
Maximum inlet pressure [kPa]	446.8	337.9
Minimum exit pressure [kPa]	1311	723
Mean exit pressure [kPa]	2106	1031
Maximum exit pressure [kPa]	2901	1810
Minimum inlet superheat [°C]	7.88	2.11
Mean inlet superheat [°C]	8.62	31.62
Maximum inlet superheat [°C]	9.49	61.40

Table 3.3 Comparison of the UIUC and Ford compressor data sets.

For the purpose of the discussion here, compressor models may be divided into three broad categories according to their level of empiricism as follows: (a) empirical models, (b) semi-empirical models, and (c) first-principles models. We shall examine each of these categories individually below beginning with empirical models (Section 3.6.1). We shall then move to the other extreme and examine first-principles models (Section 3.6.2). Lastly, we shall

consider semi-empirical models which combine elements of the previous two approaches (Section 3.6.3). We shall summarize the final semi-empirical model in Section 3.6.4.

When the clutch is disengaged, the compressor is essentially a closed valve between the accumulator and the condenser. The models described in Sections 3.6.1-3.6.4 only used when the compressor is operating. Section 3.6.5 summarizes the correlations for when the compressor is not operating.

3.6.1 Empirical Models

Empirical models are curve-fits or interpolations of calorimetry data. In stationary systems where compressor speed and inlet temperature or superheat are fixed, mass flow rate and power are commonly written as bi-quadratic functions of evaporating and condensing temperatures as follows.

$$\dot{m}_{ref} = a_{m1} + a_{m2}\,T_{evap} + a_{m3}\,T_{cond} + a_{m4}\,(T_{evap})^2 + a_{m5}T_{evap}\,T_{cond} + a_{m6}\,(T_{cond})^2 \tag{3.59}$$

$$\dot{W}_{ref} = a_{w1} + a_{w2}\,T_{evap} + a_{w3}\,T_{cond} + a_{w4}\,(T_{evap})^2 + a_{w5}T_{evap}\,T_{cond} + a_{w6}\,(T_{cond})^2 \tag{3.60}$$

Here, $\dot{m}_{ref}$ and $\dot{W}_{ref}$ are the mass flow rate and power at the reference inlet temperature or superheat. These values must be adjusted for the actual inlet temperature or superheat. Mass flow rate is typically adjusted by applying an inlet density correction factor as follows.

$$\dot{m}_{ref} = \left(\frac{\rho_{in}}{\rho_{ref}}\right)^{a_7} \dot{m} \tag{3.61}$$

where ρ_{in} is the actual inlet density, ρ_{ref} is the inlet density at the inlet pressure and reference temperature or superheat, and a_7 is an empirical coefficient typically equal to 1 based on the assumption that suction *volumetric* flow rate is independent of inlet temperature. Compressor power can be similarly corrected although the most common approach is to neglect the effect of inlet temperature altogether (i. e., $\dot{W} = \dot{W}_{ref}$). To obtain exit enthalpy, compressor heat transfer is determined using a surface temperature and overall heat transfer coefficient (UA). The exit enthalpy is calculated from the energy equation described below (Equation 3.63).

Note that the use of evaporating and condensing temperatures in formulating an empirical model is roughly equivalent to taking the logarithm of the inlet and outlet pressures.

Empirical models have one key advantage and two significant disadvantages. The key advantage is that these models are based on performance measurements and thus reflect all the complexity inherent in the real device. However, good empirical models require (a) a rich set of data and (b) a proven set of functional forms that fully represent the variation of each of the three outputs with the four inputs. The first problem is to fit a set of data with four degrees of freedom. For the limited range of operating conditions typical of stationary systems, the bi-quadratic method described above yields a reasonable fit of the data given two degrees of freedom. However, the fitting coefficients lack physical significance, and, because the fitting is done dimensionally, the number of coefficients is greater than necessary. The methods typically employed to correct for inlet temperature and, in the case of mobile systems, compressor speed are largely untested. Lastly, there is the issue of determining compressor heat transfer or, alternatively, exit enthalpy. Modeling heat transfer and using this value to obtain exit enthalpy again involves several untested assumptions. The second disadvantage of empirical models centers on the large number of data required to fully define three separate four-dimensional functions. Practicality dictates that only a subset of the possible variations be tested, yet artificially fixing one parameter to reduce the number of possible variations significantly degrades the scope of the measurements.

3.6.2 First-principles Models

A model based on first principles has only a few parameters, and these parameters can either be measured directly or else inferred from diagnostic measurements. However, in developing a first-principles model, one must necessarily make simplifying assumptions and approximations. As a result, first-principles models may fail to fully capture the true complexity of the real system. Nevertheless, a first-principles approach is highly desirable from both a conceptual and a practical perspective.

First-principles models can be developed from either a macroscopic or a microscopic viewpoint. In the macroscopic viewpoint, the compressor is treated as a continuous flow device whereas, in the microscopic viewpoint, the behavior of the fluid inside the compressor is analyzed. We shall start with the macroscopic viewpoint and then turn to the microscopic viewpoint.

From a macroscopic viewpoint, we apply the steady-state conservation equations to compressor. The conservation of mass is

$$\dot{m}_{in} = \dot{m}_{out} = \dot{m}. \tag{3.62}$$

The conservation of energy equation written in terms of enthalpy (energy equation) is

$$0 = \dot{m}(h_{in} - h_{out}) + \dot{W} - \dot{Q}. \tag{3.63}$$

The conservation of energy equation written in terms of entropy (entropy equation) is

$$0 = \dot{m}(s_{in} - s_{out}) - \int_S \frac{\mathbf{q}'' \cdot \mathbf{n}}{T} dS + \dot{S}_{internal}. \tag{3.64}$$

Finally, the second law of thermodynamics is

$$\dot{S}_{internal} = \int_{Vol} \left(\frac{(\bar{\tau} \cdot \nabla) \cdot \mathbf{V}}{T} - \frac{\mathbf{q}'' \cdot \nabla T}{T^2} \right) dVol \geq 0 \tag{3.65}$$

where

s_{in}	= inlet entropy,
s_{out}	= outlet entropy,
S	= surface of the system (control volume) ,
$\mathbf{q}''$	= heat transfer rate per unit area (a vector quantity),
$\mathbf{n}$	= unit vector normal to surface S,
$\dot{S}_{internal}$	= internal rate of entropy production ,
Vol	= system volume,
$\bar{\tau}$	= fluid shear stress, and
$\mathbf{V}$	= fluid velocity.

Several points regarding these equations warrant discussion as follows.

(a) The mass equation is trivial in that the inlet and outlet mass flow rates are implicitly assumed to be equal.

(b) Since the forces acting on the compressor are not of interest here, the momentum equation is omitted.

(c) The kinetic and potential energy terms are omitted from the energy equation. These terms are generally negligible.

(d) The energy equation may be re-written in terms of entropy using the defining relationship for entropy; namely, Tds = dh – v dP. Once this is done, physical significance can be assigned to the various terms to identify entropy inflows, outflows,

and internal production. The kinetic and potential energy terms as well as the work term do not appear in the energy equation re-written in this manner.

(e) For simplicity, we shall refer to the energy equation written in terms of entropy simply as the "entropy equation" to distinguish it from the energy equation written in terms of enthalpy which we shall simply refer to as the "energy equation". In doing so, we must remember that entropy is not a conserved quantity and the entropy equation is actually the energy equation in disguise.

(f) The second law of thermodynamics may be stated as two simple hypotheses: (i) friction always dissipates mechanical energy to heat and (ii) heat always flows from hot to cold. These hypotheses are valid independent of any constitutive relationship between shear stress and velocity or between heat transfer rate and temperature.

(g) The entropy equation contains the volume integral $\dot{S}_{internal}$ which is unknown except for the fact that it must be positive.

(h) The entropy equation includes a problematic surface integral that requires knowledge of (a) the heat transfer rate per unit area and (b) the temperature everywhere on the surface of the control volume. However, for the purpose of using the entropy equation to develop an efficiency concept, the integral can be satisfactorily approximated by

$$\int_S \frac{\mathbf{q}''\cdot\mathbf{n}}{T} dS = \frac{\dot{Q}}{T_{in}}. \tag{3.66}$$

The entropy equation thus becomes

$$0 = \dot{m}(s_{in} - s_{out}) - \frac{\dot{Q}}{T_{in}} + \dot{S}_{internal} \tag{3.67}$$

The energy equation can be used to relate heat transfer and exit enthalpy as follows.

$$\dot{Q} = \dot{m}(h_{in} - h_{out}) + \dot{W} \tag{3.68}$$

or

$$h_{out} = h_{in} + \frac{\dot{W} - \dot{Q}}{\dot{m}} \tag{3.69}$$

Because heat transfer is an "extra" output of the compressor model, the net gain is zero in terms of equations and unknowns.

Similarly, the entropy equation introduces the additional unknown $\dot{S}_{internal}$ again yielding a net change of zero in terms of equations and unknowns. However, the entropy equation allows us to define an efficiency for the compressor by comparing actual performance to the performance of an ideal device with no internal entropy generation ($\dot{S}_{internal} = 0$). The operation of the ideal compressor is identical with the actual compressor except for two variables. One variable measures performance, and the other is the exit enthalpy. The efficiency is then obtained from the ratio of the performance measures. Because the ideal device is reversible, we call this efficiency the "reversible efficiency".

In the first method for determining the reversible efficiency, we fix the (a) compressor speed, (b) heat transfer, (c) inlet pressure, (d) inlet enthalpy, (e) outlet pressure, and (f) work. We vary the mass flow rate and the outlet enthalpy. The two equations defining the ideal device performance are as follows.

$$0 = \dot{m}_{max} (h_{in} - h_{out,\,i}) + \dot{W} - \dot{Q} \tag{3.70}$$

$$0 = \dot{m}_{max} [s_{in} - s(P_{out}, h_{out,\,i})] - \dot{Q} / T_{in} \tag{3.71}$$

The reversible efficiency is then

$$\eta_{rev} = \frac{\dot{m}}{\dot{m}_{max}}. \tag{3.72}$$

In the second method for determining the reversible efficiency, we fix the (a) compressor speed, (b) heat transfer, (c) inlet pressure, (d) inlet enthalpy, (e) outlet pressure, and (f) mass flow rate. We vary the work and the outlet enthalpy. Now, the two equations defining the ideal device performance are as follows.

$$0 = \dot{m} (h_{in} - h_{out,\,i}) + \dot{W}_{min} - \dot{Q} \tag{3.73}$$

$$0 = \dot{m} [s_{in} - s(P_{out}, h_{out,\,i})] - \dot{Q} / T_{in} \tag{3.74}$$

The reversible efficiency is then

$$\eta_{rev} = \frac{\dot{W}_{min}}{\dot{W}}. \tag{3.75}$$

Both methods yield identical numerical values of the reversible efficiency, η_{rev}, for the adiabatic case. The primary difference is that Method 1 defines the efficiency as the ratio of the actual mass flow rate to the maximum mass flow rate possible given the power available whereas Method 2 defines efficiency as the ratio of the minimum power needed to produce the given mass flow rate to the actual power used by the compressor. We prefer the first method (Equation 3.72) because it is consistent with the broader definition of efficiency given by

$$\eta = \frac{\text{actual useful effect produced}}{\text{maximum useful effect produced by ideal device}}. \tag{3.76}$$

This same definition can be uniformly applied to all energy transferring devices. Most thermodynamics textbooks, however, adopt the second method for compressors, and thus this approach may be more generally familiar to the reader.

Two additional nondimensional parameters can be obtained from the macroscopic view point. The heat transfer fraction is

$$f_Q = \frac{\dot{Q}}{\dot{W}}. \tag{3.77}$$

The irreversibility fraction is

$$f_I = \frac{\dot{I}}{\dot{W}} = \frac{T_{in}\dot{S}_{internal}}{\dot{W}} \tag{3.78}$$

where $\dot{I} = T_{in}\dot{S}_{internal}$ is compressor irreversibility. Because heat transfer can, in principle, be any positive or negative value, f_Q varies between $-\infty$ and $+\infty$. In practice, however, heat transfer is always from the compressor to the ambient (i. e., positive by our sign convention) and less than the power input. Thus, the practical range of f_Q is between 0 and 1. The performance of the system is improved by making f_Q as *large* as possible although the value is

usually much less than 1. Because irreversibility is always positive, f_I varies between 0 and ∞ although the ratio is usually less than 1. The performance of the system is improved by making f_I as *small* as possible. Some authorities define $\eta_2 = (1 - f_I)$ as an additional system efficiency often designated the "second-law" efficiency to contrast it with the efficiency defined above which is designated the "first-law" efficiency. Actually, both definitions rely on the use of the Second Law, the only difference being that η_2 can be computed from the operating parameters of the real device alone without introducing the concept of an ideal device. However, because η_2 can be negative, we use the simple ratio f_I without associating an "efficiency" concept with it.

Turning to the microscopic viewpoint, we now consider what happens inside the compressor cylinder. To this end, we consider one representative cycle of the piston and define the following reference points.

State Point 1:	Cylinder volume is maximum
State Point 2:	Exhaust valve opens
State Point 3:	Cylinder volume is minimum
State Point 4:	Intake valve opens

Note that State Points 1 and 3 are defined in terms of piston position. We tacitly assume that the exhaust valve is closed at State Point 1 and opens sometime during the compression stroke (State Point 1 to State Point 3). Similarly, we assume that the intake valve is closed at State Point 3 and opens sometime during the suction stroke (State Point 3 to State Point 1). Otherwise, no further assumptions about valve operation are made.

Figure 3.17 shows this cycle on a P-Vol diagram. The macroscopic variables of mass flow rate and compressor power may be related to the cycle quantities as follows.

$$\dot{m} = \dot{N}(m_1 - m_3) \tag{3.79}$$

$$\dot{W} = \frac{\dot{N}\, W_{cycle}}{\eta_{mech}} \tag{3.80}$$

where $\dot{N}$ is compressor speed in cycles per unit time, m_1 is the cycle mass at State Point 1, m_3 is cycle mass at State Point 3, η_{mech} is the mechanical efficiency of the compressor drive system, and W_{cycle} is the cycle work given by the closed integral

$$\dot{W}_{cycle} = \int_{cycle} P \, d(Vol). \tag{3.81}$$

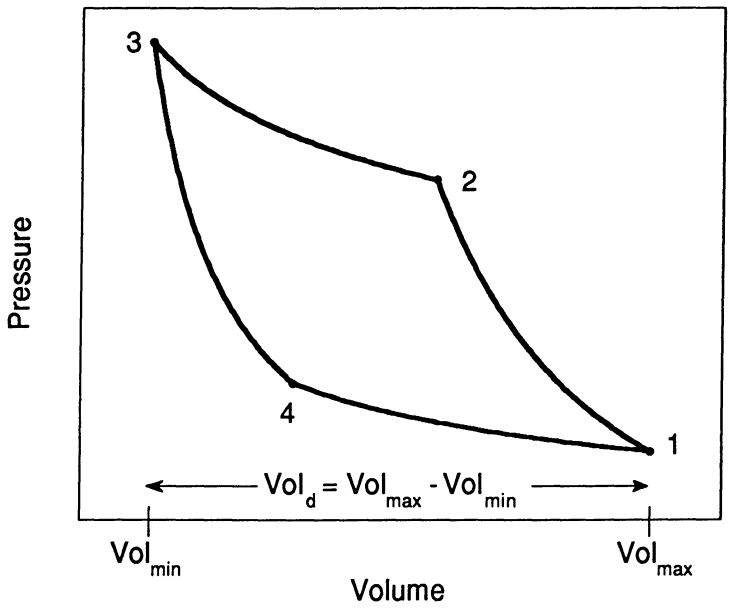

Figure 3.17 Representative cycle on P-Vol diagram.

To make use of this analysis, we require several assumptions about the processes of the cycle. The conventional assumptions as described by Threlkeld (1970) are:

1. Process 1-2 involves polytropic (isentropic) compression with $m_2 = m_1$.
2. Process 2-3 involves exhaust at constant temperature and pressure.
3. Process 3-4 involves polytropic (isentropic) expansion with $m_4 = m_3$.
4. Process 4-1 involves intake at constant temperature and pressure.
5. $P_1 = P_4 = P_{in} - \Delta P_{in}$ and $P_2 = P_3 = P_{out} + \Delta P_{out}$, where ΔP_{in} and ΔP_{out} are known valve differential pressure.

In addition to these assumptions, m, P, Vol and T are linked everywhere in the cycle by the equation of state for the working fluid.

We started with this approach in the hope of developing a first-principles model of the compressor similar to the models developed for the other system components. Based on our

analysis of the experimental data, we concluded that the assumption of constant pressure during the exhaust phase is inconsistent with observed system behavior. Even when this assumption was relaxed and the polytropic exponents and mechanical efficiency were made functions of compressor speed, we were unable to produce a reasonable collapse of the data. A first-principles model with coefficients that are complex functions of the input variables has no advantage over an empirical model that treats mass flow rate, compressor power, and exit enthalpy as empirical functions directly. We concluded that the above cycle analysis oversimplifies what actually occurs in the compressor by neglecting important flow and heat transfer effects. Consequently, it does not provide an adequate basis for practical compressor model development.

Although the processes occurring in the compressor cylinder are indeed complex, the microscopic viewpoint does provide the basis for two additional nondimensional parameters characteristic of compressor performance. One such parameter is the volumetric efficiency of the compressor. Volumetric efficiency is a nondimensional parameter between 0 and 1 that scales out the first-order effects of inlet density and compressor speed from mass flow rate. To define the volumetric efficiency, we first introduce the reference mass flow rate given by

$$\dot{m}_{ideal} = \rho_{in} \dot{N} \, Vol_d, \tag{3.82}$$

where ρ_{in} is inlet density, $\dot{N}$ is once again compressor speed, and Vol_d is displacement volume. To understand the assumptions which underlie this definition, consider the expression for mass flow rate obtained from the microscopic viewpoint and substitute the product of density and volume for mass.

$$\dot{m} = \dot{N}(m_1 - m_3) = N(\rho_1 Vol_1 - \rho_3 Vol_3) \tag{3.83}$$

If $\rho_1 = \rho_3 = \rho_{in}$, then

$$\dot{m} = \dot{m}_{ideal} = \dot{N}(\rho_1 Vol_1 - \rho_3 Vol_3) = \rho_{in}\dot{N}(Vol_1 - Vol_3) - \rho_{in}\dot{N}Vol_d. \tag{3.84}$$

The condition that $\rho_1 = \rho_3 = \rho_{in}$ is satisfied if the exit density is the same as the inlet density and the compressor operates slowly enough that equilibrium is reached at the end of the suction and exhaust strokes. The actual mass flow rate is necessarily less than this value owing to (a) nonzero pressure and temperature increases across the compressor and (b) valve restrictions

that limit flow into and out of the cylinder. Using $\dot{m}$ ideal as the reference value, the volumetric efficiency becomes

$$\eta_v = \frac{\dot{m}}{\dot{m}_{ideal}}. \tag{3.85}$$

From the above discussion, we conclude that volumetric efficiency should approach 1 as the compressor speed approaches 0 and the pressure ratio across the compressor approaches 1. We shall use this fact later in formulating a semi-empirical model.

The second nondimensional parameter derived from the microscopic viewpoint is the polytropic exponent for compression given by

$$n_{comp} = \frac{\ln(P_{out}/P_{in})}{\ln(P_{out}/P_{in})\ln(T_{out}/T_{in})}. \tag{3.86}$$

In principle, n_{comp} can vary between 0 and ∞ although, once again, the practical range is actually quite limited. Two reference values are significant. The isothermal case corresponds to $n_{comp} = 1$, and the adiabatic, frictionless (isentropic) case corresponds to $n_{comp} = n_s \approx 1.1$ for R-134a. n_{comp} is increased by friction and reduced by heat transfer. The isothermal case represents unrestricted heat transfer. Values between 1 and n_s indicate that the effect of heat transfer outweighs the effect of friction whereas values greater than n_s indicate that the effect of friction outweighs the effect of heat transfer. One may also reasonably argue that n_{comp} should rise with compressor speed because the time available for heat transfer is reduced.

Compressor speed can be made nondimensional by multiplying it by a time constant characteristic of the compressor. Two time constants are possible. One is related to the cooling rate of the compressor, and the other is related to the maximum flow rate through the valve. The latter is the more important in this analysis because it characterizes the ability of the cylinder to fill. Unfortunately, an examination of valve flow behavior requires detailed knowledge not generally available. Thus, we choose to scale the compressor speed by a reference speed as follows.

$$r = \frac{\dot{N}}{\dot{N}_{ref}}. \tag{3.87}$$

Although no specific scaling is used, the choice of reference speed is motivated by the extensive data analysis presented below.

In summary, a first-principles approach gives rise to nine nondimensional parameters that characterize compressor operation:

r = reduced compressor speed = $\dot{N} / \dot{N}_{ref}$
r_P = compressor pressure ratio = P_{out} / P_{in}
r_T = compressor temperature ratio = T_{out} / T_{in}
r_ρ = compressor density ratio = ρ_{out} / ρ_{in}
η_v = volumetric efficiency = $\dot{m} / (\rho_{in} \dot{N} \ Vol_d)$,
η_{rev} = reversible efficiency = $\dot{m} / \dot{m}_{rev}$,
f_Q = heat transfer fraction = $\dot{Q} / \dot{W}$,
f_I = irreversibility fraction = $T_{in} \dot{S}_{internal} / \dot{W}$, and
n_{comp} = polytropic exponent for compression
= $\ln (r_p) / [\ln (r_P) - \ln(r_T)]$.

3.6.3 Semi-empirical Models

Semi-empirical models seek to (a) leverage the power of nondimensionalization to minimize the number of fitting coefficients and (b) choose functional forms based on a first-principles analysis. Removing first-order dependence by scaling the variables appropriately simplifies the fitting process, and the use of physically based functional forms provides a useful starting point for the analysis.

Our development of a semi-empirical model is based on the use of the nondimensional parameters defined in the previous section and the experimental data. Figures 3.18 through 3.22 present the two sets of data in terms of the five nondimensional parameters defined in the previous section. All parameters are plotted as functions of reduced speed based on a reference speed of 6000 RPM. Specifically, Figure 3.18 shows the variation of reversible efficiency (Equation 3.72), Figure 3.19 shows the variation of irreversibility fraction (Equation 3.78), Figure 3.20 shows the variation of polytropic exponent (Equation 3.86), Figure 3.21 shows the variation of heat transfer fraction (Equation 3.77), and Figure 3.22 shows the variation of volumetric efficiency (Equation 3.85).

Figures 3.18 and 3.19 show how well the compressor performs as an energy transferring device. The primary conclusions from these results are (a) the two sets of data generally agree, (b) a slight departure is suggested at low compressor speeds although the UIUC data in this range are insufficient to draw a firm conclusion, (c) reversible efficiency η_{rev} decreases linearly from roughly 60% to 35% as reduced compressor speed increases from roughly 0.1 to 0.8, and (d) irreversibility fraction f_I increases from roughly 0.4 to 0.6 over the same speed range. Reversible efficiency and irreversibility ratio do not provide the most expedient route to a semi-empirical model owing to the need to solve simultaneous algebraic equations involving

refrigerant properties. Although solving these equations numerically is indeed possible, the added complexity proves unnecessary.

Figure 3.20 shows the variation of polytropic exponent n_{comp} with reduced speed. The two reference values noted earlier are shown. One is $n_{comp} = 1$ which corresponds to isothermal compression where heat transfer is ostensibly unrestricted. The second is $n_{comp} = n_s \approx 1.1$ which is the isentropic or frictionless-adiabatic case. Heat transfer reduces the exponent from n_s whereas friction increases the exponent. If the effect of heat transfer is greater then the exponent will lie in the sub-isentropic region ($n_{comp} < n_s$); if the effect of friction is greater then the exponent will lie in the super-isentropic region ($n_{comp} > n_s$). From the results of Figure 3.20, we see that the relative importance of friction increases as compressor speed increases but that the effect of friction always outweighs the effect of heat transfer. Because the two sets of data are in general agreement, a single fit of polytropic exponent is justified. Indeed, a simple linear fit of the form

$$n_{comp} = a_0 + a_1 r \tag{3.88}$$

appears to work nicely, and our extensive analysis of the data revealed no systematic dependence of polytropic exponent on pressure ratio, temperature ratio or density ratio. The only well defined correlation is with reduced speed. On conceptual grounds, one expects the polytropic exponent to approach the isothermal limit as compressor speed goes to zero, but as a practical matter this limit is reached only at speeds below the range of practical interest even for compressor start-up.

A correlation for polytropic exponent allows the exit temperature and thus all other exit parameters to be determined (Equation 3.86). Specifically, the exit enthalpy h_{out} can be determined from T_{out} and P_{out}. This is an important first step in obtaining a practical semi-empirical model.

Figure 3.21 shows how heat transfer fraction f_Q varies with compressor speed. Two important aspects of this figure are immediately apparent. First, we note that the two data sets show significant differences in terms of both overall magnitude and the trend at low speed. The second key observation is that this ratio is roughly constant for all operating conditions. This latter result is consistent with our hypothesis that the compressor surface temperature is driven by heat transfer rather than heat transfer being driven by a compressor surface temperature. Tying heat transfer to compressor power is decidedly preferable to computing heat transfer using a compressor surface temperature, ambient temperature, and UA value, all of which are generally unknown and generally of no practical interest to us.

Despite the differences between the Ford and UIUC data sets, we chose to approximate the ratio as a single constant based on the aggregate of the two data sets. No substantial improvement in the performance of the empirical model was realized by fitting the two data sets separately or by making the ratio a function of the nondimensional input parameters. Using this value of f_Q and h_{out} determined as noted above, compressor power can be obtained from the energy equation in the form

$$\dot{W} = \frac{\dot{m}(h_{out} - h_{in})}{1 - f_Q} \tag{3.89}$$

once the third and final variable, mass flow rate, is known.

The simplest and most direct route to mass flow rate is through the use of the volumetric efficiency. Figure 3.22 shows how volumetric efficiency varies with compressor speed. Unlike the polytropic exponent n_{comp} which we approximate as a linear function of reduced speed and the heat transfer fraction f_Q which we approximate as a constant, the volumetric efficiency depends on density differences across the compressor as well as compressor speed. Considering once again the microscopic view of the compression process as outlined in Section 3.6.2 on First-principles models, we have that

$$\eta_v = (1 + CF)\frac{\rho_1}{\rho_{in}} - CF\frac{\rho_3}{\rho_{in}} \tag{3.90}$$

where, as before, the subscripts "1" and "3" denote the beginning and end of the compression stroke, respectively, and CF is the clearance factor given by V_3 / V_d. The two density ratios are, in turn, dependent on reduced speed, pressure ratio, temperature ratio, and density ratio. Because ρ_1 and ρ_2 are not measured, we must infer their values from the volumetric efficiency. However, we have but one equation from which to determine two density factors. Because CF is small, the controlling factor is (ρ_1 / ρ_{in}); the factor (ρ_3 / ρ_{in}) is of secondary importance. We thus define $f = (\rho_{in} / \rho_1)$ and assume that $(\rho_3 / \rho_{in}) = f\,(\rho_{out} / \rho_{in})$. This later assumption does materially affect the trends obtained. The resulting expression becomes

$$\eta_v = \frac{1 + CF}{f} - CF\, f\, r_p \tag{3.91}$$

which can be solved for f. Figure 3.23 shows the results of this analysis. The UIUC data appear to be well described by a linear function of reduced speed. More importantly, these data show the expected asymptotic behavior; namely, f goes to 1 as r goes to 0. The Ford data on the other hand show a sharply different trend appearing to approach an asymptote of about 1.4 at low speed. We could find no systematic explanation for this disparity. One can theorize, for example, that the greater heat transfer evident for the Ford data corresponds to an artificially lower exit temperature and thus an incorrect exit density. Correcting for this difference has a negligible effect on the above results, however. Also, one can theorize that the pressure measurements are affected by flow related pressure drops. Unfortunately, the required correction has the opposite trend; namely, a large correction is needed at low speeds where flow rates are small. Yet another problem in calculating volumetric efficiency as shown above stems from the fact that the clearance factor is difficult to accurately determine in practice owing to the complex geometry of the head and valve regions. Changing the clearance factor cannot explain the disparity between the Ford and UIUC data sets, however.

We pursue a simpler approach. First, we write the volumetric efficiency as the product of two factors: (a) $f_P(r_P)$, the pressure-ratio factor and (b) $f_s(r)$, the speed factor. Based on the assumption that the volumetric efficiency approaches 1 as the compressor speed approaches 0 *and* the pressure ratio approaches 1, we have that (a) $f_P(r_P)$ goes to 1 as r_p goes to 0 and (b) $f_s(r)$ goes to 1 as r goes to zero. Both factors must decline monotonically as pressure ratio and reduced speed increase. This simple thinking leads to the following proposed functional forms.

$$f_P\left(r_p\right) = r_P^{-b} \tag{3.92}$$

and

$$f_s(r) = 1 - c_1 r^2. \tag{3.93}$$

We found that b = 1/4 provides a good collapse of the data. Figure 3.24 shows how the speed factor varies with reduced speed after eliminating the effect of $f_P(r_P)$. Here, we again see a clear difference between the two data sets. This difference cannot be reconciled within the context of our empirical model, nor were we able to find any explanation for the disparity other than differences in compressor installation between the two test facilities. Both sets of data are internally consistent based on their own built-in redundancy, so the possibility of a systematic experimental error in either data set seems unlikely. This difference highlights the problems inherent in transferring results between test facilities.

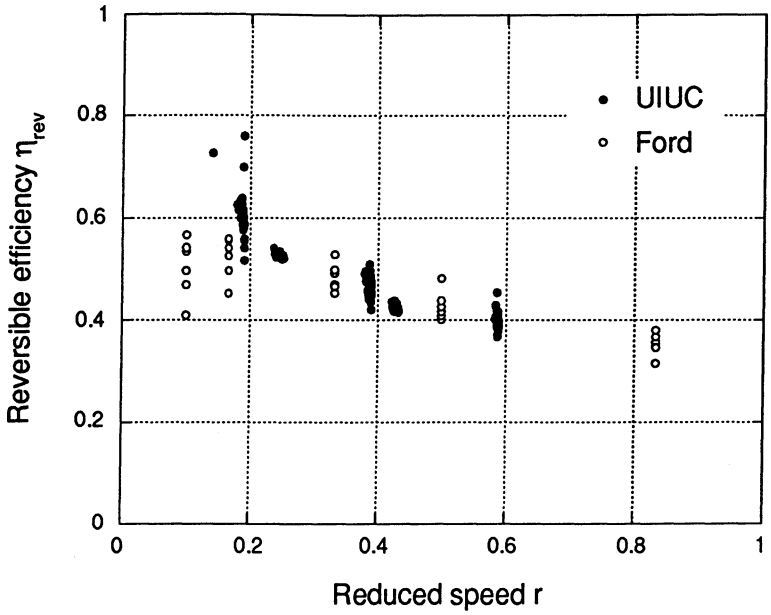

Figure 3.18 Reversible efficiency as a function of reduced speed.

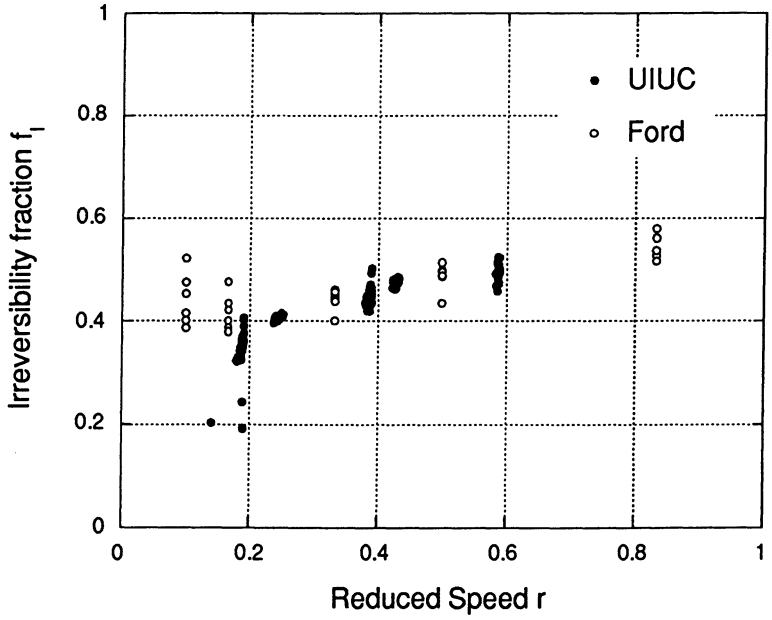

Figure 3.19 Irreversibility fraction as function of reduced speed.

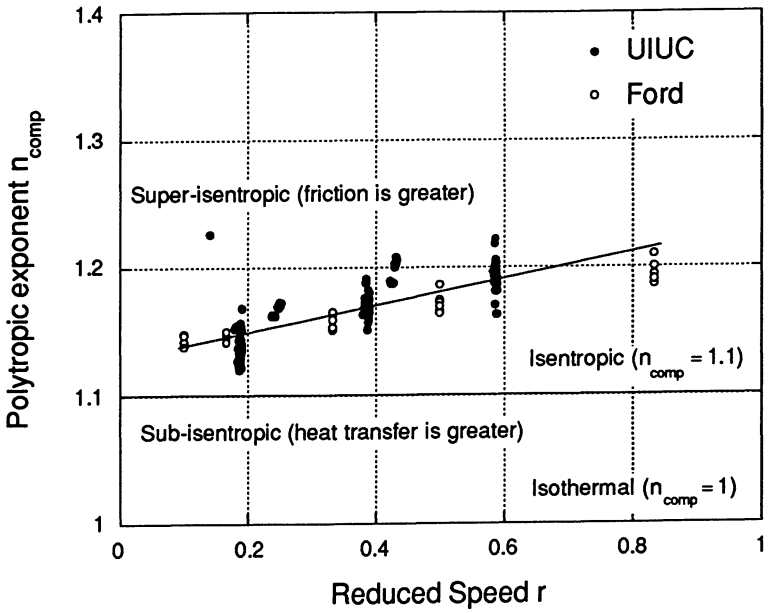

Figure 3.20 Polytropic exponent as function of reduced speed.

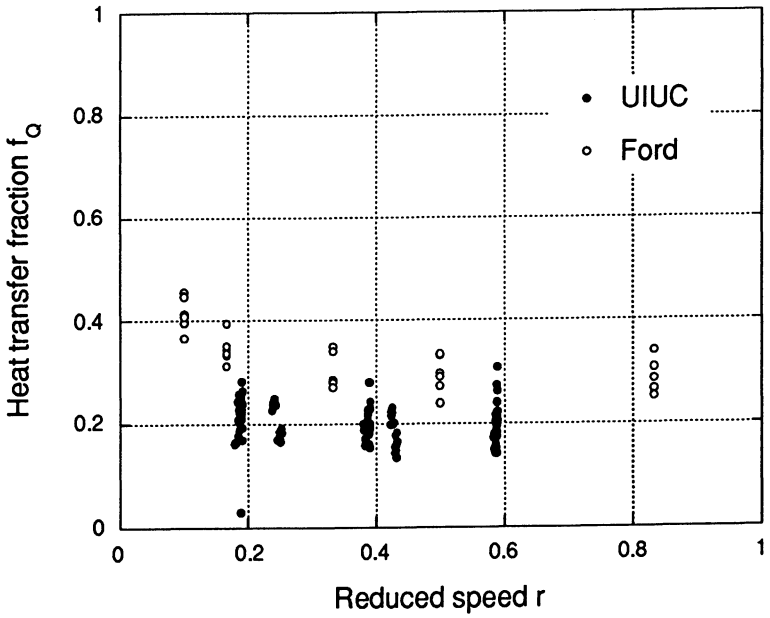

Figure 3.21 Heat transfer fraction as function of reduced speed.

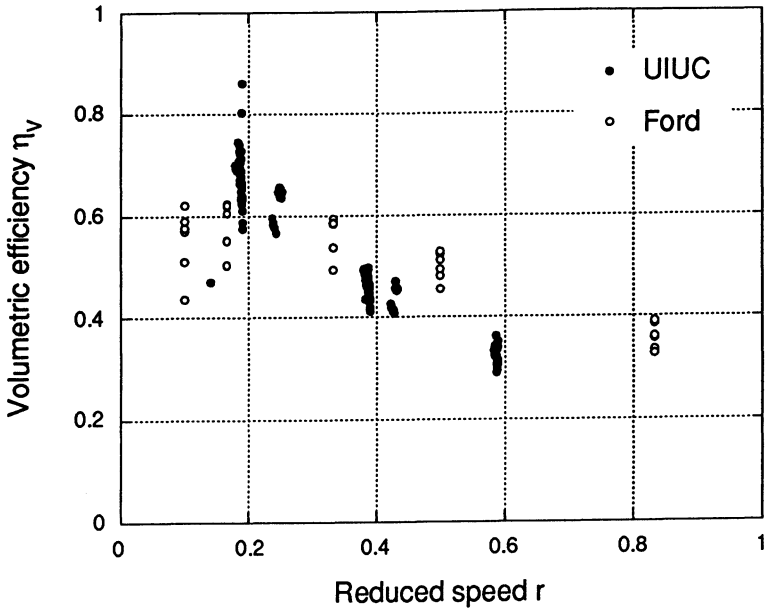

Figure 3.22 Volumetric efficiency as function of compressor speed.

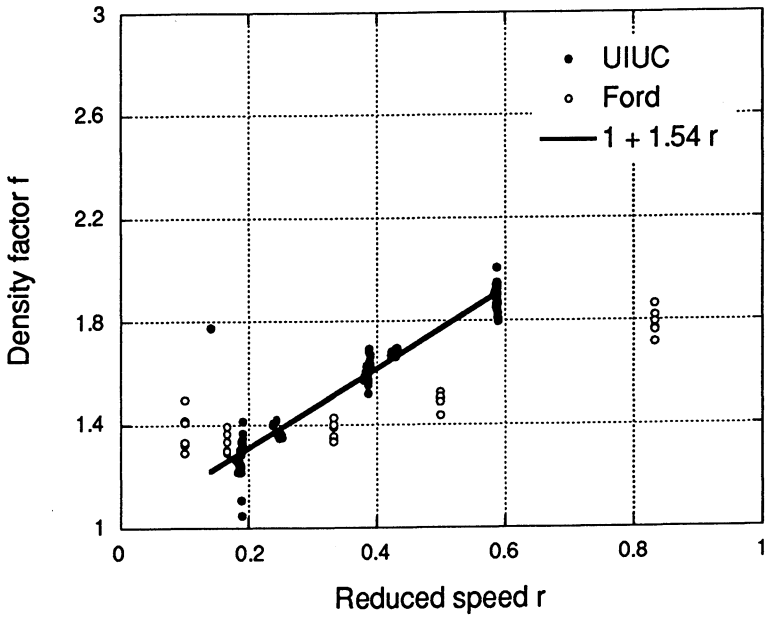

Figure 3.23 Intake density factor as a function of reduced speed.

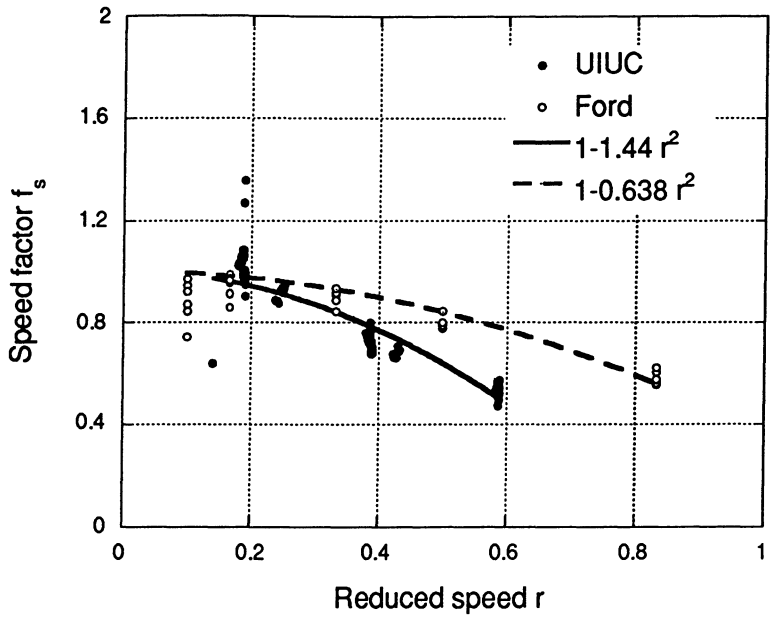

Figure 3.24 Speed adjustment factor as function of compressor speed.

3.6.4 Final Semi-empirical Compressor Model

For the sake of clarity we will summarize all of the equations here. The three residual equation used in the system model are as follows.

$$\dot{m}_{in} = \dot{m}_{comp} \tag{3.94}$$

$$\dot{m}_{out} = \dot{m}_{comp} \tag{3.95}$$

$$0 = h_{out,pred} - h_{out} \tag{3.96}$$

The mass flow rate is determined from the following equations.

$$\dot{m}_{comp} = \eta_{v,pred}\, \rho_{in}\, \dot{N}\, Vol_d \tag{3.97}$$

where

$$\eta_{v,pred} = \left(1 - b_2\left(\frac{\dot{N}}{\dot{N}_{ref}}\right)^2\right)\left(\frac{P_{out}}{P_{in}}\right)^{-c} \tag{3.98}$$

b_2 = 1.442 for the UIUC data

b_2 = 0.638 for the Ford data

c = 0.25

Vol_d = 1.7×10^{-4} m^3

The predicted outlet enthalpy is calculated from the following equations. The predicted polytropic exponent is

$$n_{comp,pred} = a_o + a_1 r. \tag{3.99}$$

where a_o = 1.128

a_1 = 0.107

The pressure exponent is

$$n_p = \frac{n_{comp,pred} - 1}{n_{comp,pred}}. \tag{3.100}$$

The predicted outlet temperature is

$$T_{out,pred} = T_{in}\left(\frac{P_{out}}{P_{in}}\right)^{n_p} \tag{3.101}$$

The predicted outlet enthalpy is calculated from the predicted outlet temperature and the outlet pressure.

$$h_{out,pred} = h\left(T_{out,pred}, P_{out}\right) \tag{3.102}$$

Finally, the compressor work is determined from the heat transfer fraction,

$$\dot{W}_{comp} = \frac{\dot{m}_{comp}\left(h_{out,pred} - h_{in}\right)}{1 - f_Q} \tag{3.103}$$

where $f_Q = 0.246$.

Figure 3.25 through 3.28 compare the predicted and observed mass flow rate, compressor power, exit temperature, and enthalpy change, respectively. The agreement between model predictions and the corresponding measured values is within experimental error. Thus, we conclude that a simple semi-empirical model with only five coefficients can adequately represent compressor performance over a wide range of inlet condition, exit condition, and compressor speed. The model performs well in terms of all three of the variables required for system modeling; namely, mass flow rate, compressor power and exit enthalpy.

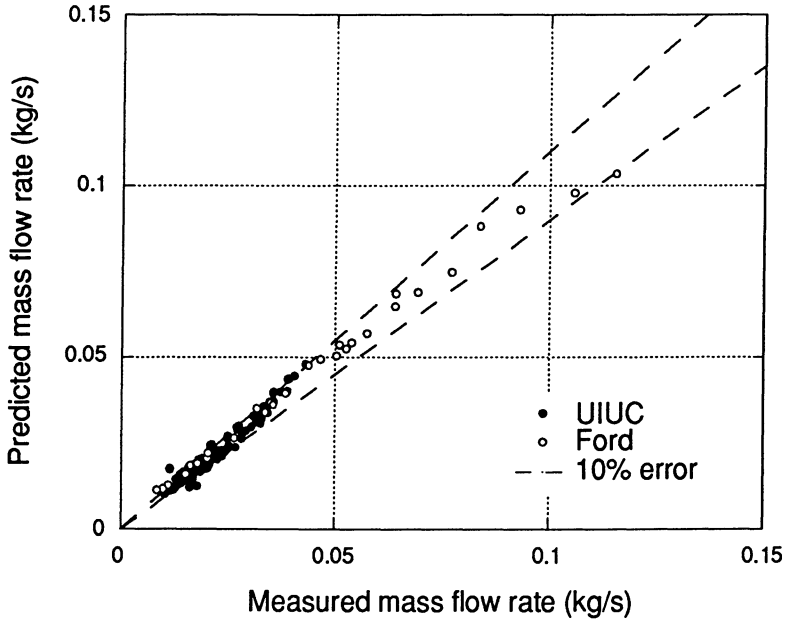

Figure 3.25 Comparison of predicted and measured mass flow rate.

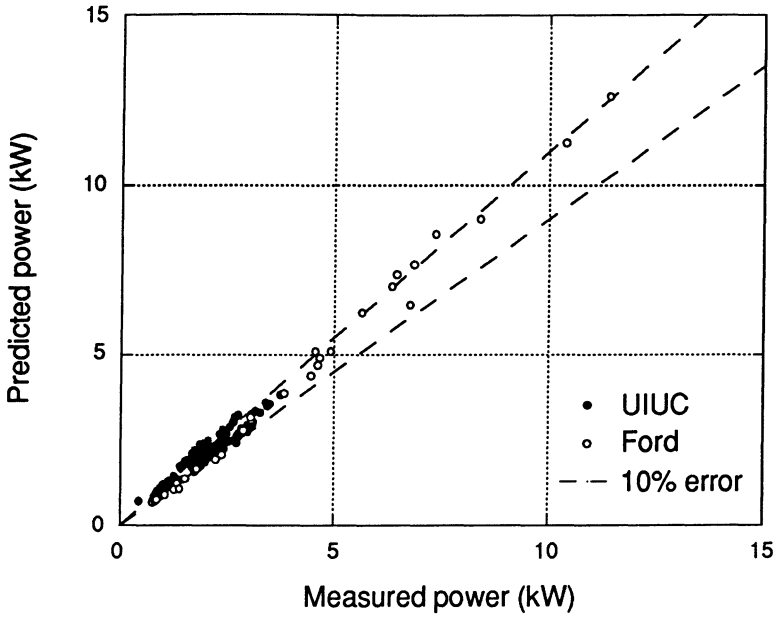

Figure 3.26 Comparison of predicted and measured compressor power.

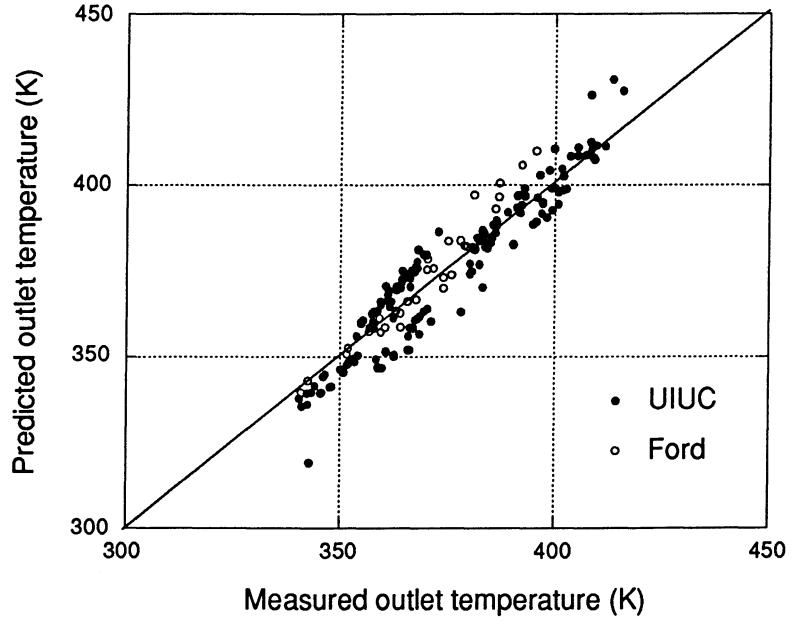

Figure 3.27 Comparison of predicted and measured outlet temperature.

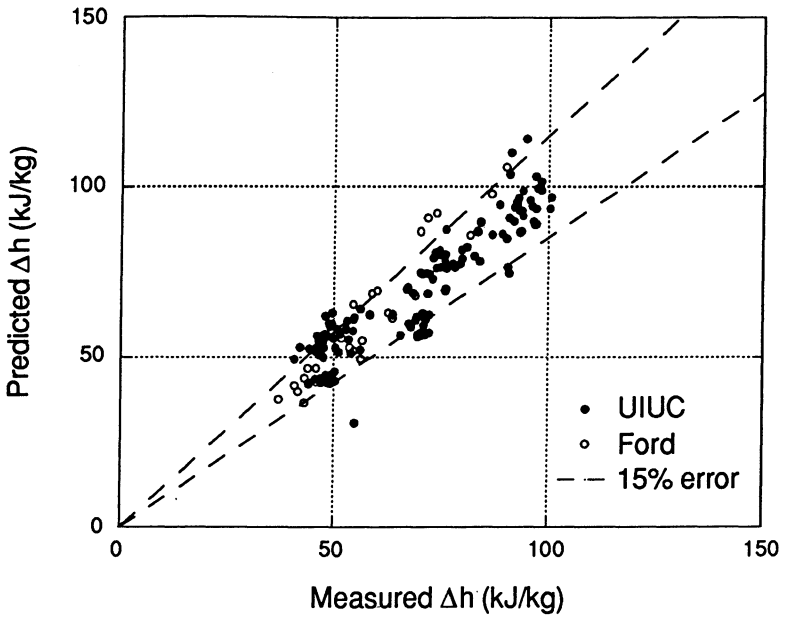

Figure 3.28 Comparison of predicted and measured enthalpy change.

3.6.5 Disengaged Clutch Model

When the compressor shuts off ($\dot{N}$= 0), we assume that it is similar to a valve closing and there is no flow between inlet and outlet. The mass flow rate and compressor power are exactly equal to zero. Equations 3.94-3.95 become

$$\dot{m}_{in} = 0 \tag{3.104}$$

$$\dot{m}_{out} = 0 \tag{3.105}$$

Because there is no refrigerant flow through the compressor, the inlet and outlet refrigerant temperature are only linked by conduction through the compressor shell. From studying experimental data, we concluded that this rate of conduction is fairly small, and the inlet and outlet refrigerant temperatures basically become decoupled after shutdown. The inlet compressor temperature becomes a function of the accumulator outlet conditions. A thermal time constant is used to determine the outlet compressor temperature.

$$\frac{T_{out} - T_{room}}{T_{initial} - T_{room}} = \exp\left(\frac{t}{\tau_{comp}}\right) \tag{3.106}$$

where

$$\tau_{comp} = 724.1 \text{ s}$$

The thermocouple which measures the outlet compressor temperature is midway between the compressor and condenser. We do not model this refrigerant line in our system model. This time constant simulates the rate at which this refrigerant cools off.

When the clutch is disengaged, we no longer have a closed loop of equations because the compressor does not allow any refrigerant flow (Section 3.1). Equations 3.104 - 3.106 become inputs to the model rather than equations solved simultaneously.

3.7 Orifice Tube Model

The conservation of mass and the conservation of energy equations for the orifice tube are quasi-steady-state. The inlet and outlet mass flow rates are equal, and they are equal to the orifice-tube mass flow rate determined from the inlet pressure, outlet pressure, and inlet enthalpy. The orifice tube has zero shaft work and is assumed to be adiabatic; therefore, the inlet enthalpy is equal to the outlet enthalpy. (Here, the term "outlet enthalpy" refers to that point downstream of the orifice tube at which all of the excess kinetic energy has been dissipated by friction.) The orifice tube equations thus are

$$\dot{m}_{in} = \dot{m}_{orifice} \tag{3.107}$$

$$\dot{m}_{out} = \dot{m}_{orifice} \tag{3.108}$$

$$h_{in} = h_{out} \tag{3.109}$$

The same three equations are used for the steady-state solution and transient solution. The only correlation needed for this model is the orifice-tube mass flow rate as a function of inlet and outlet parameters.

3.7.1 Orifice Tube Mass Flow Rate Correlation

The mass flow rate correlation was determined by Hrnjak (1998) and is valid for the standard orifice tubes found in automotive air-conditioning systems as summarized in Table 3.4

below. The geometry inputs into the model are the orifice tube length (L) and diameter (d). The orifice tube cross-sectional area ($A_{orifice}$) is determined from the diameter.

Orifice Tube	nominal diameter (mm)	length (mm)
brown	1.22	38.4
green (gray)	1.32	38.4
orange	1.45	38.4
red	1.55	38.4
blue	1.70	38.4

Table 3.4 Orifice tubes used in automotive air-conditioning systems.

The orifice-tube model is semi-empirical with coefficients determined from laboratory data. This laboratory data covers all inlet flow regimes of interest: subcooled liquid, two-phase, and superheated vapor. The flow is assumed to be choked and the refrigerant is pure R134a with no oil. The empirical fit to the data agrees to the measured value with an accuracy of ±10 %.

When the inlet is subcooled, a modified orifice flow equation is used.

$$\dot{m}_{sub} = c_1 A_{orifice} \sqrt{2\rho_f (P_{in} - P_{sat} k)} \tag{3.110}$$

P_{sat} is the saturation pressure calculated from the inlet temperature, and ρ_f is the saturated liquid density at the inlet temperature. The empirical coefficient, k, is determined from the following equation.

$$k = c_2 \left(\frac{S + 2K}{T_{crit}} \right)^{c_3} + \left(\frac{D}{1\ mm} \right)^{c_4} \left(\frac{L}{1\ mm} \right)^{c_5} + c_6 \left(\frac{L}{1\ mm} \right) + c_7 \left(\frac{P_{crit} - P_{out}}{P_{crit}} \right) \tag{3.111}$$

P_{crit} and T_{crit} are the critical pressure and temperature, respectively. S is the amount of subcooling at the orifice tube inlet in Kelvin.

When the inlet is vapor, the Fanno flow equation is used.

$$\dot{m}_{fanno} = P_{in} A_{orifice} M \sqrt{\frac{\gamma}{R T_{in}}} \tag{3.112}$$

M is the Mach number, γ is the specific heat ratio, and R is the gas constant for R134a (82.29 J/kg-K). The Mach number is determined from the Fanno flow relationship shown below.

$$\frac{4fL}{D} = \frac{1-M^2}{\gamma M^2} + \left(\frac{\gamma+1}{2\gamma}\right)\ln\left[M^2\left(\frac{\gamma+1}{2+(\gamma-1)M^2}\right)\right] \tag{3.113}$$

Here, f is the Fanning friction factor which was determined to be 0.008 through nitrogen flow tests. This equation cannot be explicitly solved for the Mach number. To simplify the calculation, we developed a curve fit for the Mach number for R134a ($\gamma = 1.13$).

$$M = 0.093931\left(\frac{4fL}{D}\right)^{-0.6385} \tag{3.114}$$

When the inlet is two-phase, the mass flow rate is determined from a quality (x_{in}) weighted average between the pure liquid flow rate equation (Equation 3.107) and pure vapor flow rate equation (Equation 3.109).

$$\dot{m}_{orifice} = \left(\dot{m}_{sub}(1-x_{in})^{c_8} + \dot{m}_{fanno}x_{in}^{c_9}\right) \tag{3.115}$$

If the refrigerant is pure liquid, then $x_{in} = 0$; if the refrigerant is pure vapor, then $x_{in} = 1$. The values of the empirical coefficients for the model are listed in Table 3.5.

Coefficient	Value	Coefficient	Value
c_1	0.265249714	c_6	0.0000218672
c_2	-0.11497189	c_7	0.0362919356
c_3	0.041465780	c_8	1.7562517005
c_4	-0.006578346	c_9	0.4970578018
c_5	0.0039000541		

Table 3.5 Empirical coefficients for the orifice tube model.

3.7.2 Comparison Between the Mass Flow Rate Correlation and Experimental Data

Figure 3.29 shows a comparison between the model predictions and experimental data using our experimental facility. Rubio-Quero, Collins, and Hemami obtained the data for the brown, green, and orange orifice tubes, respectively. In all of the cases, the refrigerant at the inlet is subcooled liquid. The model significantly overpredicts the mass flow rate for the brown and green orifice tubes. The model overpredicts the mass flow rate for the orange orifice tube data as well, but the error is within the tolerance of the model (±10%).

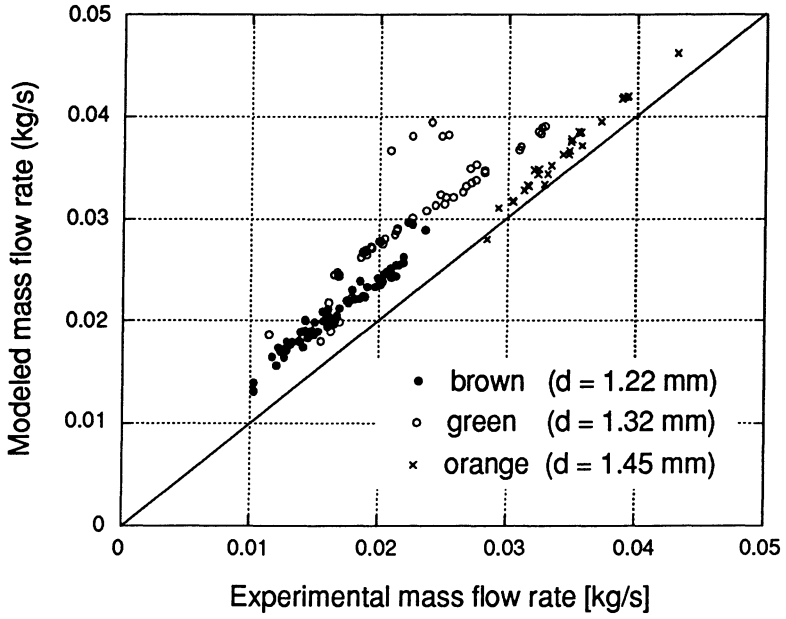

Figure 3.29 Comparison of experimental data with the orifice tube model using the correct diameters.

To understand the differences between the data obtained with the brown, green, and orange orifice tube, we must review the chronology of the data. The brown-orifice-tube data were obtained in the spring of 1995, and the green-orifice-tube data were obtained in the fall of 1996. The orange-orifice-tube data were obtained in the summer of 1997. Also, in the summer of 1997, all of the data were compared with the orifice tube model. Because the most recent data agrees well with the model while the earlier data earlier does not agree well, we can assume that the problem causing the discrepancy in the previous data has been corrected.

There appear to be two possible problems which could contribute to the discrepancy between the experimentally measured mass flow rate and the predicted mass flow rate. One possible problem is a systematic error in one or more of the measurement devices. The second

possible problem is that since the inlet pressure and temperature are not measured directly in front of the orifice tube, a restriction in the refrigerant pipe could occur between the measurement devices and the orifice tube causing a reduction in the mass flow rate.

First, we shall examine the extent to which errors in the experimental measurements could explain the apparent discrepancy. The measurements which are inputs to the model are (a) the inlet orifice tube pressure, (b) the inlet orifice tube temperature, and (c) the outlet orifice tube pressure, and the model predicts (d) the mass flow rate. In our experimental facility as shown in Figure 3.3 these four values correspond, respectively, to (a) the pressure measured at the liquid venturi, (b) the temperature measured at the liquid venturi, (c) the pressure measured at the inlet evaporator, and (d) the mass flow rate measured by the Micro Motion™ flow meter. The calibrations of these instruments did not change significantly over the two year period when we obtained the orifice tube data.

To asses the extent that experimental measurements can affect the model prediction, we determined the amount of error in the measurements required for the experimental mass flow rate to agree with the predicted mass flow rate. As a reference point, we first note that the model over predicts the mass flow rate for the brown orifice tube data by roughly 20%. First, we can eliminate errors in the mass flow rate measurement because the accuracy of the calibration of the Micro Motion™ flow meter is ± 0.2 % (Weston 1996). The only way that large errors could be reported by the mass flow meter is if the refrigerant is not subcooled liquid. However, the fact that the refrigerant is subcooled liquid is visually verified using a sightglass between the Micro Motion™ and the liquid venturi.

Turning, our attention to the three variables which are inputs to the model, we first consider the outlet pressure (P_{out}) which only affects the mass flow rate prediction through Equation 3.111. Changes in the downstream pressure have a very small effect on mass flow rate because the flow is essentially choked. In the data obtained with the brown orifice tube, P_{out} ranges from 0.14 - 0.30 MPa (21 - 44 psi). If all outlet pressures were in fact 0 Pa, the predicted mass flow rate only changes by an average of 0.4%.

The remaining input variables, inlet pressure and inlet temperature, affect mass flow rate to approximately the same degree, primarily because the saturation pressure in Equation 3.110 is a function of inlet temperature. Decreasing P_{in} by 7%, eliminates the systematic error observed for the brown orifice tube. A 7% error corresponds to a 0.05 - 0.08 MPa (7 - 12 psi) error. As mentioned above, the inlet orifice tube pressure is measured at the liquid venturi. A partially redundant pressure measurement is obtained upstream of the liquid venturi at the condenser outlet. If a 7% error exists in the liquid venturi pressure measurement, there should be a large difference between the pressure at the condenser outlet and the liquid venturi. For the data obtained with the brown orifice tube, the average difference in pressures is 8700 Pa

(1.3 psi). For the orange-orifice-tube data, the average difference in pressures is 8000 Pa (1.2 psi). Since the orange orifice tube and brown orifice tube pressure difference are comparable, we can eliminate errors in the inlet pressure measurement as causing the discrepancy between the measured and predicted mass flow rate.

Changing the orifice tube inlet temperature affects the predicted mass flow rate primarily by changing the saturation pressure (P_{sat}) in Equation 3.110. For the brown orifice tube, the inlet temperature must be increased by 3 K (5.4 F) to remove the systematic error in the predicted mass flow rate. The inlet temperature is between 296 - 306 K (73 - 91 F). Again, there is a redundant temperature measurement at the outlet of the condenser. For the brown orifice tube, the average difference in temperature is 0.48 K (0.9 °F). For the orange orifice tube, the average difference in temperature is 0.87 K (1.5 °F). Since the average temperature difference is consistently less than 1 K, we assume that the inlet temperature data cannot cause the error.

From the above analysis, we concluded that measurement errors did not cause the discrepancy between the predicted and modeled mass flow rates. Another possible problem could be in the piping. If a restriction in the pipe occurred between the measurement devices summarized above and the orifice tube, then the mass flow rate could be less than the predicted mass flow rate. Many changes were made in the test facility regarding the refrigerant pipe around the orifice tube between the fall of 1996 and the summer of 1997 (Wandell 1997). Wandell removed the refrigerant pipe between the liquid venturi and the evaporator which contained initially the brown orifice tube and later the orange orifice tube in fall of 1996. Wandell installed two parallel pipes (Figure 3.3). One contains the orifice tube and the other contains an electronic expansion valve (EEV). Ball valves were installed at the inlet an outlet of each of these parallel lines so the refrigerant flow could be switched between the two metering devices without discharging the entire loop of refrigerant. This current configuration which contains the orange orifice tube apparently does not substantially restrict the refrigerant flow.

One final possibility is that the orifice tube was clogged with debris from the circulating refrigerant. We located the original green orifice tube, and no evidence of clogging was apparent.

The data we obtained from the current test facility configuration agrees well with the orifice tube model. We cannot say for certain why the model overpredicts the experimental data for the brown and green orifice tubes. Because of the changes to the piping in the test facility, the opportunity to resolve this issue has been permanently lost.

We set the mass flow rate from the model equal to the mass flow rate in the experimental data to solve for a theoretical diameter. These empirical diameters are reported in

Table 3.6. Hrnjak reports that there is a variation in the actual diameters of the orifice tubes compared with the nominal diameter. However, the empirical diameters of the brown and green orifice tubes do not realistically fit in this range. The empirical diameter for the orange orifice tube is realistic. Figure 3.30 show a comparison between the experimental data and the model using the theoretical diameter.

In order to make use of the extensive data obtained with the brown and green orifice tube, the empirical diameter is used in all of the system model comparisons with data instead of the nominal diameter.

Orifice Tube	Nominal diameter (mm)	Empirical diameter (mm)
brown	1.22	1.097
green (gray)	1.32	1.156
orange	1.45	1.423

Table 3.6 Nominal and empirical orifice tube diameters.

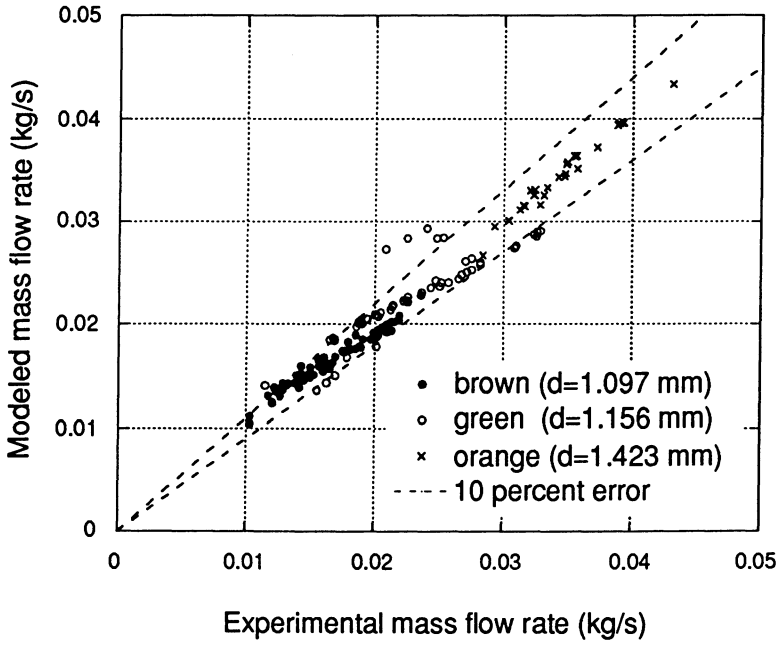

Figure 3.30 Comparison of experimental data with the orifice tube model using the corrected diameters.

3.7.3 Extensions to the Orifice Tube Mass Flow Rate Correlation

The model by Hrnjak only treats the steady-state operating conditions. We needed to extend the model to work in start-up and shut-down conditions when the flow is not choked. We must be able to predict when the flow becomes choked and nonchoked mass flow rate.

When the inlet pressure equals the outlet pressure, there is no flow through the orifice tube. As the inlet pressure drops, the mass flow rate increases and it is dependent on the difference between the inlet and outlet pressures. As the pressure drops further, eventually the Mach number at the exit of the orifice tube will equal one and the flow becomes choked. At this point, as the outlet pressure decreases, the mass flow rate and the pressure at the exit of the orifice tube will remain basically constant.

If the fluid is an ideal gas, then the Fanno flow equations can be used to determine the pressure at which the flow just becomes choked. For simplicity, we will refer to this pressure are the choked flow pressure. This pressure depends on he inlet pressure, diameter, length, and friction factor. If the outlet pressure is less than the choked pressure, then the flow is choked. However, for two-phase flow it is not trivial to determine the pressure at which the flow chokes. A solution similar to the heat exchangers must be performed where the orifice tube is discretized and the conservation equations are applied to each section. This solution is more complex than is required for a system model, therefore we will use a simplified approach to determine when the flow becomes choked and the equation for the nonchoked flow.

The nonchoked mass flow rate through an unchoked orifice tube is approximated using the orifice equation.

$$\dot{m}_{sub} = C_d A_{orifice} \sqrt{2\rho(P_{in} - P_{out})} \tag{3.116}$$

For turbulent single-phase flow (Re > 10^4), the pressure drop to acceleration losses and entrance losses is

$$\Delta P_{entrance} = (1+K)\frac{\rho V^2}{2} \tag{3.117}$$

where K = 0.5 for sudden contractions from large to small tubes (Idelchik, 1994). The pressure drop to exit losses is (Idelchik, 1994)

$$\Delta P_{exit} = \left(1 + \frac{A_{orifice}}{A_{tube}}\right)^2 \frac{\rho V^2}{2}. \tag{3.118}$$

Because the orifice tube area is much smaller than the tube area, the ratio is approximately zero. For this limiting case, Idelchik gives the discharge coefficient to be 0.667.

Instead of trying to predict the two-phase critical conditions, we shall use Equation 3.116 whenever it is less than the mass flow rate predicted by Equation 3.115. This accomplishes a smooth transition between choked and nonchoked flow.

A further extension to the orifice tube model allows for the mass flow rate to be negative when the evaporator pressure is greater than the condenser pressure. The physical difference between the inlet and outlet of the orifice tube is the shape of the screens which prevent debris from clogging the orifice tube. Hrnjak reports that the screens do not effect the mass flow through the orifice tube and the model is also valid for backwards flow.

3.8 Accumulator Model

The accumulator is basically a tank between the evaporator and compressor which prevents liquid from flowing into the compressor. Figure 3.31 show the internal geometry of the accumulator. As the refrigerant enters the accumulator, the inlet tube directs the refrigerant to the top of the accumulator (Point 1) and then down the sides of the accumulator. The liquid then remains at the bottom. Vapor enters the exit tube at Point 2. The exit tube loops down towards the bottom of the accumulator where there is an oil return hole. This hole draws in a small amount of the liquid/oil mixture, so oil can be returned to the compressor.

An accumulator is used in clutch-cycling/orifice-tube systems. During clutch-cycling conditions, the level of liquid in the accumulator is changing. When the compressor clutch disengages, the refrigerant initially migrates from the condenser to the evaporator because of the pressure difference. The evaporator cannot physically hold all of the system charge, so the refrigerant subsequently flows out of the evaporator and fills the accumulator. When the compressor is turned on again, the suction-line pressure decreases rapidly causing the refrigerant in the accumulator to begin to boil. The refrigerant vaporization causes the temperature of the liquid to drop requiring heat transfer with the ambient air to sustain the evaporator of liquid. The compressor will cycle off when the evaporator pressure decreases below a set point. At this time, the accumulator starts to fill with liquid refrigerant. During more extreme operating conditions (such as the initial pulldown) the clutch is engaged for a long period of time and all of the liquid evaporates from the accumulator. During less extreme

operating conditions, the clutch cycles more frequently and liquid refrigerant can exist in the accumulator at all times.

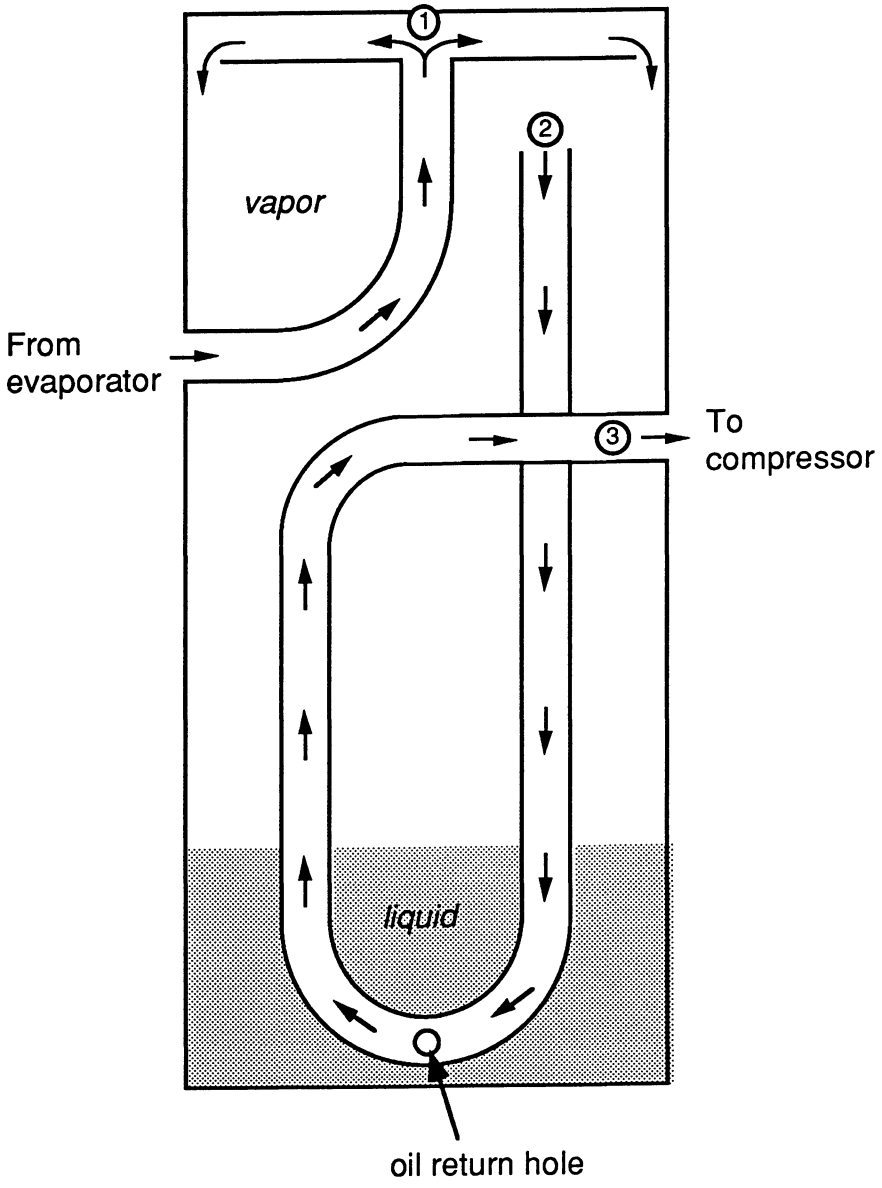

Figure 3.31 Internal accumulator geometry.

The accumulator should be sized to contain all of the refrigerant in liquid form. After shutdown, all of the charge migrates to the coldest part of the system. Immediately after shutdown, the evaporator is the coldest part of the system. The evaporator is in the cabin and can later heat up with the cabin temperature. As the evaporator heats up, most of the refrigerant migrates to the accumulator. If the accumulator is undersized, it entirely fills with liquid. Because of the geometry of the accumulator (Figure 3.31) once the accumulator has filled with liquid, liquid exits to the compressor before it exits to the evaporator. When the compressor is turned on, the liquid flowing into the compressor can remove the oil required for lubrication.

3.8.1 Steady-state Accumulator Model

We have modeled the accumulator as a single cell in the system. We will investigate two different operating conditions. The first condition occurs when the accumulator is filled with superheated vapor. The second condition occurs when the accumulator is filled with two-phase refrigerant.

When the accumulator is filled with superheated vapor it is similar to a heat exchanger. The heat transfer between the ambient air and the refrigerant in the accumulator is very small. Rubio-Quero's data set was run at a low-charge condition where the accumulator was completely vapor. From these data, we conclude there is no enthalpy change across the accumulator when it contains vapor refrigerant.

When two-phase refrigerant is in the accumulator, a steady-state condition exists when the amount of liquid and vapor refrigerant in the accumulator remain constant with respect to time. The liquid in the accumulator must be evaporating at exactly the same rate as liquid flows into the accumulator. This requirement for steady-state operation rarely occurs during normal operation. However, when the rest of the system has apparently reached a steady-state condition, the rate of evaporation is generally small enough that we can assume a quasi-steady-state condition exists.

The following equations are used to model a quasi-steady-state accumulator.

$$0 = \dot{m}_{in} - \dot{m}_{out} \tag{3.119}$$

$$0 = P_{in} - P_{out} - \Delta P_{fric} \tag{3.120}$$

$$0 = h_{out} - h_{out,calc} \tag{3.121}$$

where

$$h_{out,calc} = h_g(P_{in}) \quad \text{for } x_{in} \leq 1 \qquad (3.122)$$
$$h_{out,calc} = h_{in} \quad \text{for } x_{in} > 1$$

The frictional pressure drop and minor losses are lumped into one empirical parameter, ΔP_{fric}, as discussed in Section 3.8.3.

3.8.2 Transient Accumulator Model

The accumulator is also modeled as a single cell in the transient model. The standard conservation of mass, energy, and momentum equations apply. With the additional constraint equation, the equations are

$$\frac{dm_{acc}}{dt} = \dot{m}_{in} - \dot{m}_{out} \qquad (3.123)$$

$$\frac{d(mu)_{acc}}{dt} = \dot{m}_{in}h_{in} - \dot{m}_{out}h_{out} - UA_{acc}(T_{acc} - T_{ambient}) \qquad (3.124)$$

$$0 = P_{in} - P_{out} - \Delta P_{fric} \qquad (3.125)$$

$$0 = h_{out} - h_{out,calc} \qquad (3.126)$$

where

$$h_{out,calc} = h_g(P_{in}) \quad \text{for } x_{in} \leq 1 \qquad (3.127)$$
$$h_{out,calc} = h_{in} \quad \text{for } x_{in} > 1$$

These equations are similar to the steady-state form except for the transient term in the conservation of mass and energy equations. The state variables are m_{acc}, P_{in}, h_{out}, and $\dot{m}_{out}$. In Section 3.84 we summarize how we determine the accumulator heat transfer coefficient, UA.

In the standard heat exchanger equations (Section 3.3) the outlet enthalpy is set equal to the cell enthalpy. This assumption is not valid for the accumulator because the refrigerant at the outlet of the accumulator is always vapor regardless of the cell properties in the accumulator. As a result, we include an additional equation (Equation 3.127) and an additional variable (m_{acc}) to correctly model the accumulator.

Several additional equations are required for the accumulator model are. The density of the refrigerant in the accumulator is calculated from the refrigerant mass and the accumulator volume.

$$\rho_{acc} = \frac{m_{acc}}{Vol_{acc}} \tag{3.128}$$

The derivative in Equation 3.6 is calculated from the following equations.

$$\frac{d(mu)_{acc}}{dt} = m_{acc}\frac{du_{acc}}{dt} + u_{acc}\frac{dm_{acc}}{dt} \tag{3.129}$$

where

$$\frac{du_{acc}}{dt} = \frac{1}{Vol_{acc}}\frac{dm_{acc}}{dt}\frac{\partial u}{\partial \rho} + \frac{dP_{acc}}{dt}\frac{\partial u}{\partial P} \tag{3.130}$$

The accumulator volume includes the volume of the accumulator itself plus the refrigerant line between the evaporator and the accumulator and the accumulator and the compressor.

The results from the steady-state model are used as starting conditions for the transient model. During steady-state operation, we assume that the accumulator cell properties are equal to the inlet accumulator properties.

3.8.3 Pressure Drop Correlations

The pressure drop in the accumulator is due to frictional losses and minor losses in the entrance tube and exit tubes. An empirical parameter was determined for the pressure drop similarly to the evaporator and condenser. Different correlations were determined depending on whether the inlet refrigerant is two-phase or superheated. The data of Rubio-Quero, Collins, and Hemami were used to determine an empirical correlation for pressure drop.

$$\Delta P_{fric} = 1.13\times10^{9}\frac{\dot{m}_{in}}{\rho_{in}^{2}} \qquad \text{for } x_{in} < 1 \tag{3.131}$$

$$\Delta P_{fric} = 1.51\times10^{9}\frac{\dot{m}_{in}}{\rho_{in}^{2}} \qquad \text{for } x_{in} > 1$$

To prevent a discontinuity around $x_{in} = 1$, the equations are weighted between $x_{in} = 0.95$ and $x_{in} = 1$. Figure 3.32 provides a comparison between the model and the experimental data.

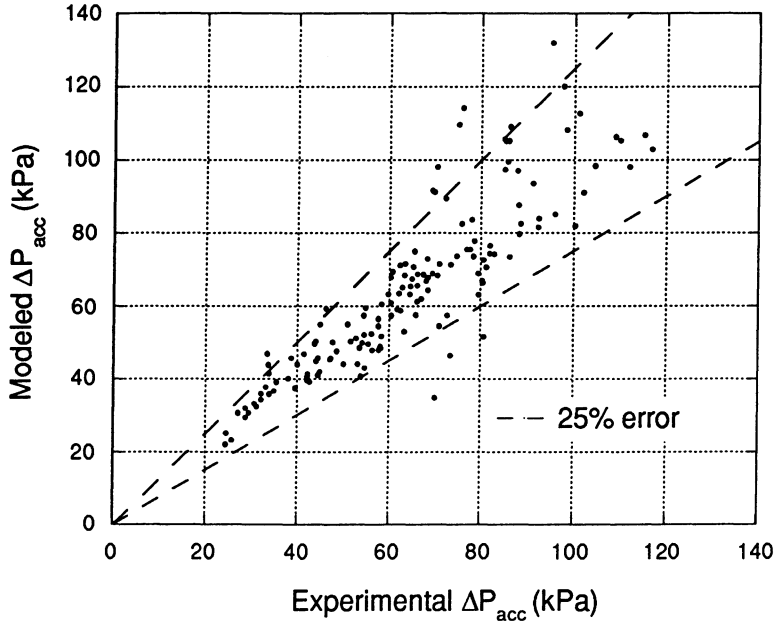

Figure 3.32 Comparison between predicted accumulator pressure drop and experimental accumulator pressure drop.

3.8.4 Heat Transfer Coefficient

Heat transfer between the accumulator refrigerant and the ambient air causes the refrigerant to evaporate. The outside surface of the accumulator is smooth and the heat transfer between the air and the surface is caused by natural convection. The interior of the accumulator is also smooth. The configuration of the entrance tube (Figure 3.31) causes the inlet refrigerant to flow down the inside of the walls which increases the heat transfer coefficient. The heat transfer coefficient is a function of the following parameters:

1) Liquid level in the accumulator,
2) Inlet quality,
3) Inlet mass flow rate,
4) Refrigerant properties,
5) Air properties, and
6) Accumulator wall properties

Currently, we use a constant value for the accumulator heat transfer coefficient. This heat transfer coefficient is calculated from the steady-state conditions.

3.9 Solution Technique

This section summarizes the solution techniques for the steady-state and transient models.

3.9.1 Steady-state Solution

The steady-state solution is needed to provide initial conditions for the transient solution and to verify the accuracy of the steady-state model. The steady-state model consists of 3 equations and 3 unknowns per cell. The unknowns are the enthalpy, pressure, and mass flow rate at the inlets and outlets of the cells (Figure 3.2). The governing equations are the conservation of mass, energy, and momentum equations. The relevant equations are summarized in Sections 3.2 - 3.8. For n cells, a set of 3n simultaneous equations are written in the following form.

$$\mathbf{F(x)} = \mathbf{0} \tag{3.132}$$

A Newton-Raphson technique (Press et al.1992) is used to solve the equations.

The Newton-Raphson algorithm must be provided with initial guesses for the unknowns, **x**. The Jacobian matrix is then calculated numerically.

$$J_{ij} = \frac{\partial F_i}{\partial x_j} \tag{3.133}$$

From the Jacobian, we solve the linear system of equations for $\delta\mathbf{x}$, which will set the equations directly equal to zero.

$$\mathbf{J} \cdot \delta\mathbf{x} = -\mathbf{F} \tag{3.134}$$

New next iteration of x is

$$\mathbf{x}_{new} = \mathbf{x}_{old} + \delta\mathbf{x}. \tag{3.135}$$

The vector x is accepted as the solution when the maximum residual (maximum value of **F**) is below a user specified tolerance or else the maximum change in the solution vector **x** is below a user specified tolerance.

If the initial guesses are poor, the above method may not converge. To avoid this situation the magnitude of the residual vector is evaluated at each step.

$$f = \frac{1}{2}\mathbf{F}\cdot\mathbf{F} \tag{3.136}$$

If the full Newton-Raphson step, $\delta\mathbf{x}$ does not reduce f then we backtrack along the Newton direction until we find an acceptable step size. This method can still fail by landing on a local minimum of f. A good initial guess must still be provided for the best convergence.

3.8.2 Transient Solution

The transient model consists of 4 transient equations per cell when we include the heat exchanger wall conservation of energy (Equation 3.10). If we do not include this equations, the transient model contains 3 transient equations per cell. In addition, we have 3 algebraic equations describing the compressor and 3 algebraic equations describing the orifice tube. A system of differential and algebraic equations has the following form.

$$\mathbf{F}(t, \mathbf{y}, \mathbf{y}') = 0 \tag{3.137}$$

$$\mathbf{y}(t_0) = \mathbf{y_0} \tag{3.138}$$

$$\mathbf{y}'(t_0) = \mathbf{y_0'} \tag{3.139}$$

Equation 3.6 is the vector of equations and Equations 3.7 and 3.8 are the initial conditions.

The solver we used is a public domain program DASSL (differential-algebraic system solver) (Brenan et al., 1996). DASSL is based on the algorithms developed by Gear (1971) for stiff systems.

The algorithms in DASSL are only briefly summarized here. The derivatives in Equation 3.6 are replaced with a kth order Backwards Difference Formula (BDF).

$$y_n = \sum_{i=1}^{k} \alpha_{ni} y_{n-i} + h_n \beta_{n0} y_n' \tag{3.140}$$

h_n is the step size. α_{ni} and β_{n0} are coefficients specific to the algorithm. The resulting equations are solved using a Newton-Raphson method similar to the one summarized in Section 3.9.1. A good initial guess for y_n and y_n' are obtained from an explicit equation called the predictor formula.

DASSL uses a variable step size (h_n) and variable order (k) method. The new order is determined by calculating the error if the previous steps had been taken at a constant step size with the current order k and the order k-2, k-1, and k+1. The new order, k_{n+1}, is lowered if the error increases as k increases and raised if the error decreases with k. Using the new order k_{n+1}, the new stepsize is chosen so the error estimate based on taking constant stepsizes, Δt_{n+1}, satisfies the error test. The coefficients α_{ni} and β_{n0} depend on the stepsize and the order.

From the author's experience, we can conclude that DASSL is an extremely robust program. However, it is not very efficient. It is extremely useful for developing models for design purposes but it is too slow to apply to a model for controls or any real time application.

When solving differential equations, one must take care to make sure no discontinuities exist in the equations. Discontinuities in the refrigerant properties or the correlations for friction factors or heat transfer coefficients will cause DASSL to take extremely small time steps and possibly fail. Removing the discontinuities from the correlations will also improve the convergence of the steady-state code.

Chapter 4
Steady-state Model Validation

In Chapter 3, we summarized the overall organization of the model, the steady-state equations, and the steady-state solution technique. Also, we validated the correlations for the heat transfer coefficient, friction factor coefficient, mass flow rates, and power with steady-state data. In this chapter, we shall combine the component models into a steady-state system model. This system model will be validated with experimental data.

4.1 Model Validation

As shown in Chapter 3, the steady-state model provides the appropriate method for validating component models. In addition, the steady-state model provides the starting point for the transient model once the system is fully in operation. The steady-state model is the same as the transient model except that the time derivatives are set to zero. The orifice-tube and compressor models are exactly the same because these models are quasi-steady-state. In the heat exchanger and accumulator models, the time derivatives in the conservation of energy equation and the conservation of mass equation are set equal to zero. The conservation of energy equation for the heat exchanger wall is not needed in the steady-state model.

The model is compared with steady-state data obtained by Rubio-Quero (1995), Collins (1996), and myself using a facility specifically designed to test mobile air-conditioners. The primary difference between the three data sets is the size of the orifice tube and amount of refrigerant mass in the system. The test facility and the associated data are discussed in detail in Section 3.2.

The steady-state equations are solved with a Newton-Raphson technique discussed in Section 3.9. The physical parameters which define the operating point of the system are

1) Evaporator inlet air temperature,
2) Condenser inlet air air temperature,
3) Ambient temperature,
4) Evaporator air mass flow rate,
5) Condenser air mass flow rate,
6) Compressor speed, and
7) Refrigerant mass.

It is very difficult to accurately predict the refrigerant mass in the two-phase regime, and as a result it is difficult to predict the amount of refrigerant mass in the system. Different two-phase void fraction correlations are summarized in Section 4.2. Instead of using refrigerant mass as an input to the model, we specified either the condenser subcooling or the evaporator superheat. The refrigerant subcooling at the condenser outlet is a good choice because predictions are very sensitive to the value selected. Section 4.1.1 summarizes the comparisons between the model predictions and data when subcooling is specified. To study the influence of selecting condenser subcooling as an input, in Section 4.2.2 we shall compare model predictions with the data using evaporator superheat as an input.

4.1.1 Results Obtained Using Condenser Subcooling as an Input

For these steady-state simulations, the only difference between the three data sets (Rubio-Quero, Collins, and Hemami) are the orifice-tube diameter and the refrigerant mass. The inputs to the steady-state model for this simulation are

1) Evaporator inlet temperature,
2) Condenser inlet air temperature,
3) Ambient temperature,
4) Evaporator air mass flow rate,
5) Condenser air mass flow rate,
6) Compressor speed, and
7) Condenser outlet refrigerant subcooling.

Figure 4.1 shows a comparison between the modeled mass flow rate and the experimental mass flow rate. The mass flow rates generally agree within 10%. During a steady-state operating condition, all of the mass flow rates at all points in the system is the same. Therefore, the mass flow rates at the orifice tube and the compressor must be equal. These mass flow rates are functions of the condenser pressure, evaporator pressure, condenser subcooling, and inlet compressor density.

Good agreement between the modeled and experimental mass flow rates suggest that we can expect good agreement between the modeled and experimental pressures. Figures 4.2 and 4.3 show comparisons between the predicted and experimental pressures for the condenser and evaporator, respectively. The experimental and predicted inlet condenser pressures agree within 10%. The experimental and predicted inlet evaporator pressures agree within 15%. Since the flow through the orifice-tube is choked, evaporator pressure has a very small effect

on the mass flow rate through the orifice tube. As a result, the evaporator pressure is difficult to predict because of the low correlation between evaporator pressure and system operation.

Next, we shall look at heat transfer and power comparisons for the system model. The heat transfer rate is computed by multiplying the refrigerant mass flow rate by the refrigerant enthalpy difference across a component. Figure 4.4 shows the comparison between the modeled and experimental condenser capacity. The system model agrees within approximately 15% of the data. The system model agrees within approximately 10% of the data for the evaporator capacity (Figure 4.5). We have good agreement between the predicted and experimental heat capacities which indicates that the heat transfer coefficients are accurate. The modeled compressor power is within approximately 10% of the experimental compressor power (Figure 4.6).

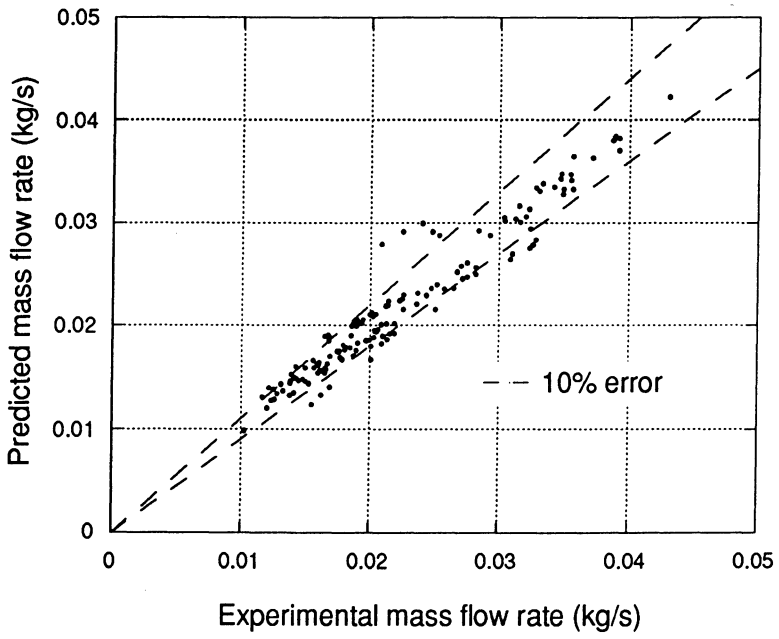

Figure 4.1 Mass flow rate validation (subcooling input).

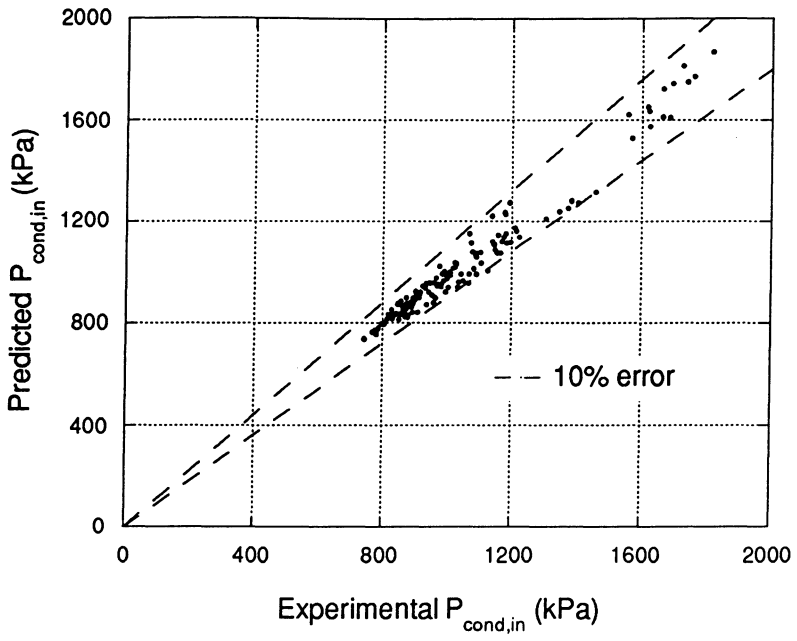

Figure 4.2 Inlet condenser pressure comparison (subcooling input).

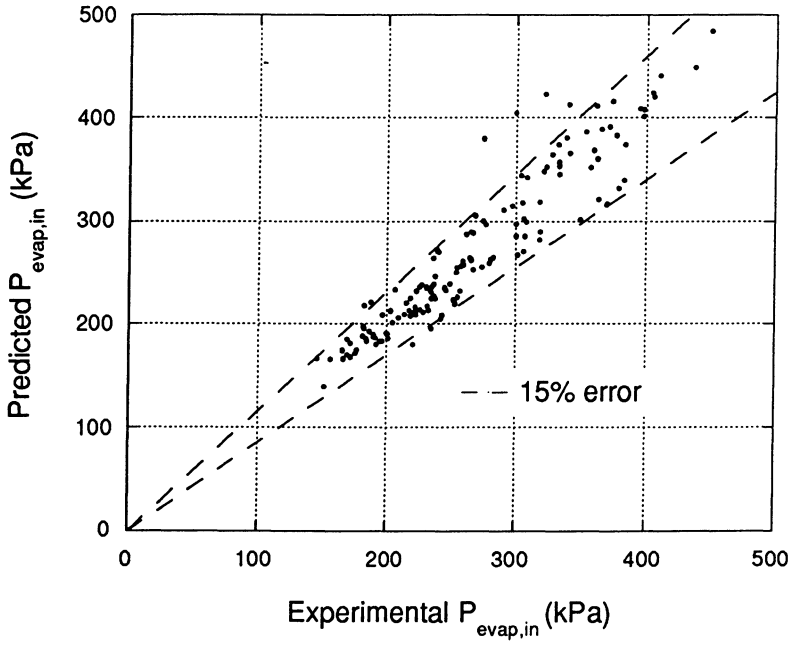

Figure 4.3 Inlet evaporator pressure comparison (subcooling input).

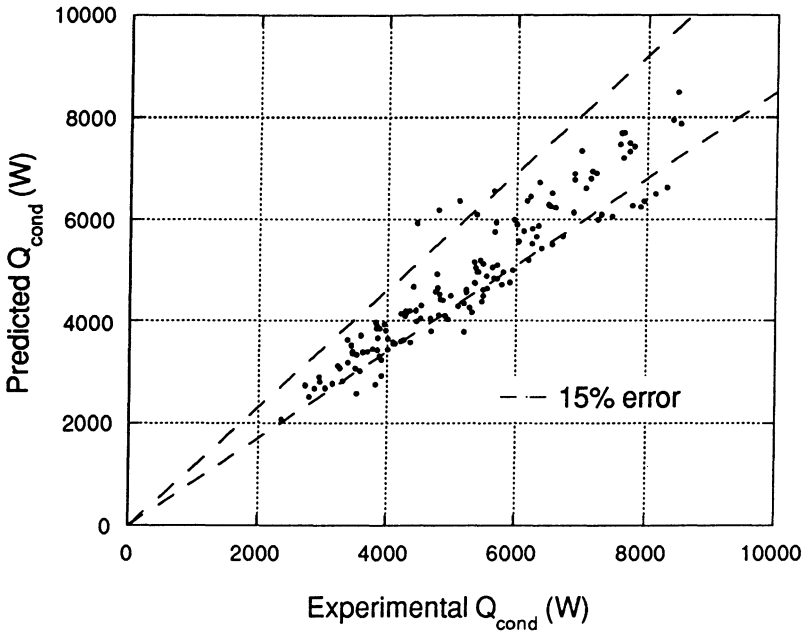

Figure 4.4 Condenser capacity comparison (subcooling input).

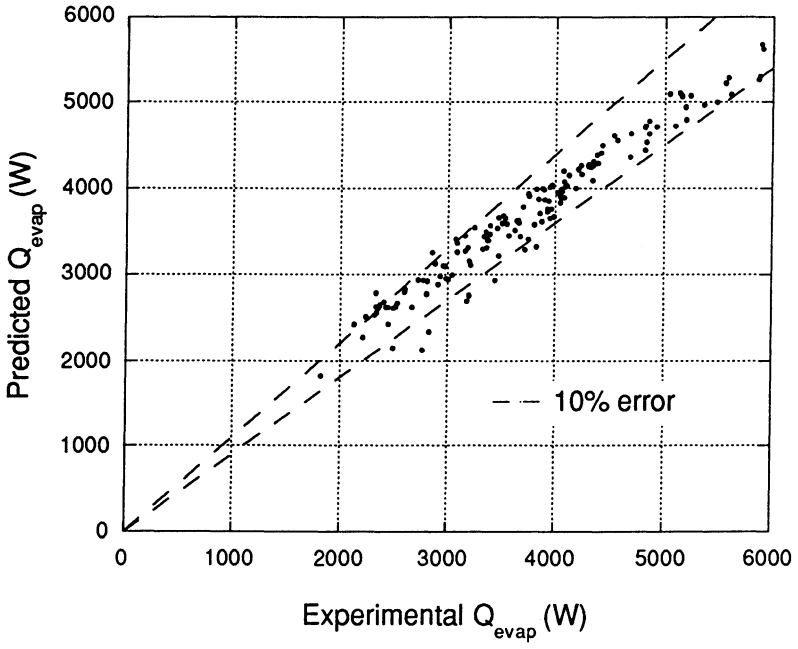

Figure 4.5 Evaporator capacity comparison (subcooling input).

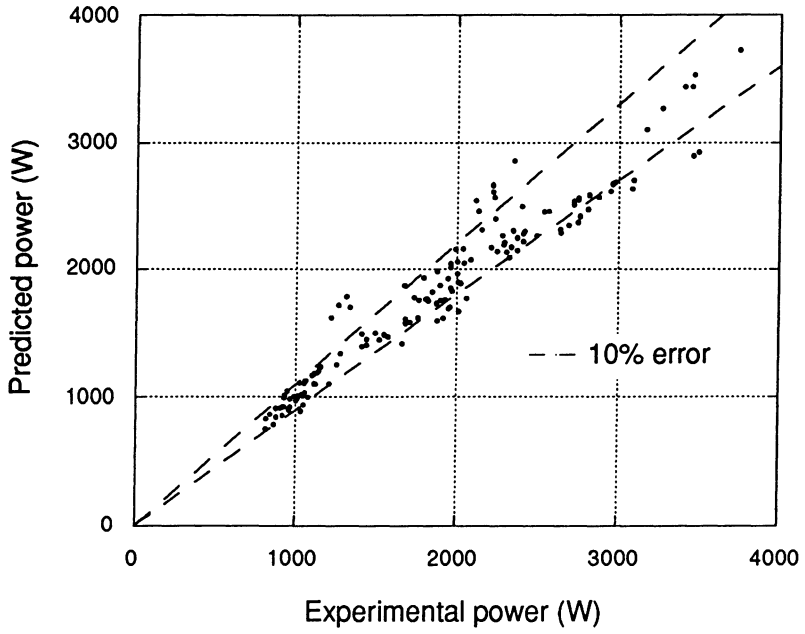

Figure 4.6 Compressor power comparison for the system model (subcooling input).

As just seen, Figures 4.1 - 4.6 provided an overview of some of the important system parameters. Figures 4.7 - 4.9 show comparisons between the predicted and experimental component pressure drops. The predicted condenser pressure drop agrees within approximately 20% of the data. The predicted evaporator pressure drop exceeds the experimental pressure drop by between 0% and 30%. The pressure drop through the evaporator is small and a larger error can be tolerated. The pressure drop through the accumulator is predicted within 20% (Figure 4.9).

Figure 4.10 shows the differences between the modeled evaporator superheat and the experimental superheat. The model predicts the evaporator superheat within 15 K. Evaporator superheat is extremely sensitive to evaporator capacity, and this error is considered to be quite good.

The system model shows good agreement with the experimental data. Having good agreement between the steady-state data and the steady-state model is the first step in having good agreement between a transient model and transient data.

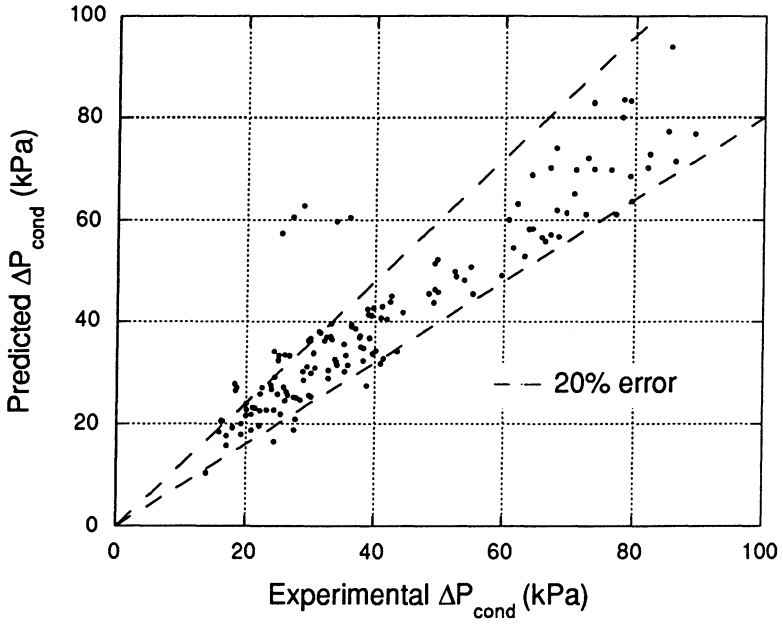

Figure 4.7 Condenser pressure drop comparison for system model (subcooling input).

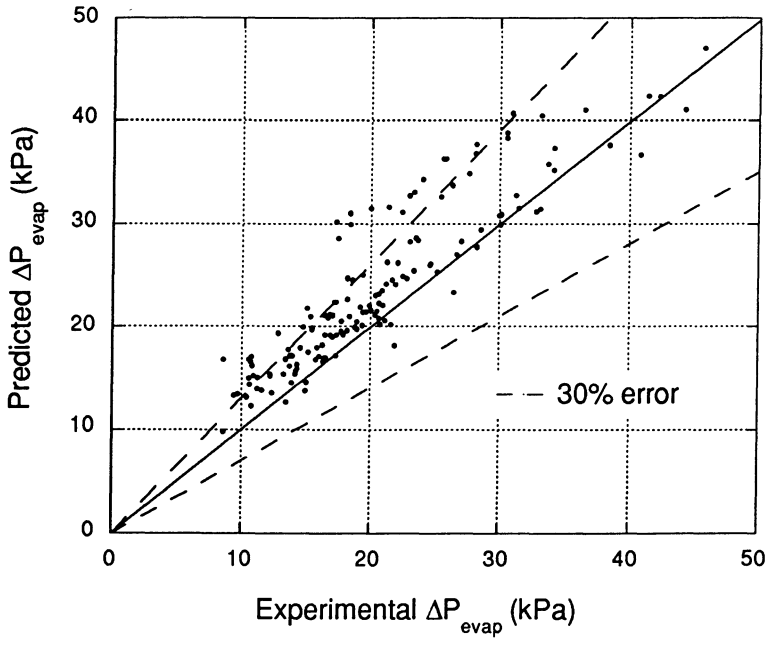

Figure 4.8 Evaporator pressure drop comparison for system model (subcooling input).

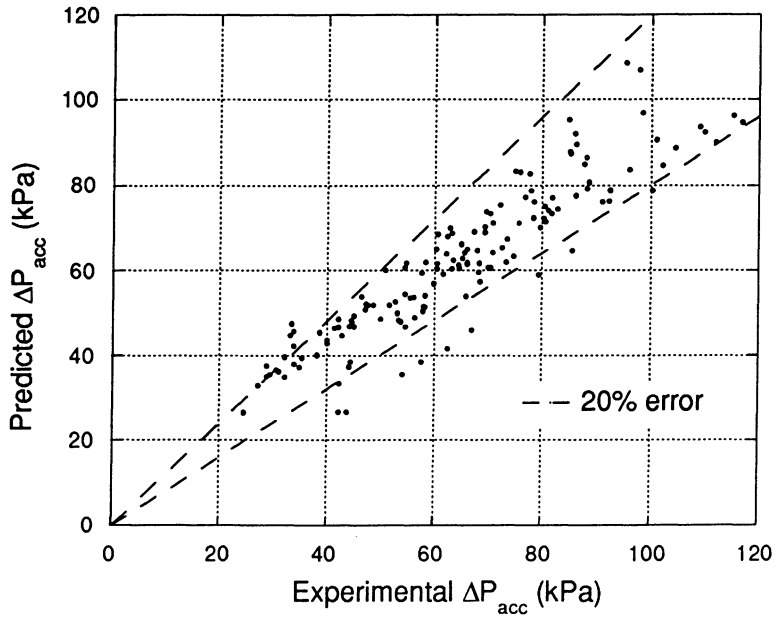

Figure 4.9 Accumulator pressure drop comparison for system model (subcooling input).

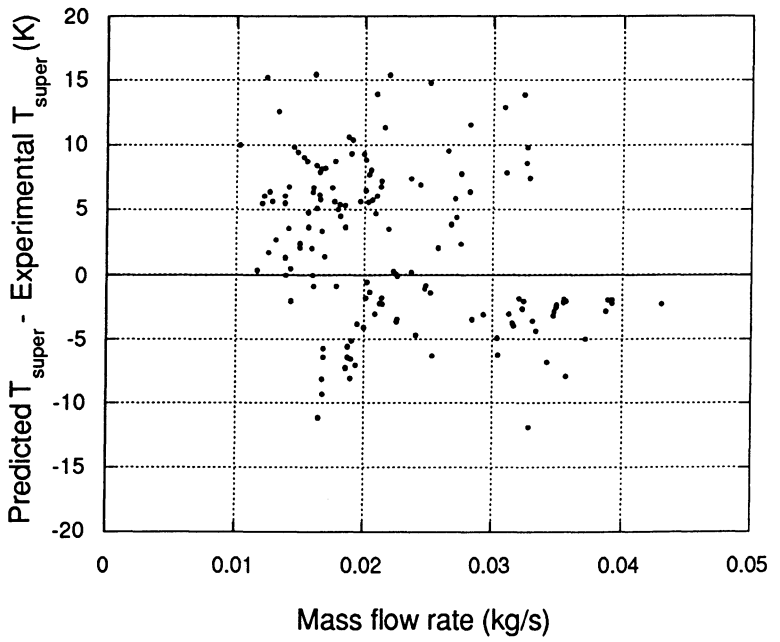

Figure 4.10 Evaporator superheat comparison (subcooling input).

4.1.2 Results Obtained Using Evaporator Superheat as an Input

As mentioned as in Section 4.1.1, using the condenser subcooling as an input could bias the comparison between model predictions and measured values. Condenser subcooling is an input to the orifice-tube model. Using condenser subcooling as an input means that it is exactly correct and helps ensure good agreement between the predicted and measured mass flow rate through the orifice tube. To determine the effect of this bias, we used evaporator superheat as an input instead of condenser subcooling. Everything else in the model remains the same as in Section 4.1.1. The inputs to the steady-state model for this simulation are then

1) Evaporator inlet air temperature,
2) Condenser inlet air temperature,
3) Ambient temperature,
4) Evaporator air mass flow rate,
5) Condenser air mass flow rate,
6) Compressor speed, and
7) Evaporator outlet refrigerant superheat.

First, we shall investigate the comparison between the experimental and predicted mass flow rate (Figure 4.11). Slightly more error exists when evaporator superheat is an input (15%) than when condenser subcooling is an input (10%). When evaporator superheat is an input, the model overpredicts at low mass flow rates and underpredicts at high mass flow rates. The predicted condenser (Figure 4.12) and evaporator (Figure 4.13) pressure agree with the experimental data within 10% and 15%, respectively, which are the same errors obtained when condenser subcooling was an input. The increase in error in the mass flow rates can be caused by the an error in the outlet condenser subcooling. Figure 4.14 shows the difference between the predicted and experimental subcooling as a function of temperature. A general trend can be seen where the subcooling is overpredicted at low mass flow rates and underpredicted at high mass flow rates. This trend seems to cause the increased error in the mass flow rate prediction. However, the mass flow rate prediction is still quite good for a system model.

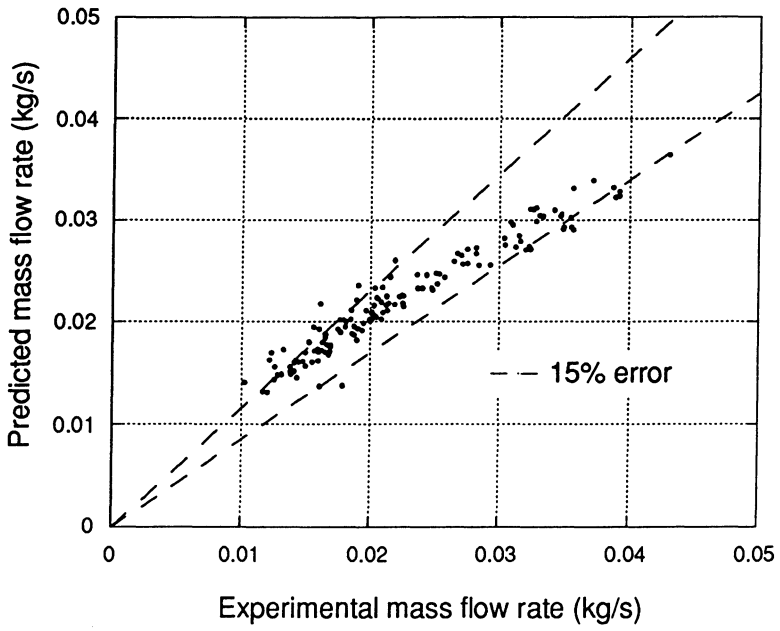

Figure 4.11 Mass flow rate validation (superheat input).

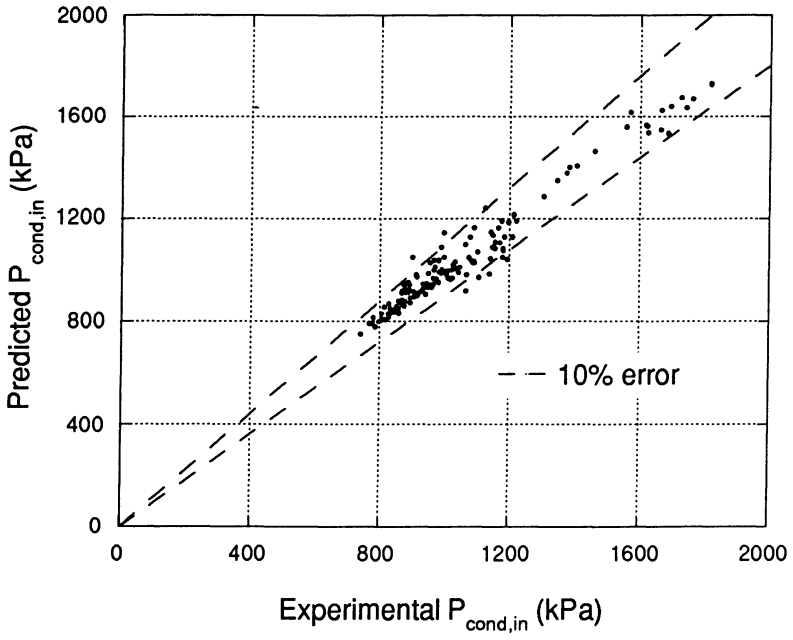

Figure 4.12 Inlet condenser pressure comparison (superheat input).

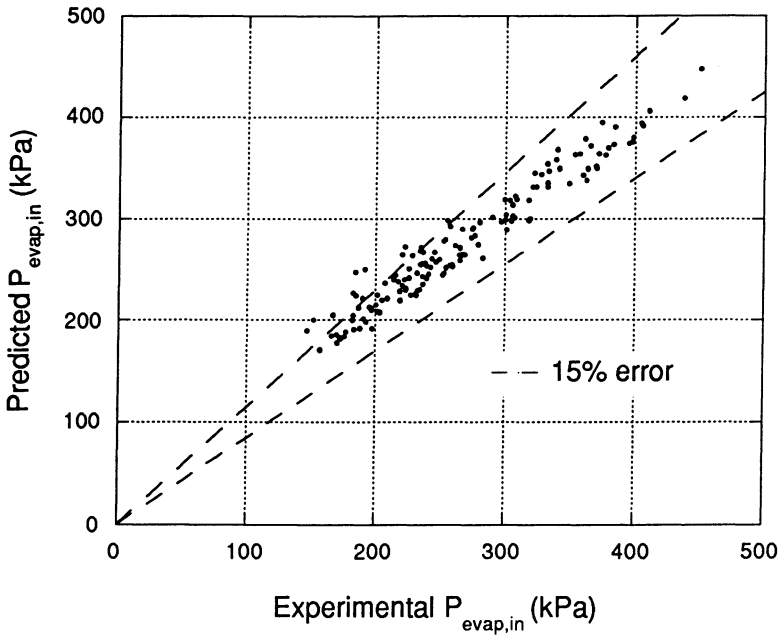

Figure 4.13 Inlet evaporator pressure comparison (superheat input).

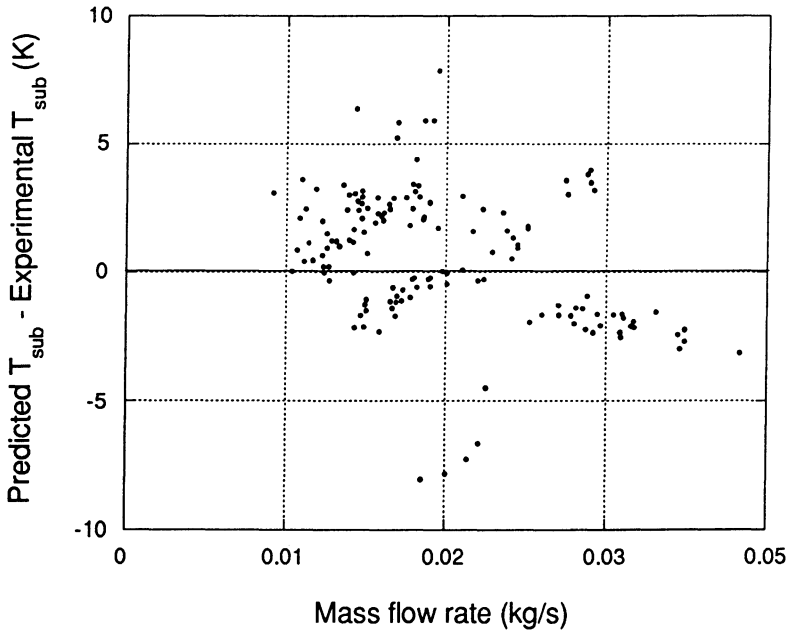

Figure 4.14 Condenser subcooling comparison (superheat input).

Figure 4.15 shows a comparison between the predicted and the experimental condenser capacity. The error is 15% which is approximately the same as the error observed in Figure 4.4. Figure 4.16 shows that the error between the modeled and experimental evaporator capacity is 15%. Comparing Figure 4.16 to Figure 4.5, we can see that the error in the evaporator capacity is slightly increased when evaporator superheat is used as an input rather then condenser subcooling. The error in the evaporator capacity (Figure 4.16) shows the same trend as the error in the system mass flow rates (Figure 4.11). The compressor power also has a slightly larger error when the evaporator superheat is an input (Figure 4.17).

The small errors in the mass flow rate show the largest affect on the pressure drops through the components. The pressure drops are modeled as empirical linear functions of mass flow rate. In Figure 4.18, we see that the pressure drop through the condenser is greatly overpredicted when the pressure drop is small. A small condenser pressure drop corresponds to a small mass flow rate; accordingly, the model overpredicts the mass flow rate when it is small. The same trends can be seen in the evaporator pressure drop (Figure 4.19) and the accumulator pressure drop (Figure 4.20).

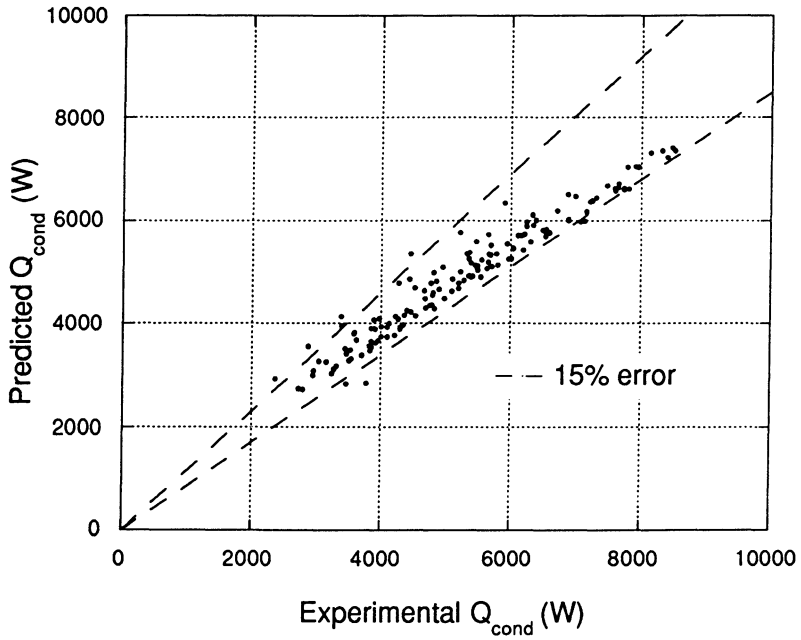

Figure 4.15 Condenser capacity comparison (superheat input).

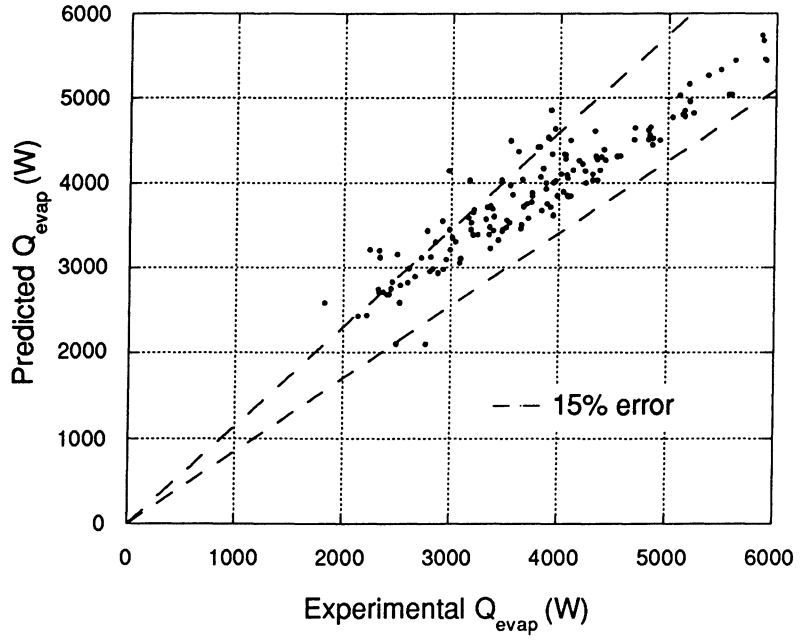

Figure 4.16 Evaporator capacity comparison (superheat input).

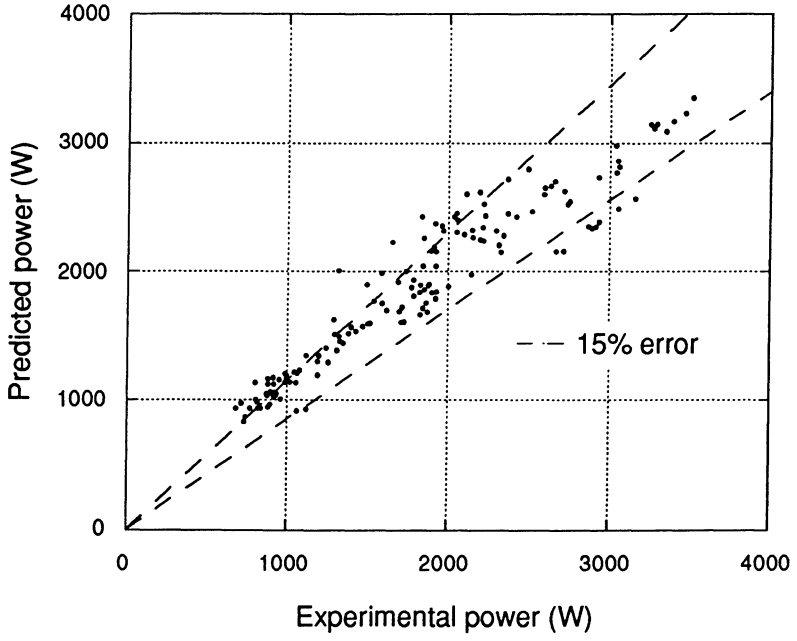

Figure 4.17 Compressor power comparison for the system model (superheat input).

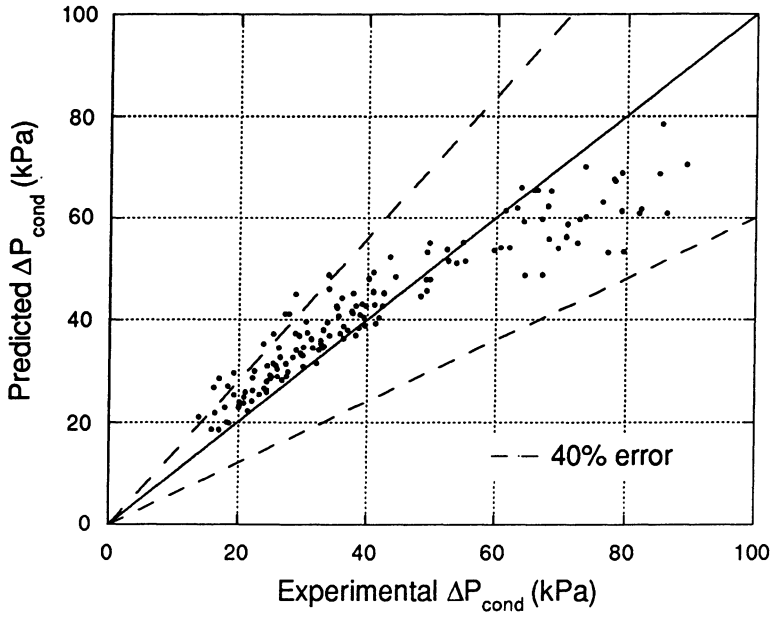

Figure 4.18 Condenser pressure drop comparison for system model (superheat input).

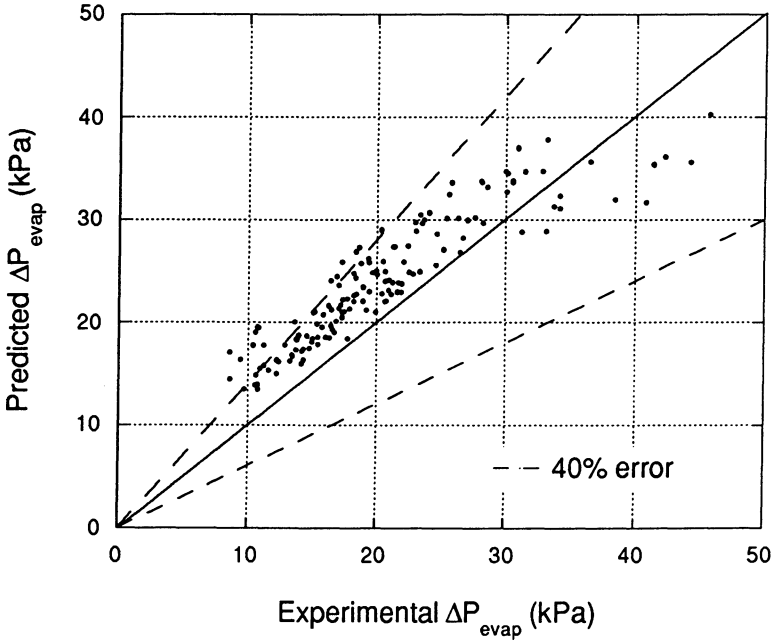

Figure 4.19 Evaporator pressure drop comparison for system model (superheat input).

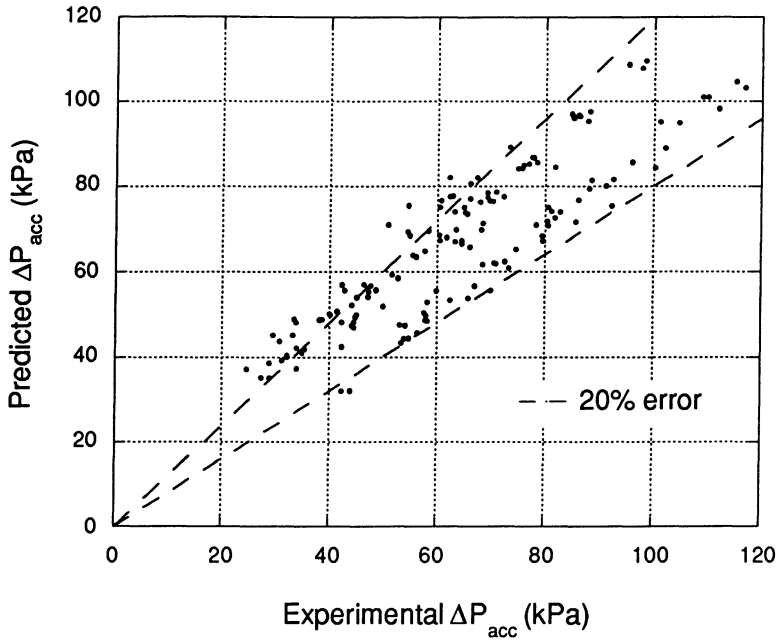

Figure 4.20 Accumulator pressure drop comparison for system model (superheat input).

In conclusion, using condenser subcooling rather that evaporator superheat as an input increases the accuracy of the model slightly. As previously noted, we traced this effect to the fact that condenser subcooling is an input to the orifice-tube equation. When the subcooling is exact, mass flow rate predictions agree better with the experimental data. Because mass flow rate influences every variable in the system, accuracy is improved. For the remainder of the steady-state simulations, condenser subcooling is the input variable used instead of evaporator superheat or refrigerant mass.

4.2 Refrigerant Mass Prediction

The steady-state solution summarized above provides the refrigerant state points throughout the system. Now, we shall use that information to predict the refrigerant mass in the system.

It is trivial to predict the refrigerant mass in a single-phase cell. As discussed in Section 3.3, the average cell pressure is determined by a downwind scheme, and the average cell enthalpy is determined by an upwind scheme.

$$P_{in} = P_{cell} \tag{4.1}$$

$$h_{out} = h_{cell} \tag{4.2}$$

The refrigerant mass in the cells is then determined by the following equations.

$$\rho_{cell} = f(P_{cell}, h_{cell}) \tag{4.3}$$

$$m_{cell} = \rho_{cell} \, Vol_{cell} \tag{4.4}$$

The pure vapor cells contribute a negligible amount of the refrigerant charge. Even if the density in a vapor cell changes by a large amount, the above algorithm gives a very small error in the overall mass prediction. The cells containing pure liquid contain an extremely large fraction of the entire refrigerant charge. The density changes in the liquid cell are small and thus contribute a very small error to the mass prediction. Thus, it is the two-phase region where mass prediction is problematic.

In our transient model, we use Equations 4.1 - 4.4 to determine the mass in the two-phase refrigerant cells. In this section, we shall determine the error which results from this method compared with void fraction correlations. In the final comparison, the above method is named the "Upwind" algorithm because the enthalpy (which is upwinded) is the variable which most strongly influences the mass of refrigerant in a cell.

The void fraction is defined as

$$\alpha = \frac{A_{vapor}}{A_{total}} . \tag{4.5}$$

The mass flux quality is

$$\phi = \frac{\dot{m}_{vapor}}{\dot{m}_{total}} . \tag{4.6}$$

Using basic algebra, we determined the relationship between the void fraction and the mass flux quality.

$$\alpha = \frac{1}{1+\left(\frac{1-\phi}{\phi}\right)\left(\frac{\rho_g V_g}{\rho_f Vf}\right)} \tag{4.7}$$

In Equation 4.7, one generally knows the mass flux void fraction, and the saturation densities can be calculated from the pressure. The ratio of the vapor velocity to the liquid velocity is not known. This ratio (or more generally the void fraction as a function of mass flux quality and pressure) can be determined from the void fraction correlation.

Equation 4.7 is used to find the void fraction at a cross sectional area. This equation must be integrated over a length to determine the average void fraction in the entire tube.

$$\alpha_{cv} = \frac{Vol_v}{Vol} = \frac{\int_{L_{in}}^{L_{out}} \alpha(L)\, dL}{\int_{L_{in}}^{L_{out}} dL} \tag{4.8}$$

In order to perform the integration in Equation 4.8, we must determine the how the mass flux quality changes with respect to length, l. This is dependent on the heat flux $f_Q(\phi)$ approximation (Rice, 1987).

$$d\dot{Q} = f_Q(\phi)\, dl = \dot{m}_{ref} h_{fg} d\phi \tag{4.9}$$

Combining Equations 4.8 and 4.9, we get

$$\alpha_{cv} = \frac{\int_{\phi_{in}}^{\phi_{out}} \frac{\alpha(\phi)}{f_Q(\phi)} d\phi}{\int_{\phi_{in}}^{\phi_{out}} \frac{1}{f_Q(\phi)} d\phi}. \tag{4.10}$$

The simplest assumption of the form of $f_Q(\phi)$ is constant heat flux. Rice (1987) determined that the heat-flux assumption is less important than the void-fraction assumption when determining two-phase mass. Assuming constant heat flux, Equation 4.10 becomes

$$\alpha_{cv} = \int_{\phi_{in}}^{\phi_{out}} \alpha(\phi)\, d\phi. \tag{4.11}$$

The mass can then be determined from the following equation

$$m_{cell} = \left[\alpha_{cv}\rho_g + (1-\alpha_{cv})\rho_f\right]Vol_{cell} \tag{4.12}$$

Integration in Equation 4.11 is performed using a Gaussian-Legendre formulation summarized in Porter (1992).

Next, we shall summarize the specific void fraction correlations which were compared with the upwind method.

The slip ratio is defined as

$$S = \frac{V_g}{V_f} \tag{4.13}$$

In the homogenous correlation, the slip ratio is set equal to one. The void fraction is simply

$$\alpha = \frac{1}{1+\frac{\rho_g}{\rho_f}\left(\frac{1-\phi}{\phi}\right)}. \tag{4.14}$$

During two-phase flow, the vapor refrigerant has a larger velocity than the liquid refrigerant. Zivi (1964) improved the homogeneous correlation by defining the slip ratio as a function of the vapor and liquid density.

$$S = \left(\frac{\rho_g}{\rho_f}\right)^{-1/3} \tag{4.15}$$

Premoli et al. (1971) used empirical equations to calculate void fraction as a function of liquid Reynolds number and the liquid Weber number. In this formulation, this slip ratio is defined as

$$S = 1 + F_1\left(\frac{y}{1+yF_2} - yF_2\right)^{1/2} \tag{4.16}$$

where

$$F_1 = 1.578\,Re_L^{-0.19}\left(\frac{\rho_f}{\rho_g}\right)^{0.22}, \tag{4.17}$$

$$F_2 = 0.0273\,We_L\,Re_L^{-0.519}\left(\frac{\rho_f}{\rho_g}\right)^{-0.08}, \tag{4.18}$$

$$y = \frac{\beta}{1-\beta}, \tag{4.19}$$

$$\beta = \frac{1}{1+\frac{\rho_g}{\rho_f}\left(\frac{1-\phi}{\phi}\right)}, \tag{4.20}$$

$$Re_L = \frac{Gd}{\mu_f}, \text{ and} \tag{4.21}$$

$$We_L = \frac{G^2 d}{\sigma\,\rho_f}. \tag{4.22}$$

The surface tension correlation needed to calculate the Weber number is from Stegou-Sagia (1996).

The final void fraction correlation investigated is from Hughmark (1962). The empirical equation for void fraction is

$$\alpha = \frac{K_H}{1+\frac{\rho_g}{\rho_f}\left(\frac{1-\phi}{\phi}\right)} \tag{4.23}$$

where

$$K_H = f(Z). \tag{4.24}$$

The values of K_H as a function of Z are provided in Table 4.1. The variable Z is determined from the following equations.

$$Z = \frac{Re_\alpha^{1/6} Fr^{1/8}}{y_L^{1/4}} \tag{4.25}$$

$$Re_\alpha = \frac{G\,d}{\mu_f + \alpha(\mu_g - \mu_f)} \tag{4.26}$$

$$Fr = \frac{V^2}{g\,d} = \frac{1}{gd}\left(\frac{G\phi}{\beta\rho_g}\right)^2 \tag{4.27}$$

$$y_L = 1-\beta \tag{4.28}$$

β is defined in Equation 4.20. Note that Reynolds number (Equation 4.26) is a function of the void fraction. These equations must be calculated iteratively.

One final note must be made on how the refrigerant mass in the two-phase region was computed. If a cell has two-phase refrigerant at both the inlet and the outlet then Equation 4.11 can be used directly. If one interface is two-phase and the other interface is single-phase, then we must predict at what point in the cell the refrigerant switches from single phase to two phase in order to obtain an accurate mass prediction. For example, if a cell in the evaporator has two-phase refrigerant at the inlet and superheated refrigerant at the exit, then the fraction of the cell which is two-phase must be determined. We again assume constant heat flux (Equation 3.9) which indicates that the enthalpy changes linearly with length. Then the fraction of the heat exchanger cell which is two-phase is calculated.

Z	K_H
1.3	0.185
1.5	0.225
2.0	0.325
3.0	0.49
4.0	0.605
5.0	0.675
6.0	0.72
8.0	0.767
10	0.78
15	0.808
20	0.73
40	0.88
70	0.93
130	0.98

Table 4.1 Hughmark flow parameter K_H.

$$f_{2phase} = \frac{h_{in} - h_g}{h_{in} - h_{out}} \tag{4.29}$$

The average void fraction in the two-phase region is determined from

$$\alpha_{cv,2phase} = \int_{\phi_{in}}^{1} \alpha(\phi)\, d\phi. \tag{4.30}$$

The mass in the two-phase region is determined from Equation 4.12. The mass in the single-phase region is determined from Equation 4.4, and the vapor density is assumed to be equal to the saturated vapor density. The refrigerant mass in the cell is then

$$m_{cell} = f_{2phase} m_{2phase} + \left(1 - f_{2phase}\right) m_{1phase} \tag{4.31}$$

A similar algorithm is used in the condenser if the inlet is superheated and the exit is two-phase, or if the inlet is two-phase and the outlet is superheated.

Now, we shall summarize the comparisons between the different void fraction correlations and the experimental data. Figure 4.21 shows the comparisons between the mass predictions and the refrigerant mass in Rubio-Quero's data set. Figure 4.22 shows the comparisons between the mass predictions and the refrigerant mass in Collins's and Hemami's data sets. The two differences between these figures is the mass in the system and the volume of the liquid line. Modifications to the liquid line were made after Rubio-Quero obtained his data in the spring of 1995 which added approximately 50% more refrigerant line between the condenser and orifice tube. This refrigerant line in our system is extremely long because it contains instrumentation to measure the oil concentration in the system. During steady-state operation, this line is filled with subcooled liquid and contains approximately 60% of the refrigerant charge.

At this point, we should also note that the volumes of the heat exchangers are known extremely well. The heat exchangers were filled with water and then weighed to determine the volumes. The volume of the refrigerant lines were calculated by physically measuring the length of the line and the diameter. Since the refrigerant lines contain such a large percentage of the charge, errors in the prediction of these volume correspond directly to errors in the prediction of the refrigerant mass.

Table 4.2 summarizes the average errors between the different void fraction correlations for both refrigerant masses. The Premoli void fraction correlations predict the refrigerant charge the most accurately. The Hughmark correlation slightly overpredicts the refrigerant mass. The upwind algorithm underpredicts the mass by approximately 4% for the case with the larger mass. This error is taken to be reasonable and the upwind correlation is a valid approximation for our model.

Void fraction correlation	Experimental mass (kg)	Average predicted mass (kg)	Error (%)
Hughmark	1.02	1.05	2.9
	1.34	1.44	7.5
Premoli	1.02	0.989	-3.0
	1.34	1.37	2.2
Zivi	1.02	0.956	-6.3
	1.34	1.32	-1.5
Upwind	1.02	0.935	-8.3
	1.34	1.29	-3.7
Homogeneous	1.02	0.863	-15.4
	1.34	1.21	-9.7

Table 4.2 Errors associated with the average predicted mass using different void fraction correlations.

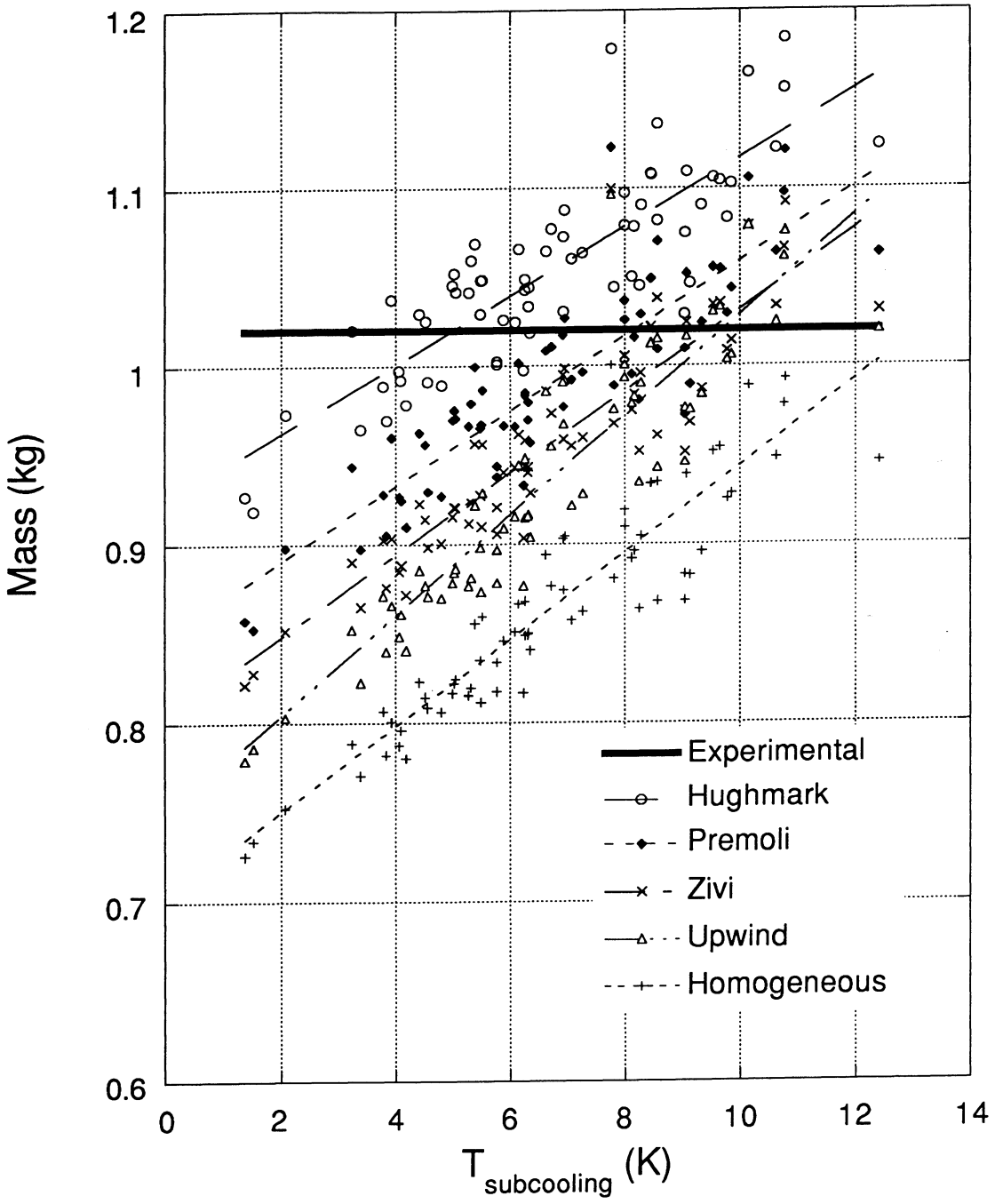

Figure 4.21 Refrigerant mass prediction using different void fraction correlations for Rubio-Quero's data.

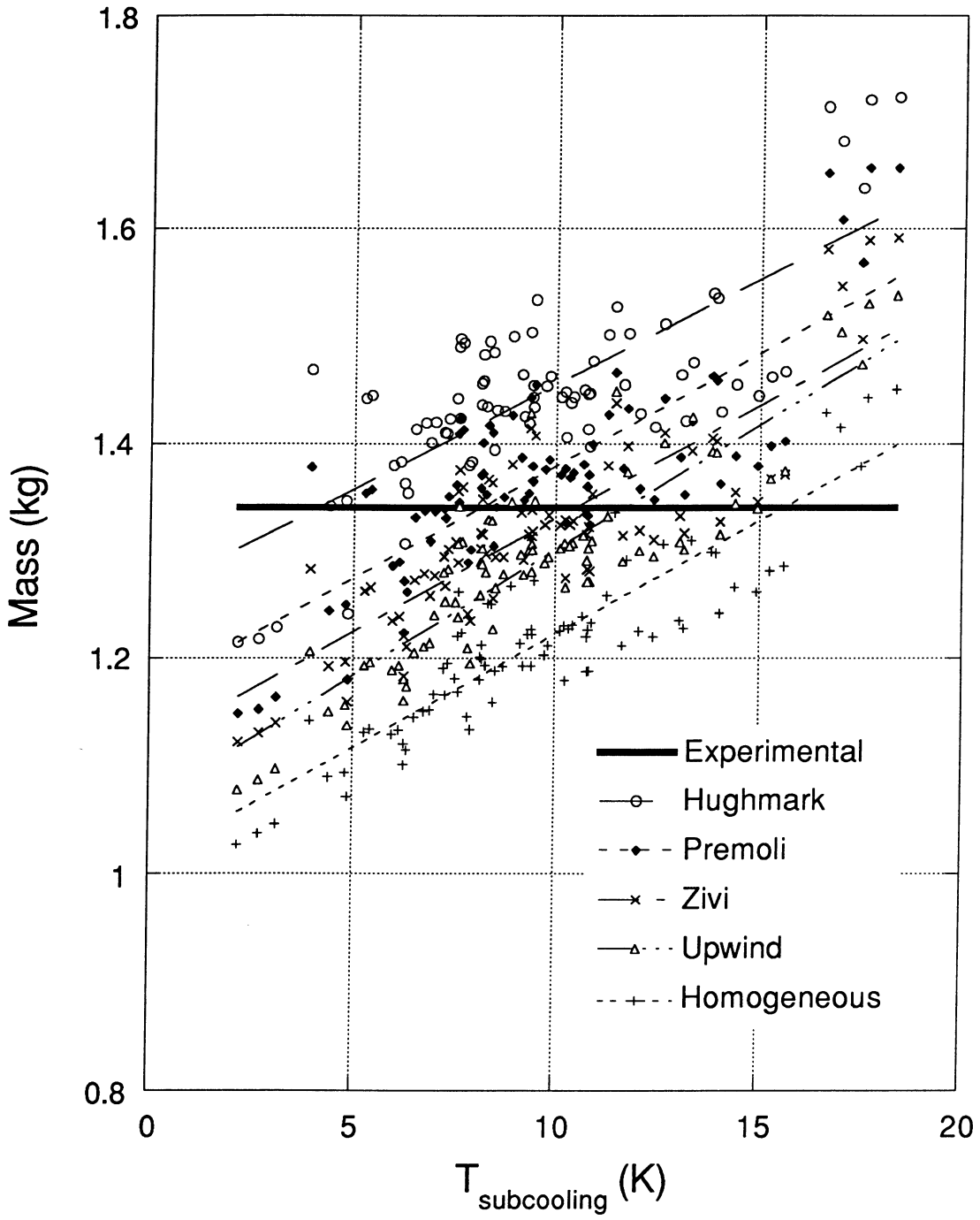

Figure 4.22 Refrigerant mass prediction using different void fraction correlations for Collins's and Hemami's data.

Chapter 5
Transient Model Validation

In Chapter 3, we presented the equations and solution technique for the transient model. In this chapter we shall validate the transient model with experimental data. All of the data for the transient tests were obtained from a Ford Crown Victoria air-conditioning system installed in the test facility described in Section 3.2. The transient data were obtained in the spring and summer of 1997 using an orange orifice tube and 1.34 kg of refrigerant charge. I personally took all of the transient data except for the clutch cycling data which were obtained by Johnston (1997).

The presentation is divided in four sections as summarized below:

1) Section 5.1 - Transient city driving cycle,
2) Section 5.2 - Final compressor shutdown,
3) Section 5.3 - Initial compressor startup, and
4) Section 5.4 - Clutch cycling.

5.1 City Driving Cycle

The city driving cycle simulates an automobile driving at 30 mph for 30 s, decelerating to 0 mph over 12 s, waiting at a stop light over 20 s, and accelerating to 30 mph over 10 s. The inputs for the driving cycle are summarized in Figure 7.1. We are simulating an outside air temperature of 309 K (96.5 °F). The evaporator is being operated without recirculation; all of the air flowing over the coil is fresh outside air at 309 K. This condition results in a high load condition so the clutch does not cycle. This specific simulation is convenient for testing the transient model without compressor cycling. The thermal capacitance of the heat exchangers was neglected in this analysis.

Figure 5.1 show how the compressor speed and condenser air flow rate change with time. The acceleration and deceleration of the compressor speed and condenser air flow rate are modeled as a linear change between their corresponding values at 0 mph and 30 mph. This simplification does not take into account the transmission changing gears or a nonlinear combination between the ram air effect and condenser fan effect.

Figure 5.2 shows good agreement between the experimental mass flow rates and the modeled mass flow rate. The mass flow rate is measured with a Micro Motion flowmeter

Input variable	units	0 mph	30 mph
Compressor speed	RPM	1085	1685
$\dot{m}_{cond,air}$	kg/s	0.84	0.92
	cfm	1480	1620
$\dot{m}_{evap,air}$	kg/s	0.11	0.11
	cfm	194	194
$T_{cond,air}$	K	309	309
$T_{evap,air}$	K	309	309
$T_{ambient}$	K	302	302

Table 5.1 Driving-cycle conditions.

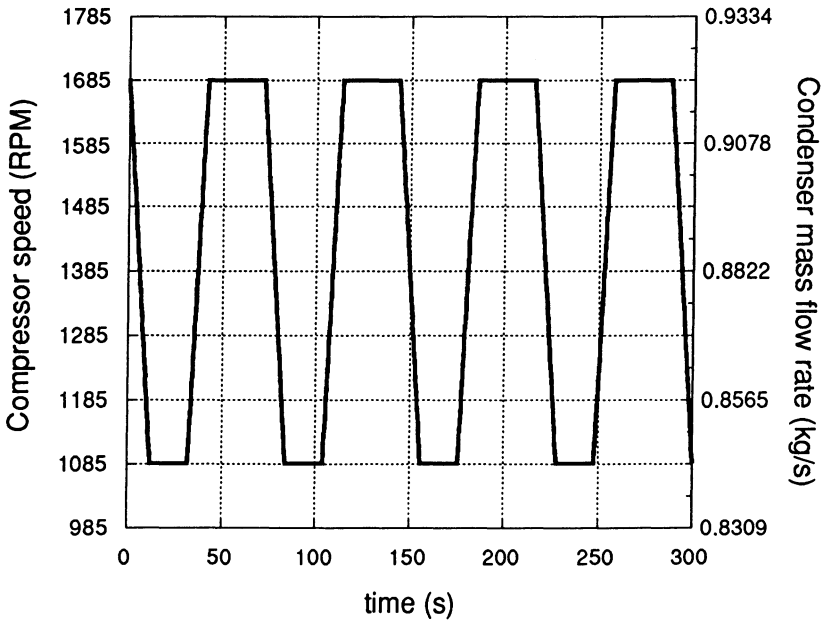

Figure 5.1 Driving-cycle transient inputs.

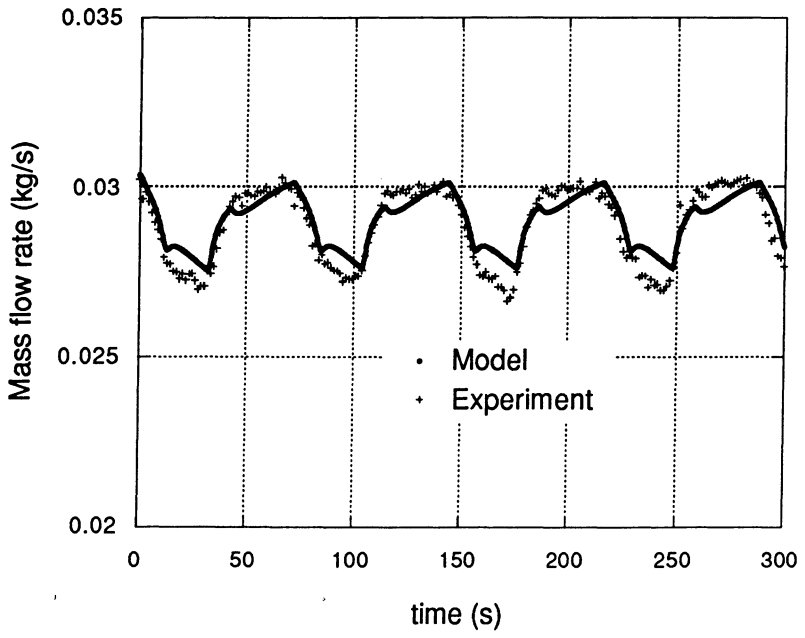

Figure 5.2 Driving-cycle mass flow rates.

between the condenser and the orifice tube. The mass flow rate follows the same trend as the compressor speed. Figure 5.3 shows a comparison between predicted and measured pressures. The condenser pressure is predicted extremely well; the evaporator pressure is slightly overpredicted.

Figure 5.4 shows a comparison of predicted and measured evaporator capacities. The predicted capacity follows the transient behavior well, but underpredicts it by about 7%. This is within the error of the model; however, it should be noted that under these operating conditions the outlet of the evaporator is two-phase. As a result, the measured air heat capacity is used to determine the outlet refrigerant enthalpy. This additional calculation adds more uncertainty to the experimental capacity measurements.

Figure 5.5 shows the calculated mass distribution in the air-conditioning system as a function of time. The majority of the mass is in the liquid line between the condenser and the orifice tube. Since this refrigerant is subcooled, the liquid-line mass remains constant with respect to time. Only very small oscillations exist in the evaporator mass (between 2.75% and 3.25% of the total charge). The majority of the mass is redistributed between the accumulator and the condenser. Decreasing the air flow across the condenser decreases the heat transfer coefficient and thus the amount of subcooled refrigerant in the condenser. This excess charge then collects in the accumulator.

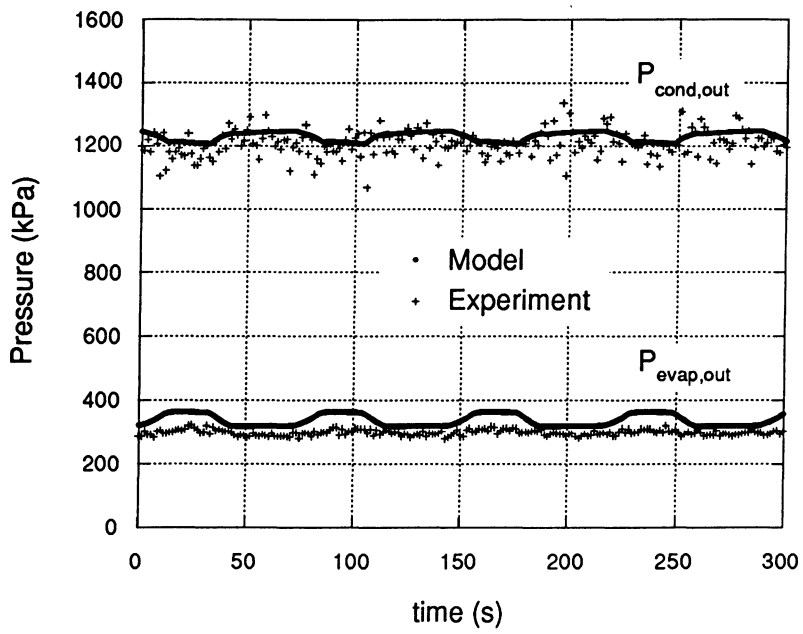

Figure 5.3 Driving-cycle evaporator and condenser pressures.

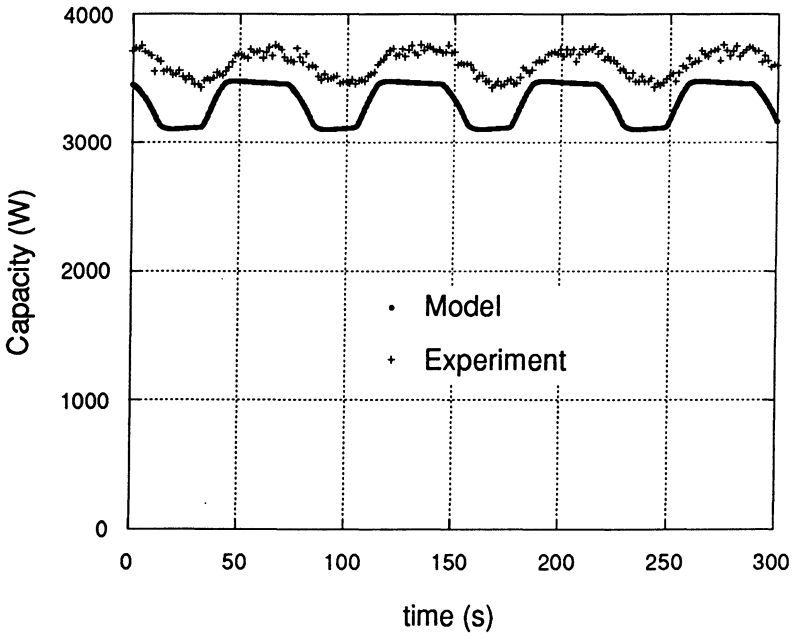

Figure 5.4 Driving-cycle evaporator capacity.

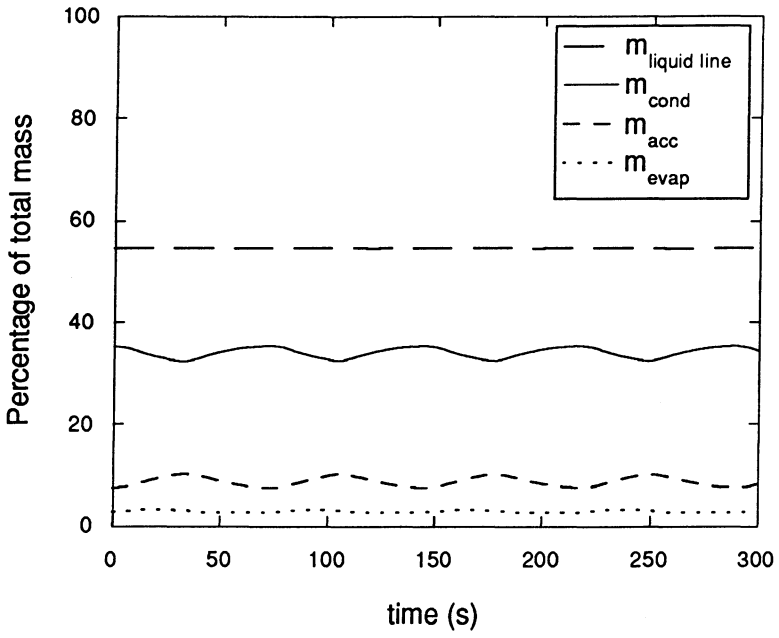

Figure 5.5 Driving-cycle mass distribution.

5.2 Compressor Shutdown

During compressor shutdown, the compressor clutch is disengaged, and the condenser and evaporator fans are turned off. After the clutch is disengaged, eventually the system comes to new steady state value where all of the pressures are equal and all of the mass flow rates are zero. The refrigerant temperature comes to equilibrium with the ambient temperature.

We have modeled two different cases. The first is a typical case when the evaporator inlet air is colder than the condenser inlet air. This occurs when the air blowing over the evaporator is recirculating from the cabin. In the second case the condenser air is colder than the evaporator air. This situation does not frequently occur during a system shutdown; however, it is interesting to note the differences between the two opposite cases.

Unlike the previous analysis, the thermal capacitance of the refrigerant walls is included here. The compressor speed ramps from the steady-state value to zero over 3 s. The evaporator and the condenser air mass flow rates ramp from their steady-state values to zero over 3 s and 12 s, respectively. When the mass flow rate over the heat exchanger is zero, so is the air heat transfer coefficient.

Table 5.2 summarizes the initial conditions for the Case 1. Figure 5.6 shows a comparison between the experimental and modeled outlet condenser pressure and outlet evaporator pressure. All of the pressures on the high side and the low side show the same basic

trend; for simplicity we only show one pressure on each side. The predicted evaporator pressure shows extremely good agreement with the experimental evaporator pressure. The modeled condenser pressure follows the predicted condenser pressure exactly for the first 6 s. At that point, the model predicts that the refrigerant entering the orifice tube changes from subcooled liquid to two-phase. In the experiment, the refrigerant became two-phase at approximately 10 s. We can determine when the refrigerant becomes two-phase by studying the mass flow rate data in Figure 5.7. The mass flow meter reads unreasonable values when the refrigerant is not single-phase. This effect can be seen between 10 s and 45 s in the experimental mass flow rate measurements. When liquid refrigerant flows through the orifice tube, the slope of the condenser pressure is much steeper than when the two-phase refrigerant flows through the orifice. Since we predict the refrigerant becoming two-phase slightly early, we overpredict the condenser pressure after 6 s. The model predicts that the orifice tube becomes unchoked at 53 s. The modeled pressures and the experimental pressures equalize at approximately the same time.

Input variable	units	Initial condition
compressor speed	RPM	2548
$\dot{m}_{cond,air}$	kg/s cfm	0.41 726
$\dot{m}_{evap,air}$	kg/s cfm	0.17 296
$T_{cond,air}$	K	316
$T_{evap,air}$	K	309
$T_{ambient}$	K	296
$T_{sub,cond}$	K	9.3

Table 5.2 Compressor shutdown initial conditions for Case 1 (the condenser is warmer than the evaporator).

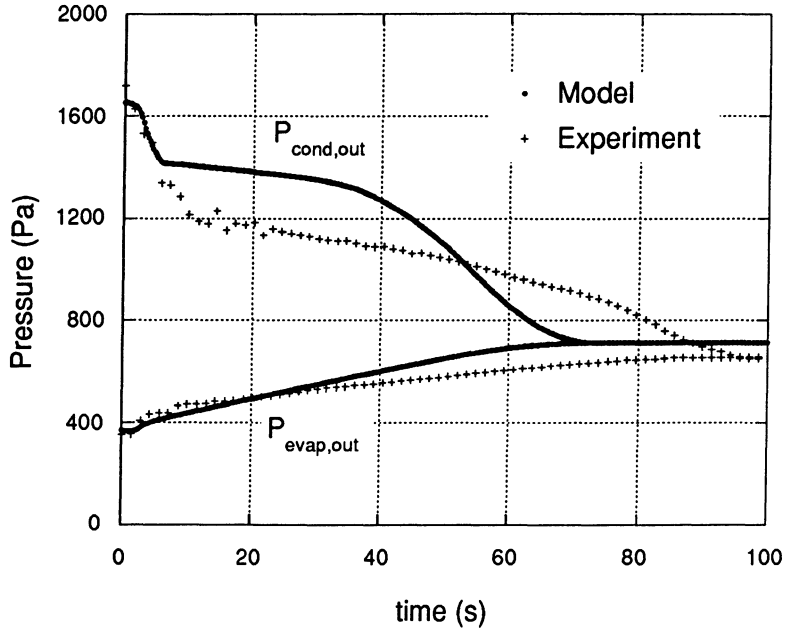

Figure 5.6 Compressor shutdown evaporator and condenser pressures for Case 1 (the condenser is warmer than the evaporator).

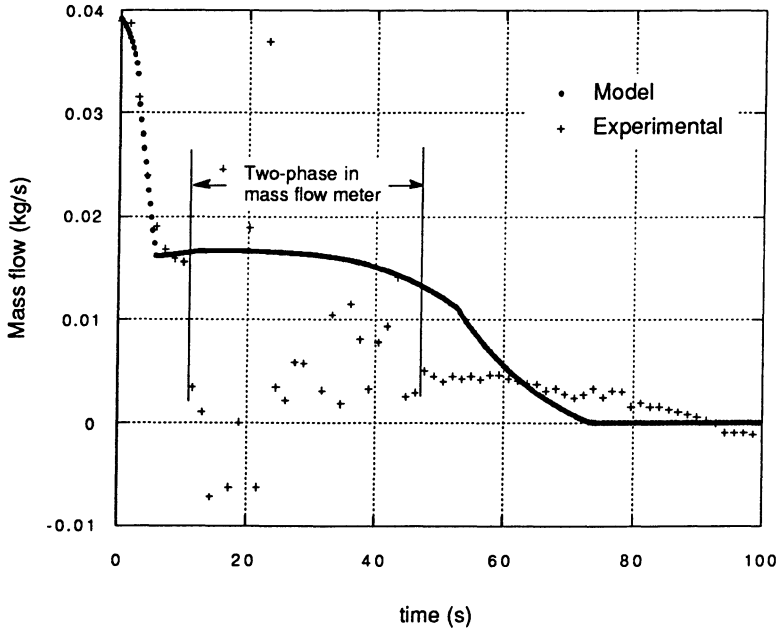

Figure 5.7 Compressor shutdown mass flow rate at the orifice tube inlet for Case 1 (the condenser is warmer than the evaporator).

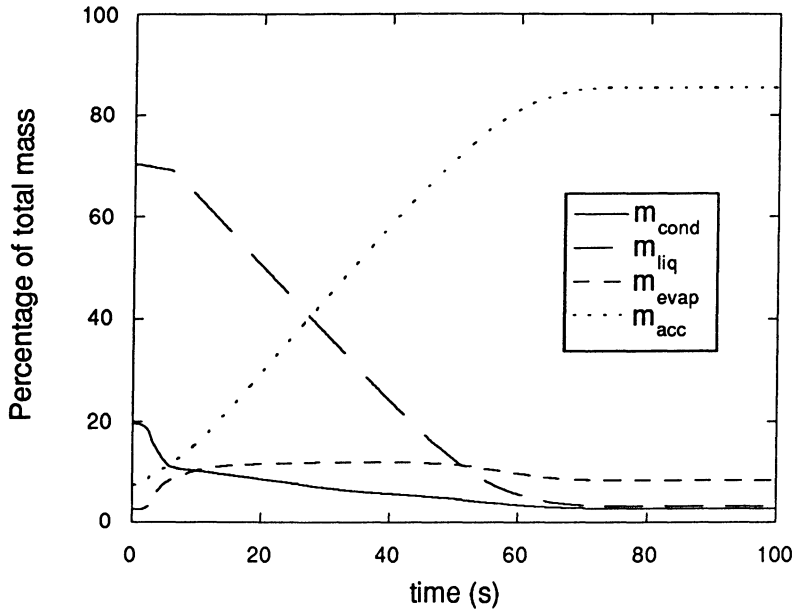

Figure 5.8 Compressor shutdown mass distribution for Case 1 (the condenser is warmer than the evaporator).

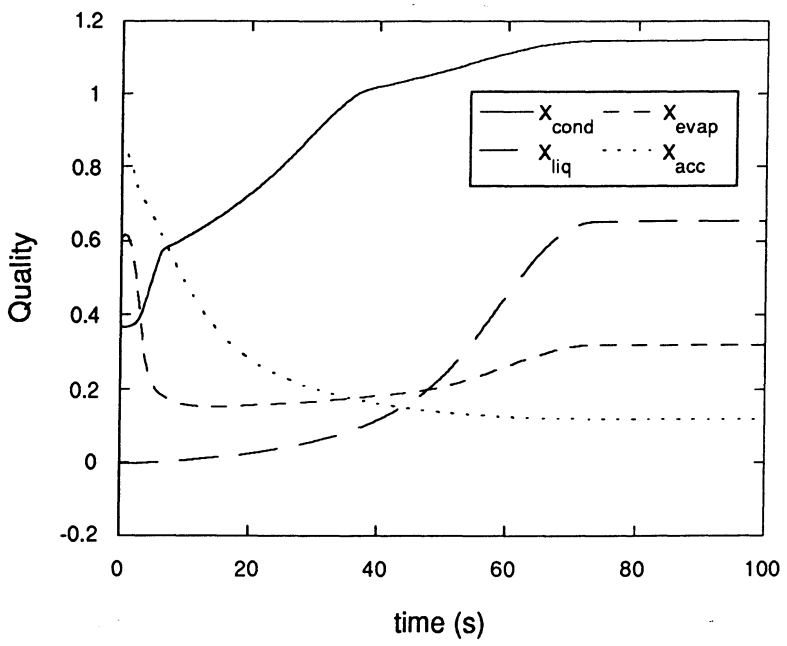

Figure 5.9 Compressor shutdown component refrigerant quality for Case 1 (the condenser is warmer than the evaporator).

Figure 5.8 shows the predicted mass distribution of the system. Initially the majority of the mass is in the liquid line. After the compressor shuts off, refrigerant begins flowing out of the condenser and liquid line into the evaporator. The evaporator cannot hold the complete system charge, so the excess flows out of the evaporator and into the accumulator. Eventually, the majority of the charge is in the accumulator.

Figure 5.9 provides some insight into the liquid distribution in the system. In this plot, we define a pseudo-quality defined by

$$x = \frac{v - v_f}{v_g - v_f}. \tag{5.1}$$

Using this definition, the pseudo-quality can be less than zero indicating a subcooled liquid state or greater than one indicating superheated vapor. The condenser eventually becomes pure vapor. The liquid line still contains liquid refrigerant after the pressures equalize. The evaporator and the accumulator are mostly filled with liquid.

Table 5.3 summarizes the initial conditions for Case 2 in which the evaporator is warmer than the condenser. Comparing Figure 5.10 to Figure 5.6, we can see that the pressures take a longer time to equalize when the evaporator is warmer than the condenser. Both figures show similar trends when the refrigerant becomes two-phase. The model predicts that the refrigerant at the orifice tube inlet becomes two-phase slightly sooner than the data show. This effect results in an overprediction of the condenser pressure for much of the shutdown. Again, the predicted evaporator pressure agrees extremely well with the experimental data. Figure 5.11 shows a comparison between the predicted and measured mass flow rates. Again, we can see the different times at which the orifice tube inlet becomes two-phase.

The mass distribution (Figure 5.12) and the component quality (Figure 5.13) show the same trends for Case 2 as for Case 1. The refrigerant migrates from the high side to the low side and the majority of the refrigerant is in the accumulator when steady-state is reached.

Input variable	units	Initial condition
compressor speed	RPM	1480
$\dot{m}_{cond,air}$	kg/s cfm	0.74 1305
$\dot{m}_{evap,air}$	kg/s cfm	0.17 296
$T_{cond,air}$	K	299
$T_{evap,air}$	K	316
$T_{ambient}$	K	299
$T_{sub,cond}$	K	9.7

Table 5.3 Compressor-shutdown initial conditions for Case 2 (the evaporator is warmer than the condenser).

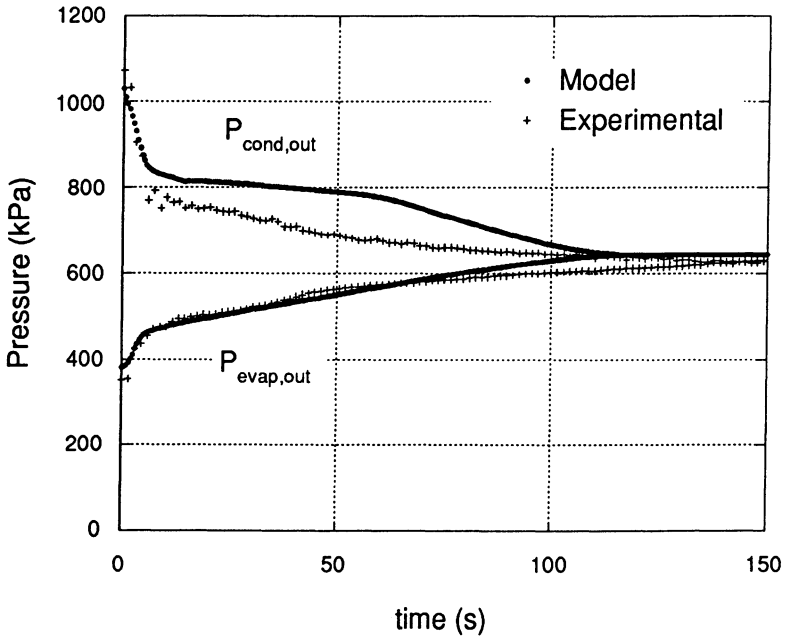

Figure 5.10 Compressor-shutdown evaporator and condenser pressures for Case 2 (the evaporator is warmer than the condenser).

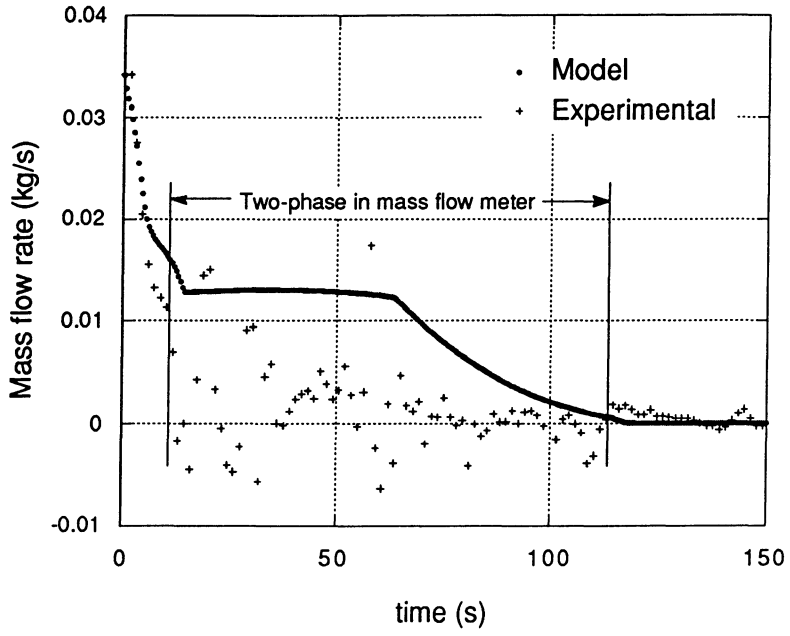

Figure 5.11 Compressor-shutdown mass flow rate at the orifice tube inlet for Case 2 (the evaporator is warmer than the condenser).

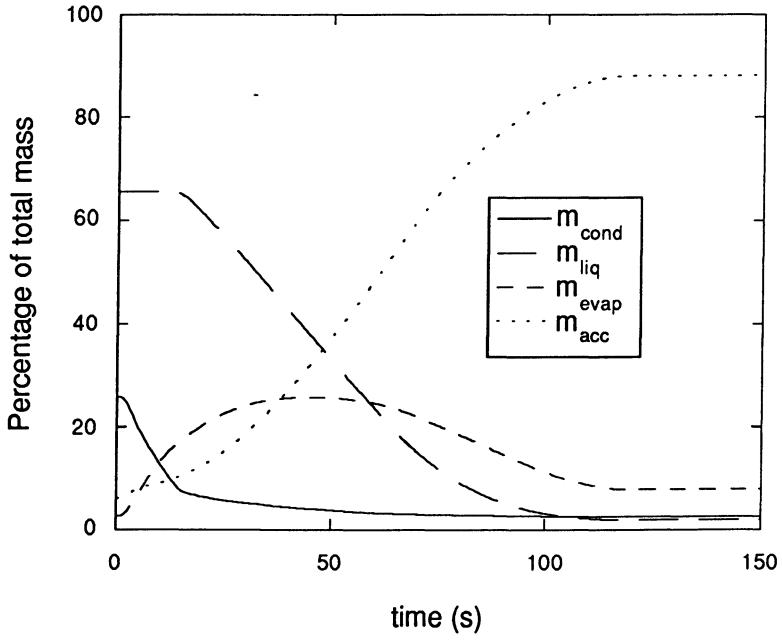

Figure 5.12 Compressor-shutdown mass distribution for Case 2 (the evaporator is warmer than the condenser).

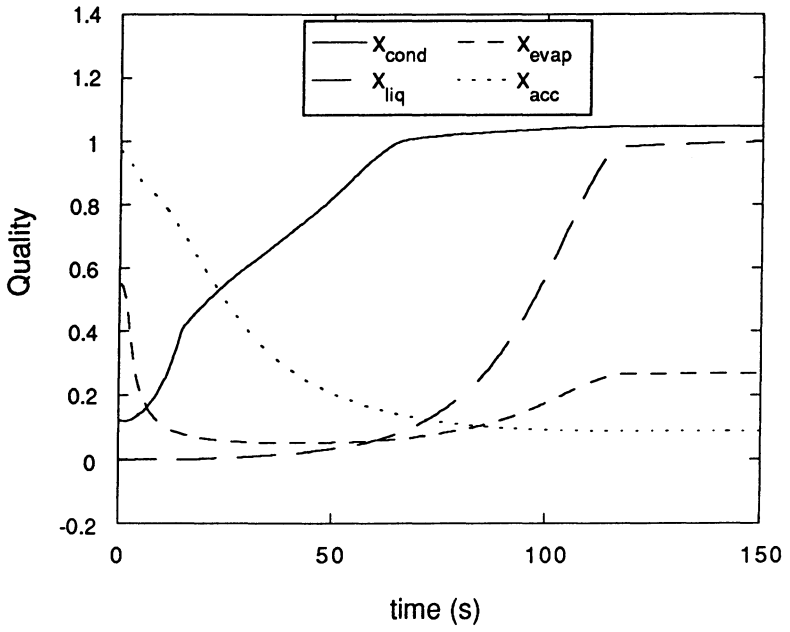

Figure 5.13 Compressor-shutdown component refrigerant quality for Case 2 (the evaporator is warmer than the condenser).

5.3 Compressor Start-up

In this section we compare the model with compressor start-up experimental data. These data were obtained after the system was allowed to sit for at least two hours before the compressor clutch is engaged. When the clutch is engaged, all of the refrigerant pressures are equal, the mass flow rates are zero, and the refrigerant temperatures are in equilibrium with the surrounding air temperatures.

We have modeled two different cases. In the first case the evaporator air is warmer than the condenser air and the ambient air. This case simulates a vehicle parked in the sun causing the air in the cabin (surrounding the evaporator) to be warmer than the air in the engine compartment (surrounding the remainder of the system). In the second case the evaporator, condenser, and ambient air temperatures are all equal. This case simulates a vehicle parked in the shade.

For these tests, the compressor is assumed to ramp to the steady-state compressor speed over a 6 s period. All of the other parameters remain constant during the simulation. The thermal capacitance of the heat exchangers was neglected in the modeling.

Input variable	units	Steady-state condition
compressor speed	RPM	1720
$\dot{m}_{cond,air}$	kg/s cfm	0.95 1675
$\dot{m}_{evap,air}$	kg/s cfm	0.12 209
$T_{cond,air}$	K	303
$T_{evap,air}$	K	319
$T_{ambient}$	K	303
$T_{sub,cond}$	K	9.0

Table 5.4 Compressor-startup initial conditions for Case 1 (the evaporator is warmer than the condenser).

Table 5.4 lists the steady-state conditions for Case 1. The refrigerant mass is calculated from the steady-state model using the steady-state conditions. It was found to be 1.37 kg. The refrigerant pressure is set equal to the saturation pressure at the lowest temperature in the system. In this case the lowest temperature is the ambient air temperature which is the same as the condenser air temperature. As a result, only saturated refrigerant exists in the condenser, accumulator, and refrigerant lines. Since the evaporator is warmer than the condenser, the evaporator is filled with superheated vapor. We define the initial mass distribution as follows:

1) Saturated vapor is in the first 5 (out of a total of 7) cells of the condenser.
2) Saturated liquid is in the last 2 cells of the condenser and the liquid line.
3) Superheated vapor is in the evaporator.
4) The remainder of the mass is placed in the accumulator.

The initial mass distribution can be seen on Figure 5.17 by observing the respective mass values at time = 0 s.

Figure 5.14 shows the comparison between the predicted and experimental condenser and evaporator outlet pressures. Both predicted pressures agree extremely well with the measured values. The pressures reach the new steady-state values in approximately 8 s. Figure 5.15 shows a comparison between the predicted and experimental mass flow rates. In our simulation, liquid refrigerant in always flowing at the inlet of the orifice tube. The flow at the exit of the orifice becomes choked at 3.75 s.

Figure 5.16 shows a comparison between the predicted and experimental evaporator capacities. The predicted capacity increases more quickly than does the experimental capacity. In Figure 5.17, we illustrate how the refrigerant mass distribution in the system changes over time. The refrigerant in the liquid line is always liquid, and thus the mass there remains relatively constant. The refrigerant mass in the condenser and evaporator increases with time, while the refrigerant mass in the accumulator decreases with time.

Figure 5.18 shows the pseudo-quality (as defined by Equation 5.1) in each component. Immediately after start-up, some of the liquid exits from the condenser, and the quality increases slightly. As the pressure rises in the condenser, the saturation temperature also increases, the refrigerant begins to condense, and the quality decreases. The quality in the evaporator immediately initially decreases rapidly as first liquid and then two-phase refrigerant begins flowing into it. Some of the low quality refrigerant empties into the accumulator and the evaporator reaches a steady-state condition. The liquid in the accumulator evaporates and eventually reaches a steady-state condition.

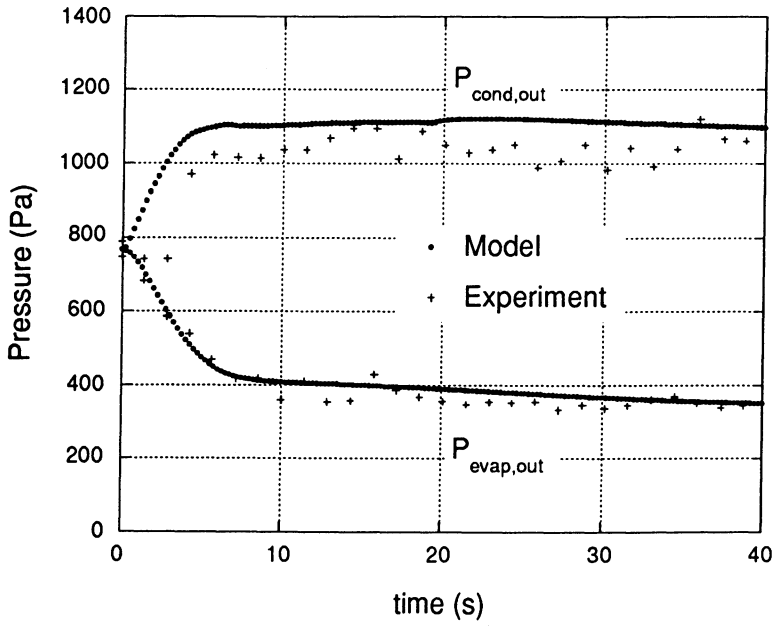

Figure 5.14 Compressor-startup pressures for Case 1 (the evaporator is warmer than the condenser).

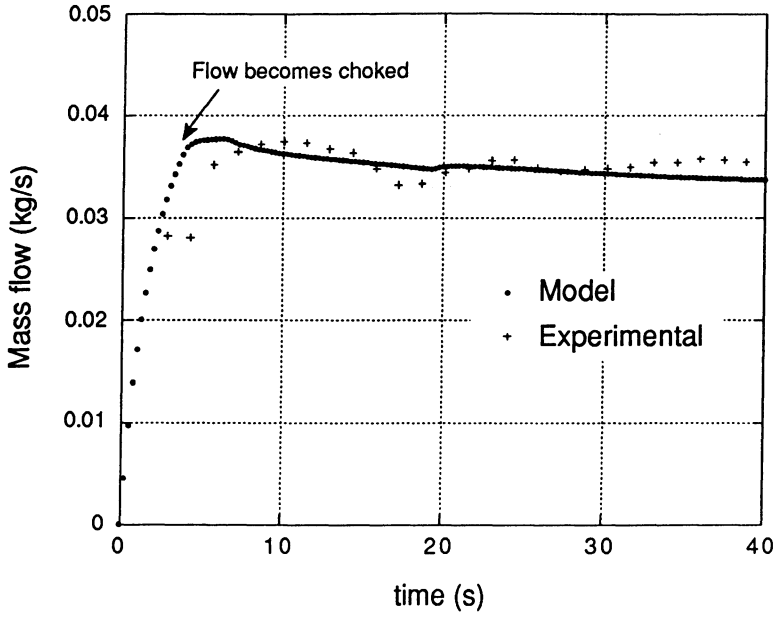

Figure 5.15 Compressor-startup mass flow rates for Case 1 (the evaporator is warmer than the condenser).

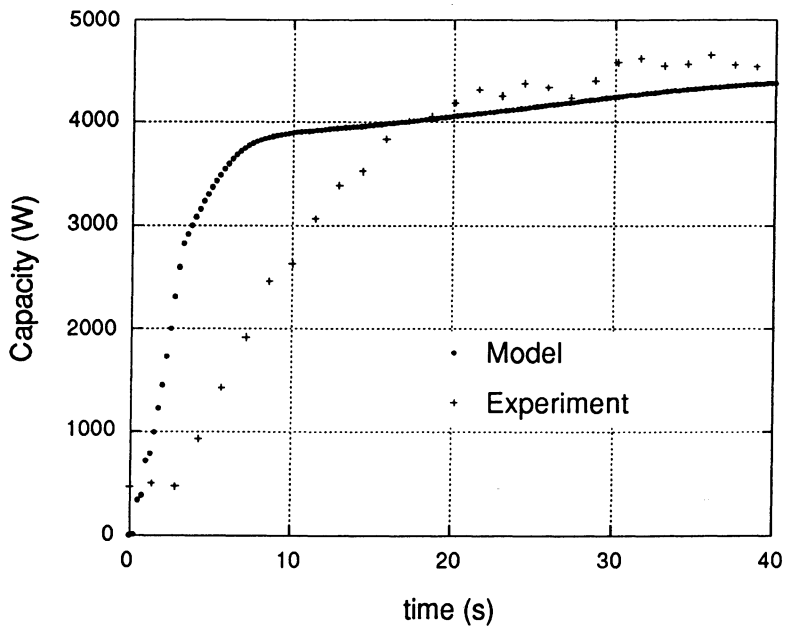

Figure 5.16 Compressor-startup capacity for Case 1 (the evaporator is warmer than the condenser).

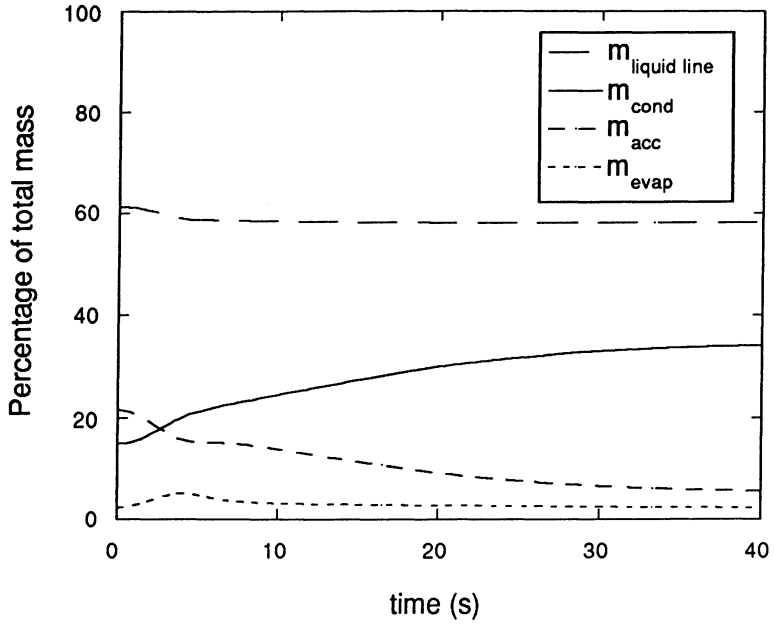

Figure 5.17 Compressor-startup mass distribution for Case 1 (the evaporator is warmer than the condenser).

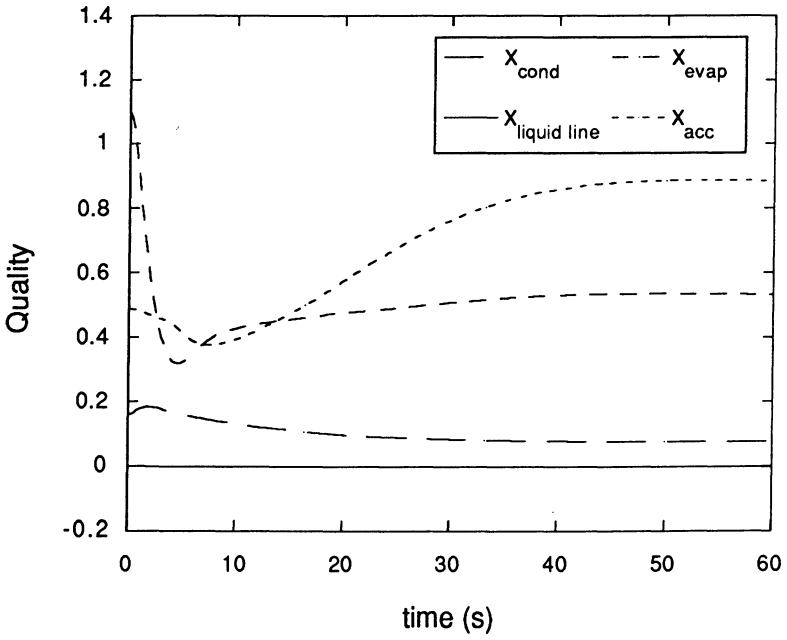

Figure 5.18 Compressor-startup component refrigerant quality for Case 1 (the evaporator is warmer than the condenser).

Table 5.5 lists the steady-state conditions for Case 2. In this case the air evaporator, condenser, and ambient temperatures are equal to each other and constant throughout the entire simulation. Only the compressor speed changes with time; it ramps from zero to the steady-state speed over a 6 s period.

Input variable	Units	Steady-state condition
compressor speed	RPM	1720
$\dot{m}_{cond,air}$	kg/s cfm	0.95 1675
$\dot{m}_{evap,air}$	kg/s cfm	0.12 209
$T_{cond,air}$	K	302
$T_{evap,air}$	K	302
$T_{ambient}$	K	302
$T_{sub,cond}$	K	5.3

Table 5.5 Compressor-startup initial conditions for Case 2 (all air temperatures are equal).

Figure 5.19 presents the condenser and evaporator pressure histories for this case. Because the system is initially in equilibrium at 302 K, the refrigerant is saturated everywhere in the system at this temperature. To obtain the initial conditions in our model, we must assume the initial distribution of liquid and vapor throughout the system.

If the liquid line is initially flooded, the model predicts a condenser pressure history similar to Figure 5.14. Comparing the experimental results shown in Figure 5.19 with the model predictions in Figure 5.14, we note two distinct differences. The first difference is that Case 1 shows an asymptotic approach to steady state pressure where Case 2 shows a distinct overshoot. The seconds difference involves the time to reach the equilibrium pressure. Case 1 reaches equilibrium after only 5 s whereas Case 2 does not reach equilibrium for more than 20 s. Because of the compressor overshoot, we are forced to conclude that the condenser and liquid line contain very little liquid. Based on these comparisons, we conclude that the assumption of the flooded liquid line does not produce the observed behavior for this case. If on the other hand we assume the liquid line is initially filled with vapor or two-phase refrigerant, then the time required to reach equilibrium pressure is much larger than indicated

by Figure 5.19. We conclude that no initial mass distribution can produce the observed behavior of the experimental system.

To understand why this problem occurs, we must consider the sequence of events following start-up. If liquid refrigerant is initially placed in the evaporator, it will move almost immediately to the accumulator after start-up. Therefore, there is practically no difference between placing the mass in the evaporator or the accumulator. Once the mass is in the accumulator, it can only leave by boiling off as vapor because liquid is preventing from flowing out of the accumulator. The compressor rapidly pulls the accumulator to a low pressure which leads to intense boiling in the accumulator. The temperature of the liquid refrigerant drops rapidly and boiling eventually becomes limited by ambient heat transfer which is quite low. Thus there is a long time constant associated with removing the liquid from the accumulator.

This problem only affects model predictions at start-up when the liquid line is not flooded. We believe that the physics of the accumulator are correctly modeled and that some other phenomenon causes the refrigerant to leave the accumulator. Figure 5.20 shows a comparison between the predicted and experimental mass flow rates exiting the compressor. The experimental mass flow rate is measured with a venturi flow meter. It appears that during the first 8 s the model greatly underpredicts the mass flow rate through the compressor. This effect can be caused by slugs of liquid traveling through the compressor and transferring a large amount of mass out of the accumulator. Our model does not account for liquid entering the compressor.

To model this case, we use the following initial distribution of liquid and vapor.

1) The condenser and liquid line contain saturated vapor.
2) The first 4 (out of a total 6) evaporator cells contains refrigerant at a quality of 0.3,
3) The last two cells of the evaporator contain saturated vapor.
4) The accumulator contains the rest of the mass.

The initial mass distribution can be seen in Figure 5.22 at time = 0 s.

To treat this very large initial mass flow rate seen in the experimental data, we artificially transfer mass from the accumulator to the liquid line.

Figure 5.19 shows a comparison between the predicted and experimental pressures. The condenser pressure is slightly underpredicted. The predicted evaporator pressure reaches the steady-state value slightly faster than the measured evaporator pressure. Figure 5.21 shows a comparison between the predicted and measured mass flow rates at the orifice tube. In the model, the mass flow rate through the orifice tube becomes choked at 2.25 s. The model predicts that the refrigerant in the liquid line becomes flooded at 13 s. We determine that the refrigerant in the experimental facility becomes flooded at approximately the same time from the mass flow meter (Figure 5.21) and the temperature at the orifice inlet (Figure 5.22). Two

interesting phenomenon an be seen in this model. First, for approximately 6 s before the liquid line becomes flooded the mass flow rate remains constant. After the liquid line floods it gradually increases to the steady-state rate. The experimental data show that the two-phase goes through the orifice tube at approximately the same time. However, the experimental mass flow rate is much greater than the modeled mass flow rate this point. This discrepancy is most likely caused by the slight overprediction of the condenser outlet pressure at this point.

Figure 5.23 shows a comparison between the predicted and measured evaporator capacity. The capacities agree extremely well. Figure 5.24 shows the distribution of the mass in the air conditioning system. Note that since we have reduced the length of the liquid line, it holds a much smaller proportion of the mass than the in the previous simulations. The mass in the liquid line increases until it becomes flooded at 13 seconds. The mass in the accumulator empties and fills the condenser. The mass in the evaporator decreases slightly. Figure 5.25 shows the pseudo-quality (Equation 5.1) for each component.

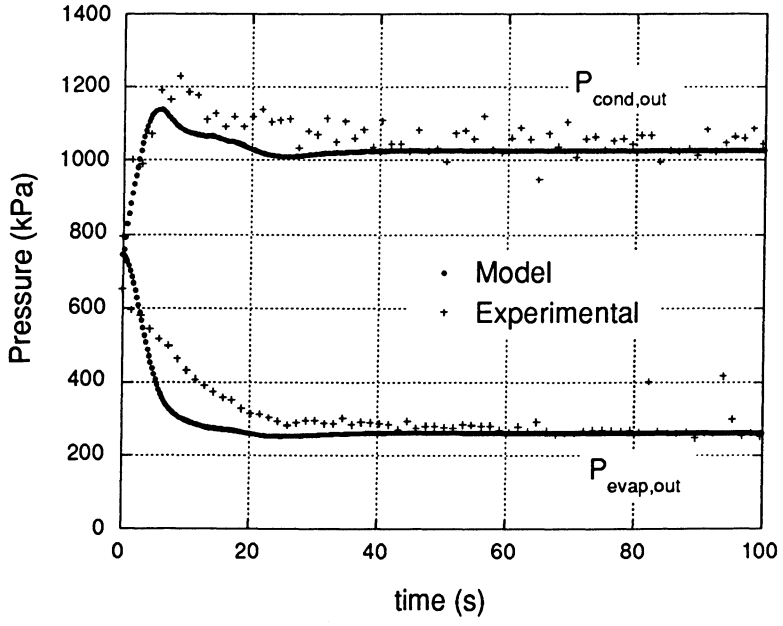

Figure 5.19 Compressor-startup pressures for Case 2 (all air temperatures are equal).

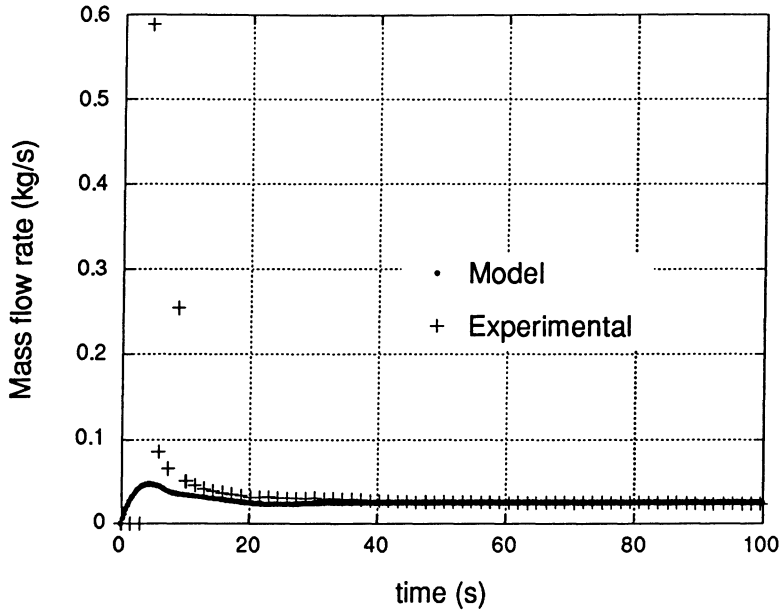

Figure 5.20 Compressor-startup compressor mass flow rate for Case 2 (all air temperatures are equal).

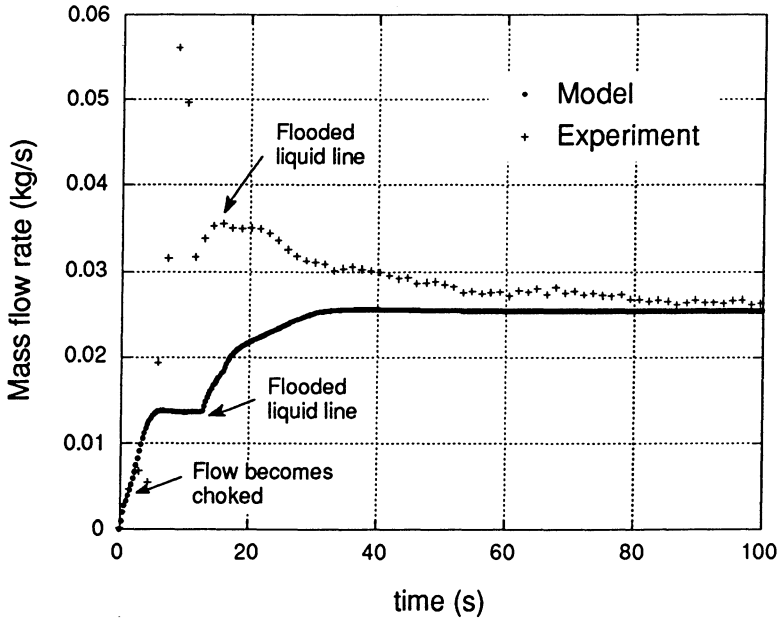

Figure 5.21 Compressor-startup mass flow rate for Case 2 (all air temperatures are equal).

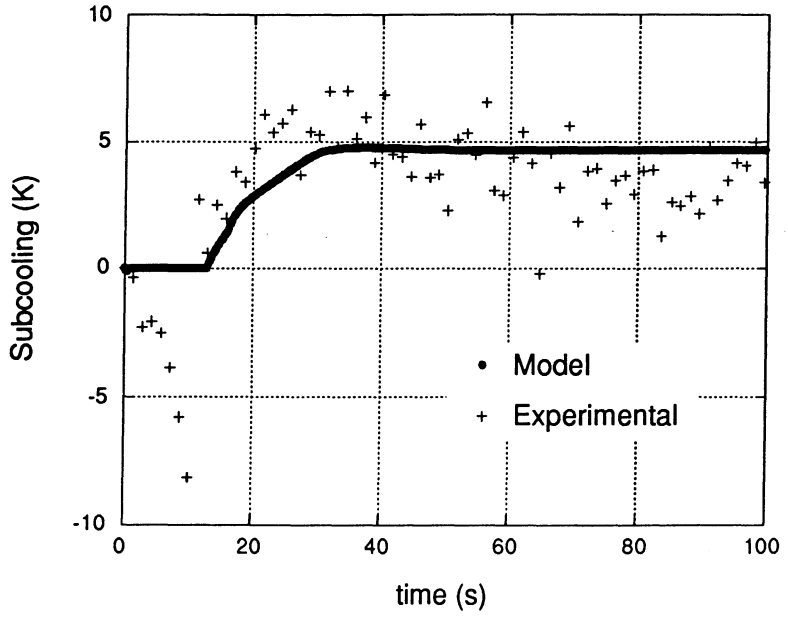

Figure 5.22 Compressor-startup orifice inlet subcooling for Case 2 (all air temperatures are equal).

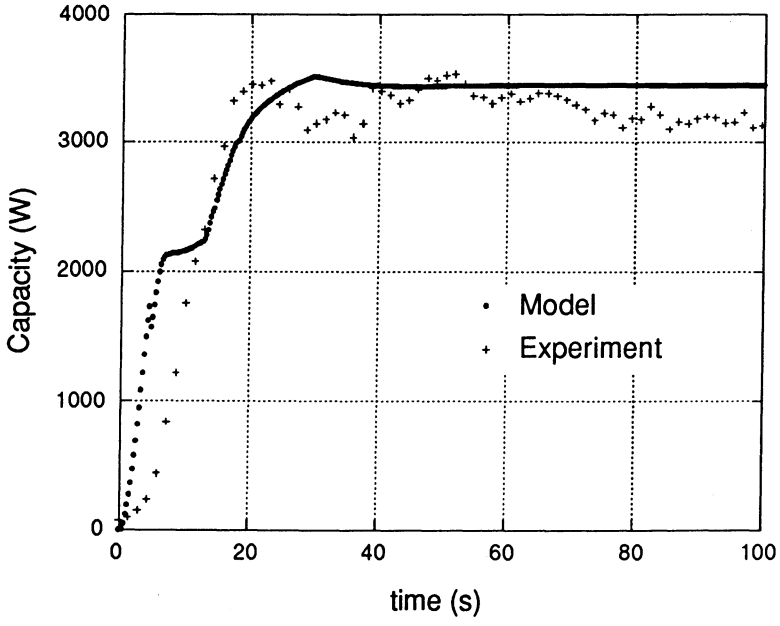

Figure 5.23 Compressor-startup capacity for Case 2 (all air temperatures are equal).

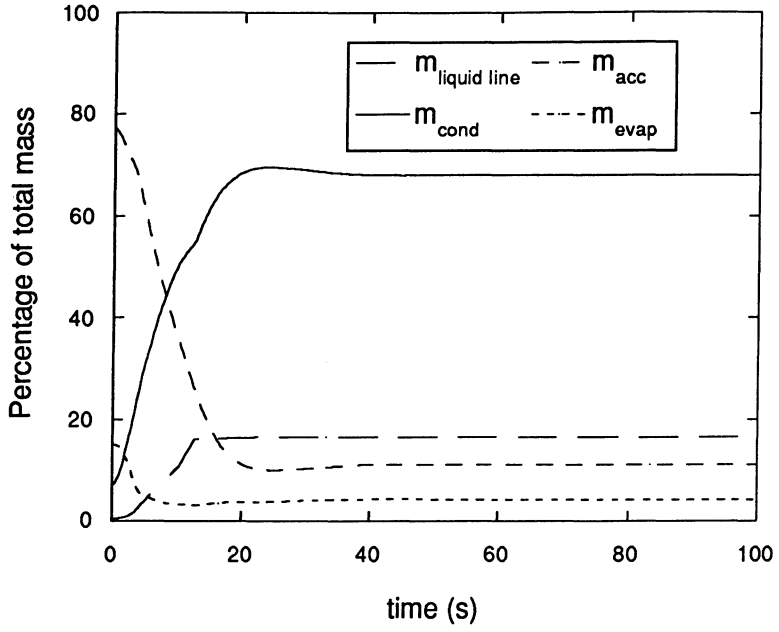

Figure 5.24 Compressor-startup mass distribution for Case 2 (all air temperatures are equal).

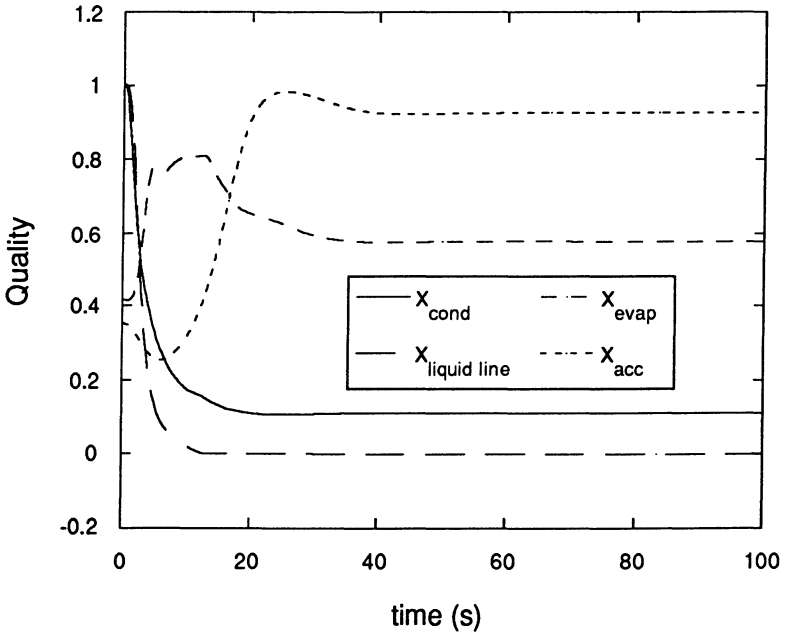

Figure 5.25 Component pseudo-quality for Case 2 (all air temperatures are equal).

5.4 Clutch cycling

On-off control (or clutch cycling) uses a pressure sensor at the exit of the evaporator to engage and disengage the clutch. This control strategy prevents the evaporator from frosting by always keeping the saturation temperature above the freezing point of water. The clutch disengages when the pressure falls below the low-pressure set point of 25 psig (approximately 270 kPa absolute) and engages when the pressure reaches a high-pressure set point of 43 psig (approximately 400 kPa absolute).

In the following simulation, we model the vehicle as driving at a steady speed (Table 5.6). The outside air temperature flowing over the condenser is at 317 K (110 °F). The air flowing over the evaporator is recirculated air from the cabin that was cooled to 295 K (72 °F). In this simulation we must use the same correction of artificially transferring liquid out of the accumulator as summarized in Section 5.3.

Figure 5.26 shows a comparison between the predicted and measured pressures for one clutch cycle. The clutch is disengaged at 0 s and re-engaged at 9 s. The trends of the predicted and measured evaporator outlet pressures agree extremely well. The trends of the predicted and measured outlet pressures agree well except that it appears that the predicted pressure leads the measured value slightly after the clutch is engaged.

Input variable	units	Steady-state condition
compressor speed	RPM	1713
$\dot{m}_{cond,air}$	kg/s cfm	0.90 1585
$\dot{m}_{evap,air}$	kg/s cfm	0.14 243
$T_{cond,air}$	K	317
$T_{evap,air}$	K	295
$T_{ambient}$	K	298
$T_{sub,cond}$	K	2.0

Table 5.6 Clutch cycling conditions.

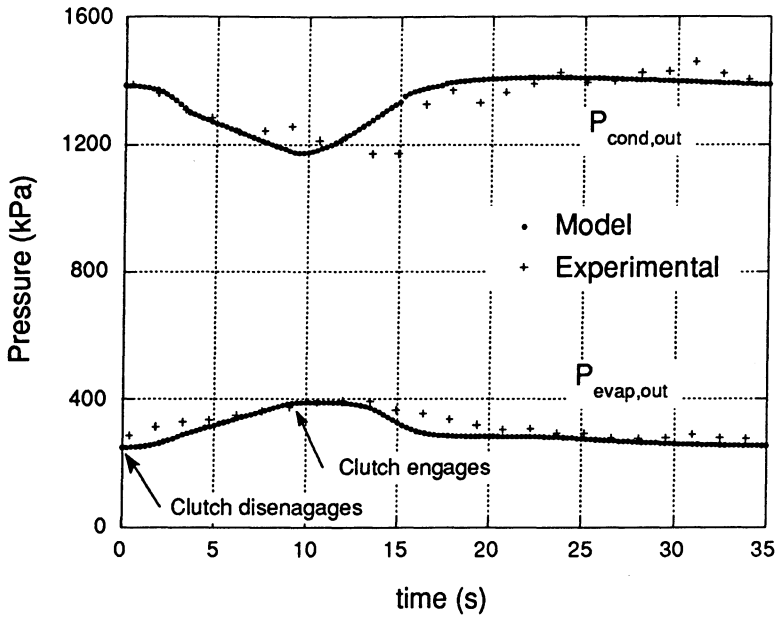

Figure 5.26 Clutch cycling pressures.

Figure 5.27 shows a comparison between the predicted and measured mass flow rates. The mass flow meter reads unreasonable values when the refrigerant is not single-phase, and we use this fact to determine when the liquid line is two-phase. The predicted and observed periods when the flow in the liquid-line is two-phase is labeled in the figure. The model predicts that the refrigerant at the orifice tube inlet becomes two-phase at 3.75 s and then is flooded again at 17.5 s. The experimental data show that the liquid line becomes two-phase approximately at the same time as the model, but does not become flooded again until 5 s after the time predicted by the model. We consider this discrepancy to be insignificant and may be an artifact of the mass flow meter itself.

A more disturbing fact is that the mass flow rate through the orifice tube is systematically underpredicted by approximately 20%. Since the condenser and evaporator pressures are predicted accurately, this error can be traced to either the orifice tube model or incorrect subcooling at the orifice inlet.

Figure 5.28 shows a comparison between the predicted and measured evaporator capacity. Since the refrigerant at the evaporator exit is two-phase for most of the simulation, the experimental capacity was determined from airside measurements. The model slightly underpredicts evaporator capacity; however, this underprediction is within experimental error. The predicted evaporator capacity shows the same trends as the measured evaporator capacity, but the predicted capacity reaches its minimum sooner than does the experimental capacity.

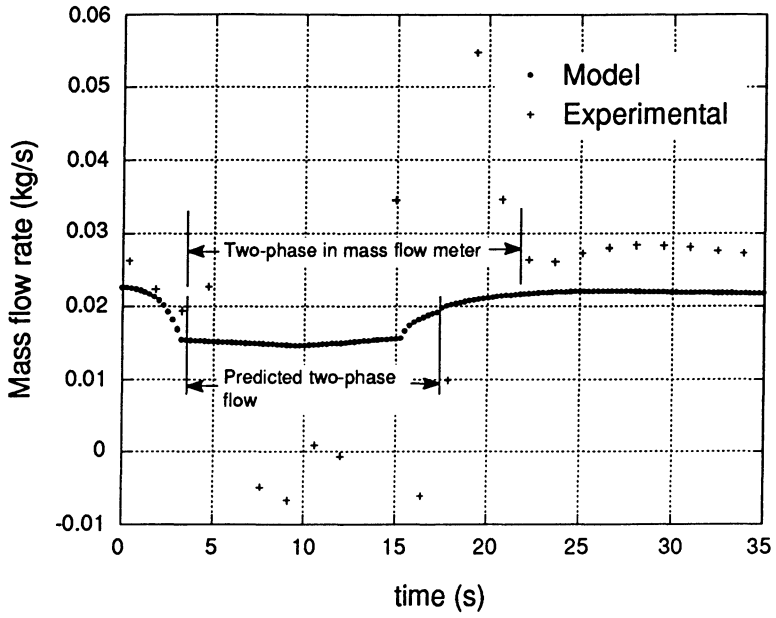

Figure 5.27 Clutch cycling mass flow rate.

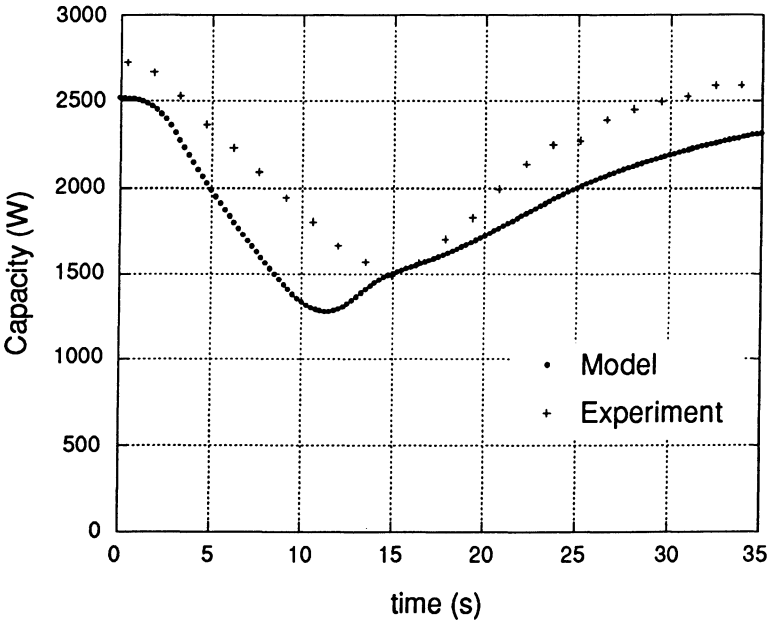

Figure 5.28 Clutch cycling evaporator capacity.

Figure 5.29 shows the refrigerant mass distribution in the system. After the clutch disengages at 0 s, mass in the condenser and liquid line empties into the evaporator and accumulator. The mass in the evaporator increases until the clutch engages again at 9 s. After this point, the evaporator empties its excess mass into the accumulator. The mass in the accumulator increases until approximately 13 s. After that, the excess mass in the accumulator is redistributed to the condenser and liquid line.

Figure 5.30 shows the pseudo-quality in each of the components. The quality in the condenser and liquid line remains relatively constant. The quality in the evaporator decreases sharply after the clutch disengages. After the clutch re-engages the evaporator essentially empties of liquid and then refills to return to approximately the same steady-state value.

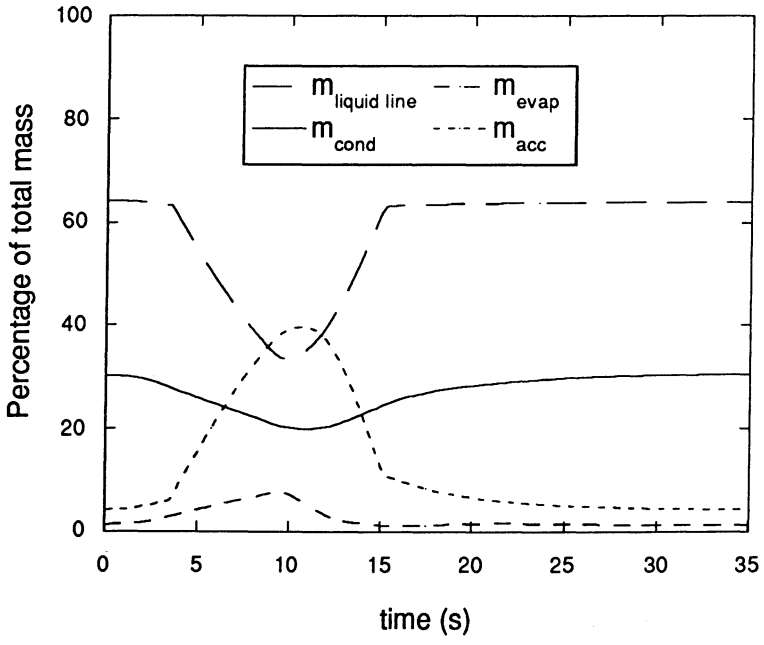

Figure 5.29 Clutch cycling mass distribution.

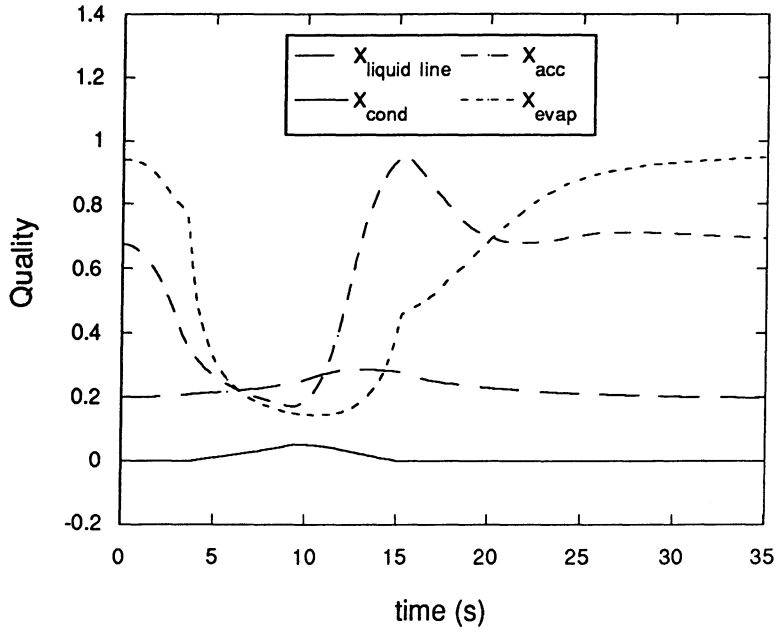

Figure 5.30 Clutch cycling component pseudo-quality.

Chapter 6
Refrigerant Property Routines Background

An important aspect of modeling any refrigeration or air-conditioning system is accurately determining the thermodynamic state and the refrigerant properties. Specifically in vapor-compression systems, it is important to accurately model the vapor, liquid, and two-phase vapor-liquid regions. Additionally, the supercritical region is important for transcritical vapor-compression cycles.

The computer codes which solve for thermodynamic properties are called refrigerant property routines. Good property routines must

1) Accurately solve for the refrigerant properties,
2) Quickly solve for the refrigerant properties,
3) Provide versatility with respect to the input properties,
4) Have a convenient user interface, and
5) Provide results for different refrigerants.

Poorly formulated property routines can cause problems in a computer model by providing inaccurate refrigerant properties and thus providing poor agreement with the experimental data. Also, numerical discontinuities in the property routines can cause problems with convergence of a simulation code.

This chapter reviews the basic thermodynamic concepts regarding thermodynamic properties and different equations of state. We also discuss how to compute properties from the equations of state, and we review currently available refrigerant property routines. The next chapter details the refrigerant property routine code written for the transient air conditioner model.

6.1 Equilibrium Thermodynamic Properties

A thermodynamic property is defined as any quantity that is dependent on the state of the system and is independent of the prior history of the system. Intensive or mass specific properties are given on a per unit mass basis. Unless otherwise specified, mass specific properties are indicated by the use of lower case letters. The thermodynamic properties discussed in this chapter are temperature (T), pressure (P), density (ρ), specific volume (v), enthalpy (h), internal energy (u), entropy (s), Gibbs free energy (g), specific heat at constant

volume (c_v), and specific heat at constant pressure (c_p). For simplicity, we will restrict this discussion of thermodynamic properties to a single component.

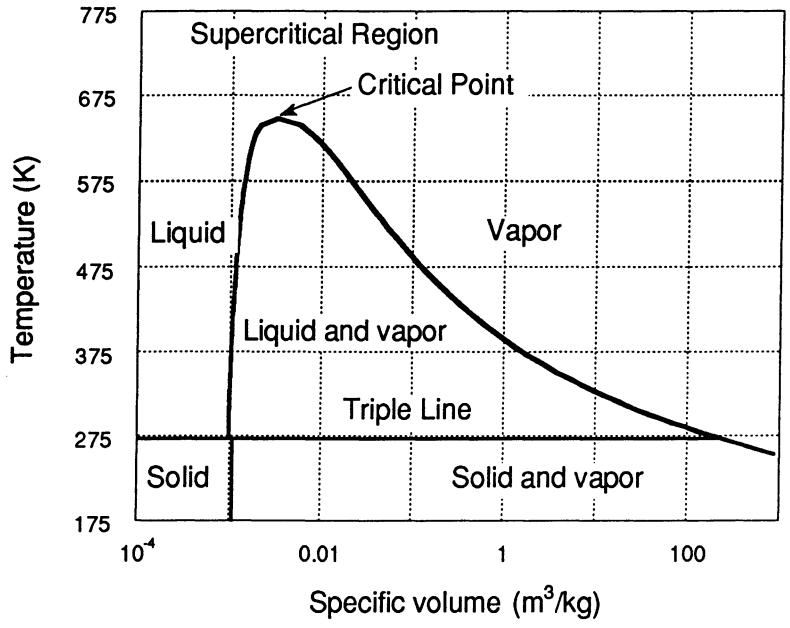

Figure 6.1 T-v phase diagram for water.

The state of a material is completely described by a three-dimensional T-v-P surface, but it is more common to see a two-dimensional projection of this surface. Figure 6.1 displays a T-v phase diagram for water. It illustrates the temperature and specific volume ranges for the solid, liquid, vapor, and two-phase regions. The two-phase liquid-solid region reduces to a line between the single phases in this two-dimensional projection. The triple-point is the only temperature at which the three phase can coexist in equilibrium. The critical point is at the maximum temperature, T_{crit}, of the liquid-vapor region. A critical pressure, P_{crit}, and critical density, ρ_{crit}, are also defined at this point. The liquid-vapor dome is the two-phase liquid-vapor region. The minimum temperature of this dome is the triple point and the maximum temperature is the critical point. Above the critical point is the supercritical region. In this region as the liquid transforms to vapor, no separable phases exist between the liquid and vapor. Vapor-compression refrigeration cycles operate in the liquid, vapor, and two-phase region. Additionally, transcritical vapor-compression cycles operate in the supercritical region. Refrigerant property routines traditionally solve for properties between the triple point temperature and a maximum temperature which is above the critical point.

According to Gibbs phase rule, two independent thermodynamic properties are required to specify the equilibrium state of a single-phase, single-component substance. One property is needed to specify the state of a two-phase, single-component substance. Figure 6.2 shows the liquid-vapor dome for R134a with equilibrium isobars in the two-phase region.

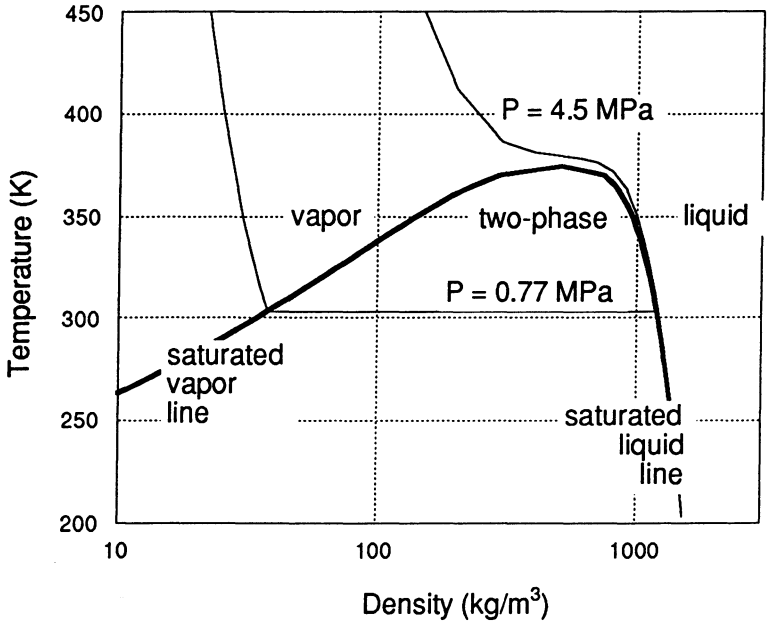

Figure 6.2 Liquid-vapor dome for R134a.

It is evident that both temperature and pressure are needed to determine the density in the liquid, vapor, and supercritical regions. Within the two-phase region, the temperature exactly defines the pressure and vice versa. The two-phase temperature and pressure are called the saturation pressure and the saturation temperature, respectively. In equilibrium, the liquid and vapor are at the same temperature (thermal equilibrium) and pressure (dynamic equilibrium).

$$T_{liquid} = T_{vapor} \tag{6.1}$$

$$P_{liquid} = P_{vapor} \tag{6.2}$$

Although either the temperature or pressure are required to specify the state in a two-phase region, this single intensive property does not provide information on the relative amounts of the two phases. An additional property is required to provide this information. The quality of a two-phase mixture is defined as

$$x = \frac{m_{vapor}}{m_{liquid} + m_{vapor}} . \tag{6.3}$$

Within the two-phase region, the liquid is at the saturated liquid state (defined by subscript f) and the vapor is at the saturated vapor state (defined by subscript g). The saturation liquid and vapor properties are defined along the saturation lines which separate the single and two-phase regions (Figure 6.2). Consequently, the two-phase specific volume, enthalpy, internal energy, and entropy are determined from the following equations.

$$v = v_f + x(v_g - v_f) \tag{6.4}$$

$$h = h_f + x(h_g - h_f) \tag{6.5}$$

$$u = u_f + x(u_g - u_f) \tag{6.6}$$

$$s = s_f + x(s_g - s_f) \tag{6.7}$$

The two-phase density is

$$\frac{1}{\rho} = \frac{1}{\rho_f} + x\left(\frac{1}{\rho_g} - \frac{1}{\rho_f}\right). \tag{6.8}$$

In conclusion, in order to determine the properties of a single-phase substance, two intensive properties are required. For a two-phase substance, either temperature and pressure are required to determine the state. An additional property is required to provide the respective amounts of liquid and vapor.

6.2 Equations of State

An equation of state is an analytical representation of the thermodynamic behavior of a substance. It is a mathematical relationship between two independent and one dependent property such as P-ρ-T (pressure, density, and temperature) and has the form

$$P = f(T, \rho) . \tag{6.9}$$

When this equation is combined with an equation for the ideal gas specific heat, c_v°, one can explicitly solve for the thermodynamic properties as a function of temperature and density (Section 7.2.1).

$$c_v^\circ = f(T) \tag{6.10}$$

The next section summarizes different types of P-ρ-T equations of states. The c_v° equation is usually in the form of a polynomial.

Another method of calculating properties is to interpolate from a thermodynamic table. The data in property tables are originally obtained from an equation of state because it is difficult to obtain an adequate amount of experimental data. Also, it is impossible to measure thermodynamic properties such as enthalpy or entropy. Using a computer program to interpolate from a table is a time efficient method but the precision depends on the density of data points in the table. The advantage of using an equation of state is that the calculated properties are as accurate as the curve fit of the P-ρ-T data.

6.2.1 Types of Equations of State

The three types of equations of state are general, theoretical, and empirical. General equations of state are used to represent property behavior over a limited region of state. Theoretical equations of state are derived from kinetic theory or statistical thermodynamics. Empirical equations of state are curve fits of experimental P-v-T data.

The ideal gas law is an example of a general equation of state.

$$Pv = RT \tag{6.11}$$

This equation of state only applies in the superheated and supercritical regions away from the critical point. The van der Walls and Redlich-Kwong equation of state attempt to modify the ideal gas equation in order to provide accurate values over a broader range of conditions.

$$P(T,v) = \frac{RT}{v-b} - \frac{a}{v^2} \qquad \text{(van der Walls)} \tag{6.12}$$

$$P(T,v) = \frac{RT}{v - b_{rk}} - \frac{a_{rk}}{v(v + b_{rk})T^{1/2}} \quad \text{(Redlich-Kwong)} \tag{6.13}$$

The coefficients for van der Walls equations (a and b) and Redlich-Kwong equation (a_{rk} and b_{rk}) can be determined analytically from the temperature and pressure at the critical point. Both equations of state increase the accuracy of the ideal gas law but none of these generalized equations are valid in the liquid, solid, or multiphase regions.

Statistical mechanics is used to predict the form of a theoretical equation of state. An example of a theoretical equation of state is the virial equation.

$$P(T,v) = \frac{RT}{v} + \frac{RT\,B(T)}{v^2} + \frac{RT\,C(T)}{v^3} + \ldots \tag{6.14}$$

The functions B and C are called the second and third virial coefficient. These coefficients can be related to parameters characterizing the intermolecular potential function. The equation is often truncated after the second coefficient and is then only valid in the vapor region for small deviations from ideal-gas behavior.

Another theoretical equation of state is based on a theoretical reference fluid. For example, the Carnahan-Starling-DeSantis (CSD) equation of state models the hard-sphere fluid (DeSantis, 1975). This fluid exhibits an infinite repulsion force for a bimolecular collision at some distance of closest approach.

$$\frac{Pv}{RT} = \frac{1 + y + y^2 - y^3}{(1-y)^3} - \frac{a}{RT(v+b)} \tag{6.15}$$

where

$$y = \frac{b}{4v}, \tag{6.16}$$

$$a = a_0\, e^{\left(a_1 T + a_2 T^2\right)}, \text{ and} \tag{6.17}$$

$$b = b_0 + b_1 T + b_2 T^2. \tag{6.18}$$

The above equation does not model a real fluid exactly, but it correctly represents the fluid in the vapor region and for saturated liquid properties. The coefficients (a_0, b_0, b_1, and b_2) for real fluids are empirically determined.

Empirical equations of state can be extremely accurate if a sufficient amount of experimental data is obtained. The minimum experimental data needed to define an equation of state consist of P-v-T data along lines of constant volume in the vapor phase, saturated liquid density and vapor pressure over a range of temperatures, and the critical point (McLinden et al., 1989). An example of an empirical equation of state is given by Martin and Hou (1955). One form of the equation is listed below; however, several modifications exist.

$$P(T,v) = \frac{RT}{(v - b)} + \sum_{i=2}^{5} \frac{1}{(v - b)^i}\left[A_i + B_i T + C_i \exp\left(\frac{-kT}{T_{crit}}\right)\right] \tag{6.19}$$

This equation is not accurate in the subcooled region.

None of the above equations of state predict refrigerant properties in the subcooled liquid region. As result, an additional model must be employed to compute the properties in this region. Another empirical equation, the Modified Benedict-Webb-Rubin (MBWR) equation of state (Jacobsen and Stewart, 1973), accurately predicts the refrigerant properties in the superheated vapor, subcooled liquid, and supercritical regions. It is widely used for the representation of hydrocarbons and cryogenic fluid. The MBWR equation has 32 adjustable parameters which provide an accurate representation of the experimental data and requires an involved fitting procedure. The form of the MBWR equation is

$$P(T,\rho) = \sum_{n=1}^{9} a_n(T)\,\rho^n + \exp\left(\frac{-\rho^2}{\rho_{crit}^2}\right)\sum_{n=10}^{15} a_n(T)\,\rho^{2n-17} \tag{6.20}$$

The form of functions a_1-a_{15} are given in Table 7.2.

The above equations of state calculate pressure as a function of temperature and density. An additional equation for the ideal gas specific heat (Equation 6.10) is needed to obtain a complete description of the thermodynamic properties. The fundamental equation of state provides a complete description of thermodynamic properties in a single equation (Lemmon et al., 1995). The Helmholtz energy is used as the dependent variable instead of pressure. The Helmholtz energy is defined as

$$a = u - Ts \tag{6.21}$$

The fundamental equation of state has the general form

$$\frac{a}{RT} = a^{\circ}(\delta,\tau) + \bar{a}(\delta,\tau) \tag{6.22}$$

where

$$\delta = \frac{\rho}{\rho_{crit}} \tag{6.23}$$

and

$$\tau = \frac{T}{T_{crit}}. \tag{6.24}$$

a° is the ideal gas contribution and $\bar{a}$ is the real fluid contribution. The specific form of these equations is summarized in Lemmon et al. (1995). An advantage of the fundamental equation of state is that the properties of mixtures can be computed by applying mixing rules to the Helmholtz energy (McLinden et al., 1998).

The final equation of state we will discuss is the extended corresponding states (ECS) model (Huber and Ely, 1994). This model is useful for fluids with limited amounts of experimental data. A reference fluid is chosen which is chemically similar to the fluid of interest and has a well defined equation of state. This model assumes that similar fluids obey the same intermolecular force laws. As a result, the real fluid contribution to the Helmholtz energies, $\bar{a}$, of different fluids are equal with the appropriate scaling of the temperature and density. The temperature and density are scaled by the critical parameters and by empirically determined coefficients.

6.2.2 Solving for Thermodynamic Properties

The above formulation of the equation of state (Equations 6.9 and 6.10) allow all of the properties to be explicitly calculated from temperature and density (Section 7.2.1). To be practical in a modeling application, a refrigerant property routine program should allow the user to input any two of the following properties: temperature, density, pressure, enthalpy, internal energy, entropy, and quality. Either a one-dimensional or two-dimensional search is

performed to calculate the correct temperature and density from which the output property is calculated. The refrigerant property routine program must be robust and accurately converge on the correct properties.

0-D Searches	1-D Searches		2-D Searches	
T, ρ	T, P	ρ, P	P, h	h, u
	T, h	ρ, h	P, u	h, s
	T, u	ρ, u	P, s	u, s
	T, s	ρ, s		

Table 6.1 Dimension of searches for combinations of single-phase input properties.

Table 6.1 summarizes the dimensions of the search required for each combination of single-phase input properties. If temperature and either pressure, enthalpy, internal energy, entropy, or quality are inputs, then a one-dimensional search is used to calculate the correct density. Similarly, a one-dimensional search calculates the correct temperature if density and one other property are inputs. If neither temperature nor density are inputs, then a two-dimensional search determines the correct temperature and density.

0-D Searches	1-D Searches		
T, x	P, x	ρ, h	x, ρ
T, ρ	P, ρ	ρ, u	x, h
T, h	P, h	ρ, s	x, u
T, u	P, u	h-u	x, s
T, s	P, s	h-s	
		u-s	

Table 6.2 Dimension of searches for combinations of two-phase input properties.

In the two-phase region, a different algorithm is used to determine the thermodynamic properties. The properties are uniquely determined by the temperature and quality. If temperature and density, enthalpy, internal energy, or entropy are inputs then the quality can be determined from Equations 6.4 - 6.8. If pressure instead of temperature is an input, then the

saturation temperature and the quality can be determined. If neither of the inputs are temperature and pressure, then a one-dimensional search is performed for the saturation temperature. The quality calculated for the two properties from the temperature must be equal. Table 6.2 summarizes the dimensions of the searches for each combination of two-phase input properties.

The property routines must be able to determine whether the state is single-phase or two-phase to determine the correct result. The specific algorithms used in our refrigerant property routines are detailed in the next chapter (Section 7.3). The following section summarizes some of the refrigerant property routines which are currently available.

6.3 Review of Refrigerant Property Routines

Some of the programs developed to solve for refrigerant properties are REFPROP, ALLPROPS, and EES. Table 6.3 shows an overall comparison between the routines. Table 6.4 shows the combinations of input properties for which each routine solves.

	ALLPROPS	REFPROP	EES
Developer	University of Idaho	NIST	F-Chart Software
Equation of State	Fundamental	MBWR, Fundamental, ECS	Martin-Hou
Number of refrigerants	43	43	43
Allows refrigerant mixtures	no	yes	no
Programming language	FORTRAN	FORTRAN	Independent PC program

Table 6.3 Comparison of refrigerant property routines.

REFPROP is a FORTRAN program developed by the National Institute of Standards and Technology (NIST) (McLinden et al., 1998). The main advantage of this program is that it determines properties for arbitrary mixtures of up to five refrigerants. The disadvantages are that it does not allow for many different combinations of input properties. Also, the FORTRAN interface is somewhat cumbersome for use in models.

ALLPROPS is a FORTRAN program developed by Center for Applied Thermodynamic Studies at the University of Idaho (Lemmon, et al., 1995). It allows for more combinations of input properties and has a better user interface than REFPROP. However it still does not allow for all of the combinations of input properties.

The Engineering Equation Solver (EES) runs on a personal computer and uses a Newton-Raphson iteration scheme to solve a set of algebraic equations. Incorporated into EES are the thermophysical properties of 43 fluids. EES allows one to calculate any thermodynamic properties from all combinations properties except for internal energy and enthalpy. It uses the Martin-Hou equation of state which is not valid in the liquid region. In the liquid region, the pressure is set equal to the saturation pressure and is independent of density. It is generally a robust program except when internal energy is used as an input variable.

6.4 Conclusion

No currently available refrigerant property routines meet all of the requirements needed for a system model. This chapter reviewed some basic definitions of thermodynamic properties and the different types of equations of states. It also explained how to calculate properties from the equations of state. The next chapter explains how this theory was implemented in a new refrigerant property routine.

Input Properties		Refrigerant Property Routines		
		ALLPROPS	REFPROP	EES
0-D Searches	T, ρ	x	x	x
1-D Searches	T, P	*	x	x
	T, h			x
	T, u			**
	T, s	x		x
	T, x			x
	ρ, P	x		x
	ρ, h	x		x
	ρ, u	x		**
	ρ, s	x		x
	ρ, x			x
2-D Searches	P, h	x	x	x
	P, u			**
	P, s	x	x	x
	P, x			x
	h, u			
	h, s			x
	h, x			x
	u, s			**
	u, x			**
	s, x			x

x = solves for properties

* = requires an initial guess for ρ

** = has convergence problems

Table 6.4 Combinations of input properties for which the property routines.

Chapter 7
Refrigerant Property Routines

A need exists for a robust set of FORTRAN refrigerant property routines which can easily be used with a computer model. We have developed a property routine which uses the Modified Benedict-Webb-Rubin (MBWR) equation of state and provides a convenient user interface. It allows for any of the following properties as inputs: temperature, density, pressure, enthalpy, internal energy, entropy, and quality. The program solves for any of the above properties as well as specific heat at constant volume, specific heat at constant pressure, the speed of sound, and Gibbs free energy.

The previous chapter provided an overview of the available property routines and their limitations. This chapter outlines the algorithms used in our property routine code. As summarized in Chapter 6, the purpose of a property routine code is to take two independent properties and to calculate a third output property. Our property routines uses the following basic procedure.

1) Obtain two independent input properties from the user interface and the desired output property.
2) Determine if the refrigerant is single phase or two-phase.
3) If the refrigerant is single phase find the correct temperature and density.
4) If the refrigerant is two-phase find the correct temperature and quality.
5) Find the correct output property.

Section 7.1 provides an overview of the user interface. It describes the FORTRAN commands used to call the property routines and the valid input and output properties. It also shows the units of the properties.

In Section 7.2, we provide details about the equation of state used in the property routines. Also, we explain how all of the output properties are calculated from the equation of state.

Section 7.3 explains how to determine if the refrigerant is single phase or two-phase. It also explains how to find saturation conditions from the equation of state.

Section 7.4 summarizes the search routines, single-phase searches and two-phase searches. In the single-phase region, the properties can be directly calculated from the temperature and density. If the two input properties are not temperature and density, then a search routine must be executed to determine the correct temperature and density. They include

1) One-dimensional search for temperature given density and one other property.
2) One-dimensional search for density given temperature and one other property.
3) Two-dimensional search for temperature and density given two other properties.

In the two-phase region, all properties can be determined from temperature and quality. The two phase searches are

1) One-dimensional search for saturation temperature given saturation pressure.
2) One-dimensional search for saturation temperature given two other properties not including pressure.

Sections 7.5 and 7.6 describe the performance and accuracy of the property routines.

7.1 User Interface

The user interface for the FORTRAN refrigerant property routines is designed to be intuitive and convenient. First, a refrigerant subroutine which initializes the program for a specific refrigerant must be called. The name of the subroutine is simply the name of the substance. For example, R134a is initialized with the following call.

```
call R134a
```

After the refrigerant is initialized, properties can be determined with a call to the FORTRAN function *prop*. This function solves for one thermodynamic property given two other thermodynamic properties.

```
OUT = prop(cout,cin1,xin1,cin2,xin2)
Inputs:     cout  =   a string of 3 characters indicating the desired output
                      property
            cin1  =   a string of 3 characters indicating the first input
                      property
```

	xin1 =	double precision value of the first input property
	cin2 =	a string of 3 characters indicating the second input property
	xin2 =	double precision value of the second input property
Outputs:	OUT =	double precision value of desired output property

For example, to determine pressure given temperature (300 K) and density (0.01 kg/m^3) the following function call is used.

```
P = prop('P  ', 'T  ', 300d0, 'rho', 0.01d0)
```

The unit system and variables used in the program are summarized in Table 7.1. All of the variables in Table 7.2 are valid outputs but only temperature, pressure, density, specific volume, enthalpy, entropy, internal energy, entropy, and quality are valid inputs.

Property	**Variable**	**Unit**	**Valid Input**	**Valid Output**
temperature	T	K	yes	yes
pressure	P	Pa	yes	yes
density	rho	kg / m^3	yes	yes
specific volume	v	m^3 / kg	yes	yes
enthalpy	h	J / kg	yes	yes
internal energy	u	J / kg	yes	yes
entropy	s	J / kg-K	yes	yes
quality	x	-----	yes	yes
specific heat at constant pressure	cp	J / kg-K	no	yes
specific heat at constant volume	cv	J / kg-K	no	yes
Gibbs free energy	g	J / kg	no	yes

Table 7.1 Description of properties used in the refrigerant property routines.

The program does some minimal error checking when the function *prop* is called. It checks that the user has not used both density and specific volume as inputs. It also verifies

that if temperature or density are inputs, they are within the correct range. How this range is determined is detailed in Section 7.2.

The refrigerant property routines have two additional user subroutines. The input for the first subroutine is the saturation temperature. The outputs are the saturation pressure and the saturated liquid and saturated vapor values for specific volume, enthalpy, and entropy.

```
subroutine sat_T(Tsat, Psat,vg,vf,hg,hf,sg,sf)
Inputs:     Tsat  =   Saturation temperature
Outputs:    Psat  =   Saturation pressure
            vg    =   Saturated vapor specific volume
            vf    =   Saturated liquid specific volume
            hg    =   Saturated vapor enthalpy
            hf    =   Saturated liquid enthalpy
            sg    =   Saturated vapor entropy
            sf    =   Saturated liquid entropy
```

The second subroutine also returns the saturation properties but the input is pressure.

```
subroutine sat_P(Psat, Tsat,vg,vf,hg,hf,sg,sf)
Inputs:     Psat  =   Saturation pressure
Outputs:    Tsat  =   Saturation temperature
            vg    =   Saturated vapor specific volume
            vf    =   Saturated liquid specific volume
            hg    =   Saturated vapor enthalpy
            hf    =   Saturated liquid enthalpy
            sg    =   Saturated vapor entropy
            sf    =   Saturated liquid entropy
```

If the input temperature or pressure is greater than the critical value, then zero is returned for all of the saturation values.

One refrigerant, R134a, has been programmed into the refrigerant property routines. The procedure for adding additional properties is detailed in Appendix E.

7.2 Equation of State

The Modified Benedict-Webb-Rubin (MBWR) equation of state is used in the refrigerant property routines. This equation of state is empirical and is extremely accurate

because it has thirty-two empirical coefficients. The MBWR equation of state is valid in the vapor, liquid, and supercritical regions. It is also a common equation of state and coefficients have been determined for many refrigerants. This equations determines pressure as a function of temperature and density. γ is a constant equal to the critical specific volume. For the below coefficients $\gamma = 1.948\ 10^{-3}$.

$$P = \sum_{n=1}^{9} a_n \rho^n + \exp\left(-\rho^2\gamma^2\right) \sum_{n=10}^{15} a_n \rho^{2n-17} \tag{7.1}$$

Coefficient	Equation
a_1	RT
a_2	$b_1T + b_2T^{0.5} + b_3 + b_4 / T + b_5 / T^2$
a_3	$b_6T + b_7 + b_8 / T + b_9 / T^2$
a_4	$b_{10}T + b_{11} + b_{12} / T$
a_5	b_{13}
a_6	$b_{14} / T + b_{15} / T^2$
a_7	b_{16} / T
a_8	$b_{17} / T + b_{18} / T^2$
a_9	b_{19} / T^2
a_{10}	$b_{20} / T^2 + b_{21} / T^3$
a_{11}	$b_{22} / T^2 + b_{23} / T^4$
a_{12}	$b_{24} / T^2 + b_{25} / T^3$
a_{13}	$b_{26} / T^2 + b_{27} / T^4$
a_{14}	$b_{28} / T^2 + b_{29} / T^3$
a_{15}	$b_{30} / T^2 + b_{31} / T^3 + b_{32} / T^4$

Table 7.2 Equations for the a_1 - a_{15} coefficients in the Modified Benedict-Webb-Rubin equation of state.

Coefficient	Value	Coefficient	Value
b_1	0.9271836240E+00	b_{17}	-0.6241811030E-13
b_2	0.3859943345E+02	b_{18}	0.3241227725E-10
b_3	0.3796685328E+03	b_{19}	-0.8832148917E-14
b_4	0.1292327632E+05	b_{20}	-0.6395014970E+05
b_5	-0.1339463227E+08	b_{21}	-0.1195678765E+08
b_6	-0.2911857245E-03	b_{22}	-0.3854864317E+00
b_7	0.2752746684E+00	b_{23}	0.9222468987E+04
b_8	-0.1554841102E+03	b_{24}	0.1621989396E-06
b_9	0.1418884002E+06	b_{25}	-0.8109327456E-04
b_{10}	0.4936522116E-07	b_{26}	-0.4771379477E-12
b_{11}	0.5019195534E-03	b_{27}	-0.1475162087E-07
b_{12}	-0.1950030878E+00	b_{28}	-0.3184879150E-18
b_{13}	-0.2425521321E-06	b_{29}	0.1146516844E-15
b_{14}	-0.4796051391E-07	b_{30}	0.6184422434E-25
b_{15}	-0.7549801475E-04	b_{31}	-0.1324227401E-21
b_{16}	0.1782613900E-09	b_{32}	0.1742223096E-20

Table 7.3 Values of the empirical coefficients of the Modified Benedict-Webb-Rubin equation of state for R134a (Huber and Ely, 1994).

Table 7.2 and Table 7.3 summarize the empirical coefficients used in the equations of state. Along with an equation for the ideal specific heat at constant volume all other properties can be determined (Section 7.2.1). Equation 7.2 is the equation for the ideal specific heat at constant volume and the coefficients are summarized in Table 7.4.

$$c_v^\circ = c_1 + c_2T + c_3T^2 + c_4T^3 + c_5T^4 + c_6T^5 + c_7T^6 \tag{7.2}$$

Coefficient	Value
c_1	-3.0112041712E+03
c_2	4.8340122646E+01
c_3	-2.6767243954E-01
c_4	7.8064012365E-04
c_5	-1.2102287867E-06
c_6	9.4181503738E-10
c_7	-2.8847327981E-13

Table 7.4 Values of coefficients of the ideal specific heat at constant volume equation (Equation 7.2) for R134a (Huber et al, 1996).

One of the main difficulties found when developing property routines using the MBWR equation of state is that multiple answers exist for some of the one-dimensional and two-dimensional searches for temperature and density. The MBWR equation is only accurate for a certain range of temperatures and densities. Outside this range, redundant solutions exist for the search parameters.

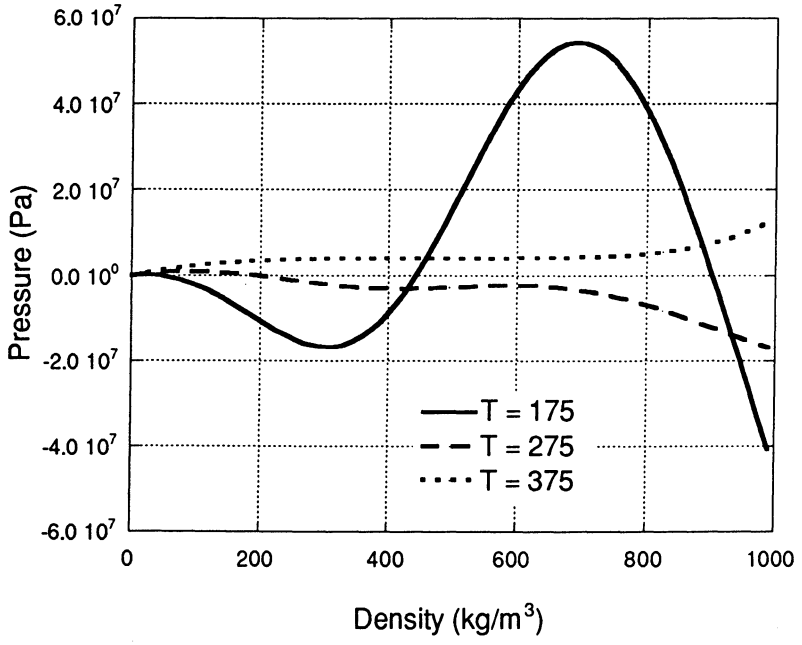

Figure 7.1 Pressure as a function of temperature and density from the MBWR equation of state.

Figure 7.1 shows an example of this phenomenon. The lowest temperature, 175 K, is below the minimum temperature for the properties. For a given pressure and density, it is possible to have two mathematically valid temperatures. However, only one of the temperatures is physically correct.

In order to ensure that the property routines converge on the correct result, a minimum and maximum temperature and a minimum and maximum density must be defined in the code. The temperature range for which the property routine is valid is generally available from the data. The valid density range is generally not always provided by the data. We used the following algorithm to determine the minimum and maximum density.

$$\rho_{min} = \frac{\rho_g(T_{min})}{10} \tag{7.3}$$

$$\rho_{max} = \rho_f(T_{min}) + 100 \tag{7.4}$$

These values provided a reasonable bound for the search routines. Table 7.5 summarizes the actual minimum and maximum temperatures and densities used for R134a.

	minimum	maximum
Temperature (K)	200	500
Density (kg/m3)	0.0001	1600

Table 7.5 Temperature and density range for R134a.

All of the algorithms and search routines discussed in this chapter were only checked with the MBWR equation of state. It is believed that these routines would be applicable for any equation of state with only minor modifications.

7.2.1 Calculating the Single-phase Properties

Pressure can be explicitly calculated from Equation 7.1. Equations for enthalpy (h), internal energy (u), entropy (s), specific heat at constant volume (c_v), specific heat at constant pressure (c_p), Gibbs free energy (g), and the speed of sound (ss) can be derived from Equation 7.1 and 7.2 using the following thermodynamic relations.

$$u(T,\rho) = \int c_v^\circ \, dT + \int \left(P - T\frac{\partial P}{\partial T} \right) \frac{d\rho}{\rho^2} \tag{7.5}$$

$$h(T, \rho) = u + \frac{P}{\rho} \tag{7.6}$$

$$s(T,\rho) = \int \frac{c_v^\circ}{T} dT + \int \frac{1}{\rho^2} \frac{\partial P}{\partial \rho} d\rho \tag{7.7}$$

$$c_v(T,\rho) = c_v^\circ - T\int \left(\frac{\partial^2 P}{\partial T^2} \right) \frac{d\rho}{\rho^2} \tag{7.8}$$

$$c_p(T, \rho) = c_v + \frac{\partial P}{\partial T} \tag{7.9}$$

$$g(T,\rho) = h - Ts \tag{7.10}$$

$$ss(T,\rho) = \sqrt{\left(\frac{\partial P}{\partial \rho} \right)_s} \tag{7.11}$$

Equations 7.1 and 7.2 are plugged into Equations 7.5 - 7.11 which results in a set of algebraic equations where all of the above properties can be directly calculated from temperature and density (Appendix D). Also, the derivatives with respect to temperature and density of all of the above equations are determined. If temperature and density are not inputs into the property routines, a search routine must be performed to determine the correct temperature and density. These search routines are summarized in Section 7.4

7.2.2 Calculating Two-phase Properties

The MBWR equation accurately predicts gas properties, liquid properties, supercritical properties, and saturation properties. The properties predicted in the two-phase region are not

equal to the equilibrium values. As a result, a different algorithm determines the properties in the two-phase region.

Temperature and quality uniquely define the properties in the two-phase region. The two-phase specific volume, enthalpy, internal energy, entropy, and density are determined from Equations 6.4 - 6.8. If temperature and quality are not inputs to the property routines, the appropriate algorithm must be used to determine the temperature and quality (Section 7.4.3). The next section discusses how to determine the saturation properties and the phase of the refrigerant.

7.3 Determining the Phase of the Refrigerant

There are different methods for determining the phase of the refrigerant for different pairs of input properties. If temperature (T) is one of the inputs then it trivial to determine the phase of the refrigerant with any other input (Table 7.6). Alternatively, if pressure is an input then the saturation temperature can be calculated and the phase is determined from the Table 7.6. If one of the inputs is quality, then it is known that the refrigerant is in the two-phase region (qualities less than zero or greater than one are not accepted as a valid input). It is not trivial to determine the phase of the refrigerant if none of the inputs are temperature, pressure, or quality.

Phase	**INPUTS**		
	T and ρ	**T and h (or T and s or T and u)**	**T and P**
vapor	$\rho \leq \rho_g(T)$	$h \geq h_g(T)$	$P < P_{crit}$
liquid	$\rho \geq \rho_f(T)$	$h \leq h_f(T)$	$P > P_{crit}$
two-phase	$\rho_g(T) < \rho < \rho_f(T)$	$h_g(T) > h > h_f(T)$	$P = P_{crit}$
supercritical	$T > T_{crit}$	$T > T_{crit}$	$T > T_{crit}$

Table 7.6 Conditions for determining the phase of the refrigerant if temperature is an input.

No experimental data from the two-phase region is used to determine the coefficients in the Modified Benedict-Webb-Rubin equation of state. The answers returned from the MBWR equation in the two-phase region are not equal to the equilibrium thermodynamic properties. For example, in the two-phase region the equilibrium pressure remains constant along an isotherm. Figure 7.2 illustrates the isotherms returned by the MBWR equation in the two-phase region. Although the pressure varies greatly, it always remains within the two-phase dome.

We can use this information to determine if the properties are in the single-phase or two-phase region.

The following algorithm is used if the input properties include two of the following properties: density, enthalpy, internal energy, or entropy. The appropriate single-phase search is performed to calculate a single-phase temperature, T_{1phase}, and density, ρ_{1phase}, (Section 7.4.2). If T_{1phase} and ρ_{1phase} are in the two-phase region (Table 7.6) then the correct two-phase properties temperature and quality must be determined (Section 7.4.3). If T_{1phase} and ρ_{1phase} are in the single-phase region, then they are correct. This algorithm works for all combinations of the input properties (density, enthalpy, internal energy, or entropy) except for enthalpy and internal energy. These properties are not independent in the two-phase region as summarized in Section 7.5.

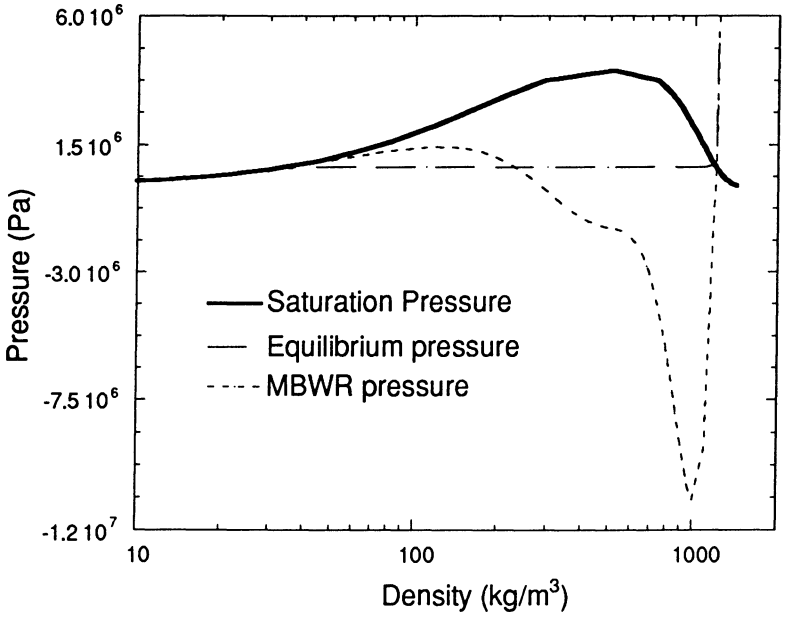

Figure 7.2 A comparison of the two-phase equilibrium pressure with the pressure determined from the MBWR equation of state.

In order to determine the phase of the refrigerant, it is necessary to be able to calculate the saturation properties at a given temperature. The following sections describe that procedure.

7.3.1 Calculating the Saturation Properties

When different phases of a pure substance are in equilibrium, each phase must have the same temperature, pressure, and Gibbs free energy per unit mass.

$$T_{liquid} = T_{vapor} \tag{7.12}$$

$$P_{liquid} = P_{vapor} \tag{7.13}$$

$$g_{liquid} = g_{vapor} \quad \text{or} \quad g_f = g_g \tag{7.14}$$

Given a temperature, a two-dimensional search is performed to find the corresponding saturated liquid density and saturated vapor density. The two equations for the search are Equations 7.13 and 7.14. The trivial answer for those equations is

$$\rho_f = \rho_g = \rho \tag{7.15}$$

where ρ can be any value. In order to solve for two distinct values of ρ_f and ρ_g initial guesses which are close to the actual value must be provided. Curve fits of the saturation properties were developed for this purpose.

7.3.2 Determining Curve Fits of the Saturation Properties

In order to develop curve fits for the saturation properties, the saturation properties first need to be obtained from the equation of state. A program independent of the property routines was developed for this purpose. An array of temperature T_n is created from the minimum valid temperature to the critical temperature. Since the saturation densities change greatly near the critical point, many temperatures should be clustered around the point. A seed is given for the initial guess for ρ_f and ρ_g at T_{min} which can be obtained from a table of refrigerant properties. The program calls a two-dimensional Newton-Raphson search routine as specified below.

Inputs:	T_i
Unknowns:	ρ_f, ρ_g
Initial guess:	$\rho_f = \rho_{f,i-1}$
	$\rho_g = \rho_{g,i-1}$

Equations:

$$P(T_i,\rho_g) = P(T_i,\rho_f) \tag{7.16}$$

$$g(T_i,\rho_g) = g(T_i,\rho_f) \tag{7.17}$$

After the search routine has converged on a the saturation vapor density and the saturation liquid density, these values are used a initial guesses for the search at the next temperature. Using this method, the saturation dome was created for R134a (Figure 7.3).

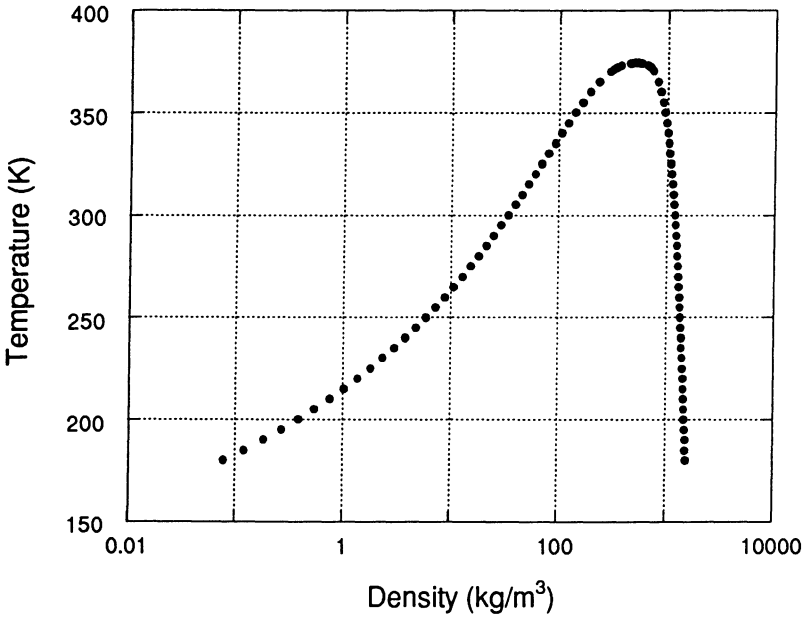

Figure 7.3 Saturation dome for R134a.

A curve fit of ρ_f vs. T and P_{sat} vs. T was created from this data for R134a (Figure 7.4 and Figure 7.5). The form of the saturated liquid density equation is

$$\rho_f = r_0 + r_1(T^*) + r_2(T^*)^2 + r_3(T^*)^3 + r_4(T^*)^4 \tag{7.18}$$

where

$$T^* = \left(1 - \frac{T}{T_{crit}}\right)^{1/3} \tag{7.19}$$

$r_0 = 520.73223019$

$r_1 = 718.02485183$

$r_2 = 1477.8123759$

$r_3 = -1987.0643174$

$r_4 = 1299.9953261$

$T_{crit} = 374.18$

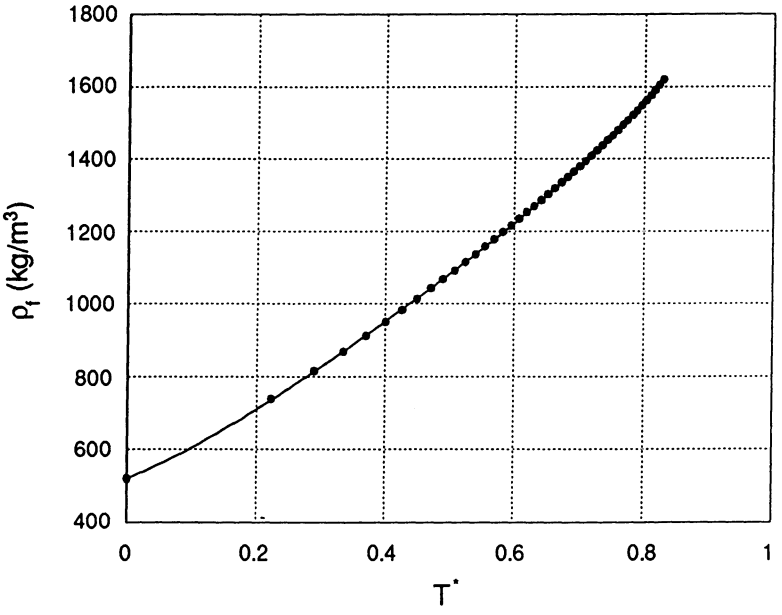

Figure 7.4 Curve fit for the saturated liquid density of R134a.

The form of the saturation pressure curve fit is

$$\ln(P_{sat}) = p_0 + p_1 T + p_2 T^2 + p_3 T^3 + p_4 T^4 + p_5 T^5 \tag{7.20}$$

where

$p_0 = -67.372739467$

$p_1 = 1.0348363554$

$p_2 = -0.0058497264175$

$p_3 = 1.7771926183e-05$

p_4 = -2.7991145435e-08

p_5 = 1.8003152482e-11

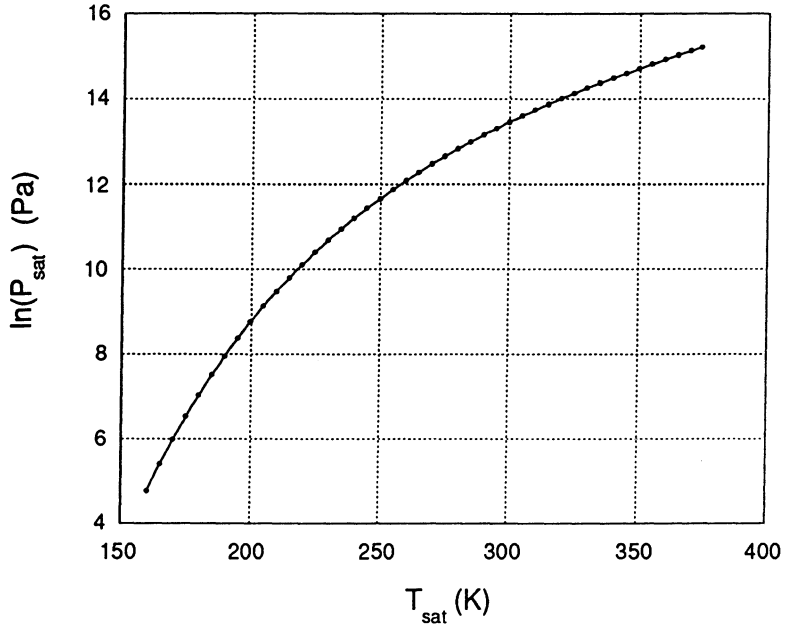

Figure 7.5 Curve fit for the saturation pressure of R134a.

Reid, Prausnitz, and Poling (1987) have examples of different forms of these curve fits.

The actual subroutine which calculates the saturation properties in the property routines is called *Subroutine sat*. This subroutine calculates the saturation pressure (P_{sat}), saturated liquid density (ρ_f), and saturated vapor density (ρ_g) at a given temperature. The initial guess for the saturated liquid density is calculated from the curve fit of ρ_f versus T. The initial guess for the saturated vapor density is determined from the ideal gas law.

Subroutine sat

Inputs: T

Unknowns: ρ_f, ρ_g

Initial guess: $\rho_f = \rho_f(T)$ from Equation 7.18

$$\rho_g = \frac{P}{RT} \text{ where } P = P_{sat}(T) \text{ from Equation 7.20} \qquad (7.21)$$

Equations:

$$P(T,\rho_g) = P(T,\rho_f) \qquad (7.22)$$

$$g(T,\rho_g) = g(T,\rho_f) \tag{7.23}$$

The code verifies that ρ_g is in the vapor region by checking if $\partial P/\partial\rho$ is less than zero. If $\partial P/\partial\rho$ is greater than zero, the code halves ρ_g until the derivative is less than zero. The search routine is a two-dimensional Broydn's method or multidimensional secant method.

Near the critical point, the program tends to converge on the same density for both unknowns since the difference between saturation densities is small. The initial guesses must be extremely close to the actual values for the two-dimensional search to converge on the correct densities. A different algorithm is used to find the initial guesses if $T \geq 0.975\ T_{crit}$. The saturation liquid density determined from the curve fit is assumed to be correct. Then a one-dimensional search is performed to calculate the saturated vapor density. After this program has converged, the results are used in the two-dimensional search to find the exact answer.

7.3.3 Notes about the Critical Point

The critical point is illustrated in Figure 6.1. It is the maximum temperature and pressure of the two-phase region. The critical point is defined by

$$\left(\frac{\partial P}{\partial \rho}\right)_T = 0 \tag{7.24}$$

$$\left(\frac{\partial^2 P}{\partial \rho^2}\right)_T = 0 \tag{7.25}$$

The critical point defined by the equations of state does not exactly meet both of these conditions.

A two-dimensional search was performed to find the temperature and density at the critical point using the above equations as residuals. The search was given several initial guesses very close to the critical point. For R134a, the search consistently returned the same temperature, 374.182 K, for various initial guesses. It always returned a density close to the initial guess rather than the actual critical density. From this search the saturation temperature and saturation pressure were determined to be 374.182 K and 4.05598 MPa. The critical density was determined from the two-dimensional search detailed in Section 7.3.1 and is 512.658 kg/m^3.

7.4 Overview of Search Routines and Solvers

In Section 7.3, we discussed how to determine the phase of the refrigerant. In the single-phase region, the temperature and density are required to find the output property. In the two-phase region, temperature and quality are required to find the output property. This section summarizes the different search routines which are required to find the correct temperature, density, or quality.

Figure 7.6 shows the different algorithms required to find the output property for each pair of input properties. Each box refers to an algorithm. Table 7.7 shows where each of those algorithms is discussed in the text.

Algorithm	Section
Find the phase	Table 7.6
Find T	Section 7.4.1.1
Find ρ	Section 7.4.1.2
Find T, ρ	Section 7.4.1.3
Find x	Section 7.2.2
Find T_{sat} 1	Section 7.4.2.1
Find T_{sat} 2	Section 7.4.2.2

Table 7.7 Key for Figure 7.6.

'Find the phase' requires temperature and one other property as an input. It determines whether the properties are one-phase or two-phase.

In the single-phase region, all output properties can either be calculated from temperature and density. 'Find T' performs a one-dimensional search for temperature given density and one other property. If temperature is one of the input properties, then a one-dimensional search for density is performed in 'Find ρ.' 'Find T, ρ' performs a two-dimensional search for temperature and density.

In the two-phase region, temperature and quality are needed to find the output properties. 'Find Tsat 1' executes a one-dimensional search for saturation temperature given pressure. 'Find Tsat 2' performs a one-dimensional search for saturation temperature and given two properties not including pressure. 'Find x' solves for the quality from the equations in Section 7.2.2.

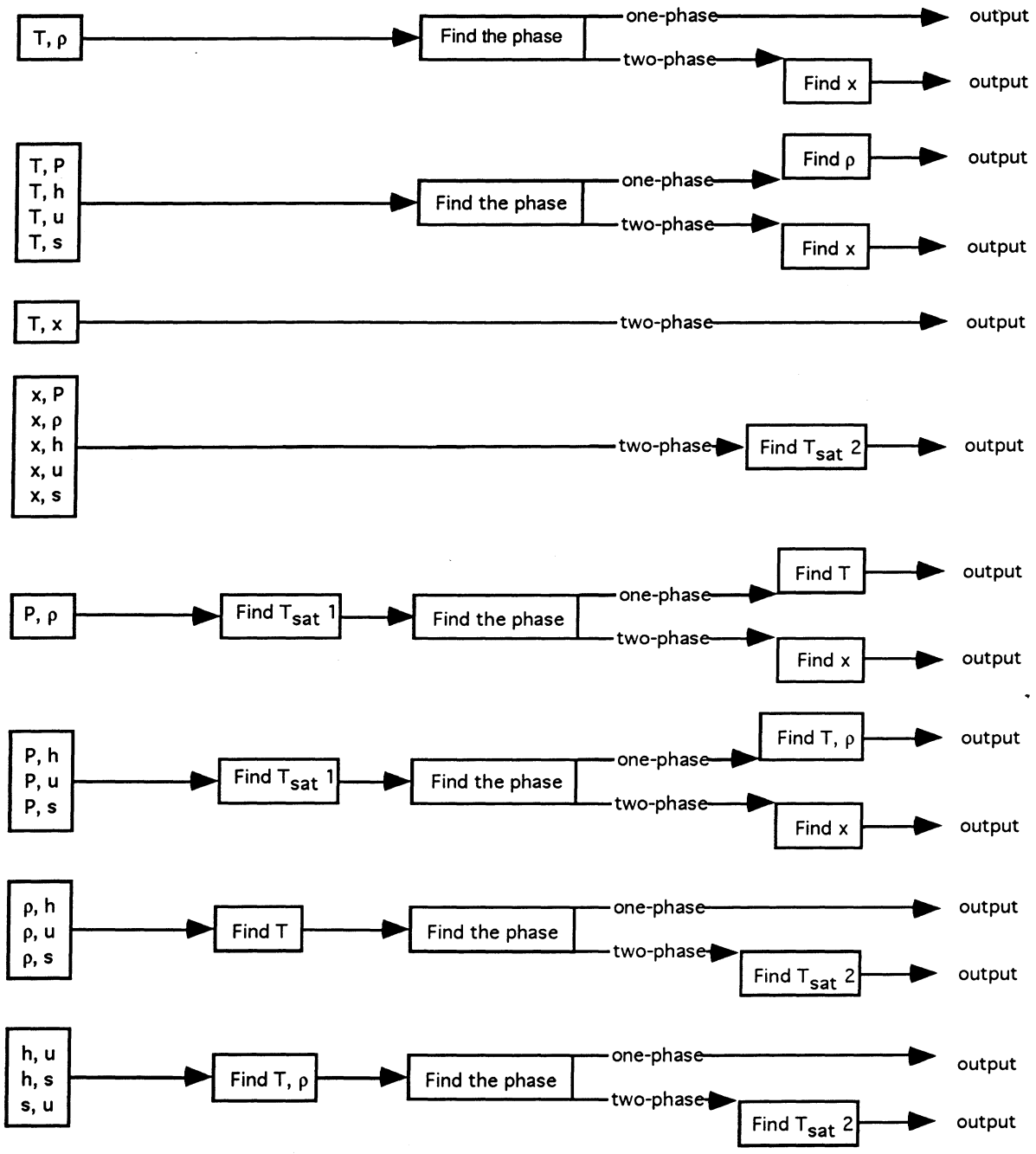

Figure 7.6 Search algorithms for each pair of input properties.

Section 7.4.1 summarizes the solver required for the four one-dimensional searches, 'Find T', 'Find ρ', 'Find Tsat 1', and 'Find Tsat 2'. There is one two-dimensional search, 'Find T, ρ'. The two-dimensional solver is summarized in that section 7.4.2.3.

7.4.1 One-dimensional Solver

The purpose of solver is solve for *n* unknowns given *n* equations. The equations are defined as

$$\mathbf{f(x)} = 0 \tag{7.26}$$

where **x** are the unknowns. The solver attempts to minimize the residuals r(i).

$$\mathbf{r(i)} = \mathbf{f_i(x_n)} \tag{7.27}$$

The search routines used in the property routines must be efficient and calculate output with a minimum number of iterations. They must also be robust and always converge on the correct answer.

An extremely efficient solution technique is the Newton-Raphson solver. In this method both the function **f(x)** and the derivative of the function **f'(x)** are calculated. The tangent line **f'(x)** is then extended until it crosses zero, and the next guess is at the zero crossing point. This solution technique is very efficient and converges quadratically. One drawback to the Newton-Raphson technique is that it requires the derivative of the function. We have already explicitly calculated the derivatives of each property with respect to temperature and density from the MBWR equation of state (Appendix D). As a result, the derivative is computed quickly and accurately. A second drawback to the Newton-Raphson solution technique is that it needs an extremely good initial guess. If the initial guess isn't close to the actual solution, the next guess obtained from the zero crossing point of the tangent can be extremely far from the solution. This can cause problems with robustness.

One dimensional searches are performed to find either temperature or density. Finding a good initial guess for temperature is fairly easy. The equation of state is usually only valid over several hundred degree Kelvin. An initial guess of the critical value or the average of the minimum or maximum temperature is generally good enough. It is much more difficult to provide a good initial guess for density. Valid densities range over several orders of magnitude. With such a large range, a Newton-Raphson routine can easily converge to a negative density or an extremely large density.

An extremely robust one-dimensional search routine is bisection. Bisection is guaranteed to return a solution. Bisection routines are provided a minimum and maximum value of the unknown. The residual must have different signs at the brackets to guarantee at least one solution. The bisection algorithm evaluates the sign at the midpoint of the minimum and maximum value. The midpoint replaces the endpoint which has the same sign of the residual. After each iteration the size of the region containing the roots decreases by a factor of two. This method is slower than Newton-Raphson and only converges linearly.

Our one-dimensional solver is a combination of the Newton-Raphson and bisection searches. The solver uses a Newton-Raphson algorithm to determine the next guess for the unknown. If the next guess is outside of the minimum and maximum bounds, the solver switches to a bisection routine for one iteration.

The next two sections summarize the single-phase and two-phase search routines. The specifications for each one-dimensional search are listed in the sections.

7.4.2 Single-Phase Search Routines

If density is one input and either pressure, enthalpy, internal energy, or entropy is the other input, then a one-dimensional search is performed to find the temperature. This search is summarized in Section 7.4.1.1. A one-dimensional search for density is performed if temperature and either pressure, enthalpy, internal energy, or entropy are inputs (Section 7.4.1.2). If neither temperature or density are inputs (the inputs include pressure, enthalpy, internal energy, or entropy) then a two-dimensional search is conducted to find the temperature and density (Section 7.4.1.3).

7.4.1.1 Search for Temperature

A one-dimensional search is performed for temperature when the inputs are density and either pressure, enthalpy, internal energy, or entropy. The parameters for the one-dimensional search for temperature are defined below.

Subroutine FIND_T

Inputs:	ρ, y
	(y = P, h, u, or s)
Unknowns:	T
Minimum:	T_{min}
Maximum	T_{max}
Initial guess:	T_{crit}

Equations: $y = y(T,\rho)$ (7.28)

T_{min} and T_{max} are the bounds for which the equation of state is valid defined (Section 7.2). T_{crit} is determined directly from the equation of state. This is a straightforward search routine because there is a small range (less than an order of magnitude) of valid temperatures.

If pressure is an input, it known before the one-dimensional search whether the properties are in the single phase or two-phase region. If enthalpy, energy, or internal energy are inputs, the program must check whether the properties are in the single-phase or two-phase regions after the search routine returns a temperature.

7.4.1.2 Search for Density

A one-dimensional search is performed for density when the inputs are temperature and either pressure, enthalpy, internal energy, or entropy. Searching for density is challenging because there is a wide range of valid densities between the minimum density and the maximum density. Also, the minimum and maximum density are only correct at the minimum temperature (Section 7.2). We can guarantee convergence on the correct density because we can provide the search routine with a very good initial guess. The phase of the refrigerant is already known since temperature is an input (Table 7.6). Since the phase is known, an extremely good initial guess can be provided to the search routine. The parameters for the search are as follows.

Subroutine FIND_rho

Inputs:	T, y	
	(y = P, h, u, or s)	
Unknowns:	ρ	
Minimum:	ρ_{min}	
Maximum	ρ_{max}	
Initial guess:	ρ_g	$(T < T_{crit},\ y \geq y_g)$
	ρ_f	$(T < T_{crit},\ y \leq y_f)$
	$\rho_{crit} / 10$	$(T > T_{crit})$
Equations:	$y = y(T,\rho)$	(7.29)

This search is robust and will converge on the correct answer even if multiple answers exits between the minimum and maximum density. The one-dimensional search will converge on the density closest to the initial guess.

7.4.2.3 Two-dimensional Search for Temperature and Density

A two-dimensional search is performed when neither of the two inputs are temperature or density. The valid inputs for this search are pressure, enthalpy, internal energy, and entropy. The search routine is a globally convergent multidimensional Newton-Raphson method. This search does not allow minimum or maximum bounds to be set for each variable. In order to guarantee convergence, extremely good initial conditions must be defined.

The challenges of the two-dimensional search is similar to the challenges of the one-dimensional search for density. The valid range of values for density encompasses several orders of magnitude. If the fluid is liquid (the density is large) and the initial guess of density is small, the solver can easily wander into regions of extremely large density. This could cause the property calls to fail because one coefficient in the equation of state would become larger than the FORTRAN compiler could evaluate. If the fluid is vapor (density is small) and the initial guess for density is too large, then the Newton-Raphson routine could converge on a negative density which would cause the equations of state to fail. It is important to give the search routine a reasonably close guess for the density.

Subroutine FIND_Trho

Inputs:	y, z	
	(y = P, h, u, or s)	
	(z = P, h, u, or s)	
Unknowns:	T, ρ	
Initial guess:	$T = (T_{min}+T_{crit}) / 2$	
	$\rho = \rho^*$	
Equations:	$y = y(T, \rho)$	(7.30)
	$z = z(T, \rho)$	(7.31)

The initial guess for density is determined by trying an array of different densities between the minimum and maximum density.

$$\rho_i = \rho_{min} * 10^i \tag{7.32}$$

$$i = 0 \text{ to } n \text{ where } \rho_{n+1} > \rho_{max}$$

Next we find the residuals for Equations 7.30 and 7.31 at each combination of the initial temperature, T_{init}, and density, ρ_i. An error is associated with each pair of residuals.

$$r(1) = \frac{y - y(T_{init}, \rho_i)}{y} \tag{7.33}$$

$$r(2) = \frac{z - z(T_{init}, \rho_i)}{z} \tag{7.34}$$

$$err(i) = \left(r(1)^2 + r(2)^2\right)^{1/2} \tag{7.35}$$

The initial guess for density is the density associated with the minimum value of the error.

$$\rho^* = \rho_i \text{ at the minimum err(i)} \tag{7.36}$$

Instead of iterating on temperature and density, the solver iterates on the following variables.

$$x(1) = \frac{T - T_{crit}}{T_{crit} - T_{min}} \tag{7.37}$$

$$x(2) = \log \rho \tag{7.38}$$

Taking the logarithm of density prevents it from becoming negative. Temperature is constrained between -1 and $(T_{max}-T_{crit}) / (T_{crit}-T_{min})$. For R134a, the logarithm of density (in kg/m^3) is constrained approximately between -4 and 3.2. The multi-dimensional Newton-Raphson solver generally converges better if the unknowns and the residuals are of the order one.

As discussed in Section 7.3, if the temperature and density returned from *Subroutine FIND_Trho* are in the two-phase region, then the solution should also be in the two-phase region. Also, if the temperature is less than the minimum temperature, this indicates that the

properties are in the two-phase region as well. The algorithms used to find two-phase properties are summarized in Section 7.5.

7.4.3 Two-phase Search routines

Section 7.3 summarizes how the program determines if the properties are in the single-phase or the two-phase region. If the properties are two-phase, then the temperature and quality must be determined to find the output property.

If pressure is an input, then a search must be performed to find the saturation temperature (Section 7.4.3.1). If neither pressure nor temperature are inputs, then a different search must be performed to find the saturation temperature (Section 7.4.3.2).

7.4.3.1 Search for Saturation Temperature Given Saturation Pressure

This subroutine performs a bounded one-dimensional search for temperature. It solves for the saturation temperature given pressure.

Subroutine FIND_Tsat1

Inputs:	P	
Unknowns:	T_{sat}	
Minimum:	T_{min}	
Maximum	T_{crit}	
Initial guess:	$T_{init} = (T_{min} + T_{crit}) / 2.$	
Equations:	$P = P_{sat}(T)$	(7.39)

Two one-dimensional searches are performed in this subroutine. The first search solves uses the curve fit of saturation pressure (Equation 7.20) for Equation 7.39. The saturation temperature determined from this search is used as an initial guess for the second search. The second search uses *Subroutine sat* (Section 7.3.1) to accurately solve for the saturation pressure. The first search is very fast since the computer can very quickly solve a polynomial. The second search is much slower because each time the subroutine sat is called a two-dimensional search for ρ_f and ρ_g is performed. The temperature determined from the first search is generally good enough that only one or two iterations of the second search are required.

7.4.3.2 Search for Temperature in the Two-phase Region

If the input properties include density, enthalpy, internal energy, entropy, and quality, a search must be performed to find the saturation temperature.

Subroutine FIND_Tsat2

Inputs:	y, z
	(y = ρ, h, u, s, or x)
	(z = ρ, h, u, s, or x)
Unknowns:	T_{sat}
Minimum:	T_{min}
Maximum	T_{crit}
Initial guess:	$T_{init} = (T_{min} + T_{crit}) / 2.$
Equations:	$x(T_{sat}, y) = x(T_{sat}, z)$ (7.40)

Subroutine FIND_Tast2 returns a temperature and the quality calculated in equations 7.41. This program will generally converge on a quality between zero and one. If the final value of x_1 and x_2 is greater than 1.00001 or less than -0.00001, then another search must be performed to find the correct quality. This only occurs when the properties are near the saturation line or when the temperature is close to the minimum temperature.

To perform another search, the initial guess of the temperature is changed. If the quality is greater than one, then the then the program has converged on a temperature which is too large. The minimum temperature is decreased by 5 K. The initial guess is still $(T_{min} + T_{max}) / 2$. If the quality is less than zero, then the then the program has converged on a temperature which is too small. The new initial guess for the temperature is $(T_{min} + T_{max} + 5\ K) / 2$.

If the solver returns the same temperature and quality after the above modifications are made, then the two-dimensional search for temperature and density is called (Section 7.4.3). If the quality is greater than one that means the fluid is in the vapor region. The initial guesses for the density is the saturated vapor density. If the quality is less than the zero, then the initial guess for density is the saturated liquid density.

7.5 Performance of the Property Routines

The following procedure is used too determine if the search routines are converging on the correct solution. It is not attempting to determine if the accuracy of the property routines. That is summarized in Section 7.6.

7.5.1 Test Procedure

The following procedure is used to test the property routines. An array of temperatures is created between the minimum and critical temperatures. For each temperature, nine densities are tested which are summarized in Table 7.8.

The code determines whether the properties are one-phase or two-phase and then calculates the pressure, enthalpy, internal energy, and entropy from the temperature and pressure. The code then performs all combinations of one-dimensional and two-dimensional searches to calculate temperature and density. An error check is performed comparing the actual temperature or density with the calculated one. An error is documented if

$$\frac{|T_{act} - T_{calc}|}{T_{act}} > 10^{-4} \quad \text{or} \quad \frac{|\rho_{act} - \rho_{calc}|}{\rho_{act}} > 10^{-4} \tag{7.41}$$

Number	Region	Calculation
1	vapor	$\rho_g / 2$
2	two-phase	$(\rho_f + \rho_g) / 2$
3	liquid	$\rho_f + 10$ kg/m^3
4	saturated vapor	ρ_g
5	high quality	$\rho_g * 1.01$
6	low superheat	$\rho_g / 1.01$
7	saturated liquid	ρ_f
8	low quality	$\rho_f / 1.01$
9	low subcool	$\rho_f * 1.01$

Table 7.8 Test array of densities for each temperature below the critical temperature.

Number	Calculation
1	ρ_{min}
2	$\rho_{crit} / 2$
3	ρ_{crit}
4	$\rho_{crit} + 100$

Table 7.9 Test array of densities for each temperature above the critical temperature.

These values should not be interpreted as an accuracy. Rather they are used to indicate that the property routine is converging on values and that there aren't multiple answers. The same tests are performed for another array of temperature between the critical temperature and the maximum temperature. The densities are summarized in Table 7.9.

The following sections summarize the results from this test.

7.5.1.1 Vapor and Supercritical Regions

The program consistently converges to the correct answer for all combinations of input in the vapor as long as the density is within the proper range. The routines will not always converge for extremely small densities in both regions and extremely large densities in the supercritical region. The MBWR equation of state was not fitted to this region and as a result and incorrect answer will be returned. In the supercritical region the program returns incorrect answers for enthalpy and internal energy for larger densities. This error occurs for the same reason as in the liquid region. The region surrounding the critical point is summarized in Section 7.5.1.3.

7.5.1.2 Two-phase Region

Multiple answers occur in the two-phase region for inputs of quality and either enthalpy, internal energy, and entropy. The code tends to converge on the smallest correct temperature. The one-dimensional search finds temperature from the following residual for an input of, for example, quality and enthalpy.

$$r = x - \frac{h - h_f}{h_g - h_f} \tag{7.42}$$

The residual of the equation when it converged on an alternate temperature was on the order of 10^{-13}. This tends to happen closer to the saturated vapor line than to the saturated liquid line.

Multiple answers occur in the two-phase region for inputs of enthalpy and internal energy. This is a result of the definition of enthalpy rather than the equation of state. Enthalpy is defined as

$$h = u + \frac{P}{\rho} \tag{7.43}$$

An infinite number of combinations of pressure and density occur for any given enthalpy and internal energy. In the one-phase region

$$P = f(T,\rho) \tag{7.44}$$

The above two equations have two unknowns, temperature and density, so there is a unique answer for temperature and density. In the two-phase region pressure is only a function of temperature.

$$P = f(T) \tag{7.45}$$

Since pressure and density are not related, the solution is an infinite number of combinations of temperature and density.

7.5.1.3 Liquid Region

In the previous section it was documented how multiple answers exist for an input of enthalpy and internal energy in the two-phase region. A similar problem exists in the liquid region. In the two-phase region multiple answers were returned because pressure is only a function of temperature. In the liquid region, the fluid is incompressible so again pressure is only a function of temperature. As a result, many answers exist for an input of enthalpy and internal energy. It is strongly recommended that the programmer does not use enthalpy and internal energy in the liquid region because the program can completely fail if it starts to converge on a density which is too large.

Redundant densities exist for inputs of temperature and enthalpy in the two-phase region and the liquid region. Figure 7.7 shows a an isotherm on a plot of enthalpy versus density. The enthalpy decreases as density increases in the two-phase region. In the liquid region, enthalpy increases as density increases. This effect occurs because enthalpy is such a strong function of pressure. In the liquid region, small changes in the density cause large

changes in the pressure. When the density increases slightly, the pressure increases much more and the enthalpy will also increase. It is obvious from Figure 7.7 that redundant densities exist for temperature and enthalpy near the saturated liquid line. Our property routines always return the two-phase density.

7.5.1.4 Properties Near the Critical Point

Near the critical point, the saturation densities change greatly with temperature. As a result a much finer temperature grid is used. The property routines converged extremely well to the correct temperature and pressure except within 0.005 K of the critical temperature. Given pressure and either enthalpy, entropy, or internal energy the program converges to the wrong the density. The density has at most 0.3% error.

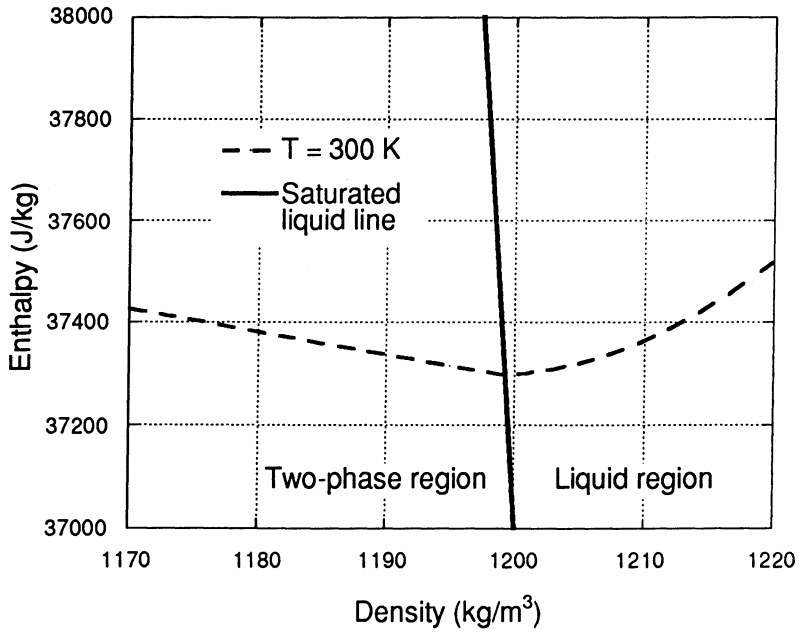

Figure 7.7 Enthalpy as a function of density and temperature near the saturated liquid line.

7.5.2 Summary

For the majority if the inputs the code will converge to the correct input. Table 7.10 summarizes the combinations of inputs and the region in which the code will fail to return the correct answer.

Input 1	Input 2	Region
quality	enthalpy	two-phase
quality	internal energy	two-phase
quality	entropy	two-phase
enthalpy	internal energy	two-phase, liquid supercritical - high densities
temperature	enthalpy	liquid

Table 7.10 Conditions for which the property routines will fail to return a correct answer.

7.6 Accuracy of the Refrigerant Property Routines

To determine the accuracy of our property routines, we compared our property routines to experimental data documented in the literature. We compared the model with a) single-phase P-v-T data, b) saturation pressure data, c) saturated liquid density data, and d) speed of sound data. The results of all of the comparison are in Table 7.11. Tables 7.12 - 7.15 summarize the data sets used for each comparison.

Data comparison	Number of points	Average absolute error	Percentage of data with greater than 1% absolute error
P-v-T	1613	0.14%	1.7%
P_{sat}	223	0.16	1.8
ρ_f	94	0.19	3.2
ss	298	0.14	1.3

Table 7.11 Summary of the comparison between the properties calculated by the property routines and experimental data.

Figure 7.8 shows that the density predictions from the property routines are in extremely good agreement with the experimental P-v-T data. Most of the large deviations are close to the critical point. At 423 K, three of the data points obtained from Tillner-Roth and Baehr (1991) have errors less than -2%. All of these data points were obtained at the lowest pressures at that temperature (0.2-0.7 MPa).

Figure 7.9 illustrates the comparison between the predicted saturation pressure and the experimental saturation pressure. All of the data are in extremely good agreement except at low temperatures. The data points with errors below -0.75% and temperatures below 250 K were obtained by Wilson and Basu (1988). The one data point with an error below -1% at 280 K was obtained by Maezawa et al. (1990). All of these outlying data points were the lowest temperature data point obtained for each data set.

In Figure 7.10, we can see that the calculated saturated liquid density agrees very well with the experimental values near the critical point. Near the critical point, small changes in temperature result in a large changes in the saturated liquid density. For example at the critical temperature (374.182 K) the property routines predict the saturation density to be 512.6 kg/m^3. At 372 K the property routines predict the saturation density to be 690.5 kg/m^3.

A comparison between the calculated speed of sound and experimental speeds of sound is shown in Figure 7.11. All of the outliers were obtained by Guedes and Zollweg (1992). No apparent discrepancy could be found with this data except that they are all at approximately the same temperature (360-380 K) and at a low pressure ranges for those temperatures (3.5 MPa - 5.2 MPa).

7.7 Conclusions

We have developed refrigerant property routines which use the Modified Benedict-Webb-Rubin (MBWR) equation of state to calculate the thermodynamic properties for R134a. Our property routines have a convenient user interface, and they allow for any permutation of input properties. Section 7.5 verified that the properties are robust and converge to the appropriate answer. As seen in Section 7.6, the properties determined by the routines agree well with experimental data in the literature. These property routines can easily be expanded to include other refrigerant.

Table 7.16 compares our refrigerant property routines, prop.f, with those available in the literature. Our property routines have been developed work for all possible combinations of input properties. ALLPROPS and REFPROP are the other available FORTRAN subroutines which only work for a limited combination of properties. EES, which can not be called from FORTRAN programs, works for all combinations of inputs except those that involve internal energy.

Source	Number of data points	Temperature range (K)		Pressure range (MPa)	
		minimum	maximum	minimum	maximum
Diller et al. (1991)	63	200	300	0.62	33.7
Hou et al. (1992)	417	180	380	0.75	70.9
Laesecke et al. (1992)	215	200	390	0.05	68.2
Maezawa et al. (1990)	10	280	340	0.51	2.0
Magee (1992)	141	200	320	2.58	29.2
McLinden et al. (1989)	22	250	250	0.10	0.10
Morrison and Ward (1991)	120	280	370	0.70	5.8
Piao et al. (1990)	159	310	420	0.80	11.8
Tillner-Roth and Baehr (1991)	410	290	450	0.08	16.4
Weber (1989)	56	320	420	1.23	5.32

Table 7.12a Summary of experimental P-v-T data.

Source	Absolute error	
	average	maximum
Diller et al. (1991)	0.06%	0.10%
Hou et al. (1992)	0.14	1.26
Laesecke et al. (1992)	0.15	2.19
Maezawa et al. (1990)	0.14	0.18
Magee (1992)	0.07	0.20
McLinden et al. (1989)	0.06	0.13
Morrison and Ward (1991)	0.06	0.80
Piao et al. (1990)	0.37	1.93
Tillner-Roth and Baehr (1991)	0.11	4.09
Weber (1989)	0.07	0.20

Table 7.12b Summary of errors for the P-v-T data.

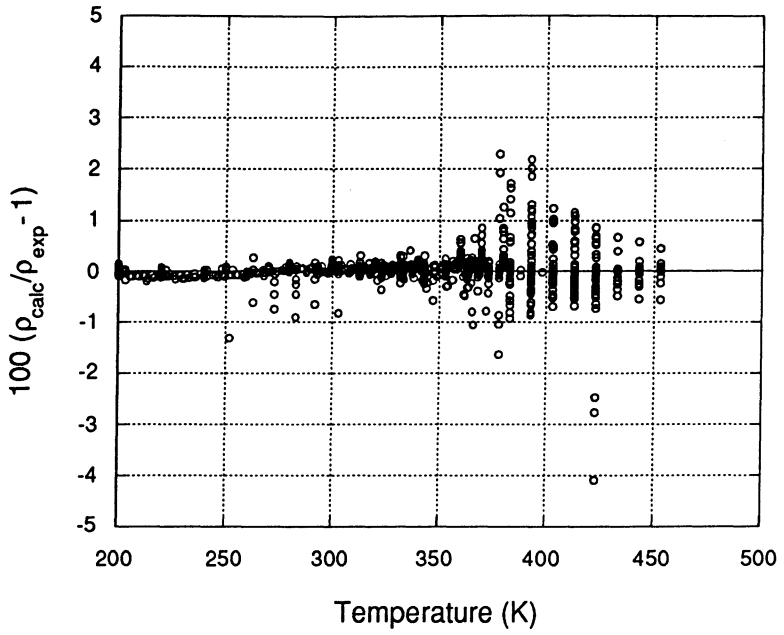

Figure 7.8 R134a density comparison with P-v-T experimental data.

Source	Number of data points	Temperature range (K)		Absolute error	
		minimum	maximum	average	maximum
Baehr and Tillner-Roth (1991)	37	300	374	0.01%	0.02%
Kubota et al. (1989)	25	250	373	0.23	0.60
Maezawa et al. (1990)	13	280	350	0.38	1.66
Magee and Howley (1992)	17	180	350	0.23	0.56
Morrison and Ward (1991)	11	270	374	0.09	0.31
Piao et al. (1990)	46	310	374	0.09	0.27
Wilson and Basu (1988)	32	210	370	0.34	2.34
Zhu et al. (1992)	42	280	360	0.08	0.25

Table 7.13 Summary of experimental saturation pressure data.

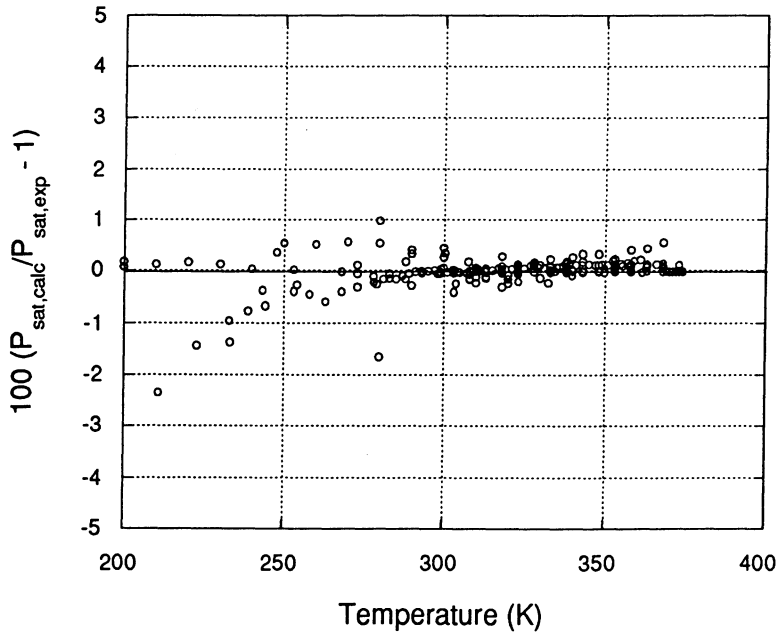

Figure 7.9 R134a saturation pressure comparison with experimental data.

Source	Number of data points	Temperature range (K)		Absolute error	
		minimum	maximum	average	maximum
Diller et al. (1991)	25	200	320	0.05%	0.08%
Kabata et al. (1989)	9	340	374	1.05	3.87
Maezawa et al. (1990)	24	210	370	0.11	1.04
McLinden et al. (1989)	1	247		0.09	
Morrison and Ward (1991)	26	270	370	0.12	0.90
Wilson and Basu (1988)	9	240	370	0.14	0.24

Table 7.14 Summary of experimental saturated liquid density data.

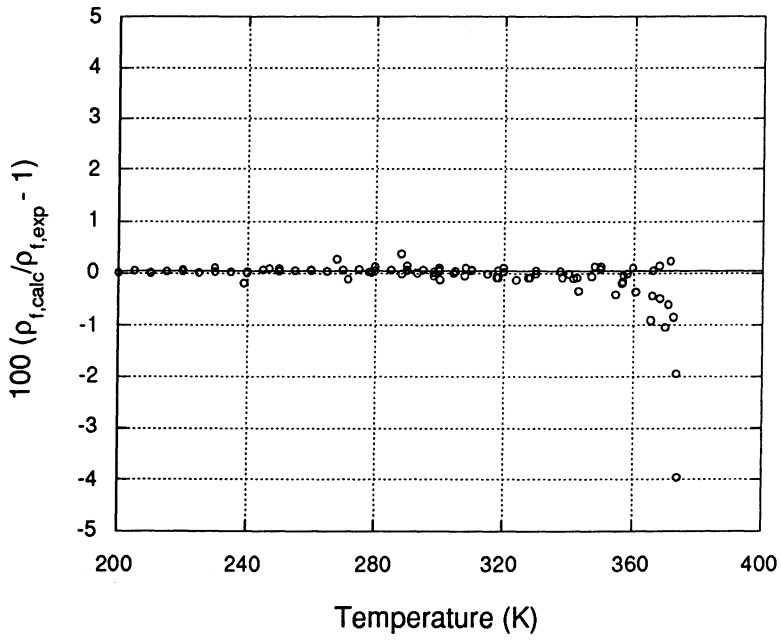

Figure 7.10 R134a saturated liquid density comparison with experimental data.

Source	Number of data points	Temperature range (K)		Pressure range (MPa)	
		minimum	maximum	minimum	maximum
Goodwin and Moldover (1990)	93	230	340	0.005	0.058
Guedes and Zollweg (1992)	184	200	380	0.13	70
McLinden et al. (1989)	21	300	350	0.10	0.10

Table 7.15a Summary of experimental single-phase speed of sound data.

Source	Absolute error	
	average	maximum
Goodwin and Moldover (1990)	0.01%	0.04%
Guedes and Zollweg (1992)	0.22	2.32
McLinden et al. (1989)	0.02	0.04

Table 7.15b Summary of errors for experimental single-phase speed of sound data.

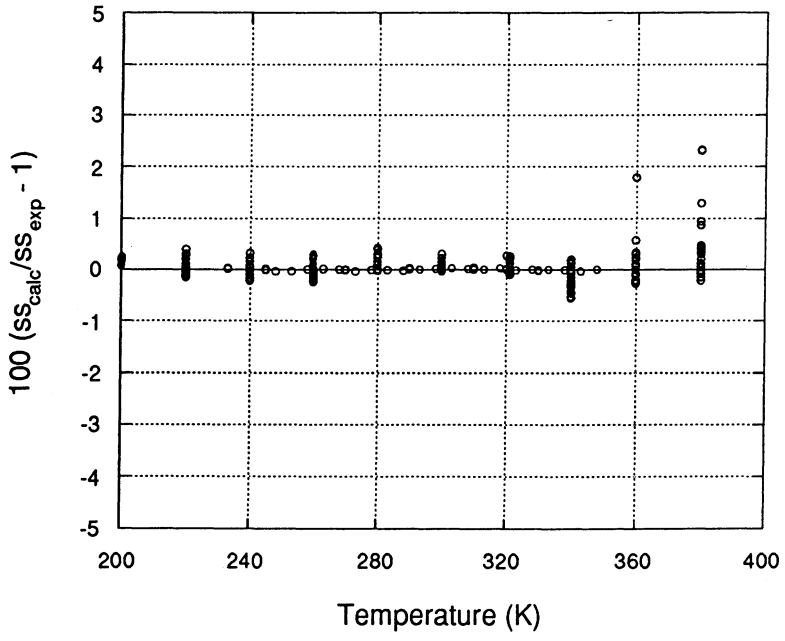

Figure 7.11 R134a single-phase speed of sound comparison with experimental data.

Input Properties		Refrigerant Property Routines			
		ALLPROPS	REFPROP	EES	prop.f
0-D Searches	T, ρ	x	x	x	x
1-D Searches	T, P	*	x	x	x
	T, h			x	***
	T, u			**	x
	T, s	x		x	x
	T, x			x	x
	ρ, P	x		x	x
	ρ, h	x		x	x
	ρ, u	x		**	x
	ρ, s	x		x	x
	ρ, x			x	x
2-D Searches	P, h	x	x	x	x
	P, u			**	x
	P, s	x	x	x	x
	P, x			x	x
	h, u				****
	h, s			x	x
	h, x			**	**
	u, s			**	x
	u, x			**	**
	s, x			**	**

x = solves for properties

* = requires an initial guess for ρ

** = has convergence problems

*** = problems in the liquid region

**** = only independent in the vapor region

Table 7.16 Combinations of input properties for which the property routines.

Chapter 8
Conclusions

In this thesis, a transient model was developed to predict the behavior of the vapor compression cycle of a mobile air-conditioning system. Mobile air-conditioning systems operate in a transient mode due to the variations in compressor speed, condenser air flow rate, and the control strategy such as clutch-cycling. The majority of transient models in the literature are for stationary systems which operate under different transient conditions than do mobile systems. Because an important part of the system model involves calculating the refrigerant properties correctly, we developed property routines to accurately compute the properties of R134a in the transient model.

A review of the work concerning transient modeling is provided in Section 8.1. Section 8.2 summarizes the work regarding the property routines. Section 8.3 provides suggestions for future work.

8.1 Transient Mobile Air-conditioning System Model

Our transient model treats the components in a vapor compression refrigeration system including the compressor, condenser, orifice tube, evaporator, and accumulator. Each component model is designed to use enthalpy (h), pressure (P), and mass flow rate ($\dot{m}$) as inlet and outlet properties.

The model operates in three different modes: (a) as a steady-state model, (b) as a compressor-on transient model, and (c) as a compressor-off transient model. The above models were validated with experimental data obtained from a test facility specifically designed to simulate mobile air conditioners.

We model the heat exchangers using a control-volume approach. The refrigerant circuit in the evaporator and condenser is divided into a series of constant-volume cells. The conservation of mass, conservation of energy, and conservation of momentum equations are applied to each cell. Between simulations, the number of cells and/or the volume of the cells can be modified in order to change the resolution of the model.

The condenser is a fin-tube heat exchanger, and the evaporator is a plate-fin heat exchanger. It is necessary to separately model the air and refrigerant heat transfer coefficient in order to simulate the correct behavior during compressor start-up and shut-down. In the condenser model, we use the following heat transfer correlations: a) Hiller and Glicksman

(1976) for the vapor flow, b) Dobson et al. (1994) for two-phase flow, c) Dittus-Boelter (1930) for liquid flow, and d) Gray and Webb (1986) for the air flow. We use the following heat transfer correlations in the evaporator model: a) Kandlikar (1991) for two-phase flow, b) Robertson and Lovegrove (1983) for vapor flow, and c) Manglik and Bergles (1995) for the air flow. The refrigerant pressure drop correlation is empirical for both heat exchangers.

A semi-empirical model is used for the compressor. We based the compressor model on data acquired in our own laboratory (UIUC data) and data obtained by Ford Motor Company (Ford data) for the exact same compressor. The mass flow rate equation is based on the volumetric efficiency and requires different coefficient for the UIUC data and Ford data. After extensive analysis of the data, we concluded that the differences arise from different installation of the compressors between the two test facilities. The outlet temperature is predicted by assuming a polytropic process. Compressor power is directly proportional to the mass flow rate and enthalpy change across the compressor.

The orifice tube model is semi-empirical and was developed by Hrnjak (1998). It is valid when the inlet refrigerant is subcooled liquid, two-phase, and superheated vapor and the flow is choked. When the inlet is subcooled, a modified orifice flow equation is used. When the inlet is vapor, the Fanno flow equation is used. When the inlet is two-phase, the mass flow rate is determined from a quality weighted average between the pure liquid flow rate and pure vapor flow rate. We compared the model with experimental data acquired from our test facility using three different diameter orifice tubes. The model accurately predicts the mass flow rate for the third tube tested, but significantly overpredicts the mass flow rate for the first tubes tested. The refrigerant pipes around the orifice tube were modified after tests with the first two tubes were completed. This modification to the refrigerant pipes is the only systematic difference we could identify to explain the disparity. An empirical correction was made to bring the mass flow rates for the first two orifice tubes in agreement with the model .

The accumulator model is a slight modification of the heat exchanger model. The conservation of energy, conservation of momentum, and conservation of mass equations are applied to the accumulator. An additional equation constrains the accumulator exit to be vapor.

The equations for the component models are combined into a system model. The steady-state equations are solved using a globally convergent Newton-Raphson technique. The transient equations are solved using a public domain program DASSL which solves a combination of algebraic and differential equations.

The steady-state model was compared to experimental data. The predicted and measured mass flow rates agree within 10%. The model predicts the condenser pressure within 10% and the evaporator pressure within 15% of the measured values. The predicted and measured condenser and evaporator capacities agree within 10% and 15%, respectively.

The transient model was compared with a) city driving cycle data, b) compressor shut-down data, c) compressor start-up data, and d) clutch-cycling data. The model predictions agree extremely well with the city driving cycle data. The model agrees well with the two different compressor shut-down simulations. The model predicted that the liquid line becomes two-phase sooner than the experimental data indicates. This difference in time causes a slight overprediction in the condenser pressure.

The transient model predictions agree well with the first case of the compressor start-up data in which the liquid line was flooded. In the second case, the experimental data indicate that the liquid line is initially either vapor or two-phase refrigerant. The model predicts that the liquid line took much longer to flood than seen in the experimental data. We believe that during the initial start-up, slugs of liquid refrigerant are exiting the accumulator, traveling through the compressor, and filling the liquid line. Our model does not account for liquid entering the compressor. To treat this very large initial mass flow rate seen in the experimental data, we artificially transfer mass from the accumulator to the liquid line. After this modification is made, the model provides good agreement with the experimental data for the second case of the compressor start-up and the clutch cycling case.

8.2 Refrigerant Property Routine

We developed a computer program to calculate the temperature, pressure, density, enthalpy, internal energy, entropy, quality, specific heat at constant pressure, specific heat at constant volume, Gibbs free energy, and speed of sound of R134a in the liquid, vapor, two-phase, and supercritical regions using any reasonable pair of these parameters.

We use the Modified Benedict-Webb-Rubin (MBWR) equation of state in the property routines because it is extremely accurate, it is valid in the vapor, liquid, and supercritical regions, and the coefficients have already been determined for many refrigerants. This equation determines the pressure as a function of temperature and density. When this equation of state is combined with an equation of the ideal specific heat at constant volume, all other single-phase properties can be determined explicitly as a function of temperature and density.

The two-phase properties can be explicitly calculated from the temperature, quality, and saturation properties. As a result, we need to be able to calculate the saturation properties as a function of temperature. The saturated liquid and vapor properties are defined as having the same temperature, pressure, and Gibbs free energy. We developed a two-dimensional search routine to find the saturation densities and pressure at a given temperature.

Our property routines compute an output property from any combination of the following input properties: temperature, pressure, density, enthalpy, internal energy, entropy, and quality. In the single-phase region, unless both temperature and density are given, we first

perform a search routine to find these parameters from which we compute all other output properties. If either temperature or density is an input, then a one-dimensional search must be performed to find the other one. If neither temperature nor density are given, then a two-dimensional search must be performed to find both temperature and density. In the two-phase region, temperature and quality are required to compute the output property. If pressure is an input, then a one-dimensional search is performed to determine the saturation temperature. If neither temperature nor pressure are inputs, then a one-dimensional search is performed to determine the correct saturation temperature and quality.

The MBWR equation of state is only accurate for a certain range of temperatures and densities. Outside of this range, redundant solutions exist for the search parameters. As a result, the above search routines must be constrained.

We must be able to determine whether the refrigerant is in the single-phase or two-phase region. If either temperature or pressure are an input property, it is trivial to determine the phase by directly calculating the saturation properties. If neither temperature nor pressure are inputs, then we use a single-phase search to find the temperature and density. We then determine if these properties are in the single-phase or the two-phase region. If they are in the single-phase region then the temperature and density are correct. If they are in the two-phase region, we must perform a two-phase search to calculate the correct temperature and quality.

We tested the property routines to ensure that the search routines converge on the correct properties. The property routines converged to the correct answer whenever the input properties uniquely defined the state. Redundant answers exist in the liquid region for a) temperature and enthalpy and b) enthalpy and internal energy. In the two-phase region, redundant answers exist for a) quality and enthalpy, b) quality and internal energy, and c) quality and entropy, and d) enthalpy and internal energy.

To determine the accuracy of our property routines, we compared predictions to experimental a) single-phase P-v-T data, b) saturation pressure data, c) saturated liquid density data, and d) speed of sound data. The property routines agree extremely well with the experimental data found in the literature.

8.3 Recommendations for Future Work

The transient mobile system model can be extended in several different directions. The model can be modified to include other control strategies such as thermal or electronic expansion valves. Also, the vapor compression model can be combined with an airside model which can predict the vehicle cabin temperature. The evaporator model can be extended to include the effects of humidity and frosting on the heat transfer coefficient. Finally, the

slugging phenomena through the compressor at start-up should be investigated more thoroughly.

Regarding the refrigerant property routines, these can easily be extended to include more refrigerants and more equations of state. Also, an important extension involves adding transport properties, predicting the properties of refrigerant mixtures, and adding oil/refrigerant mixtures.

References

Baehr, H. D. and R. Tillner-Roth (1991) "Measurement and Correlation of the Vapour Pressures of 1,1,1,2-Tetrafluoroethane (R134a) and of 1,1-Difluoroethane (R152a)." Journal of Chemical Thermodynamics, Vol. 23: pp. 1063-1068.

Bajpai, A. (1994) "An Expert System Approach to Design of Automotive Air-conditioning Systems." Artificial Intelligence for Engineering Design, Analysis, and Manufacturing, Vol. 8: pp. 1-11.

Brenan, K. E., S. L. Campbell, et al. (1996) Numerical Solution of Initial-Value Problems in Differential-Algebraic Equations. Philadelphia, SIAM, Philadelphia.

Bridges, B. D. and C. W. Bullard (1995) "Simulation of Room Air Conditioner Performance." ACRC TR-79.

Carey, V. P. and G. D. Mandrusiak (1986) "Annular Film-flow Boiling of Liquids in a Partially Heated, Vertical Channel with Offset Strip Fins." International Journal of Heat and Mass Transfer, Vol. 29(6): pp. 927-939.

Chen, Z. and W. Lin (1991) "Dynamic Simulation and Optimal Matching of a Small-Scale Refrigeration System." International Journal of Refrigeration, Vol. 14: pp. 329-335.

Cherng, J. G. and W. J. Wu (1989) "Design Tool for Climatic Control of an Automotive Vehicle." SAE Technical Papers Series, paper number 891966.

Chi, J. and D. Didion (1982) "A Simulation Model of the Transient Performance of a Heat Pump." International Journal of Refrigeration, Vol. 5: pp. 176-184.

Colding, L., J. Holst, et al. (1991) "Dynamic Model of Refrigerating Systems Using Air Cooled Condensers." 18th International Congress of Refrigeration, Vol. 3: pp. 1208-1212.

Collins, C. D. and N. R. Miller (1996) "Experimental Study of Mobile Air Conditioning System Transient Behavior." ACRC TR-102.

Crawford, R. R. and D. B. Shirey (1987) "Dynamic Modeling of a Residential Heat Pump From Actual System Performace Data." ASHRAE Transactions, Vol. 93 part 2: pp. 1179-1190.

Crawford, R. R. and J. E. S Woods (1988) "A Method for Deriving a Dynamic System Model from Actual Building Performance Data." ASHRAE Transactions, Vol. 91 part 2: pp. 1859-1874.

Darrow, J. B., S. J. Lovatt, et al. (1991) "Assessment of a Simple Mathematical Model for Predicting the Transient Behavior of a Refrigeration System." 18th International Congress of Refrigeration, Vol. 3: pp. 1189-1192.

DeSantis, R., F. Gironi, et al. (1976) "Vapor-Liquid Equilibrium from a Hard-Sphere Equation of State." Industrial and Engineering Chemistry, Vol. 15(3): pp. 183-189.

Dhar, M. and W. Soedel (1979-a) "Transient Analysis of a Vapor Compression Refrigeration System: Part I - The Mathematical Model." XVth International Congress of Refrigeration, Venice. pp. 1035-1048.

Dhar, M. and W. Soedel (1979-b) "Transient Analysis of a Vapor Compression Refrigeration System: Part II - Computer Simulation and Results." XVth International Congress of Refrigeration, Venice. pp. 1049-1067.

Diller, D. E. et al. (1991) "Measurements of the Viscosities of Saturated and Compressed Liquid 1,1,1,2-Tetrafluoroethane (R134a), 2,2-Dichloro-1,1,1-trifluoroethane (R123) and 1,1,-Dichloro-1-fluoroethane (R141b)." 11th Symposium on Thermophysical Properties, Boulder, Colorado.

Dittus, F. W. and L. M. K. Boelter (1930) University of California Publications on Engineering. University of California, Berkeley. Vol. 2: p. 443.

Dobson, M. K., J. C. Chato, et al. (1994) "Heat Transfer and Flow Regimes During Condensation in Horizontal Tubes." ACRC TR-57.

DuPont Chemicals (1992) "Product Information: Transport Properties of SUVA Refrigerants." DuPont Chemicals Fluorochemicals Customer Service Center, Wilmington, Delaware. Stock No. H-43855-1.

Eaton Co. (1993) "Thermostatic Expansion Valves for Automotive A/C Application." published by EATON Automotive Controls Division. Prepared for University of Brighton Symposium: Developments in Air Conditioning Systems (20-23 April 1993).

Farzad, M. and D. L. O'Neal (1994) "The Effect of Void Fraction Model on Estimation of Air Conditioner System Performance Variables Under A Range of Refrigerant Charging Conditions." International Journal of Refrigeration, Vol. 12(2): pp. 85-93.

Gear, C. W. (1968) "The Automatic Integration of Stiff Ordinary Differential Equations." Proceedings of the IFIP Congress, Amsterdam. pp. 187-193.

Gear, C. W. (1971) "Simultaneous Numerical Solution of Differential-Algebraic Equations." IEEE Transactions on Circuit Theory, Vol. CT-18(1): pp. 89-95.

Ginsberg, C. (1994) "EASY5 Vapor Cycle (VC) Library User's Guide." The Boeing Company. Report No. 20491-0550.

Goodwin, A. R. H. and M. R. Moldover (1990) "Thermophysical Properties of Gaseous Refrigerants from Speed of Sound Measurements. Part I: Apparatus, Model, and Results for 1,1,1,2-Tetrafluoroethane R134a." Journal of Chemical Physics, Vol. 93: pp. 2741-2753.

Gray, D. L. and R. L. Webb (1986) "Heat Transfer and Friction Correlations for Plate Finned-Tube Heat Exchangers Having Plain Fins." Proceedings of the 8th International Heat Transfer Conference, San Francisco. pp. 2745-2750.

Gruhle, W. D. and R. Isermann (1985) "Modeling and Control of a Refrigerant Evaporator." Journal of Dynamic Systems, Measurement, and Control, Vol. 107: pp. 235-240.

Guedes, H. J. R. and J. A. Zollweg (1992) "Speed of Sound in Liquid R134a." International Journal of Refrigeration, Vol. 15: pp. 381-385.

Hahn, G. W. and C. W. Bullard (1991) "Modeling Room Air Conditioner Performance." ACRC TR-40.

He, X., S. Liu, et al. (1997) "Modeling of Vapor Compression Cycles for Multivariable Feedback Control of HVAC Systems." ASME Journal of Dynamic Systems, Measurements, and Control, Vol. 119: pp. 183 - 191.

Hiller, C. C. and L. R. Glicksman (1976) "Improving Heat Pump Performance via Compressor Capacity Control - Analysis and Tests." MIT Energy Laboratory MIT-EL 76-001.

Hou, H. and et al. (1992) "Experimental Densities for Compressed R134a." International Journal of Refrigeration, Vol. 15: pp. 365-371.

Hrnjak, P. (1998) Personal communication. Work in progress: Singh, G., M.S. Thesis, University of Illinois at Urbana Champaign.

Huber, M. L. and J. F. Ely (1994) "A Predictive Extended Corresponding States Model for Pure and Mixed Refrigerants Including an Equation of State for R134a." International Journal of Refrigeration, Vol. 17(1): pp. 18-31.

Huber, M., J. Gallagher, et al. (1996) "NIST Thermodynamic Properties of Refrigerants and Refrigerant Mixtures Database (REFPROP) Version 5.0." National Institute of Standards and Technology, Gaithersburg, MD.

Hughmark, G. A. (1962) "Holdup in Gas-Liquid Flow." Chemical Engineering Progress, Vol. 58(4): pp. 62-65.

Idelchik, I. E. (1994) Handbook of Hydraulic Resistance. CRC Press, Inc., Boca Raton.

Incropera, F. P. and D. P. DeWitt (1990) Fundamentals of Heat and Mass Transfer. John Wiley & Sons, New York.

Inoue, A., J. Ichikawa, et al. (1988) "Evaluation of Infinitely Variable Displacement Compressors with Thermal Expansion Valves in a Motor Vehicle Air Conditioning System." SAE Technical Papers Series, paper number 880052.

Jacobsen, R. T. and R. B. Stewart (1973) "Thermodynamic Properties of Nitrogen Including Liquid and Vapor Phases from 63 K to 2000 K with Pressure to 10,000 Bar." Journal of Physical and Chemical Reference Data, Vol. 2: pp. 757-922.

Johnston, C. E., N. R. Miller, et al. (1997) "Refrigerant Charge Loss Detection for a Mobile Air Conditioning System." ACRC TR-125.

Jung, D. S. and R. Radermacher (1989) "Transport Properties and Surface Tension of Pure and Mixed Refrigerants." ASHRAE Transactions, Vol. 97(1): pp. 90-99.

Kabata, Y. and et al. (1989) "Measurements of the Vapor-Liquid Coexistence Curve and the Critical Parameters for 1,1,1,2-Tetrafluoroethane." International Journal of Thermophysics, Vol. 10(3): pp. 605-615.

Kandilkar, S. G. (1991) "A Model for Correlating Flow Boiling Heat Transfer in Augmented Tubes and Compact Evaporators." Journal of Heat Transfer, Vol. 113: pp. 966 - 972.

Kays, W. M. and A. L. London (1984) Compact Heat Exchangers. McGraw-Hill Book Company, New York.

Kubota, H. and et al. (1989) "Vapor Pressures of New Fluorocarbons." International Journal of Thermophysics, Vol. 10(3): pp. 629-637.

Kyle, D. M., V. C. Mei, et al. (1993) "An Automobile Air Conditioning Design Model." SAE Technical Paper Series, paper number 931137.

Laesecke, A. and et al. (1992) "Thermal Conductivity of R134a." Fluid Phase Equilibria, Vol. 80: pp. 263-274.

Lemmon, E. W., R. T. Jacobsen, et al. (1995) "Computer Programs for Calculating Thermodynamic Properties of Fluids of Engineering Interest Version 4.1." Center for Applied Thermodynamic Studies at the University of Idaho. Report 95-1.

MacArthur, J. W. and E. W. Grald (1989) "Unsteady Compressible Two-phase Flow Model for Predicting Cyclic Heat Pump Performance and a Comparison with Experimental Data." International Journal of Refrigeration, Vol. 12: pp. 29-41.

Maezawa, Y., H. Sato, et al. (1990) "Saturated Liquid Densities of HCFC 123 and HFC 134a." Journal of Chemical Engineering Data, Vol. 35: pp. 224-228.

Magee, J. W. (1992) "Measurements of Molar Heat Capacity at Constant Volume (Cv) for 1,1,1,2-tetrafluoroethane (R134a)." International Journal of Refrigeration, Vol. 15: pp. 372-380.

Magee, J. W. and J. B. Howley (1992) "Vapour pressure measurements of 1,1,1,2-tetrafluoroethane (R134a) from 180 to 350 K." International Journal of Refrigeration, Vol. 15: pp. 362-364.

Manglik, R. M. and A. E. Bergles (1995) "Heat Transfer and Pressure Drop Correlations for the Rectangular Offset Strip Fin Compact Heat Exchanger." Experimental Thermal and Fluid Science, Vol. 10: pp. 171-180.

Martin, J. J. and Y. C. Hou (1955) "The Development of an Equation of State for Gases." AICHE Journal, Vol. 1(2): pp. 142-151.

McLinden, M. O. and et al. (1989) "Measurement and Formulation of the Thermodynamic Properties of Refrigerants 134a (1,1,1,2-Tetrafluoroethane) and 123 (1,1-Dichloro-2,2,2-Trifluoroethane)." ASHRAE Transactions, Vol. 95(2): pp. 263-283.

McLinden, M. O., S. A. Klein, et al. (1998) "NIST Thermodynamic and Transport Properties of Refrigerants and Refrigerant Mixtures - REFPROP Version 6.0 Users' Guide." National Institute of Standards and Technology, Gaithersburg, MD.

Mitsui, M. (1987) "Improvement of Refrigerant Flow Control Method in Automotive Air Conditioners." SAE Technical Papers Series, paper number 870029.

Morrison, G. and D. K. Ward (1991) "Thermodynamic Properties of Two Alternative Refrigerants: 1,1-Dichloro-2,2,2-Trifluoroethane (R123) and 1,1,1,2-Tetrafluoroethane (R134a)." Fluid Phase Equilibria, Vol. 62: pp. 65-86.

Murphy, W. E. and V. W. Goldschmit (1984) "Transient Response of Air Conditioners- A Qualitative Interpretation Through a Sample Case." ASHRAE Transactions, Vol. 90(1a): pp. 997-1008.

Murphy, W. E. and V. W. Goldschmidt (1985) "Cycling Characteristics of a Residential Air Conditioner-Modeling of Start-Up Transients." ASHRAE Transactions, Vol. 91(2): pp. 427-444.

Murphy, W. E. and V. W. Goldschmidt (1986) "Cycling Characteristics of a Residential Air Conditioner-Modeling of Shutdown Transients." ASHRAE Transaction, Vol. 92: pp. 186-202.

Nyers, J. and G. Stoyan (1994) "A Dynamical Model Adequate for Controlling the Evaporator of a Heat Pump." International Journal of Refrigeration, Vol. 17: pp. 101-108.

O'Neal, D. L. and S. Katipaluma (1993) "Development of Nondimensional Cycling Model for Estimating the Seasonal Performance of Air Conditioners" Transactions of the ASME, Vol. 115: pp. 176-181.

Piao, C. C. and et al. (1990) "An Experimental Study for PvT Properties of CFC Alternative Refrigerant 1,1,1,2-tetrafluoroethane (R-134a)." ASHRAE Transactions, Vol. 96(1): pp. 132-140.

Ploug-Sorensen, L., J. P. Fredsted, et al. (1997) "Improvements in the Modeling and Simulation of Refrigeration Systems: Aerospace Tools Applied to a Domestic Refrigerator." HVAC&R Research, Vol. 3(4): pp. 387-403.

Porter, K. J. (1992) "Modeling and Sensitivity Analysis of a Refrigerator/Freezer System." ACRC TR-31.

Premoli, A., D. D. Francesco, et al. (1971) "A Dimensional Correlation for Evaluating Two-phase Mixture Density." La Termotechnica, Vol. 25(1): pp. 17-26.

Press, W. H., S. A. Teukolsky, et al. (1992) Numerical Recipes in FORTRAN: The Art of Scientific Computing. Cambridge University Press, New York.

Reid, R. C., J. M. Prausnitz, and B. M. Poling (1987) The Properties of Gases and Liquids. McGraw-Hill Book Company, New York.

Rice, C. K. (1987) "The Effect of Void Fraction Correlation and Heat Flux Assumption on Refrigerant Charge Inventory Predictions." ASHRAE Transactions, Vol. 93: pp. 341-367.

Robertson, J. M. and P. C. Lovegrove (1983) "Boiling Heat Transfer with Freon 11 (R11) in Brazed Aluminum, Plate-Fin Heat Exchangers." ASME Journal of Heat Transfer, Vol. 105: pp. 605-620.

Rubio-Quero, J. E., W. E. Dunn, et al. (1995) "A Facility for Transient Testing of Mobile Air Conditioning Systems." ACRC TR-80.

Sami, S. M., T. N. Duong, et al. (1987) "Prediction of the Transient Response of Heat Pumps." ASHRAE Transactions, Vol. 93(2): pp. 471-490.

Sami, S. M. and M. A. Comeau (1992) "Development of a Simulation Model for Predicting Dynamic Behavior of Heat Pump with Non-Azeotropic Refrigerant Mixtures." International Journal of Energy Research, Vol. 16: pp. 431-444.

Sami, S. M. and Y. Zhou (1995) "Numerical Prediction of Heat Pump Dynamic Behavior Using Ternary Non-Azeotropic Refrigerant Mixture." International Journal of Energy Research, Vol. 19: pp. 19-35.

Skinner, T. J. and R. L. Swadner (1985) "V-5 Automotive Variable Displacement Air Conditioning Compressor." SAE Technical Paper Series, paper number 850040.

Sonntag, R. E. a. G. J. V. W. (1991) Introduction to Thermodynamics: Classical and Statistical. John Wiley & Sons, New York.

Stegou-Sagia, A. (1996) "Properties of New Refrigerants and Predictions for Condensation Heat Transfer Enhancements with Low-Finned Tubes." Energy, Vol. 21(12): pp. 1189-1199.

Threlkeld, J. L. (1970) Thermal Environmental Engineering. Prentice-Hall Inc., Englewood Cliffs, New Jersey.

Tillner-Roth, R. and H. D. Baehr (1991) "Burnett Measurements and Correlation of Gas-phase (P, ρ, T) of 1,1,1,2-tetrafluoroethane (R134a) and of 1,1-difluoroethane (R152a)." Journal of Chemical Thermodynamics, Vol. 24: pp. 413-424.

Tojo, K., K. Takao, et al. (1990) "Dynamic Behavior of Variable Displacement Compressor for Automotive Air Conditioners." SAE Technical Papers Series, paper number 900084.

Tollefson, J. and J. Harrison (1992) "EASY5 Technical Overview." The Boeing Company. Report No. 20491-0601.

Vargas, J. C. and J. A. R. Parise (1995) "Simulation in Transient Regime of a Heat Pump with Closed-Loop and On-Off Control." International Journal of Refrigeration, Vol. 18(4): pp. 235-243.

Wandell, E. W., W. E. Dunn, et al. (1997) "Experimental Investigation of Mobile Air Conditioning System Control for Improved Compressor Reliability." ACRC TR-128.

Weber, L. A. (1989) "Vapor Pressures and Gas-Phase PvT Data for 1,1,1,2-Tetrafluoroethane." International Journal of Thermophysics, Vol. 10(3): pp. 617-627.

Wedekind, G. L., B. L. Bhatt, et al. (1978) "A System Mean Void Fraction Model for Predicting Various Transient Phenomena Associated with Two-phase Evaporating and Condensing Flow." International Journal of Multiphase Flow, Vol. 4: pp. 97-114.

Weston, P. G., W. E. Dunn, et al. (1996) "Design and Construction of a Mobile Air Conditioning Test Facility for Transient Studies." ACRC TR-97.

Whitchurch, M. R., W. E. Dunn, et al. (1997) "Humidity Effects in Mobile Air-conditioning Systems." ACRC TR-126.

Wilson, D. P. and R. S. Basu (1988) "Thermodynamic Properties of a New Stratospherically Safe Working Fluid - Refrigerant 134a." ASHRAE Transactions, Vol. 94(2): pp. 2095-2118.

Yasuda, H., S. Touber, et al. (1983) "Simulation Model of a Vapor Compression Refrigeration System." ASHRAE Transactions, Vol. 89(2a): pp. 408-425.

Zhu, M. and et al. (1992) "New Experimental Vapor Pressure Data and a New Vapor Pressure Equation for HFC134a." Fluid Phase Equilibria, Vol. 80: pp. 99-105.

Zivi, S. M. (1964) "Estimation of Steady-state Stream Void Fraction by Means of the Principle of Minimum Energy Production." ASME Transactions, Journal of Heat Transfer, Series C, Vol. 86: pp. 247-252.

Appendix A
Transport Properties for R134a

This appendix summarizes the correlations for the liquid and vapor transport properties for R134a. All of these equations were obtained from technical manuals provided by DuPont Co. (1992). The equation for the liquid viscosity is valid between -57 °C and 93 °C.

$$\mu_{liquid} = 267.67 - 3.6494\,T + 3.9304*10^{-2}\,T^2 - 2.191*10^{-4}\,T^3 \qquad (A.1)$$

The equation for the vapor viscosity is valid between 38 °C and 149 °C.

$$\mu_{vapor} = 11.021 + 3.8599*10^{-2}\,T \qquad (A.2)$$

The units for Equations A.1 and A.2 are μPa·s for viscosity and °C for temperature.

The liquid and vapor thermal conductivity for R134a are

$$k_{liquid} = 9.537*10^{-2} - 5.17d0*10^{-6}\,T \qquad (A.3)$$

$$k_{vapor} = 1.212*10^{-2} + 9.60*10^{-5}\,T \qquad (A.4)$$

The unit of thermal conductivity is W/m·K and the unit of temperature is °C. The range of the liquid thermal conductivity is between -60 °C and 60 °C. The range of the vapor thermal conductivity is between 0 °C and 120 °C.

Appendix B
Dry Air Properties

This appendix summarizes the correlations for dry air properties used in the transient system model. These properties are used to find the air heat transfer coefficient for the heat exchangers. All of these properties are at atmospheric pressure.

The equation for the thermal conductivity of air was developed from data obtained from Incropera and DeWitt (1990). It is valid between 200 and 400 K. The units of the thermal conductivity is (W/m·K) and the units of temperature are (K).

$$k_{air} = 2.54*10^{-3} + 7.82*10^{-5}\ T \tag{B.1}$$

The equation for the viscosity was also obtained from data compiled in Incropera and DeWitt (1990). It is also valid between 200 and 400 K. The unit of the viscosity is Pa·s and the unit of temperature is K.

$$\mu_{air} = 3.672*10^{-6} + 4.876*10^{-8}\ T \tag{B.2}$$

The specific heat is assumed to be constant.

$$c_{p,air} = 1007\ J/kg{\cdot}K \tag{B.3}$$

Appendix C
Heat Exchanger Geometry Calculations

C.1 Condenser

A description of the fin-tube condenser is provided in Section 3.4. This section describes the calculations performed to obtain the diameters, area, and volumes required for the heat exchanger model.

C.1.1 Condenser Refrigerant-side Geometry

In the condenser the refrigerant flows through round tubes and round manifolds (Figure 3.4). The following parameters are measured from the heat exchanger.

D_{in} = Inner diameter of the refrigerant tube
L_{tube} = Length of a single refrigerant tube
Vol_{tot} = Total internal volume
N_{tot} = Total number of tubes

The total internal volume is determined by filling the heat exchanger with water and measuring the volume of the water.

The cross sectional area of a tube is used to compute the mass flux.

$$A_{cs} = \frac{\pi}{4} D_{in}^2 \tag{C.1}$$

The surface area of a tube is multiplied by the refrigerant heat transfer coefficient. We only include the surface area of the tubes.

$$A_{surface} = \pi D_{in} L_{tube} \tag{C.2}$$

The volume of the tubes is needed to find the refrigerant mass in the system.

$$Vol_{tube} = \frac{Vol_{tot}}{N_{tot}} \tag{C.3}$$

To determine the surface area, cross sectional area, and volume of a pass, the values computed above must be multiplied by the number of tubes in a pass.

C.1.2 Condenser Air-side Geometry

The following equations were obtained from Fisher and Rice (1983) and Bridges (1995) for computing the geometry dimensions for plain fins. The following dimensions define the airside of the condenser.

h_{hx}	= Height of the heat exchanger
d_{hx}	= Depth of the heat exchanger
L_{hx}	= Length of the heat exchanger
D_{out}	= Outer tube diameter
$N_{tubes,tot}$	= Total number of tubes in the airflow direction
$N_{tubes,front}$	= Total number of tubes in the airflow direction
S_T	= Tube spacing transverse to the air flow direction
S_L	= Tube spacing in the air flow direction
F_{th}	= Fin thickness
fp	= Fin pitch

The effective diameter is used in finding the airside Reynolds number.

$$D_{eff} = D_{out} + 2F_{th} \tag{C.4}$$

The minimum free flow area is used to the determine mass flux.

$$A_{freeflow} = A_{hx,frontal} - A_{tubes,front} - A_{fins,front} \tag{C.5}$$

The frontal area of the heat exchanger is

$$A_{hx,frontal} = L_{hx}h_{hx}. \tag{C.6}$$

The frontal area of the refrigerant tubes is

$$A_{tubes,front} = N_{tubes,front}\, D_{out}\, L_{exposed} \tag{C.7}$$

where $L_{exposed}$ is the length of tube not covered by fins.

$$L_{exposed} = L_{hx}(1 - fp\, F_{th}) \tag{C.8}$$

The frontal area of the fins is

$$A_{fins,front} = h_{hx}(fp\, L_{hx})F_{th}. \tag{C.9}$$

The surface area is multiplied by the heat transfer coefficient to find the heat transfer resistance. The surface area of the tubes is

$$A_{tubes} = N_{tubes,tot}\, \pi\, D_{out}\, L_{exposed}. \tag{C.10}$$

The surface area of the fins is

$$A_{fin} = 2\, fp\, L_{hx}\left[h_{hx}d_{hx} - N_{tubes,tot}\frac{\pi}{4}D_{out}^{2}\right]. \tag{C.11}$$

A surface efficiency accounts for the fact that the fin temperature is not the same as the tube temperature. First we must compute the fin efficiency for thin sheet fins.

$$\eta_{fin} = \frac{\tanh(m\, L_{fin,eff})}{m\, L_{fin,eff}} \tag{C.12}$$

When the fin extends from tube to tube, the effective fin length is half the tube spacing. In our condenser, the transverse fin spacing is different from the tube spacing in the flow direction. We take an average of the spacing in the two directions.

$$L_{fin,eff} = \frac{\left(\frac{S_T}{2} + \frac{S_L}{2}\right)}{2} \tag{C.13}$$

The fin parameter is

$$m = \sqrt{\frac{2\, h_{air}}{k_{wall}\, F_{th}}} \tag{C.14}$$

where h_{air} is the airside heat transfer coefficient and k_{wall} is the thermal conductivity of the wall.

The surface efficiency is

$$\eta_{surf} = \frac{A_{tube} + \eta_{fin} A_{fin}}{A_{tube} + A_{fin}}. \tag{C.15}$$

The surface efficiency is used to find the in the overall heat transfer coefficient for the air.

$$UA_{air} = \eta_{surf}(A_{tube} + A_{fin})h_{air} \tag{C.16}$$

The above calculations are for the entire heat exchanger.

C.2 Evaporator

A description of the plate-fin evaporator is given in Section 3.5. This section describes the calculations performed to obtain the diameters, area, and volumes needed for the heat exchanger model.

C.2.1 Evaporator Refrigerant-side Geometry

In the evaporator the refrigerant flows through flat plates with fins. The following parameters are specified.

L_{plate} = Length of the plate in the flow direction
N_{fin} = Number of fins perpendicular to the flow direction
L_{fin} = Fin length

h_{fin} = Fin height

s_{fin} = Spacing between adjacent fins

t_{fin} = Fin thickness

Vol_{tot} = Total internal volume

N_{tot} = Total number of plates

The fins in the evaporator are modeled as serrated fins (Section 3.5.1) The hydraulic diameter is determined by the following equation (Manglik and Bergles, 1995).

$$D_h = \frac{4 A_c}{A_{surface}/L} = \frac{4 s_{fin} h_{fin} L_{fin}}{2(s_{fin} L_{fin} + h_{fin} L_{fin} + t_{fin} h_{fin}) + t_{fin} s_{fin}} \tag{C.17}$$

The cross sectional area is determined from the following equation.

$$A_{cs,plate} = s_{fin}\, h_{fin}\, (N_{fin} + 1) \tag{C.18}$$

The surface area per plate is

$$A_{surface,plate} = 2\,(N_{fin} + 1)(h_{fins} + s_{fins})\, L_{plate} \tag{C.19}$$

Because the height of the fins is small compared with the spacing between the fins, the surface efficiency is modeled as equal to unity. As a result, we do not need to distinguish between the area of the plate and the area of the fins.

The total internal volume is again determined by filling the evaporator with water and measuring the volume of the water. The volume of the plate is

$$Vol_{plate} = \frac{Vol_{tot}}{N_{tot}}. \tag{C.20}$$

Above dimensions are all given for a single plate. To find the dimensions of a pass, the cross sectional area, surface area, and volume must be multiplied by the number of plates per pass.

C.2.2 Evaporator Air-side Geometry

The fins on the airside are modeled as offset-strip fins (Figure 3.10). A single row of fins exists between each refrigerant plate. The following dimensions define the evaporator airside.

h_{hx} = Height of the heat exchanger
d_{hx} = Depth of the heat exchanger
L_{hx} = Length of the heat exchanger
$N_{fin,rows}$ = Number of rows of fins
fp = fin pitch
F_{th} = Fin thickness
h_{fin} = Fin height
s_{fin} = Spacing between adjacent fins
L_{fin} = Fin length
t_{fin} = Fin thickness
N_{plate} = Number of total plates
h_{plate} = Height of the outside of the plate

In the specific evaporator used in the model, three different lengths of airside fins exists. The following parameters must be computed for each length of fins.

The hydraulic diameter is the same as Equation C.17. The minimum freeflow frontal area is

$$A_{freeflow} = A_{hx,frontal} - A_{plates,front} - A_{fins,front}. \quad (C.21)$$

The total frontal area of the heat exchanger is

$$A_{hx,frontal} = L_{hx}\, h_{hx}. \quad (C.22)$$

The frontal area of the plates is

$$A_{plate,frontal} = N_{plate}\, L_{hx}\, h_{plate}. \quad (C.23)$$

The frontal area of the fins is

$$A_{fins,front} = 2\, N_{fin,rows}\, (fp\, L_{hx})\, t_{fins}\, h_{fins}. \tag{C.24}$$

The surface area of plates is

$$A_{plate} = 2\, N_{plates}\, d_{hx}\, L_{hx}. \tag{C.25}$$

The surface area of fins is

$$A_{fins} = 2\, N_{fins,rows}\, (fp\, L_{hx})\, d_{hx}\, h_{fins}. \tag{C.26}$$

The fin efficiency for offset-strip fins is (Carey and Mandrusiak , 1986)

$$\eta_{fin} = \frac{\tanh(m\, h_{fins})}{m\, h_{fins}} \tag{C.27}$$

where the fin parameter is

$$m = \sqrt{\frac{2\, h_{air}(t_{fins} + L_{fins})}{k_{wall} t_{fins} L_{fins}}}. \tag{C.28}$$

h_{air} is the heat transfer coefficient of the air and k_{wall} is the thermal conductivity of the wall. The surface efficiency is

$$\eta_{surf} = \frac{A_{plate} + \eta_{fin} A_{fin}}{A_{plate} + A_{fin}}. \tag{C.29}$$

The surface efficiency is used in the following overall heat transfer coefficient calculation.

$$UA = \eta_{surf}\left(A_{plate} + A_{fin}\right)h_{air} \tag{C.30}$$

The above calculations are for the entire heat exchanger.

Appendix D
Calculating Properties from the Modified Benedict Webb Rubin Equation of State

D.1 Calculating Thermodynamic Properties from an Equation of State

This section documents how to calculate thermodynamic properties explicitly from an equation of state of the following form.

$$P(T,\rho) = \sum_{i=1}^{N_f} f_i(T)\, g_i(\rho) \tag{D.1}$$

$$c_v^{\circ}(T) = \sum_{i=1}^{N_c} c_i\, d_i(T) \tag{D.2}$$

Using the above two equations, internal energy, enthalpy, entropy, Gibbs free energy, specific heat at constant volume, specific heat at constant pressure, and the speed of sound can be explicitly calculated as a function of temperature and density. The forms of the functions f_i and g_i are unique to the specific equation of state. The function d_i is generally a polynomial and c_i is a vector of constants.

The nomenclature defined below is used to simplify the documentation of the equations.

$$f_i'(T) = \frac{df_i}{dT} \tag{D.3}$$

$$f_i''(T) = \frac{d^2 f_i}{dT^2} \tag{D.4}$$

$$g_i'(T) = \frac{dg_i}{dT} \tag{D.5}$$

$$G_i(\rho) = \int \frac{g_i(\rho)}{\rho^2}\, d\rho \tag{D.6}$$

$$D_i(T) = \int d_i(T)\, dT \tag{D.7}$$

$$E_i(T) = \int \frac{d_i(T)}{T}\, dT \tag{D.8}$$

The functions summarized above are used to solve for the thermodynamic properties explicitly as a function of temperature and density. We will also solve for the derivatives of each thermodynamic property with respect to temperature and density.

D.1.1 Pressure Equations

Pressure is determined from Equation D.1. The derivatives of pressure are

$$\frac{\partial P}{\partial T}(T,\rho) = \sum_{i=1}^{N_f} f_i'(T)\, g_i(\rho) \tag{D.9}$$

$$\frac{\partial P}{\partial \rho}(T,\rho) = \sum_{i=1}^{N_f} f_i(T)\, g_i'(\rho) \tag{D.10}$$

D.1.2 Internal Energy Equations

Internal energy can be calculated from temperature and density with the following thermodynamic equations.

$$u(T,\rho) = \int c_v^{\circ}\, dT + \int \left(P - T\frac{\partial P}{\partial T} \right) \frac{d\rho}{\rho^2} \tag{D.11}$$

Calculating internal energy from equation D.1 and D.2 gives

$$u(T,\rho) = \sum_{i=1}^{N_c} c_i\, D_i(T) + \sum_{i=1}^{N_f} \left[f_i(T) - T f_i'(T) \right] G_i(\rho) \tag{D.12}$$

The derivatives of internal energy are

$$\frac{\partial u}{\partial T}(T,\rho) = \sum_{i=1}^{N_c} c_i\, d_i(T) - T\sum_{i=1}^{N_f} f_i''(T)\, G_i(\rho) \tag{D.13}$$

$$\frac{\partial u}{\partial \rho}(T,\rho) = \frac{1}{\rho^2}\left[\sum_{i=1}^{N_f} f_i(T)\, g_i(\rho) - T\sum_{i=1}^{N_f} f_i'(T)\, g_i(\rho)\right] \tag{D.14}$$

D.1.3 Enthalpy Equations

The definition of enthalpy is

$$h(T,\rho) = u + \frac{P}{\rho} \tag{D.15}$$

The equation for enthalpy from Equation D.12 and D.1 is

$$h(T,\rho) = \sum_{i=1}^{N_c} c_i\, D_i(T) + \sum_{i=1}^{N_f}\left[f_i(T) - T f_i'(T)\right] G_i(\rho) + \frac{1}{\rho}\sum_{i=1}^{N_f} f_i(T)\, g_i(\rho) \tag{D.16}$$

The derivatives of enthalpy are

$$\frac{\partial h}{\partial T}(T,\rho) = \sum_{i=1}^{N_c} c_i\, d_i(T) - T\sum_{i=1}^{N_f} f_i''(T)\, G_i(\rho) + \frac{1}{\rho}\sum_{i=1}^{N_f} f_i'(T)\, g_i(\rho) \tag{D.17}$$

$$\frac{\partial h}{\partial \rho}(T,\rho) = -\frac{T}{\rho^2}\sum_{i=1}^{N_f} f_i'(T)\, g_i(\rho) + \frac{1}{\rho}\sum_{i=1}^{N_f} f_i(T)\, g_i'(\rho) \tag{D.18}$$

D.1.4 Entropy Equations

Entropy can be calculated from temperature and density with the following thermodynamic equations.

$$s(T,\rho) = \int \frac{c_v^\circ}{T} dT + \int \frac{1}{\rho^2} \frac{\partial P}{\partial \rho} d\rho \qquad (D.19)$$

Plugging Equation D.1 and D.2 into D.19 we get

$$s(T,\rho) = \sum_{i=1}^{N_c} c_i E_i(T) - \sum_{i=1}^{N_f} f_i'(T) G_i(\rho) \qquad (D.20)$$

The derivatives of equation D.20 are

$$\frac{\partial s}{\partial T}(T,\rho) = \frac{1}{T} \sum_{i=1}^{N_c} c_i d_i(T) - \sum_{i=1}^{N_f} f_i''(T) G_i(\rho) \qquad (D.21)$$

$$\frac{\partial s}{\partial \rho}(T,\rho) = -\frac{1}{\rho^2} \sum_{i=1}^{N_f} f_i'(T) g_i(\rho) \qquad (D.22)$$

D.1.5 Gibbs Free Energy Equations

The equations for Gibbs free energy is

$$g(T,\rho) = h - Ts \qquad (D.23)$$

From Equations D.16 and D.20 we get

$$g(T,\rho) = \sum_{i=1}^{N_c} c_i [D_i(T) - T E_i(T)] - \sum_{i=1}^{N_f} f_i(T) \left[G_i(\rho) + \frac{g_i(\rho)}{\rho} \right] \qquad (D.24)$$

The derivatives are

$$\frac{\partial g}{\partial T}(T,\rho) = \frac{1}{T}\sum_{i=1}^{N_c} c_i E_i(T) + \sum_{i=1}^{N_f} f_i'(T)\left[G_i(\rho) + \frac{g_i(\rho)}{\rho}\right] \tag{D.25}$$

$$\frac{\partial g}{\partial \rho}(T,\rho) = \sum_{i=1}^{N_f} f_i'(T)\frac{g_i'(\rho)}{\rho} \tag{D.26}$$

D.1.6 Specific Heat at Constant Volume

The specific heat at constant volume is calculated from the following equation.

$$c_v(T,\rho) = c_v^\circ - T\int\left(\frac{\partial^2 P}{\partial T^2}\right)\frac{d\rho}{\rho^2} \tag{D.27}$$

From Equation D.1 and D.2 we get

$$c_v(T,\rho) = \sum_{i=1}^{N_c} c_i d_i(T) - T\sum_{i=1}^{N_f} f_i''(T) G_i(\rho) \tag{D.28}$$

D.1.7 Specific Heat at Constant Pressure

The thermodynamic equation of the specific heat at constant pressure is

$$c_p(T,\rho) = c_v + \frac{\partial P}{\partial T} \tag{D.29}$$

From Equations D.28 and D.1 we get

$$c_p(T,\rho) = \sum_{i=1}^{N_c} c_i d_i(T) - T\sum_{i=1}^{N_f} f_i''(T) G_i(\rho) + \sum_{i=1}^{N_f} f_i'(T) g_i(\rho) \tag{D.30}$$

D.1.8 Speed of Sound Equations

The speed of sound is defined

$$ss(T,\rho) = \sqrt{\left(\frac{\partial P}{\partial \rho}\right)_s} \tag{D.31}$$

The property is calculated from the following equations

$$ss(T,\rho) = \sqrt{\frac{dP}{d\rho} - \frac{\frac{dP}{dT}\frac{ds}{d\rho}}{\frac{ds}{dT}}} \tag{D.32}$$

The derivatives in the above equations are calculated from Equations D.19, D.10, D.21, and D.22.

D.2 Functions for the Modified Benedict Webb Rubin Equation of State

The Modified Benedict Webb Rubin (MBWR) equation of state has the following form.

$$P = \sum_{n=1}^{9} a_n \rho^n + \exp\left(\frac{-\rho}{\rho_{crit}}\right) \sum_{n=10}^{15} a_n \rho^{2n-17} \tag{D.33}$$

If we write it in the notation defined in Equation D.1, the parameters for the functions f_i and g_i are summarized in Table D.1. The variables b_1-b_{32} are empirical coefficients. To compute f' (Equations D.3) the following equation is used.

$$\frac{d}{dT} T^n = nT^{n-1} \tag{D.34}$$

To compute f'' (Equations D.4) the following equation is used.

$$\frac{d^2}{dT^2} T^n = n(n-1)T^{n-2} \tag{D.35}$$

i	$f_i(T)$	$g_i(\rho)$
1	RT	ρ
2	$b_1T + b_2\sqrt{T} + b_3 + b_4/T + b_5/T^2$	ρ^2
3	$b_6T + b_7 + b_8/T + b_9/T^2$	ρ^3
4	$b_{10}T + b_{11} + b_{12}/T$	ρ^4
5	b_{13}	ρ^5
6	$b_{14}/T + b_{15}/T^2$	ρ^6
7	b_{16}/T	ρ^7
8	$b_{17}/T + b_{18}/T^2$	ρ^8
9	b_{19}/T^2	ρ^9
10	$b_{20}/T^2 + b_{21}/T^3$	$\rho^3\exp(-\gamma\rho^2)$
11	$b_{22}/T^2 + b_{23}/T^4$	$\rho^5\exp(-\gamma\rho^2)$
12	$b_{24}/T^2 + b_{25}/T^3$	$\rho^7\exp(-\gamma\rho^2)$
13	$b_{26}/T^2 + b_{27}/T^4$	$\rho^9\exp(-\gamma\rho^2)$
14	$b_{28}/T^2 + b_{29}/T^3$	$\rho^{11}\exp(-\gamma\rho^2)$
15	$b_{30}/T^2 + b_{31}/T^3 + b_{32}/T^4$	$\rho^{13}\exp(-\gamma\rho^2)$

Table D.1 Functions which define the MBWR equation of state.

To compute g' (Equations D.5) the following equations are used.

$$\frac{d}{dT}\rho^n = n\rho^{n-1} \tag{D.36}$$

$$\frac{d}{dT}\left[\rho^n \exp\left(-\gamma\rho^2\right)\right] = \left(n - 2\gamma\rho^2\right)\rho^{n-1}\exp\left(-\gamma\rho^2\right) \tag{D.37}$$

To compute G (Equations D.6) the following equations are used.

$$\int \rho^n \frac{1}{\rho^2} d\rho = \begin{cases} \dfrac{\rho^{n-1}}{n-1} & n \neq 1 \\ \log(\rho) & n = 1 \end{cases} \tag{D.38}$$

$$\int \rho^{2n+3} \exp\left(-\gamma\rho^2\right)\frac{1}{\rho^2}d\rho = \frac{-\exp\left(-\gamma\rho^2\right)}{2\gamma}\sum_{i=0}^{n}\frac{n!}{(n-i)!}\frac{\rho^{2(n-i)}}{\gamma^i} \tag{D.39}$$

The equation for the ideal gas specific heat at constant volume is

$$c_v^{\circ} = c_1 + c_2T + c_3T^2 + c_4T^3 + c_5T^4 + c_6T^5 + c_7T^6 \tag{D.40}$$

To compute D (Equations D.7) the following equation is used.

$$\int T^n dT = \frac{T^{n+1}}{n+1} \tag{D.41}$$

To compute E (Equations D.7) the following equation is used.

$$\int T^n \frac{1}{T} dT = \frac{T^n}{n} \tag{D.42}$$

Appendix E
Adding New Refrigerants to Prop.f

Three subroutines must be added and two functions must be modified to add a new refrigerant to the property routines. One subroutine must be added to initialize the coefficients of the refrigerant, for example *Subroutine R134a*. This subroutine must be called by the user before properties of the new substance can be computed. In this procedure we will call this *Subroutine X*. A subroutine must be added which contains the curve fit of the saturation pressure as a function of temperature. Another subroutine must be added which contains the curve fit of the saturated liquid density as a function of temperature. For R134a these subroutines are called *Subroutine PsatT_r134a* and *Subroutine rhofT_r134a*. In this procedure we will call the new subroutine *Subroutine PsatT_X* and *Subroutine rhofT_X*. *Function PsatT* must be modified to call the *Subroutine PsatT_X* and *Function rhofT* must by modified to call *Subroutine rhofT_X*. The following procedures list what specific changes must be made to the program to add a new refrigerant.

1) Find the coefficients for the MBWR equation of state and the ideal specific heat (c_v°) equation for the new refrigerant.

2) Convert the coefficients to the correct units which are K, Pa, and kg/m^3 for temperature, pressure, and density, respectively. Table E.1 summarizes the units for each coefficient in the MBWR equation of state.

3) Copy *Subroutine R134a* and modify it for the new the refrigerant. Set all of the constants equal to zero. At this point

A) Change the subroutine name to one appropriate for the refrigerant (e.g. *Subroutine X*).
B) Change *refname* to an unused integer
C) Change the ideal gas constant and the molecular weight.
D) Change the coefficients of the MBWR equations of state.
E) Change the coefficients of the specific heat equations.

F) Change the minimum and maximum temperature as specified by the equation of state.

b	unit	b	unit	b	unit	b	unit
1	$\frac{Pa}{(kg/m^2)^2K}$	9	$\frac{Pa\,K^2}{(kg/m^2)^3}$	17	$\frac{Pa\,K}{(kg/m^2)^8}$	24	$\frac{Pa\,K^2}{(kg/m^2)^7}$
2	$\frac{Pa}{(kg/m^2)^2K^{0.5}}$	10	$\frac{Pa}{(kg/m^2)^4K}$	18	$\frac{Pa\,K^2}{(kg/m^2)^8}$	26	$\frac{Pa\,K^2}{(kg/m^2)^9}$
3	$\frac{Pa}{(kg/m^2)^2}$	11	$\frac{Pa}{(kg/m^2)^4}$	19	$\frac{Pa\,K^2}{(kg/m^2)^9}$	27	$\frac{Pa\,K^4}{(kg/m^2)^9}$
4	$\frac{Pa\,K}{(kg/m^2)^2}$	12	$\frac{Pa\,K}{(kg/m^2)^4}$	20	$\frac{Pa\,K^2}{(kg/m^2)^3}$	28	$\frac{Pa\,K^2}{(kg/m^2)^{11}}$
5	$\frac{Pa\,K^2}{(kg/m^2)^2}$	13	$\frac{Pa}{(kg/m^2)^5}$	21	$\frac{Pa\,K^3}{(kg/m^2)^6}$	29	$\frac{Pa\,K^3}{(kg/m^2)^{11}}$
6	$\frac{Pa}{(kg/m^2)^3K}$	14	$\frac{Pa\,K}{(kg/m^2)^6}$	22	$\frac{Pa\,K^2}{(kg/m^2)^5}$	30	$\frac{Pa\,K^2}{(kg/m^2)^{13}}$
7	$\frac{Pa}{(kg/m^2)^3}$	15	$\frac{Pa\,K^2}{(kg/m^2)^6}$	23	$\frac{Pa\,K^4}{(kg/m^2)^6}$	31	$\frac{Pa\,K^3}{(kg/m^2)^{13}}$
8	$\frac{Pa\,K}{(kg/m^2)^3}$	16	$\frac{Pa\,K}{(kg/m^2)^7}$	24	$\frac{Pa\,K^2}{(kg/m^2)^7}$	32	$\frac{Pa\,K^4}{(kg/m^2)^{13}}$

Table E.1 Units of the empirical coefficients of the MBWR equation of state.

4) Determine the saturation densities and pressures. Find the critical point from a table of refrigerant properties. Create an array of temperatures between the minimum and critical temperature; cluster a lot of points around the critical value. From a table of refrigerant properties find an initial guess for ρ_g and ρ_f at T_{min}. Perform a two-dimensional search to find the saturation properties as described in Section 7.3.1.

5) Find the critical point using the two-dimensional search described in Section 7.3.3. After determining the critical temperature, repeat Step 4 using the correct critical temperature for the equation of state to find the critical density. Changing the critical temperature, pressure, and density in *Subroutine X*.

6) Take the saturation data obtained in Step 4 and determine curve fits for the saturated liquid density and saturation pressure as functions of temperature. Reid et al. (1987) document

possible forms of the curve fits. Place the equations for the curve fits in *Subroutine PsatT_X* and *Subroutine rhofT_X*. Modify *Function PsatT* and *Function rhofT* to call the *Subroutine PsatT_X* and *Subroutine rhofT_X* when *refname* equals the integer specified in Step 3.

8) Next find the constants to define the reference state for enthalpy and entropy. To use the ASHRAE standard use the following steps.

A) Make uc(1) = - prop('h ','T ',233.15,'x ',0d0)
B) Make sc(1) = - prop('s ','T ',233.15,'x ',0d0)

If instead you would like to use the international standard use the following steps.

A) Make uc(1) = - prop('h ','T ',273.15,'x ',0d0) + 200
B) Make sc(1) = - prop('s ','T ',273.15,'x ',0d0) + 1

Change *uc(1)* and *sc(1)* in *Subroutine X*.

9) Begin analyzing the performance of the property routine as described in Section 7.5. If the density range is unknown use the following equations.

$$\rho_{min} = \frac{\rho_g(T_{min})}{10} \tag{E.1}$$

$$\rho_{max} = \rho_f(T_{min}) + 100 \tag{E.2}$$

Change *rhomin* and *rhomax* to the correct value in *Subroutines X*.

Vita

Tara Lynn Hemami was born on October 11, 1970 in Columbus, Ohio to Hooshang and Anita Hemami. Upon graduating from Worthington High School in 1989, she attended the University of Illinois at Urbana-Champaign. Tara received the NSF Undergraduate Research Fellowship for Women and Minorities in the spring of 1992. Also in the summer of 1992 Tara headed the HVAC Design Team and the Sponsorship Team for Ford's Hybrid Electric Vehicle Challenge. In January, 1993 Tara received a B.S. in Mechanical Engineering and began graduate school at the University of Illinois at Urbana-Champaign. She performed research on the transient behavior of automotive air-conditioning systems and refrigerant property routines. Upon completing the requirements for the Ph.D., Tara will work for the heat and fluids research group at Cummins Engine in Columbus, Indiana. She married Anthony Brazelton on June 24, 1995.